

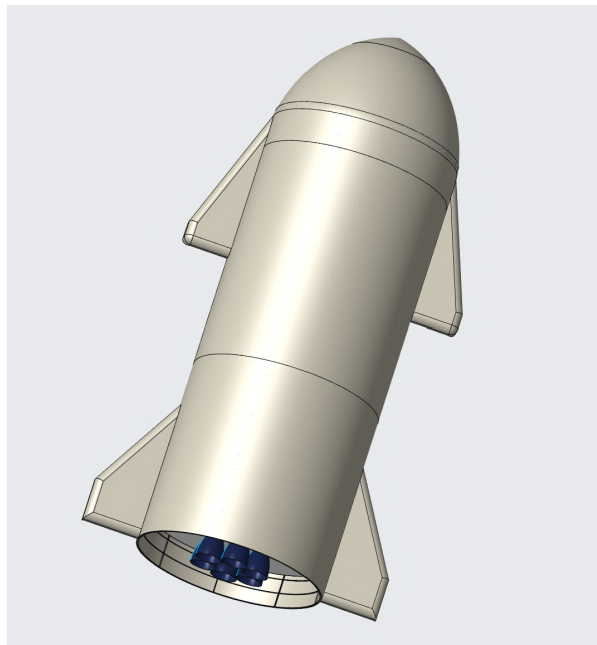


TECHNICAL REPORT - STARCHEAP

ITP PROJECT

Charlotte Bergot, Rémi Caresche, Davia Franceschini,
Maxence Goubaud, Guillaume Lopere

Advanced Master TAS ASTRO
April, 2025



2024-2025

Contents

1 Abbreviations	8
2 Introduction	10
3 Mission Analysis	11
3.1 Launch Strategy	11
3.2 Mission Outline	12
3.2.1 Concept of Operation	13
3.2.2 Propulsion choice and first orbit iteration	17
3.2.3 Refined orbit iteration	19
3.2.4 Reentry Trajectory	22
3.2.5 Reentry trajectory with Python	26
3.3 Environment	28
3.3.1 Environmental Modeling	29
3.3.1.1 Charged Particle Flux	29
3.3.1.2 Plasma Environment	30
3.3.1.3 Micrometeoroids and Debris	31
3.3.1.4 Atomic Oxygen	31
3.3.1.5 Electromagnetic Radiation	32
3.3.2 Effects on the Mission and Subsystems	32
3.3.2.1 Radiation Effects	32
3.3.2.2 Charging Effects	34
3.3.2.3 Impact Risk	34
3.3.2.4 Chemical and Thermal Degradation	34
3.3.2.5 Contamination	35
3.3.3 Analysis and Recommendations	36
4 Propulsion	38
4.1 Engine design	40
4.2 RCS Engine design	44
4.3 Injectors	46
4.4 Ignitor	47
4.5 Cooling system	49
4.6 Gimballing	52
4.6.1 Choice of architecture	52
4.6.2 Design considerations	54
4.6.3 Mount	54
4.6.4 Design of the gimbal	56
4.6.4.1 Gimbal angle	56
4.6.4.2 Frame and actuators	57
4.7 Tank design	60
4.7.1 NOFBX tank design	60
4.7.2 Pressurant System	61
4.8 Mass budget	63
5 AOCS	67
5.1 AOCS requirements	67

5.2	System choices	68
5.3	System efforts dimensioning	70
5.3.1	Human factors	71
5.3.2	Reentry & Atmospheric flight	72
5.3.3	Hover flip	75
5.3.4	Orbital flight	76
5.3.5	Rendezvous	77
5.3.6	Docking	79
5.3.7	Debris capture	80
5.3.8	Orbital insertion	82
5.3.9	Failure scenarios	82
5.3.10	Hardware approach	84
5.3.11	Obtained System Limits	84
5.4	Design of the control means	85
5.4.1	Reaction Control System	85
5.4.1.1	Thrust Assessment & Axis Control	86
5.4.1.2	Engine Choice	88
5.4.2	Flaps	90
5.4.2.1	Required aerobraking surface	90
5.4.2.2	Validation of Control Authority	94
5.4.2.3	Flaps geometry	95
5.5	Sensors Design	101
5.5.1	Navigation	102
5.5.1.1	GNSS (Global Navigation Satellite System)	102
5.5.1.2	Inertial Measurement Unit (IMU))	102
5.5.1.3	Altimeters (Radar or Laser)	102
5.5.1.4	Light Detection and Ranging (LiDAR)	103
5.5.2	Attitude	103
5.5.2.1	IMU	103
5.5.2.2	Star tracker	103
5.5.2.3	Earth Horizon Sensor	104
5.6	Integration and Rendundancy considerations	104
6	Structure	106
6.1	Propulsive module	107
6.1.1	Carbon shell	107
6.1.2	Reinforcement rings	107
6.1.3	Reinforcement stringers	107
6.1.4	Thrust ring	108
6.1.5	Structural mass	108
6.1.6	Verifications	109
6.2	Cargo Module	110
6.2.1	Shell sizing	111
6.2.2	Reinforcements Sizing	113
6.2.3	Large Opening Door	115
6.2.4	Preliminary Verification	116
6.3	Crew module	116
6.3.1	Carbon shell	117

6.3.2	Reinforcement rings	117
6.3.3	Reinforcement stringers	118
6.3.4	Separation ring	118
6.3.5	Verification	118
6.3.5.1	Vibrational modes	118
6.3.5.2	Dynamic Pressure	119
6.4	Computer Aided Design	121
6.5	Abort system	125
6.6	Conclusion	126
7	Communication	127
7.1	Requirements	127
7.2	Needs Analysis	127
7.3	Communication Strategy	128
7.3.1	Continuous Link with Relays	128
7.3.2	Direct Link with Ground	128
7.3.3	Direct Link with Station	130
7.3.4	Global Architecture	131
7.4	Links budget calculation	132
7.4.1	Communication with Relay - SES O3b mPOWER	132
7.4.2	Direct Communication with Ground	134
7.4.3	Communication with Station	137
7.5	Physical Layer Architecture	139
7.6	Protocol, Packet, Safety	140
7.6.1	Protocol	140
7.6.2	Packet	140
7.6.3	Safety	141
8	Power	142
8.1	Requirements	142
8.2	Power Budget	142
8.3	Primary Energy Source Design	143
8.3.1	State of the Art	143
8.3.2	Technology Trade-Off	144
8.3.3	Fuel Cell Design	144
8.3.4	Tank Design	146
8.4	Secondary Source Design	148
8.4.1	State of the Art	148
8.4.2	Batteries Design	148
8.5	Power Control and Distribution	150
8.5.1	Power Control Strategy	150
8.5.2	Power Distribution Topology	150
8.5.3	Fault Tolerance	150
8.6	Environmental Considerations	151
8.7	Lifespan and Reusability	151
9	Life Support	153
9.1	Requirements	153
9.2	Environment	155

9.2.1	State of the art & Design Considerations	155
9.2.1.1	ISS ECLSS	155
9.2.1.2	Orion ECLSS	155
9.2.1.3	CrewDragon ECLSS	156
9.2.2	System Design	156
9.2.2.1	Cabin Atmosphere Composition and Pressure Control .	157
9.2.2.2	Carbon Dioxide and Humidity Control	160
9.2.2.3	Trace Contaminant and Particulate Filtration	162
9.2.2.4	Thermal and Humidity Regulation	164
9.2.2.5	ECLSS Mass Budget	165
9.3	Safety Procedures	165
9.3.1	Solar flares procedures	165
9.3.2	Fire Detection and Suppression	165
9.4	Food management	166
9.4.1	Astronauts Needs	166
9.4.2	Food distribution & storage	167
9.4.3	Food and mass budget	168
9.5	Medical Necessities	169
9.5.1	TASTrain recommendations	170
9.5.2	Procedures classification	171
9.5.3	Crew Health Monitoring	172
9.5.4	Medical computer	172
9.5.5	Medical Area	173
9.5.6	Medical Mass Budget	173
9.6	Crew Module/Living Quarters	175
9.6.1	EVA	175
9.6.2	Habitacle	175
9.6.3	Hygiene on board	175
9.6.4	Absence of Artificial Gravity and a Gym	177
9.7	Water management	177
9.7.1	Water Budget	178
9.7.2	Fuel cell water recovery	178
9.7.3	Water management along the mission	180
9.7.4	Storage : Tanks design	183
9.7.5	Water distribution	187
9.7.6	Monitoring	189
9.7.7	Final architecture	190
9.7.8	Mass budget	190
9.7.9	Limits of the drinkable water system design	191
9.8	Waste Management System	191
9.8.1	Waste budget	193
9.8.2	Tank Dimensioning	194
9.8.3	Toilet Architecture and Design	195
9.8.4	Vacuum cleaner	195
9.8.5	Mass budget	196
9.9	ECLSS Mass budget	196

10 Thermal	197
-------------------	------------

10.1 Requirements	197
10.2 Heat Shield design	198
10.2.1 Objectives: Methodology for Heat Shield Design	199
10.2.2 Application of the pre-design methodology	200
10.2.3 Feasability & limits	209
10.3 Shuttle thermal exposure in orbit	210
10.4 Thermal budget	211
10.5 Passive Thermal Control System (PTCS)	212
10.5.1 Systema Analysis : Thermal context	212
10.5.2 Systema analysis results	215
10.5.3 Final coatings choices	218
10.6 Active Thermal Control System (ATCS)	221
10.6.1 Active Thermal Control requierments	221
10.6.2 Active Thermal Control equipements	223
10.6.3 Feasibility and Limitations of the ACTS	224
11 Docking	226
11.1 Introduction	226
11.2 Requirement	226
11.2.1 System of systems Docking Requirements	227
11.2.2 Functional requirements	228
11.2.3 IDSS Requirements	228
11.3 Docking phases	231
11.3.1 Description	231
11.3.2 Phasing and pre-homing :	231
11.3.3 Homing :	231
11.3.4 Closing :	232
11.3.5 Final Approach :	232
11.3.6 Docking Phase – Procedure with Station ASTROIKOS	232
11.4 Architecture	233
11.4.1 SCS	234
11.4.2 HCS	235
11.5 Interfaces	236
11.5.1 Additional Interfaces	236
11.5.2 Interfaces Location :	236
11.5.3 Interfaces Specifications	237
11.5.4 Interface Design	239
11.6 Actuators Definition of the Docking System	240
11.6.1 HCS Actuators	240
11.6.2 SCS Actuators	240
11.6.3 Other Actuators	241
11.7 Sensors Definition	241
11.7.1 Proximity Sensors	241
11.7.2 Force Sensors	242
11.8 Docking System Power Supply	245
11.9 Conclusion	245
12 Command Data Handling	246

12.1	CDH requirements	247
12.2	Critical analysis	248
12.3	Management Mode analysis	249
12.3.1	Principal Management Mode	249
12.3.2	Docking Management Mode	250
12.3.3	Capture Management Mode	251
12.3.4	Landing Management Mode	253
12.4	CDH Architecture	256
12.4.1	Global Architecture	256
12.4.2	SpaceWire links	256
12.4.3	Subsystems network	258
12.5	Component definition	258
12.5.1	OBC : On-Board Computer	259
12.5.2	TCM : Telemetry, Command, and Mass Memory	259
12.5.3	RTU : Remote Terminal Unit	260
12.5.4	Sensors	260
12.6	Conclusion	260
13	Debris Capture	262
13.1	Requirements	262
13.2	System Analysis	262
13.3	Debris use case characteristics	263
13.4	Choice of Mechanism	264
13.4.1	Tentacle-Based Clasping Mechanisms	264
13.4.2	Robotic Manipulators	265
13.4.3	Mothership-CubeSat (Deorbiter Satellite) Approach	265
13.4.4	Sling-Sat Method	265
13.4.5	Tether-Based Systems	266
13.4.6	Soft Gripper Technologies	266
13.4.7	Net-Based Capture	266
13.4.8	ElectrodynamiC Tether Capture (EDDE)	267
13.4.9	Tethered Gripper Systems	267
13.4.10	Harpoon-Based Tether Systems	268
13.4.11	Solar Concentrator Methods	268
13.4.12	Laser-Based Removal	268
13.4.13	Ion Beam Shepherding	268
13.4.14	Origami-Inspired Capture Mechanism	268
13.5	Results and Choice	269
13.6	System Specifications	270
13.6.1	Deployment Mechanism	270
13.6.2	Tether	271
13.6.3	Capture Mechanism - Net	271
13.6.3.1	Geometric Design and Sizing	271
13.6.3.2	Closure Mechanism	272
13.6.3.3	Summary of Net Specifications	273
13.6.4	Retrieval Mechanism	273
13.6.5	Specification Synthesis	275
13.7	System Limitations	275

13.8 Operational Assessment	275
14 System Lifecycle Implementation	277
14.1 Manufacturing	277
14.1.1 Supplier Strategy and Make-or-Buy Logic	277
14.1.2 Quality Control and Inspections	277
14.2 Assembly, Integration and Testing	277
14.2.1 Assembly	277
14.2.2 Integration	278
14.2.3 Testing Campaign	278
14.3 Maintenance and Refurbishment	279
14.3.1 Post-Mission Preliminary Inspection	280
14.3.2 Diagnostic Testing	280
14.3.3 Corrective Maintenance After Anomalies	280
14.3.4 Maintenance Scheduling and Cycles	280
14.4 End-of-Life and Sustainability	281
14.4.1 End-of-Life Strategy	281
14.4.2 Environmental Impact	281
15 Conclusion	282

1 Abbreviations

ACTS : Active Thermal Control System
AFC : Alkaline Fuel Cells
AOCS : Attitude and Orbit Control System
ATOX : Atomic Oxygen
BDM : Berthing Docking Mode
CAD : Computer Aided Design
CM : Crew Member
CM-d : Crew member for each day
CMG : Control Moment Gyroscope
COPV : Composite Overwrapped Pressure Vessels
CSM : Command and Service Module
DCM : Deployment Capture Mode
EBM : Ejection Bay Mode
ECLSS : Environment and Control Life Support System
ECM : Escape Capture Mode
EDM : Escape Docking Mode
EEP : Error End of Packet
EER : Estimated Energy Requirement
EOP : End of Packet
EPS : Electrical Power System
ESA : European Space Agency
EVA : Extravehicular Activity
FEM : Finite Element Method
FOM : Fail Operational Mode
FSM : Fail Safe mode
GCR : Galactic Cosmic Rays
GMAT : General Mission Analysis Tool
GNC : Guidance, Navigation and Control
GSFC : Goddard Space Flight Center
HCM : Hard Capture Mode
HDM : Hard-Dock Mode
ICM : Inspection Capture Mode
INM : Initialization Mode
ISS : International Space Station
ITU : International Telecommunication Union
LAM : Launch Mode
LEO : Low Earth Orbit
LM : Landing Mode
Max-Q : Maximum dynamic pressure
MEO : Medium Earth Orbit
MLI : Multilayer Insulation
NASA : National Aeronautics and Space Administration
NOFBX : Nitrous Oxide Fuel Blend Experimental
NOM : Nominal Operation Mode
OBC : On-Board Computer
OBDH : On-Board Data Handling

OTM : Orbit Transfert Mode
PCDU : Power and Control Distribution Unit
PEMFC : Proton Exchange Membrane Fuel Cells
PTCS : Passive Thermal Control System
RCM : Rendezvous Capture Mode
RCS : Reaction Control System
RDM : Refueling Docked Mode
RM : Re-entry Mode
RTU : Remote Terminal Unit
RVDM : Rendezvous Docking Mode
SBLM : Stand-by Landing Mode
SCM : Safe Capture Mode
SCREAM : Storable propellant Combustion Rocket Engine with Acoustic Ignition Mechanism
SDM : Safe Docking Mode
SEE : Single Event Effects
SFDM : Soft Docked mode
SLM : Safe Landing Mode
SIFLET : Sonic Ignition For Liquid Engine Technology
SMAD : Space Mission Analysis and Design
STB : Stand-by mode
TBC : Thermal Barrier Coating TCM : Telemetry, Command, and Mass Memory
TID : Total Ionizing Dose
TNID : Total Non-Ionizing Dose
TPS : Thermal Protection System
TUFİ : Toughened Uni-piece Fibrous Insulation
TVC : Thrust Vector Control
UN : United Nations
UV : UltraViolet

2 Introduction

The space shuttle StarCheap is designed to operate within a system of systems that includes a secondary shuttle, a space station, a training center, and a launcher. This network is illustrated in Figure 1, which shows the interfaces and interactions among these components.

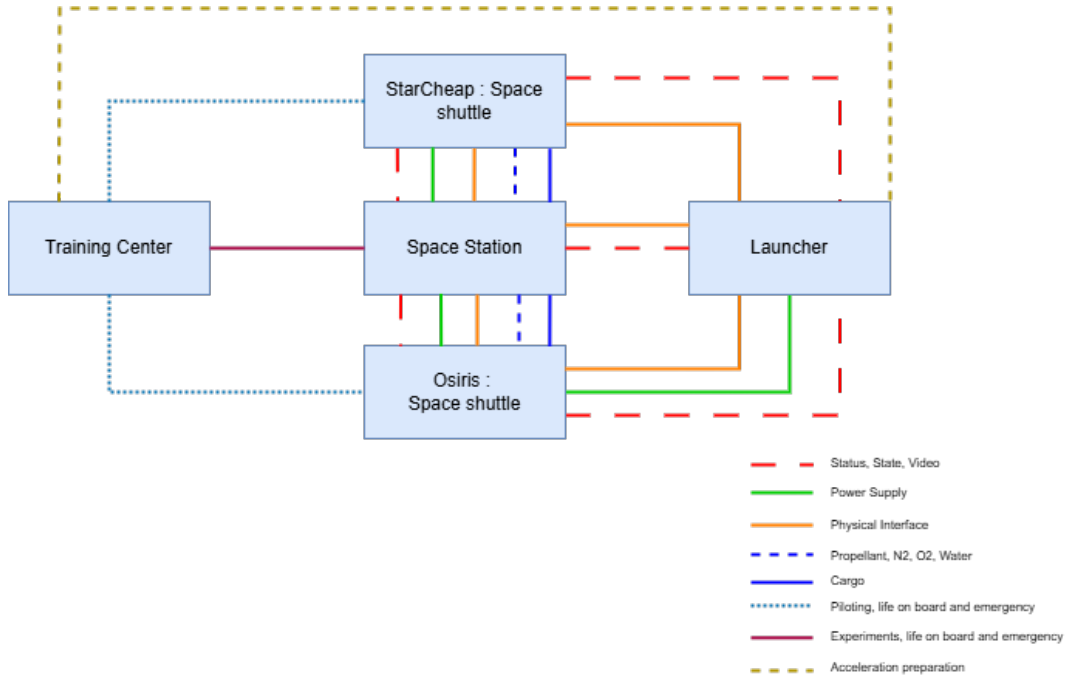


Figure 1: System of System interfaces

The StarCheap shuttle is thought to transport three astronauts and cargo into orbit. Additionally, it performs debris retrieval missions. Its design ensures interoperability with other system components.

One of the shuttle's functions is debris retrieval, which helps maintain a safe orbital environment. Its re-entry capabilities ensure the return of astronauts to Earth.

Operating at various altitudes, the shuttle accesses different orbits to support diverse mission profiles. The system of systems approach provides advantages such as increased coverage, optimized resource management, and enhanced mission reliability. If one component fails, others can compensate to ensure mission continuity.

3 Mission Analysis

This section aims to provide a comprehensive analysis of the overall mission architecture and its associated constraints. It presents the orbital parameters, mission phases, operational assumptions, and preliminary simulations that support the design of the StarCheap system.

The mission is designed to launch a crewed shuttle capable of autonomous operation and debris collection in Low Earth Orbit (LEO). The shuttle must be able to dock with a predefined space station orbiting at 500 km altitude and 50° inclination, perform long-duration missions (up to 6 months), and return safely to Earth via a controlled reentry.

The table below summarizes the high-level mission requirements derived from operational objectives and environmental constraints.

Requirement	Associated Parameter
Support launch external environment	50 kPa, 3300 °C
Support launch	Up to 6g, 100 Hz
Shuttle must take 3 astronauts	3 seats
Shuttle must dock and undock to a defined station	Station at 500 km, 50° inclination
Shuttle must support autonomous operations	3 days (autonomous ops duration)
Mission duration	6 months (5 months docking, 3 days mission)
Shuttle can travel to a defined debris	Range: [40°; 60°] inclination, [400 km; 1000 km] altitude
Shuttle can catch a debris	RDV: 20 m distance, capture debris up to shuttle hold size
Shuttle can store debris	Shuttle hold size: 5 m × 3 m × 3 m
Shuttle can free the debris	Release at 200 km circular orbit
Shuttle must perform a safe reentry	Reentry path planned (200 km to 0 km)
Shuttle must perform safe landing	Vertical landing
Shuttle should have a lifespan of 5 years	Lifetime: 5 years
Shuttle must have a cargo section	Cargo = shuttle hold size
Debris resistance	>10 cm (collision avoidance), 0.01–1 cm (shielding)
Failure rate	10^{-9}

Table 1: Mission Requirements and Associated Parameters

3.1 Launch Strategy

This section presents the launch strategy to place our shuttle into a circular orbit at an altitude of 500 km with an inclination of 50 degrees and an initial RAAN of -1.38429×10^{-6} radians. The characteristics of the orbit come from the space station

Orbital Parameters

- Altitude: 500 km
- Inclination: 50°
- Initial RAAN: -1.38429×10^{-6} radians from space Station information
- Semi-major axis (a): 6878 km
- Mean motion (n): 0.001 109 rad s $^{-1}$

Calculation of RAAN Drift :

The drift of the ascending node is calculated using the following formula:

$$\dot{\Omega}_{drift} = -\frac{3}{2}J_2 \left(\frac{R_e}{a}\right)^2 n \cos(i)$$

where $J_2 = 1.08263 \times 10^{-3}$ and $R_e = 6378$ km.

Launch Windows :

The launch windows are calculated for the next 10 days starting from April 17, 2025. Here are the results:

Day	Launch Window
1	April 16, 2025 at 23:59:59
2	April 17, 2025 at 23:36:25
3	April 18, 2025 at 23:12:50
4	April 19, 2025 at 22:49:16
5	April 20, 2025 at 22:25:41
6	April 21, 2025 at 22:02:06
7	April 22, 2025 at 21:38:32
8	April 23, 2025 at 21:14:57
9	April 24, 2025 at 20:51:22
10	April 25, 2025 at 20:27:48

Table 2: Launch windows for the next 10 days.

There is about one launch window per day. This is one sidereal day minus the drift of the station in orbit. We only take into account launches to the North-East of Kourou, as the South-East launches fly over inhabitable areas.

3.2 Mission Outline

The mission outlines defines the trajectory and operational constraints of the system. It serves as a foundational element, bridging vehicle capabilities with mission objectives. In this section, we outline the overall strategy from launch to debris recovery and reentry, providing insight into orbital maneuvers, propulsion system sizing, and operational feasibility. The analysis combines analytical estimations and simulations to iteratively refine the mission design.

3.2.1 Concept of Operation

These following pictures provides a detailed analysis of a space mission aimed at sending three astronauts and cargo to a 500 km altitude and 50-degree inclination orbit where the space station is located. The mission also involves debris recovery and disposal, followed by the spacecraft's re-entry and landing.

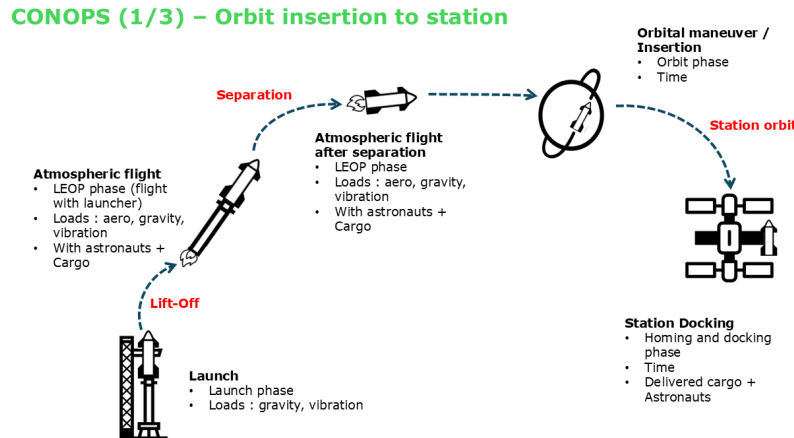


Figure 2: ConOps phase 1

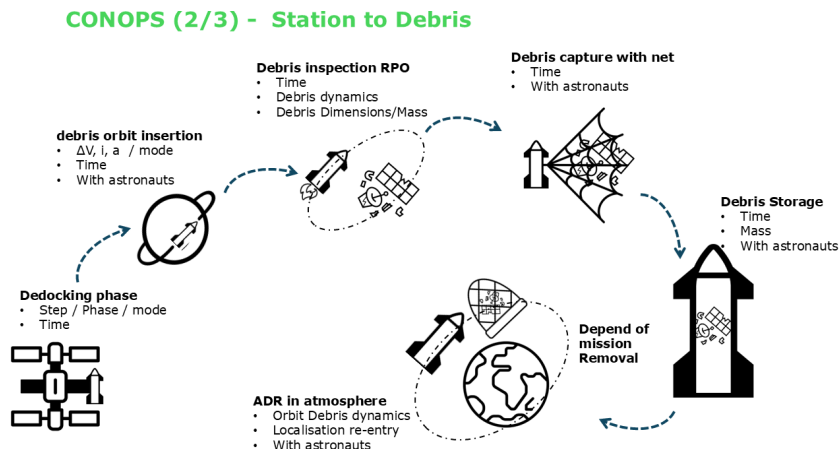


Figure 3: ConOps phase 2

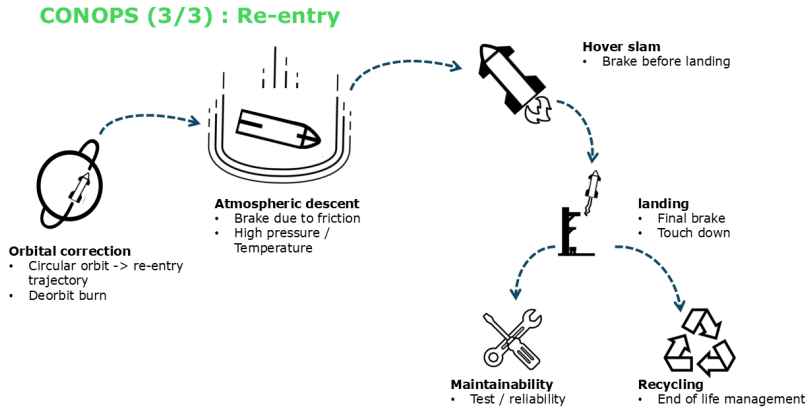


Figure 4: ConOps phase 3

Phases/Modes notes

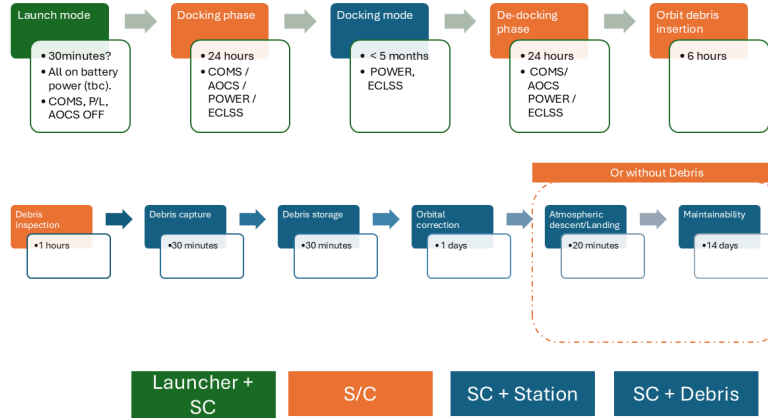


Figure 5: ConOps phases/modes

The mission begins with the launch of the spacecraft carrying astronauts and cargo with a third of its propellant on board. During the atmospheric flight phase, the spacecraft handles aerodynamic, gravitational, and vibrational loads. Post-separation from the launcher, it performs orbital maneuvers to reach the space station's orbit at 500 km altitude and 50 degrees inclination. Upon docking, the cargo and astronauts are delivered to the station.

After undocking, and following the station operations, the spacecraft transitions to debris recovery mission, with astronauts on-board. It inspects the debris to determine its dynamics and dimensions, captures it using a net, and stores it within the spacecraft. The spacecraft manages the disposal of the debris and prepares for its atmospheric re-entry. At an altitude of 200 km, the debris is released from the spacecraft. In the event of a maintenance problem on the space shuttle, the astronauts are certified by TAstrain to carry out an EVA.

The spacecraft then initiates its own re-entry process, performing orbital corrections and descending through the atmosphere while experiencing high pressure and temperature conditions. The re-entry sequence includes a hover slam to brake before landing, culminating in a vertical touchdown. Post-landing, the spacecraft undergoes maintenance and reliability checks, followed by end-of-life management and recycling procedures.

Throughout the mission, various phases and modes are meticulously planned, with specific durations allocated for each step, ensuring coordination between the launcher, spacecraft, station, and debris handling operations.

Debris Analysis

The accumulation of space debris in Earth's orbit poses significant risks to operational satellites and spacecraft, threatening the sustainability of space activities. As the number of objects in orbit continues to grow, the likelihood of collisions increases, potentially leading to catastrophic events that could render entire orbital regions unusable. Retrieving space debris is not only an environmental responsibility but also a strategic necessity to ensure the safety and longevity of space operations.

ID : NO-RAD	Altitude (km)	Inclination (°)	Mass	RCS	Country	Size
25912	957	51.96	1,210 kg wet, 820 kg dry	8.460 m ²	Russia	Large
8352	1095	46.99	105 kg wet, 105 kg dry	2.243 m ²	Japan	Medium
44784	896	45.01	1,000 kg wet, 1,000 kg dry	9.057 m ²	China	Large

Table 3: Characteristics of the selected debris.

We have chosen debris 44784 to dimension our mission as it is situated at a relatively high altitude of 896 km and, more importantly, has an inclination of 45°. This inclination is critical for dimensioning our spacecraft in terms of propellant requirements. Additionally, this debris is categorized as LARGE on satcat.com website, with a Radar Cross Section (RCS) of 9 m², which is essential for dimensioning our cargo hold. The spatial environment analysis of the debris around the spacecraft is detailed in Figure 6. The selection of this particular debris dimensions our spacecraft in such a way that it enables the retrieval of other debris in the vicinity of the station.

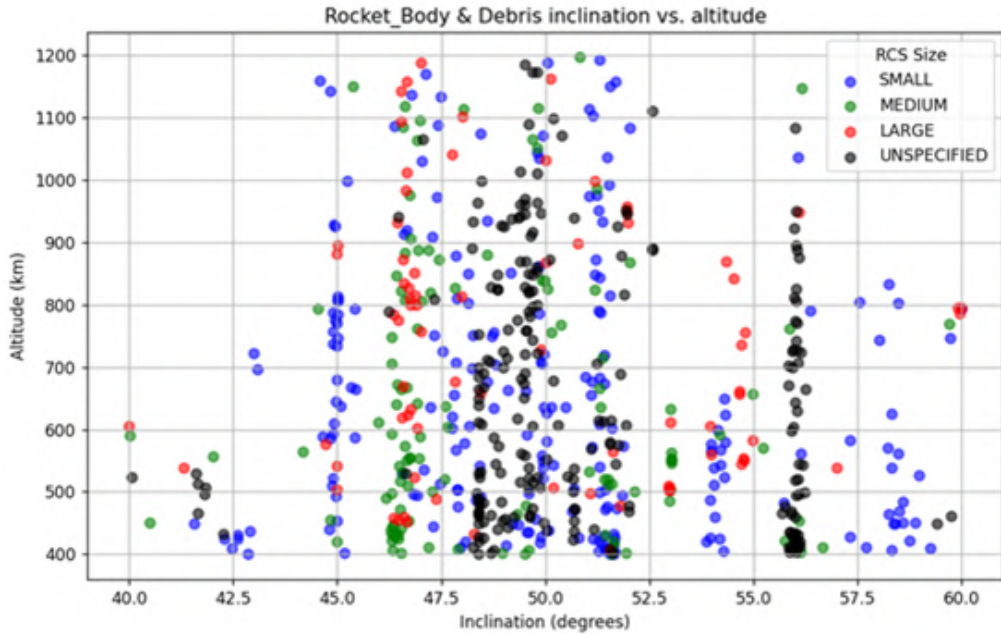


Figure 6: Debris Inclinaison vs. altitude

Legal Framework for Space Operations

Our company, based in France and operating from France, launches its shuttle from a French launch pad and through a European company (assumed). We are therefore subject to the LOS, the Law on Space Operations. In this context, we must submit mastery forms to the authorities according to the elaborated space activities. According to Law No. 2008-518 of June 3, 2008, relating to space operations, we must provide the following documents:

- **Mastery Authorization for Post-Separation Phase:** Authorization for the phase after separation with the launcher until docking.
- **Mastery Authorization for Station Contact:** Authorization for contact with the space station.
- **Mastery Authorization for Debris Capture:** Authorization for debris capture. In this specific case, a contract between the country owning the debris and our company is required. According to the mission analysis, several debris have been selected as potential candidates, whose nationality is Chinese, Russian, or Japanese. The current context would favor an exchange with Japan, as our relations between space agencies are very active. Another attempt would be to propose a collaboration with the Chinese to open a large-scale project in space between our countries, knowing that China is growing in this field.
- **Return Authorization:** Our shuttle, which must land, will need to complete a return authorization.

Several other contracts need to be added: a launch contract, a station contract, and a landing site contract. Finally, our space vehicle must be registered with the French space agency, which will transfer its registration certificate to the UN (United Nations).

A request for the use of the necessary frequency bands must be submitted to the ITU (International Telecommunication Union).

3.2.2 Propulsion choice and first orbit iteration

In the preliminary phase of mission analysis, we defined the two key orbits for our system insertion in space: a circular parking orbit for the station at 500 km altitude and 50° inclination, and a lower release orbit for the shuttle at 200 km altitude and 50° inclination.

To estimate the propulsion requirements, we used classical orbital mechanics models. In particular, we relied on Hohmann transfer approximations to compute the ΔV needed for altitude changes between circular orbits. For inclination changes, we used the formula derived from the vector difference of orbital velocities, assuming maneuvers are performed at the ascending or descending node for optimal efficiency. For a Hohmann transfer between two circular orbits of radii r_1 and r_2 , the total required ΔV is the sum of the two impulses at perigee and apogee:

$$\Delta V_{\text{total}} = \Delta V_1 + \Delta V_2 = \sqrt{\frac{\mu}{r_1}} \left(\sqrt{\frac{2r_2}{r_1 + r_2}} - 1 \right) + \sqrt{\frac{\mu}{r_2}} \left(1 - \sqrt{\frac{2r_1}{r_1 + r_2}} \right) \quad (1)$$

where μ is Earth's gravitational parameter ($\mu = 3.986 \times 10^{14} \text{ m}^3/\text{s}^2$). Inclination changes were estimated using the expression:

$$\Delta V_{\text{inc}} = 2V \sin \left(\frac{\Delta i}{2} \right) \quad (2)$$

where V is the orbital velocity at the node and Δi is the inclination difference. To compute the needed mass of propellant we use the Tsiolkovsky rocket equation,

$$\Delta V = I_{sp} \cdot g_0 \cdot \ln \left(\frac{m_0}{m_f} \right) \quad (3)$$

This method provides an estimation of the required ΔV and Δm , suitable for preliminary design and trade-off analyses.

We selected a "green hydrazine" chemical propulsion system with a specific impulse $I_{sp} = 300 \text{ s}$. This choice stems from multiple constraints:

- Cryogenic options were excluded due to the mission's 6-month docked duration, which renders long-term cryo storage unfeasible.
- Hydrazine, despite its flight heritage, was rejected due to its toxicity and current trends in favor of green propellants.
- Nuclear and hybrid propulsion systems were also dismissed due to high mass, radiation hazards, and in-orbit refueling complexity.

We ultimately selected NOFBX (Nitrous Oxide Fuel Blend), a green monopropellant with an ISP of 300 s, making it a viable alternative to hydrazine for small-scale orbital maneuvers. On the following graph, the required propellant mass for station orbit insertion is plotted as a function of the total shuttle mass.

Characteristic	Type of propu	mean ISP
Cryogenics	LH2+LOX (Shuttle USA)	400
	Kero+LOX	325
corrosif, possible RCS with monoprop hydrazine (Shuttle USA)	(N2O4/MMH/UDMH) (shuttle USA)	300
Simple	Hybride (Solid+LOX)	320
Radiations, mass	Nuclear - thermal	900
green hypergoliques ergols	Green propellants (HAN/ADN + Perchlorate)	275
Hypergolic	NOFBX	310
Storable, simple, Liquid + Liquid	H ₂ O ₂ + Hydrocarbon Fuel	310
Hypergolique	MOFBX	320

Figure 7: Propellant characteristics

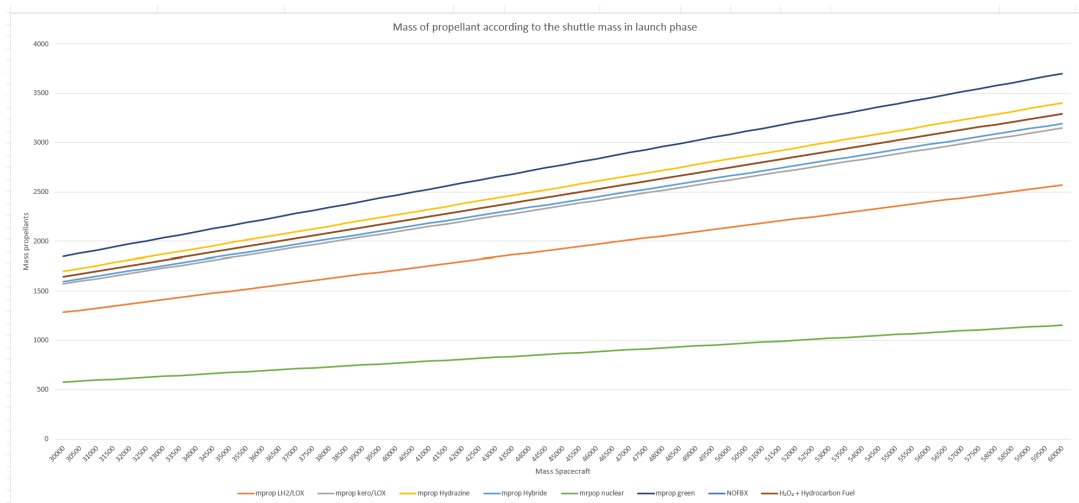


Figure 8: Propellant mass for insertion depending on propellant choice

Given the shuttle's multi-purpose role, we allocate up to 40% of its total mass to the propulsion subsystem (propellant + engines). With this constraint, we assess which orbital maneuvers are feasible. We compute the fuel mass Δm required for various mission scenarios, ranging from altitude changes to inclination maneuvers.

Based on the results we observe that:

- Altitude changes are affordable in terms of fuel mass.
- Inclination changes are prohibitively expensive. A change of more than 10° consumes a large fraction of the total propellant capacity.

We therefore constrain our operational domain to the following:

- Maximum altitude: 1200 km
- Maximum inclination change: $\Delta i \leq 10^\circ$

A debris object was selected as our reference target to size the shuttle, accounting for worst-case ΔV scenarios. The choice of this debris is study in the previous part.

3.2.3 Refined orbit iteration

Following the preliminary estimation and the propulsion system selection, we refined our mission analysis using simulations in GMAT. The objective was to validate the feasibility of the trajectory and fuel consumption through a complete mission scenario targeting a representative debris object.

For this analysis, we selected the "ideal" debris located at approximately 900 km altitude with a 45° inclination. Starting from the initial orbit of the shuttle (200 km altitude, 50° inclination), the maneuver plan involved:

- A Hohmann transfer to reach the 500 km circular orbit of the station.
- A plane change maneuver to match the debris inclination at the ascending node.
- A second Hohmann transfer to raise the apogee to 900 km.
- A final Hohmann transfer phase to 200 km for deorbit maneuver.

The maneuver sequence was implemented in GMAT using a series of finite burns. The following figures summarize the simulation results:

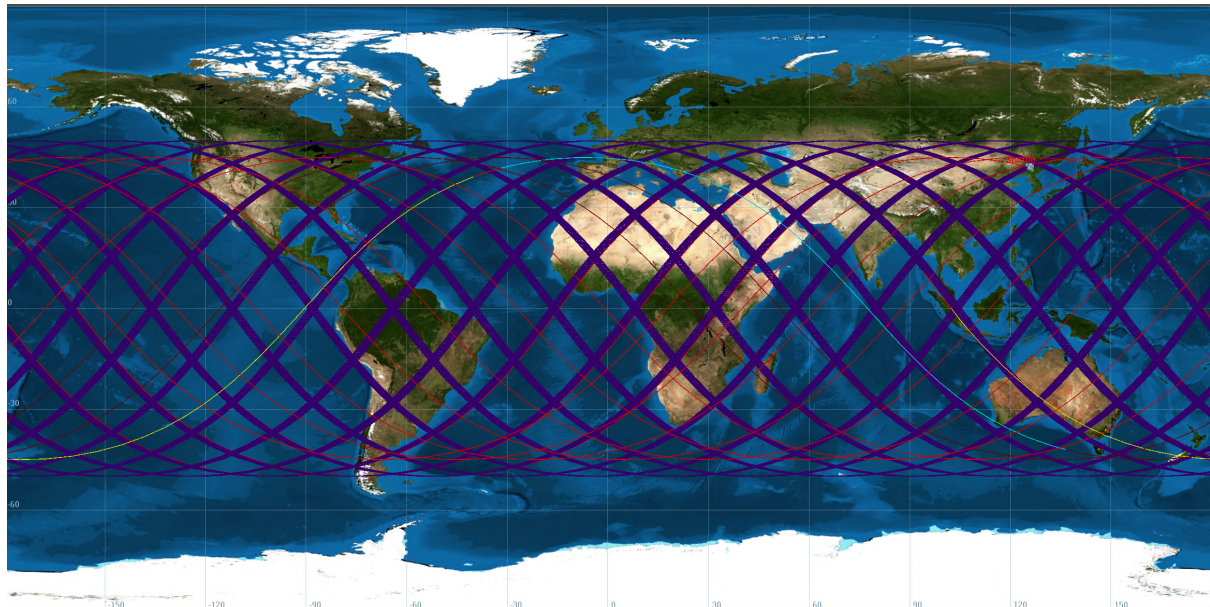


Figure 9: Trajectory representation

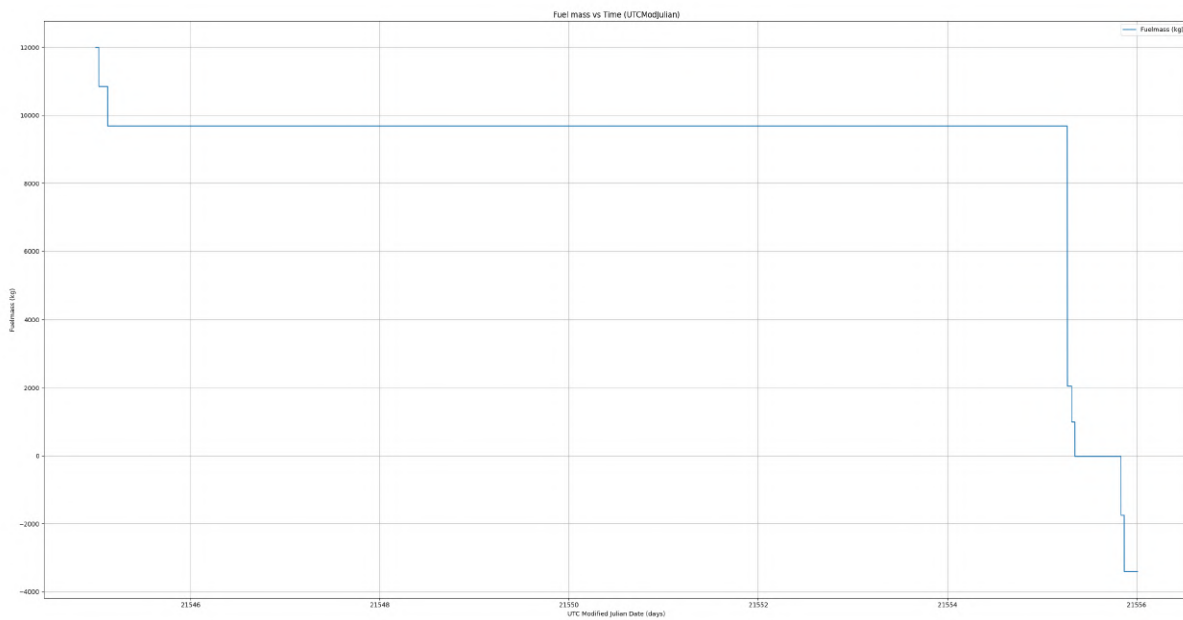


Figure 10: Remaining fuel mass

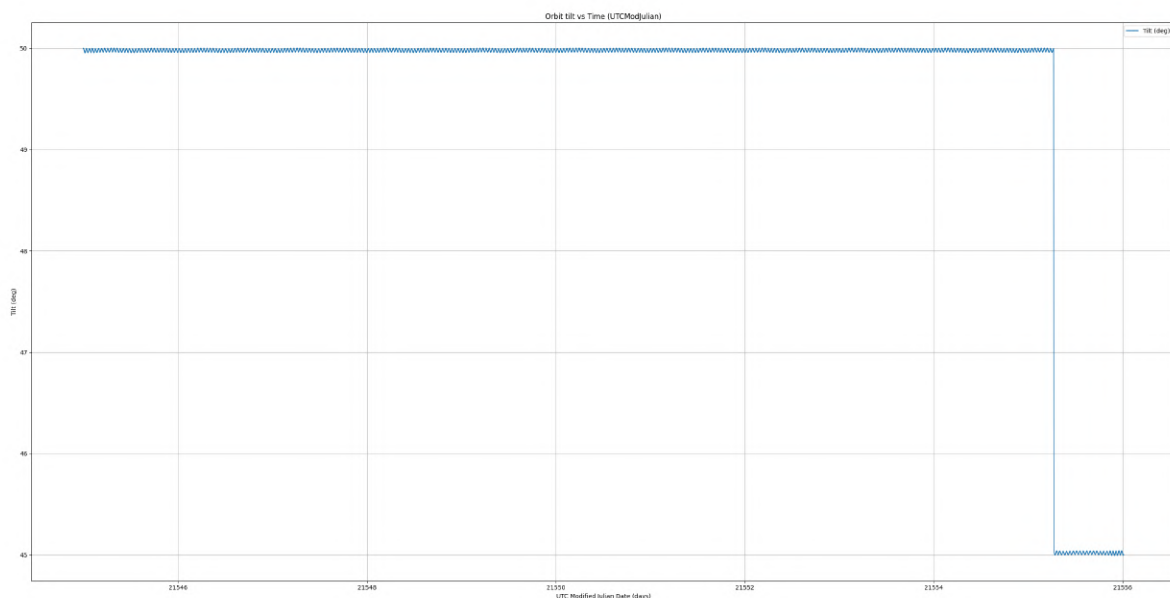


Figure 11: Inclination (tilt) evolution

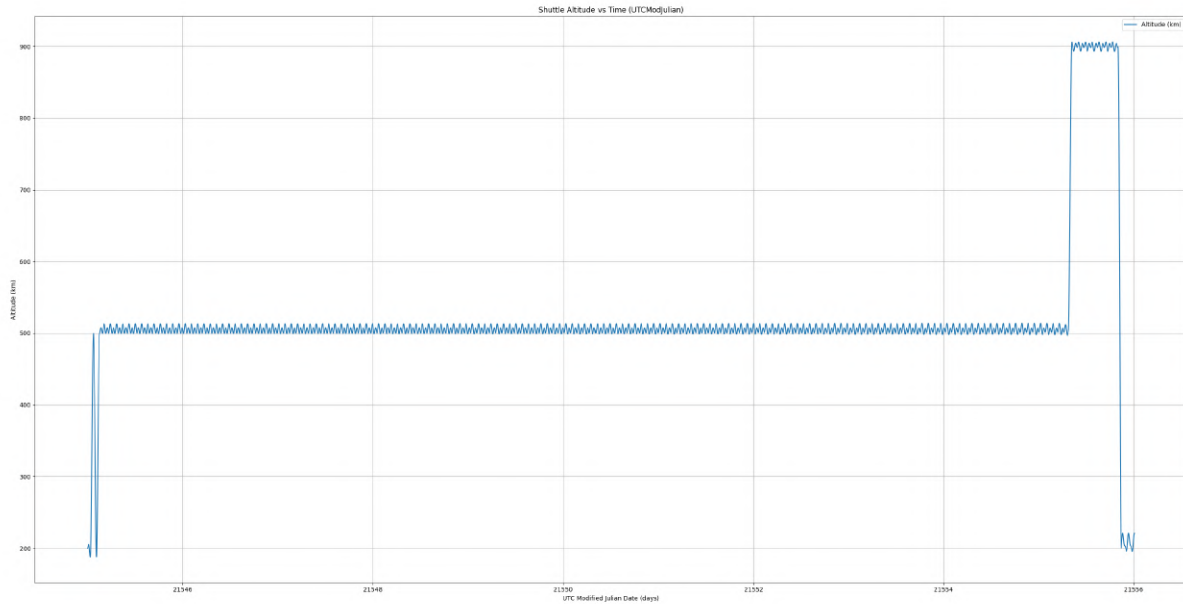


Figure 12: Altitude evolution

These results validate the overall feasibility of the debris rendezvous mission, but they also show an operational constraint. The shuttle requires a complete refueling at the station to accomplish the full mission profile. The propellant mass drops close to zero at the end of the debris retrieval sequence, even after a full refuel of up to 12 tonnes during docking. This highlights the demanding nature of the trajectory, especially the inclination change and high-altitude transfer, both of which are propellant-intensive. While the maneuver sequence remains compatible with the NOFBX system and propulsion parameters, the mission would not be achievable without the intermediate refueling capability provided by the station.

3.2.4 Reentry Trajectory

Table 4: Preliminary Reentry Estimation with Psimu

Parameter	Value
Reentry altitude	200 km
Reentry date	21/04/2025 11:50:00
Initial velocity	7.8 km/s
Vehicle shape	Cylindrical
Diameter	5 m
Height	15 m
Drag coefficient (C_D)	1.2
Lift coefficient (C_L)	0.3
Initial mass (wet)	28000 kg
Available propellant	2000 kg
Available thrust	690000 N
Specific impulse (I_{sp})	300 s
Atmospheric model	US76
Maneuver ΔV	220 m/s
Maneuver duration	10 s
Maneuver start time	$t = 5$ s
Numerical integrator	Prince-Dormand
Stop condition	Altitude = 0 km

Obtained results:

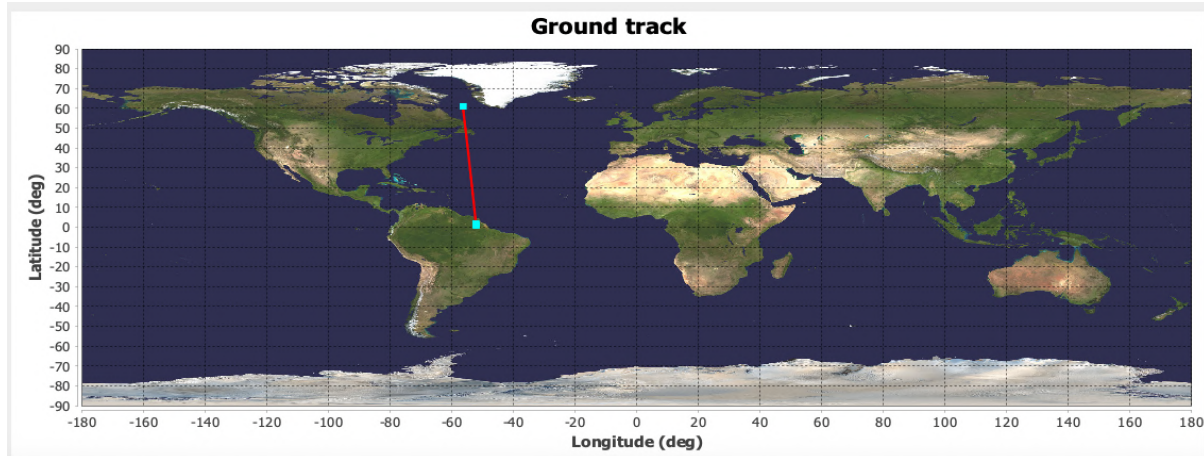


Figure 13: Psimu Reentry Ground track

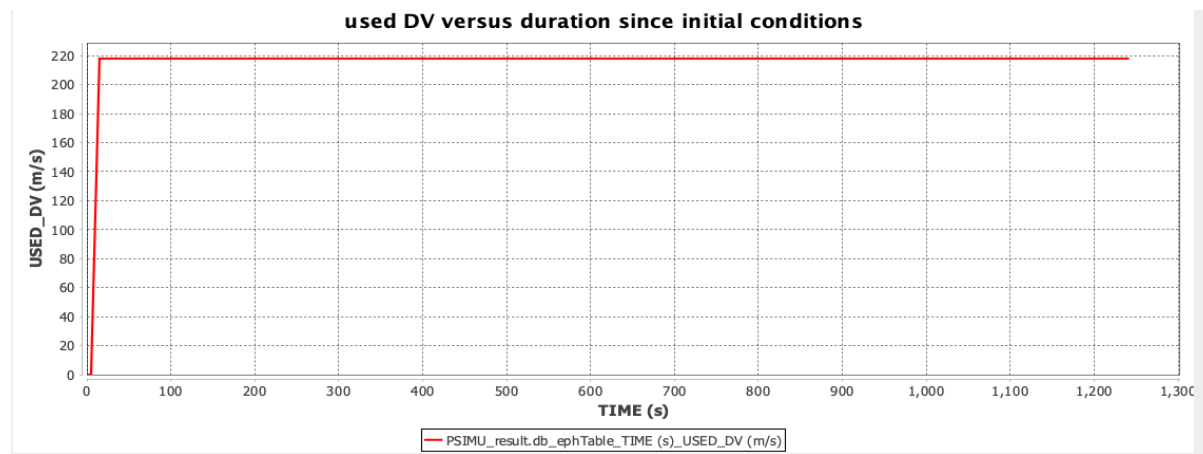


Figure 14: Psimu Reentry Used DeltaV Plot

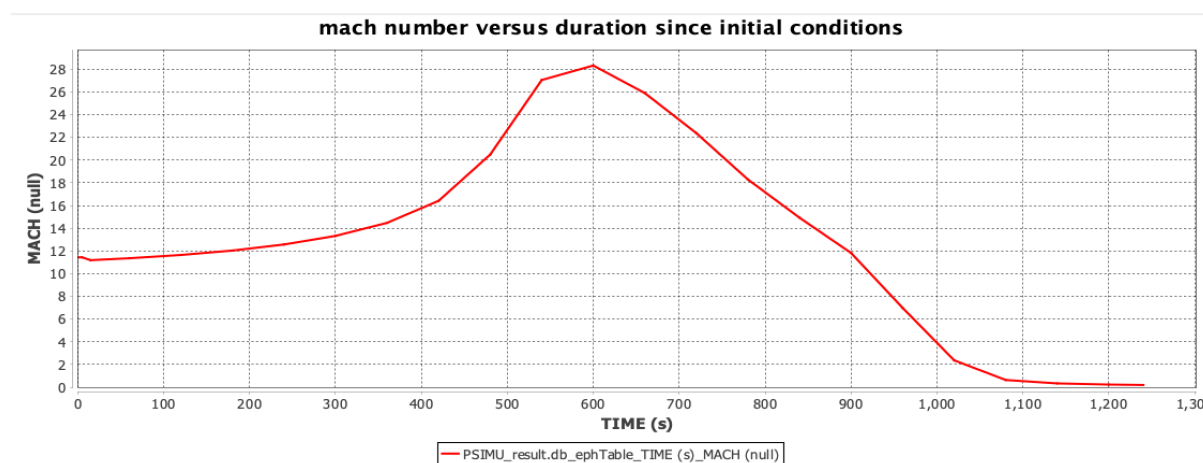


Figure 15: Psimu Reentry Mach vs Time Plot

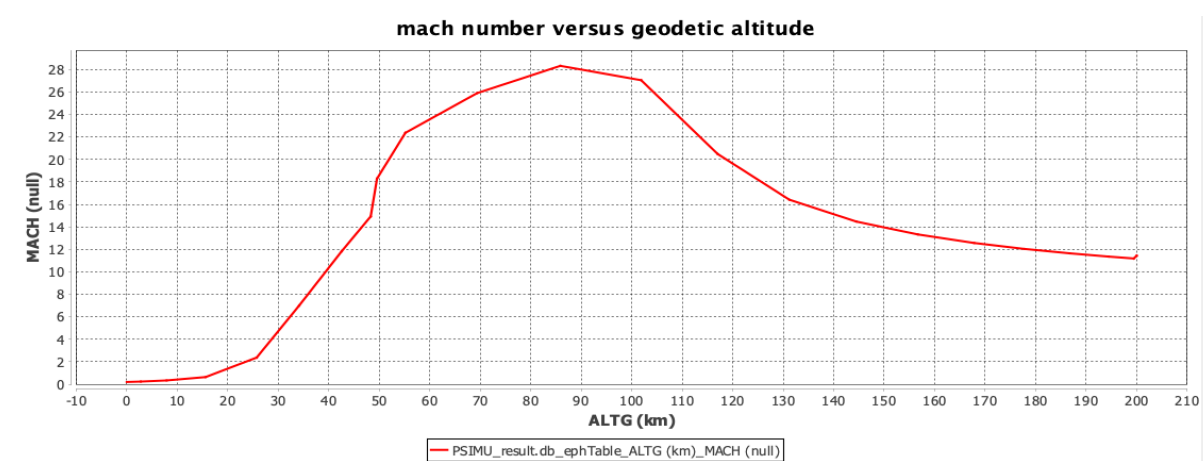


Figure 16: Psimu Reentry Mach vs Altitude Plot

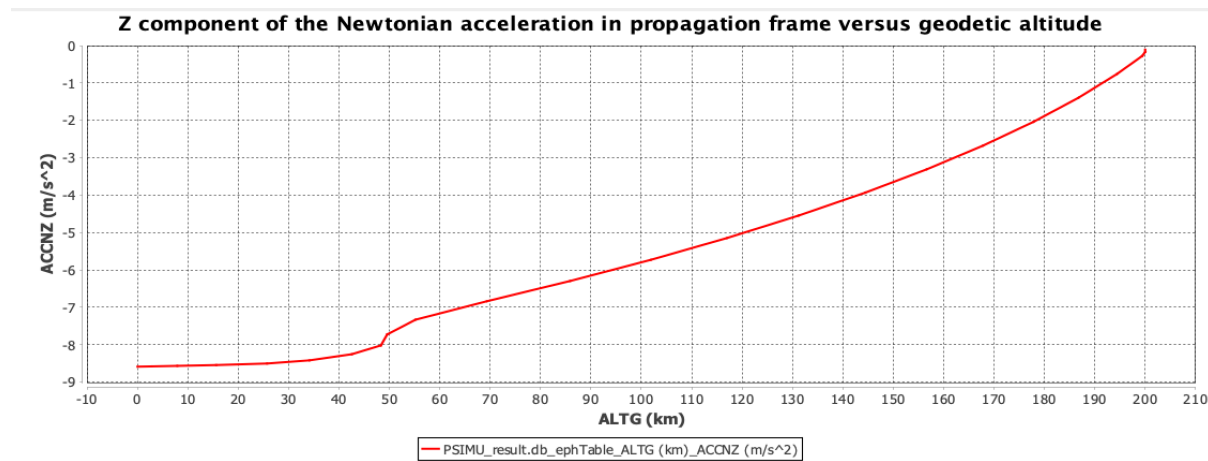


Figure 17: Psimu Reentry Acceleration vs Altitude Plot

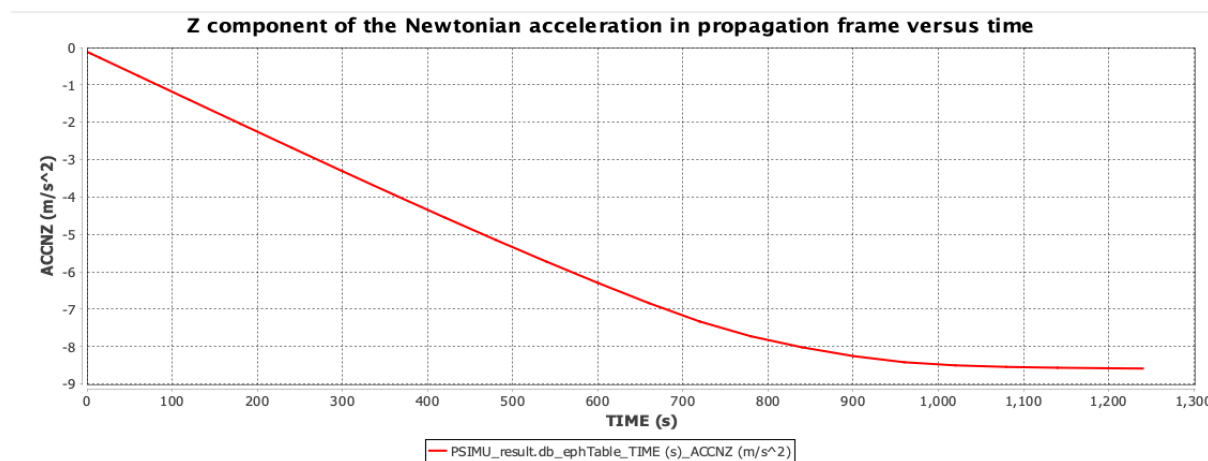


Figure 18: Psimu Reentry Acceleration vs Time Plot

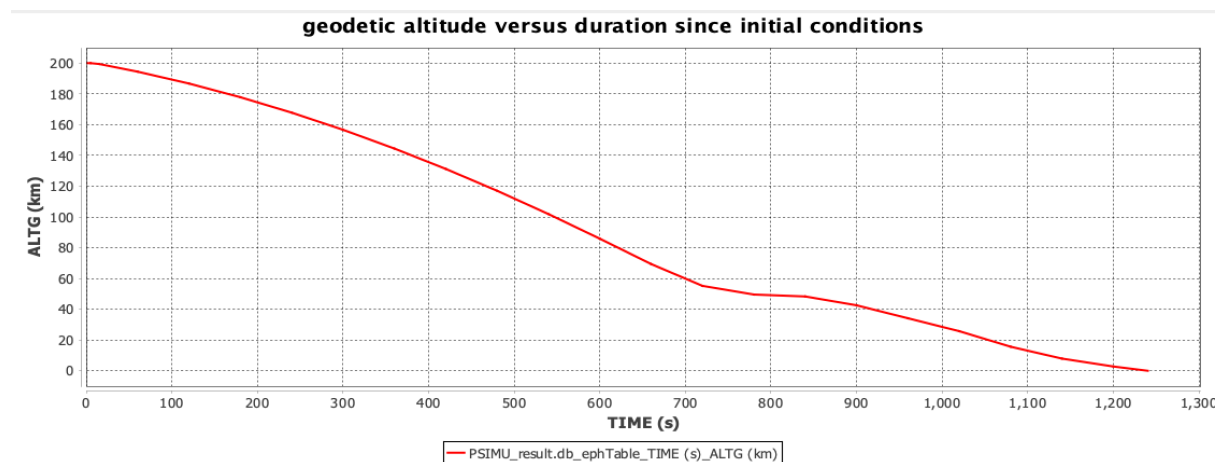


Figure 19: Psimu Reentry Altitude vs Time Plot

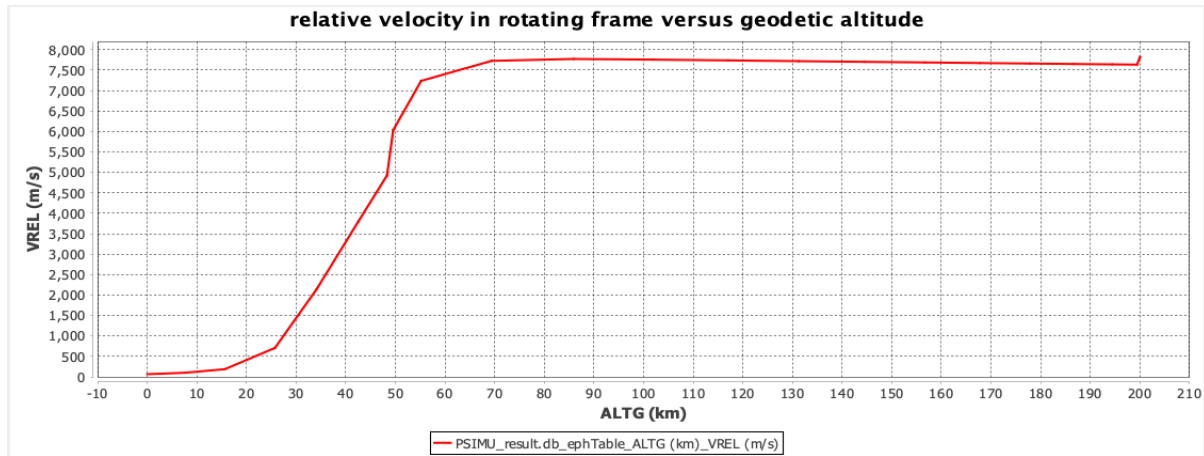


Figure 20: Psimu Reentry Velocity vs Altitude Plot

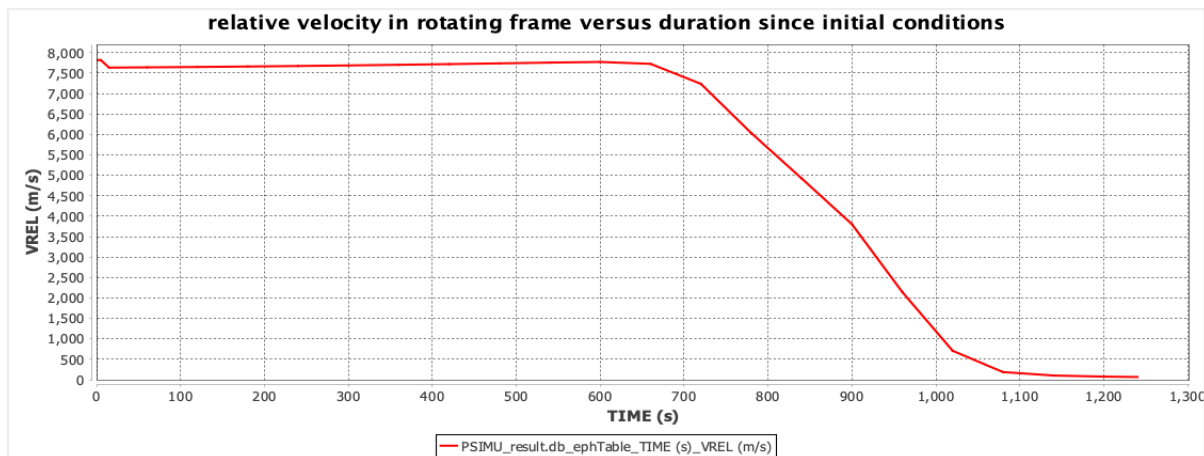


Figure 21: Psimu Reentry Velocity vs Time Plot

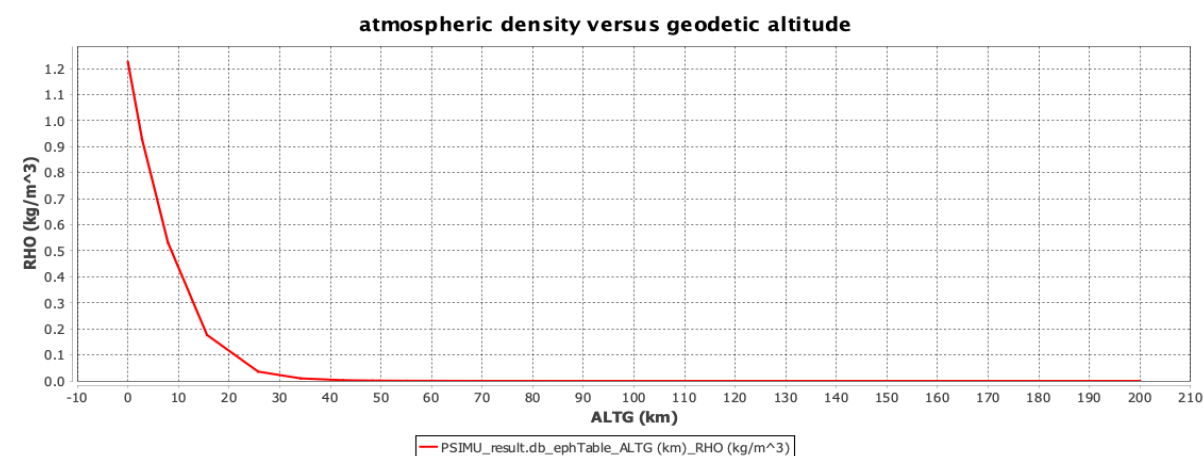


Figure 22: Psimu Atmospheric Density Model US76

We note that, for the selected maneuver parameters, the totality of the remaining propellant onboard (2 tons) is consumed during the burn. In comparison, increasing the available propellant to 3 tons under the same conditions results in a remaining fuel mass

of approximately 650 kg. This confirms that the margin is extremely tight and would require a smaller of possible debris.

The resulting reentry trajectory computed with Psimu is purely ballistic, i.e., it does not include any active control or lift modulation during atmospheric flight. While this approach is not suitable for crewed missions due to the extreme deceleration and thermal loads involved, it provides a valuable first-order estimation of the energy and fuel requirements for atmospheric entry.

3.2.5 Reentry trajectory with Python

This part presents the simulation of a more probable spacecraft's atmospheric reentry, starting from a near-orbital altitude and velocity. A smooth transition from hypersonic reentry to subsonic controlled descent (bellyflop maneuver) is implemented, mimicking vehicles like SpaceX's Starship Neumann and Sippel [2022]. The reentry is initiated at:

Parameter	Value
Initial altitude h_0	100 km
Initial velocity v_0	7419 m/s
Flight path angle γ_0	-1°
Mass m	30,000 kg
Reference area S_{ref}	15 m ² → 22 m ² (during descent)
Drag coefficient C_d	1.2 → 2.5 (during descent)

Table 5: Initial Conditions and Aerodynamic Properties for Reentry

The atmospheric density is modeled using the US Standard Atmosphere 1976 (NOAA and U.S. Air Force [1976]), with stratified temperature and pressure models. The air density $\rho(h)$ is calculated as:

$$\rho = \frac{P}{RT} \quad (4)$$

with pressure P and temperature T derived from altitude-dependent lapse rates. The model includes the troposphere, stratosphere, and lower mesosphere.

The vehicle is subjected to aerodynamic drag and gravitational forces. Assuming 1D motion with flight path angle γ , the drag force is:

$$D = \frac{1}{2}\rho v^2 S_{ref} C_d \quad (5)$$

The total vertical acceleration is:

$$a = \frac{F_{net}}{m} = \frac{T + D - mg}{m} \quad (6)$$

where T is thrust (zero except near landing), and g is gravity at sea level (9.80665 m/s²). The velocity and altitude are updated at each time step Δt as:

$$v_{i+1} = v_i - a \cdot \Delta t \quad (7)$$

$$h_{i+1} = h_i - v_i \sin(\gamma) \cdot \Delta t \quad (8)$$

The stagnation point heat flux is computed using the Chapman equation (Chapman [1958]):

$$\dot{q} = 2.0254 \times 10^8 \sqrt{\frac{\rho}{\rho_{ref}} \frac{R_{ref}}{R_n}} \left(\frac{v}{v_{ref}} \right)^{3.05} \quad (9)$$

with $\rho_{ref} = 1.225 \text{ kg/m}^3$, $v_{ref} = 10,000 \text{ m/s}$, and $R_n = 2 \text{ m}$ the nose radius. This model assumes convective heating dominates.

To simulate a controlled deceleration and increase drag, a smooth transition is applied when velocity drops below 340 m/s. The transition spans a chosen duration (e.g., 100 seconds), during which:

- The flight path angle γ goes from -1° to -90°
- C_d increases from C_{d0} to $C_{d_{max}}$
- S_{ref} increases accordingly

The smooth transition is implemented using a sigmoid function:

$$s(t) = \frac{1}{1 + \exp(-k(t - 0.5))} \quad (10)$$

where k controls the steepness of the curve. This avoids sudden jumps in dynamics. At 200 m altitude, if velocity is still non-zero, a terminal thrust is applied:

$$T = 2mg \quad (11)$$

Despite the parameter sweep and the use of established models, we were unable to converge toward a satisfactory reentry trajectory. The domain of atmospheric reentry is highly sensitive and nonlinear, involving coupled effects from aerodynamics, propulsion, and atmospheric density. Our simplified model, while capturing the main dynamics (ballistic flight, deceleration, heating profile), failed to produce a trajectory that both ensures vehicle survivability and satisfies realistic entry constraints (acceptable heat load, structural stress, and G-load limits).

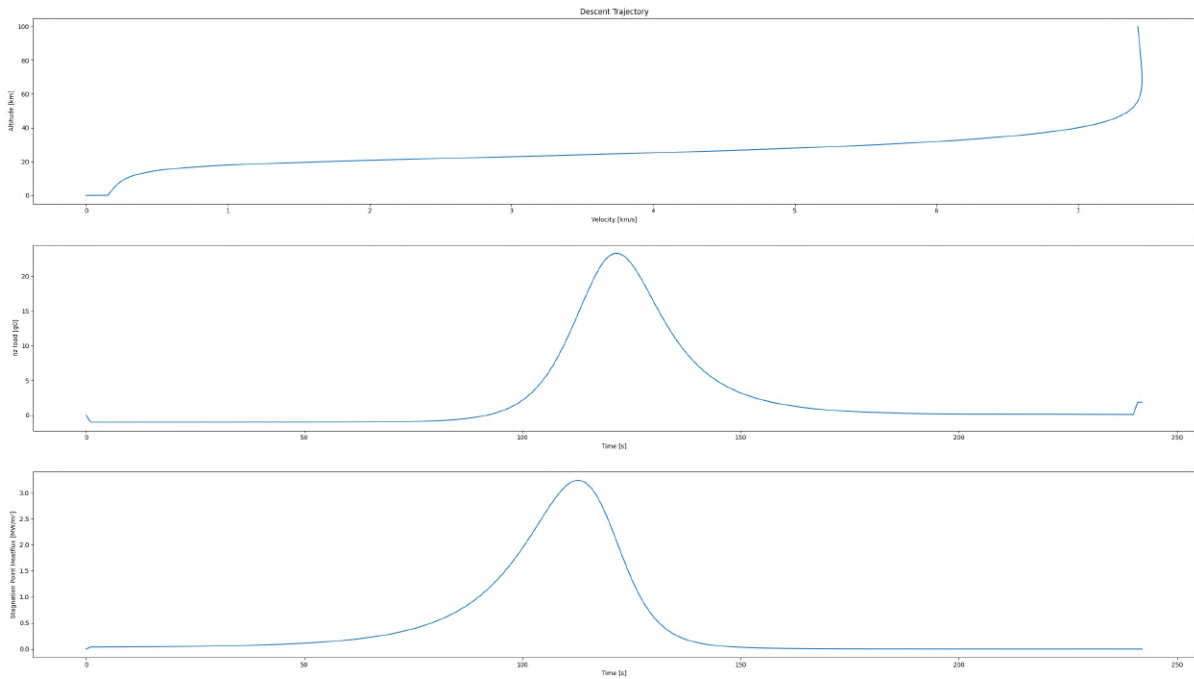


Figure 23: Atmospheric Re-entry

3.3 Environment

Space missions operating in LEO face a complex and dynamic environment that affects both spacecraft performance and astronaut safety. Exposure to radiation, micrometeoroids, plasma interactions, atomic oxygen, and contamination can degrade materials, disrupt electronic systems, and impact overall mission success. Understanding these environmental factors is essential for designing a reliable and resilient system.

This study assesses the space environment across multiple orbital regimes, including the orbit of the ASTROIKOS space station and three representative debris orbits. These trajectories were selected to capture variations in radiation exposure, debris density, plasma conditions, and atomic oxygen concentration. The goal is to quantify potential risks and evaluate their impact on mission longevity, subsystems, and astronaut safety.

Orbit	Altitude [km]	Inclination [°]
Station	500	50
Debris 1	25912	51.96
Debris 2	8352	46.99
Debris 3	44784	45.01

Table 6: Different orbits of the environment study

By modeling the environment using tools such as OMERE, we will analyze key factors. The results will guide design decisions, operational strategies, and mitigation measures to enhance mission reliability.

We present with the graph below the anomalies causes and their importance.

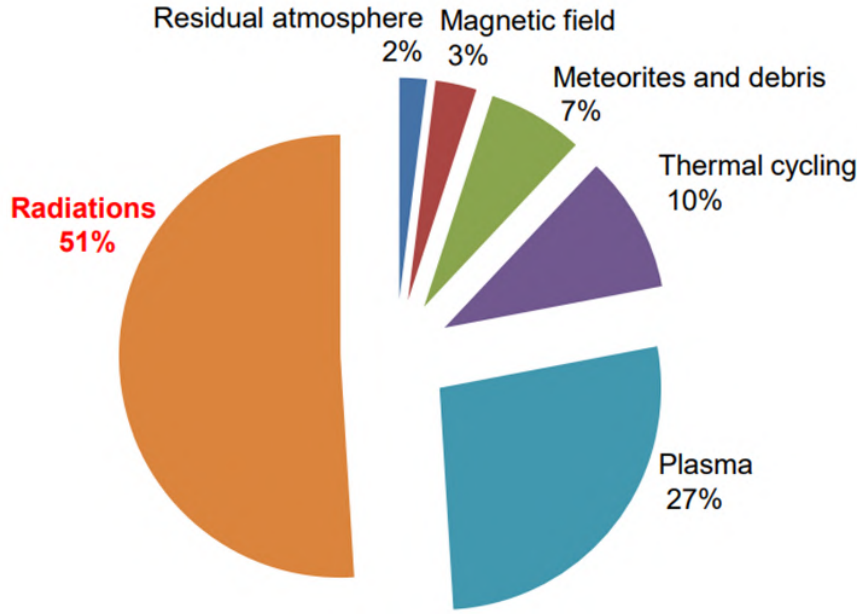


Figure 24: Anomalies environment causes

3.3.1 Environmental Modeling

3.3.1.1 Charged Particle Flux

We know that the main cause of the anomalies comes from radiations that can be regrouped in three distinct categories.

Trapped Particles

Trapped particles refer to charged particles, primarily electrons and protons, that are confined by Earth's magnetic field within the Van Allen radiation belts. These particles originate from solar wind and cosmic rays and are concentrated in specific regions, such as the inner and outer radiation belts. Their flux and energy distribution vary with altitude and geomagnetic conditions.

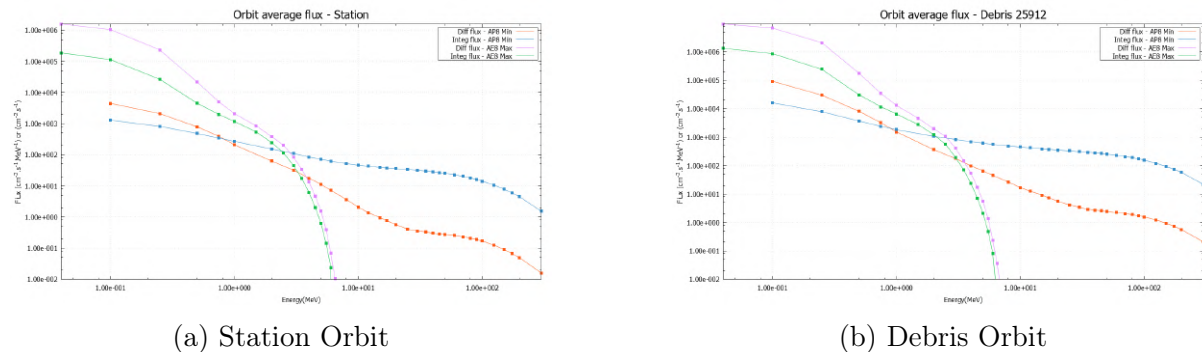


Figure 25: Orbit Average Flux

Comparing the two orbits, the debris orbit is more exposed to these trapped particles, leading to a higher radiation environment than the station.

Solar Particles

Solar particles, mainly composed of protons and heavy ions, originate from solar flares and coronal mass ejections. Their flux varies with solar activity and follows an energy-dependent distribution.

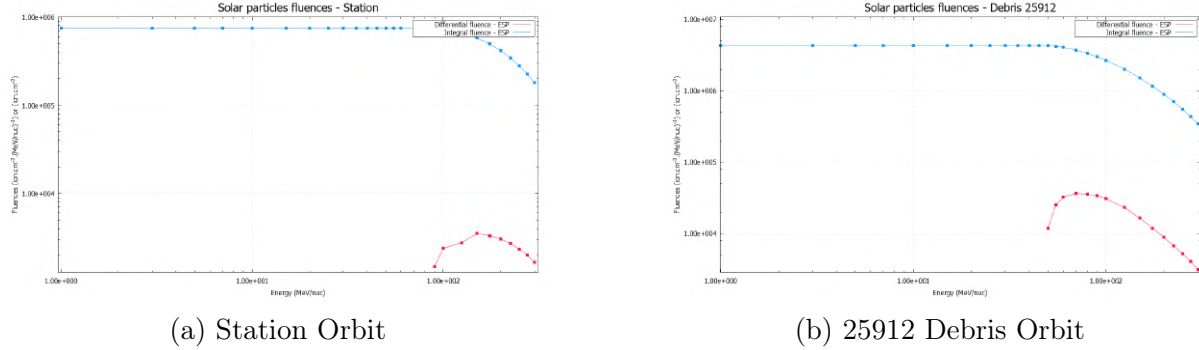


Figure 26: Solar Particle Fluences

When we compare the two graphs, the differential fluence is significantly higher debris than for the station, indicating greater exposure. However, a distinct peak is noticeable at higher energies, which can be attributed to specific solar events. These peaks indicate transient solar particle events, where a sudden influx of high-energy particles temporarily enhances the overall radiation environment. Such events must be accounted for in space mission planning.

Cosmic Rays

Galactic cosmic rays (GCRs) are high-energy charged particles originating from outside the solar system. Their flux is primarily modulated by solar activity, with lower intensities observed during periods of high solar activity due to the increased solar wind and magnetic shielding. The modeling of cosmic rays requires considering their interaction with Earth's magnetosphere and atmosphere, which influences their penetration depth and energy distribution.

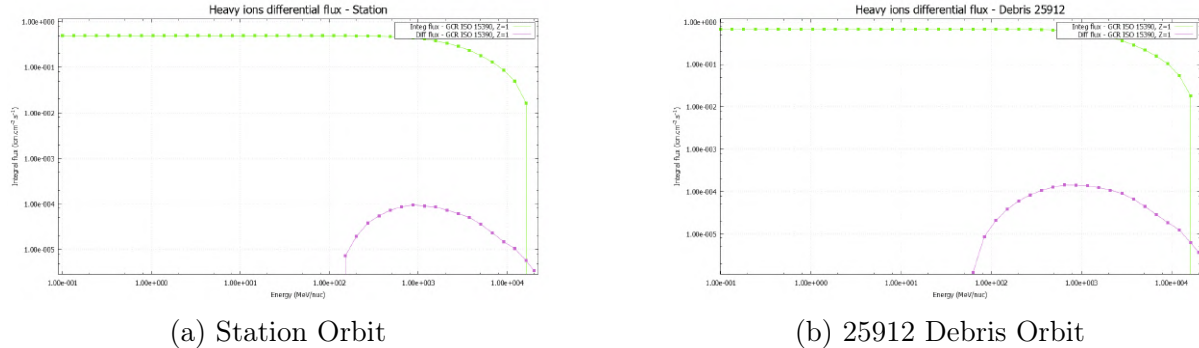


Figure 27: Heavy Ions Fluxes

We observe that the integral flux remains relatively constant at lower energy levels before gradually declining. There is no variation in flux between the station and the debris orbits.

3.3.1.2 Plasma Environment

Plasma is the second source of anomalies for spacecraft. In fact, in LEO spacecraft are

exposed to a complex plasma environment primarily composed of charged particles from the Earth's ionosphere and magnetosphere, as well as solar wind interactions. Containing high-energy protons and electrons, and free electrons and ions (O^+ , H^+ , He^+), these charged particles will interact in different ways with the spacecraft and could damage it. The shuttle will be exposed to various plasma conditions depending on its altitude and mission profile.

3.3.1.3 Micrometeoroids and Debris

Representing 7% of the anomalies causes on a space system, we shouldn't omit them since they are hard to predict and can have various consequence from benign to malignant. These objects, ranging from millimeter-sized fragments to large defunct satellites, travel at extremely high velocities (up to 15 km/s), making them a critical threat to space missions.

In fact, the number of debris keeps increasing over time, increasing the probability of impact, notably in Low Earth Orbit, where the density of debris is the highest due to past missions, Kessler syndrome and satellite's end of life.

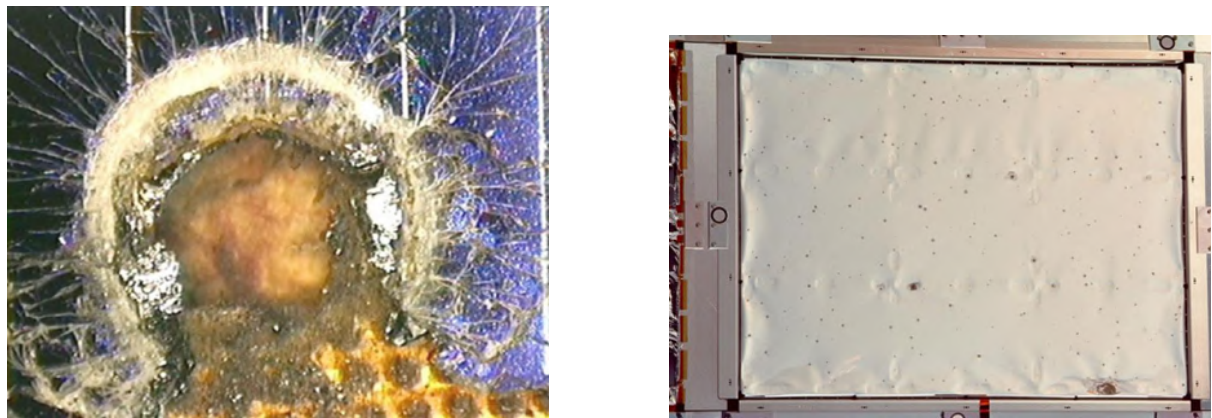


Figure 28: Meteoroids impacts in LEO over 5,7 years (LDEF mission)

3.3.1.4 Atomic Oxygen

Atomic oxygen (ATOX) is the dominant species in the Low Earth Orbit environment, formed by the dissociation of molecular oxygen due to solar UV radiation.

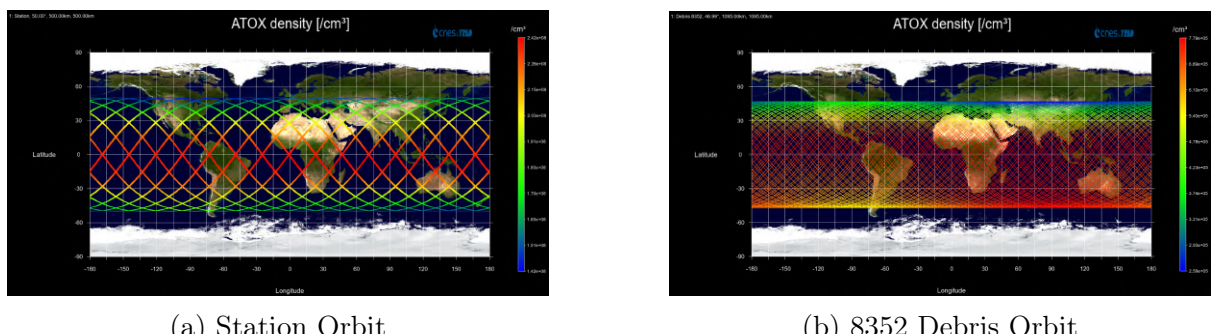


Figure 29: O^+ density on Station & Debris orbits

ATOX density is highly dependent on altitude, solar activity, and geographic location. At low altitudes, such as those corresponding to the station-like orbit (first image), atomic

oxygen concentration is most prominent between 200 and 600 km, with peak densities of $2.4 \times 10^8 \text{ cm}^{-3}$ occurring in equatorial and mid-latitude regions. The second image, corresponding to the debris orbit, exhibits a similar latitudinal distribution but with slight variations in density due to altitude differences. These variations in atomic oxygen exposure must be considered.

3.3.1.5 Electromagnetic Radiation

Electromagnetic radiation in space, particularly in the ultraviolet (UV) and X-ray ranges, originates mainly from the Sun and magnetic field. UV radiation spans wavelengths from approximately 10 nm to 400 nm, with solar extreme ultraviolet (EUV) emissions around 10–121 nm being highly variable due to solar activity. X-rays, with wavelengths shorter than 10 nm, are primarily emitted during solar flares, with intensities varying by several orders of magnitude during peak events.

For reference, the solar UV flux in the EUV range can reach around 0.1 W/m^2 , while solar X-ray emissions, particularly during strong flares, can peak at intensities of 10^{-3} to 10^{-2} W/m^2 in the 0.1–0.8 nm band.

3.3.2 Effects on the Mission and Subsystems

3.3.2.1 Radiation Effects

Total Ionizing Dose (TID)

The Total Ionizing Dose is a critical factor in assessing radiation effects on astronauts and onboard systems. It represents the accumulated energy deposited by ionizing radiation over time, leading to the progressive degradation of materials and biological tissues.

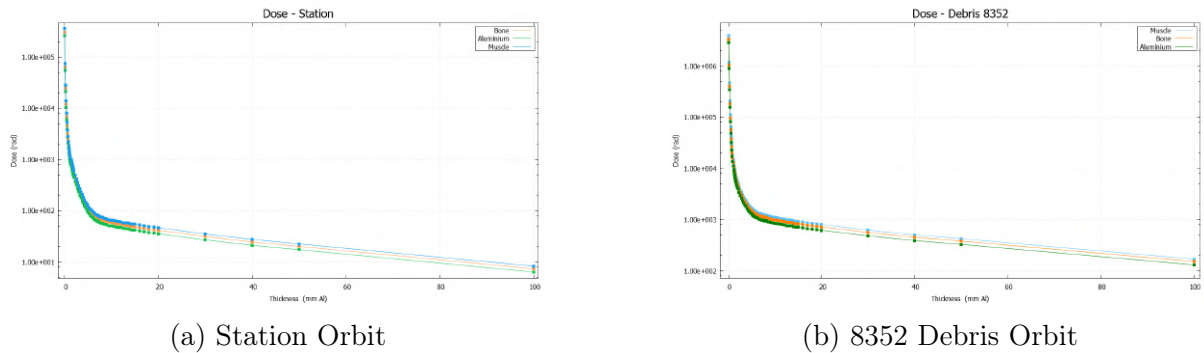


Figure 30: Dose in function of the thickness on Station & Debris orbits

The graphs above illustrate the dose-depth curves for different materials (muscle, bone, and aluminum) in two distinct orbital environments. In both cases, the radiation dose decreases exponentially as shielding thickness (expressed in mm of aluminum equivalent) increases.

At low shielding thicknesses (<10 mm Al), the radiation dose is significantly higher, with values exceeding 10^3 rad(Si) , indicating that unshielded electronic components or human tissue would experience substantial radiation exposure. As shielding increases, the dose

follows an exponential decay, converging to values close to 101-102 rad(Si) at 100 mm Al.

The overall dose levels in the Debris (8352) orbit appear higher than in the Station orbit, suggesting a possible variation in trapped particle flux or shielding effects from the geo-magnetic field. However, the TID profiles for muscle, bone, and aluminum are similar, with slight variations due to material composition and density differences.

In the context of human spaceflight, it is critical to note that acute radiation events such as solar flares can dramatically increase exposure levels within a short period. During such events, astronauts in inadequately shielded regions of the spacecraft could receive potentially hazardous doses, especially in low-shielding zones (<10 mm Al), emphasizing the need for storm shelters or predictive warning systems in mission planning.

Single Event Effects (SEE)

Single Event Effects (SEE) occur when energetic particles, such as protons or heavy ions, interact with electronic components, potentially causing disruptions or failures. The SEE rate is highly dependent on the flux of high-energy protons and heavy ions.

Orbit	Heavy Ions Total Rate	Protons Total Rate	Total Rate
Station	2.33e-04	2.40e+04	2.40e+04
Debris	3.40e-04	2.31e+05	2.31e+05

Table 7: Single Event Effects results (/device/day)

From the table, we observe that the dominant contribution to SEE comes from protons. The SEE rate due to protons is significantly higher than the rate due to heavy ions, reaching 2.40×10^4 events/device/day for the station and increasing by an order of magnitude to 2.31×10^5 events/device/day for the debris orbit. Consequently, the total SEE rate follows the same trend, with the debris orbit experiencing nearly ten times more events per day than the station orbit.

Atomic Displacement (TNID)

The TNID (Total Non-Ionizing Dose) quantifies the displacement damage induced in materials by energetic particles. These interactions create defects in the crystal structure of semiconductor components, potentially degrading their performance over time.

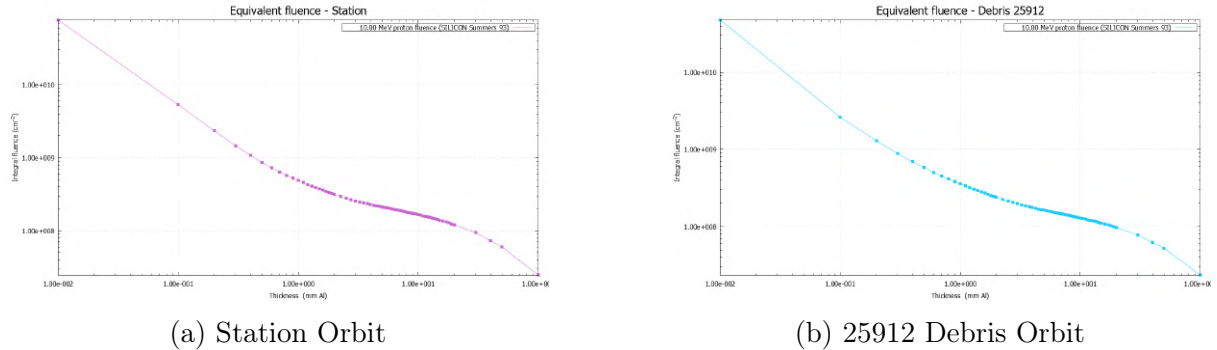


Figure 31: TNID Equivalent Fluences

The graphs illustrate the equivalent fluence of 10 MeV protons as a function of shielding thickness. In both cases, fluence exhibits a logarithmic decrease with increasing shielding,

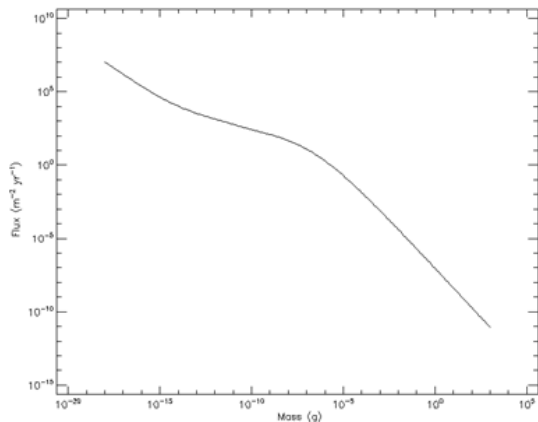


Figure 32: Grun Meteroid Flux on Station Orbit

highlighting the attenuation effect of the material. For both orbits, the initial proton fluence is on the order of 10^{11} protons/cm 2 , reducing below 10^8 protons/cm 2 at a shielding thickness of 10 mm Al. The similar shape of the curves suggests that shielding has a comparable impact in both environments.

3.3.2.2 Charging Effects

Spacecraft charging can result from interactions with plasma, leading to electrostatic discharges that may damage electronic systems or disrupt the on-board systems. The impact of this phenomenon depends on the spacecraft's orbital region and its exposure to plasma. This risk needs to be minimized as much as possible since 45% of the anomalies on flights are due to electronics.

3.3.2.3 Impact Risk

The craters impact can be of few millimetres and caused a partial melting of the materials. It can also damage solar panels and thus reduce their efficiency. Multiple impact during a long exposure gradually removes the surface layers of exposed materials. Based on previous missions of the American space shuttle and on the ISS, we can have an idea of the probability of collision with debris and micrometeoroid and thus develop solution to mitigate theses risk.

The graph above shows the mass of the encountered meteoroid per surface of the spacecraft on the station orbit. Having this in mind, we are able to provide efficient recommendation according to this impact probabilities.

3.3.2.4 Chemical and Thermal Degradation

Chemical and thermal degradation of materials is primarily driven by interactions with atomic oxygen and electromagnetic radiation. These factors contribute to the erosion, embrittlement, and gradual deterioration of exposed surfaces, particularly for polymers and composite materials.

The presence of ATOX at high velocities leads to surface erosion through oxidation reactions. Polymers, such as Kapton and Mylar, are particularly vulnerable, with erosion rates depending on material composition, exposure time, and atomic oxygen flux.

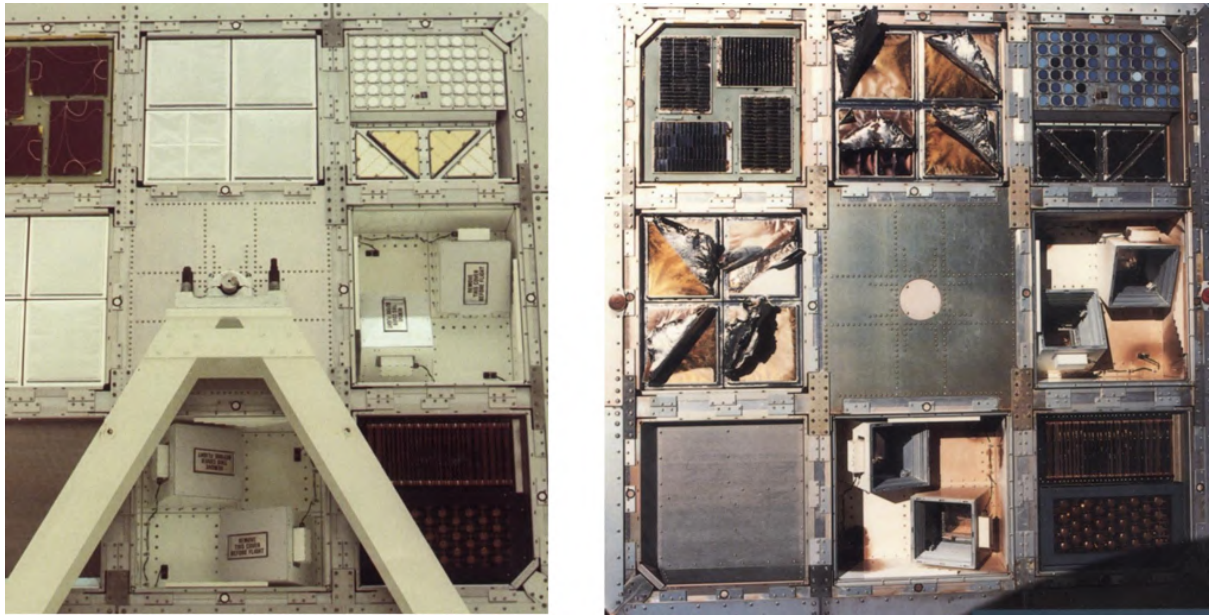


Figure 33: Comparison of different materials exposed to a LEO orbit over 5.7 years (LDEF mission)

In addition, prolonged exposure to solar UV and X-rays can cause photo-induced degradation, leading to discoloration, embrittlement, and loss of mechanical properties. For instance, UV radiation can break molecular bonds in polymers, accelerating their degradation, while X-rays contribute to deeper material penetration and potential structural weakening.

The intensity of UV radiation in LEO reaches approximately 1360 W/m^2 , while X-ray fluxes vary depending on solar activity. Materials used for external spacecraft surfaces, such as thermal blankets and optical coatings, must be carefully selected to withstand these effects. A more detailed thermal analysis will be conducted later to assess the impact of temperature variations and thermal cycling on material performance.

3.3.2.5 Contamination

Contamination in space come from multiple sources, including debris, micrometeoroid, outgassing from materials, and propellant residues. Over time, these contaminants can degrade optical surfaces, electronic instruments, and structural components, reducing their efficiency and operational lifespan.

One significant source of contamination is high-velocity impacts from micrometeoroids and debris, which can vaporize materials upon collision. The resulting particles can settle on surfaces, forming deposits that obscure sensors, degrade solar panels, and reduce the efficiency of thermal coatings. This accumulation can be particularly problematic for spacecraft operating in LEO, where debris density is higher due to human-made space activities.

Additionally, spacecraft materials such as polymers, adhesives, paints, and lubricants – can release volatile organic compounds (VOCs) when exposed to the harsh conditions of space, including vacuum and extreme temperature fluctuations. These vapours can

then condense on colder surfaces, particularly optical components, cameras, and thermal radiators, leading to reduced transparency, imaging quality, and heat dissipation performance.

3.3.3 Analysis and Recommendations

The following recommendations should be implemented:

REQ-ENV-001 – The StarCheap shall use materials with conductive properties to maintain an equipotential state across the spacecraft's surface.

REQ-ENV-002 – The StarCheap shall use materials with high density properties in critical areas, such as polyethylene.

REQ-ENV-003 – The StarCheap shall use materials with low outgassing properties.

REQ-ENV-004 – The StarCheap shall be protected from small meteoroids and debris (<1g) with a Whipple shield protection integrated in critical areas which also help to mitigate contamination effects.

This shield is made of three layers of three different materials to mitigate the impact.



Figure 34: Whipple Shield used on NASA's stardust probe

REQ-ENV-005 – The StarCheap shall use protective coatings to minimize erosion.

These coatings, such as silicon-based or metal oxide layers, aim to be placed on sensitive areas like solar panels, exposed electronics, or pressurized modules.

REQ-ENV-006 – The StarCheap shall use radiation-hardened electronic components with a total dose tolerance of at least 50 krad.

REQ-ENV-007 – The StarCheap shall ensure proper grounding to prevent differential charging.

REQ-ENV-008 – The StarCheap shall implement venting systems.

REQ-ENV-009 – The StarCheap shall monitor propellant leak to avoid contamination.

REQ-ENV-010 – The StarCheap shall use clean propellant to reduce the risk of residue accumulation.

REQ-ENV-011 – The StarCheap shall implement an emergency procedure to alert astronauts of solar flares and enable them to reach a designated area within 10 minutes, ensuring a reduction of at least 90% in received radiation doses.

REQ-ENV-012 – The StarCheap shall ensure continuous communication during solar flares with no more than 10% signal loss and establishing a secure protocol.

REQ-ENV-013 – The StarCheap shall be able to operate avoidance manoeuvres, in case of massive debris or clusters.

This continuous monitoring will be done with the help of catalogues and maps of massive debris. We will also rely on the space surveillance on ground using predictive models.

REQ-ENV-014 – The StarCheap shall be tested in representative environments.

REQ-ENV-015 – The StarCheap shall follow a maintenance plan including regular renewal of coatings.

4 Propulsion

This section presents the propulsion system of the orbital shuttle, focusing on the main engine architecture, cooling and ignition subsystems, tank pressurization strategies, and overall mass budget. The propulsion system is based on the use of a green monopropellant—NOFBX—which offers a safer and more environmentally friendly alternative to traditional hypergolic propellants, while maintaining performance compatible with orbital maneuvers and retropropulsion phases.

Figure 35 illustrates the high-level functional diagram of the propulsion system. It includes the NOFBX propellant tank, helium pressurization system, and the engine assembly. While this report focuses on the structural and thermofluidic design of the main components (chambers, nozzles, tanks, cooling, ignition), it is important to note that the complete fluidic architecture also includes:

- Non-return valves on each feed line to prevent backflow,
- Electrically or pneumatically actuated pressurization valves,
- Redundant pressure and temperature sensors placed at key locations (e.g., downstream of tanks, at injector inlet, near ignitors).

These components are critical for safe operation, feedback control, and system health monitoring. However, for simplicity and clarity, their detailed integration is not addressed in this preliminary design report.

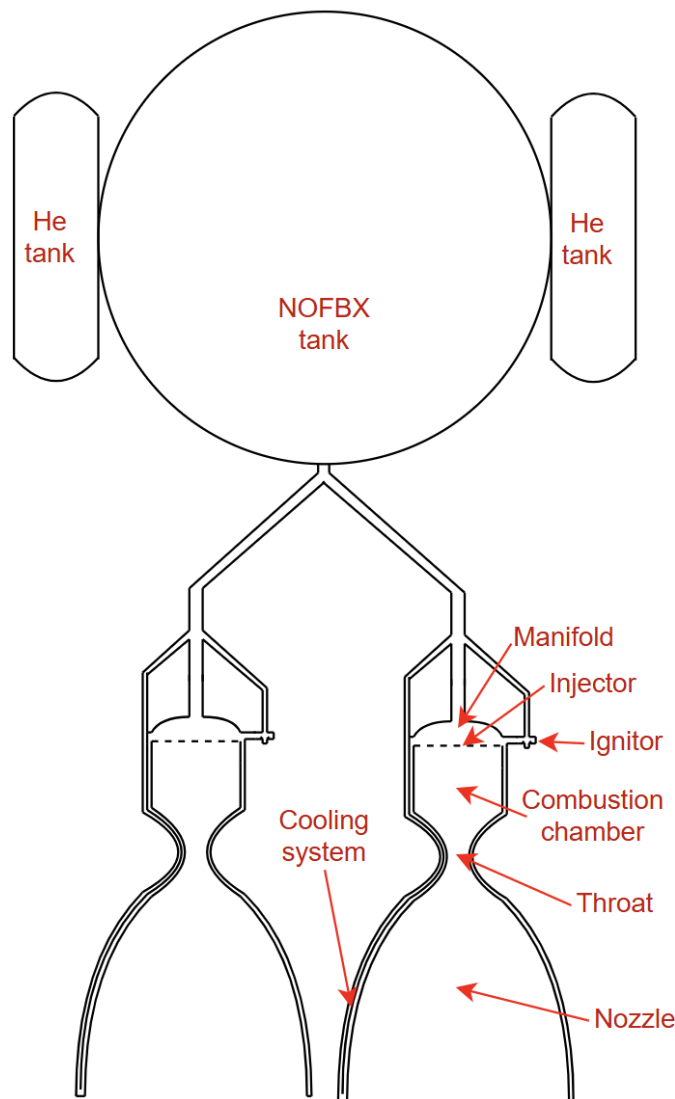


Figure 35: Architecture diagram of the propulsion system

The rest of this section details the engine geometry and performance, injector and ignition design, regenerative cooling system, tank architecture, helium pressurization, and the complete propulsion mass budget according to the following book Huzel and Huang [1992]. The design requirements used throughout the propulsion analysis are summarized in Table 8.

Table 8: Propulsion requirements

Requirement Category	Numerical Data / Specification
Capability to Achieve and Maintain Orbit	Station: 500 km, 50°
Redundancy and Fault Tolerance	10^{-9}
Propellant Tank Safety	T = [0,100]°C, 100 bar
Minimal Environmental Impact	No debris generated and no pollution
Reburn	No fully solid propulsion
Reusability	10 reuse cycles, lifetime 5 years
Mass	40%, 16000 kg
Refuel	possible
Efficiency and Performance	ISP = 300 s

Table 9: Propulsion requirements

4.1 Engine design

This part summarizes the assumptions and equations used to perform a preliminary design of a rocket engine called SCREAM (Storable propellant Combustion Rocket Engine with Acoustic Ignition Mechanism). This rocket engine is made for a reusable orbital shuttle using a green propellant (NOFBX). The engine is based on a closed-cycle architecture with regenerative cooling. The design is built around a target thrust-to-weight ratio of $T/W = 1.75$ (needed for a retropropulsion sequence) for a shuttle mass of $m = 40$ tonnes. All the calculations are based on the following physical constants and parameters:

Parameter	Value
Chamber pressure P_c	50 bar
Chamber temperature T_c	3200 K
Specific heat ratio γ	1.2
Gas constant R	346 J/(kg · K)
Expansion ratio ε	30
Propellant density ρ	1170 kg/m ³
Number of engines N_{engines}	6

Table 10: Main Engine Parameters

For this preliminary engine design, the chamber pressure was set to 50 bar, which is representative of typical values found in current orbital propulsion systems. For instance, the Shuttle's OMS engine operated at approximately 50 bar, and NOFBX-based systems such as those tested for CubeSats and satellite maneuvering systems operate with chamber pressures ranging from 30 to 50 bar. This level ensures a good balance between engine performance, system compactness, and structural reliability.

The chamber temperature was assumed to be 3200 K, reflecting the thermal output expected from high-energy green propellants like LMP-103S or NOFBX. These values are supported by experimental campaigns from NASA and ECAPS Mungas et al. [2008], IspKart [2019], and fall within the upper range of typical combustion temperatures. This temperature remains compatible with regeneratively cooled combustion chambers using

modern copper alloys or ceramic coatings. The thrust required per engine is calculated from the total thrust as:

$$T_{\text{total}} = \frac{T}{W} \cdot m \cdot g_0 \quad T_e = \frac{T_{\text{total}}}{N_{\text{engines}}} \quad (12)$$

Where T_{total} is the total thrust needed for retropropulsion, g_0 is standard gravity, and T_e is the thrust per engine. From the target specific impulse $I_{sp} = 300$ s, the corresponding mass flow rate is obtained via:

$$\dot{m} = \frac{T_e}{I_{sp} \cdot g_0} \quad (13)$$

Assuming ideal gas behavior and isentropic choked flow, the throat conditions (pressure P_t and temperature T_t) are computed as:

$$P_t = P_c \cdot \left(\frac{2}{\gamma + 1} \right)^{\frac{\gamma}{\gamma - 1}}, \quad T_t = T_c \cdot \left(\frac{2}{\gamma + 1} \right) \quad (14)$$

From these, the local speed of sound at the throat is:

$$a_t = \sqrt{\gamma R T_t} \quad (15)$$

The throat area A_t is calculated using the classical isentropic flow relation for choked conditions:

$$A_t = \frac{\dot{m}}{P_c} \cdot \sqrt{\frac{RT_c}{\gamma}} \cdot \left(1 + \frac{\gamma - 1}{2} \right)^{\frac{\gamma+1}{2(\gamma-1)}} \quad (16)$$

The exit area A_e (D_e corresponding diameter) is then defined from the expansion ratio $\varepsilon = A_e/A_t$ as:

$$A_e = \varepsilon \cdot A_t \quad D_e = 2\sqrt{\frac{A_e}{\pi}} \quad (17)$$

The length L_n of the nozzle is defined as follow, based on the expansion ratio and throat diameter D_t :

$$L_n = 1.2 \cdot D_t \cdot \sqrt{\varepsilon} \quad (18)$$

The combustion chamber is assumed to be cylindrical. The chamber volume V_c is computed using the characteristic length L^* and the throat area A_t :

$$V_c = L^* \cdot A_t \quad (19)$$

Assuming the chamber diameter is twice the throat diameter ($D_c = 2D_t$), the corresponding chamber length L_c is:

$$L_c = \frac{V_c}{\pi \cdot (D_c/2)^2} \quad (20)$$

The nozzle exit velocity v_e is related to the specific impulse by:

$$v_e = I_{sp} \cdot g_0 \quad (21)$$

Finally, the nozzle contour is described using a simplified version of the Rao method, which provides a smooth and optimized expansion profile:

$$r(x) = \begin{cases} R_c + (R_t - R_c) \cdot \frac{x}{L_c}, & \text{for } x \in [0, L_c] \\ R_t + (R_e - R_t) \cdot \left(1.5 \cdot \frac{x - L_c}{L_d} - 0.5 \cdot \left(\frac{x - L_c}{L_d} \right)^3 \right), & \text{for } x \in [L_c, L_c + L_d] \end{cases} \quad (22)$$

This profile describes a simplified Rao expansion contour. R_c is the chamber radius, R_t the throat radius, R_e the exit radius, and L_d the nozzle divergent length. We obtain the following results for our principal engine.

Parameter	Value
Total Thrust	686,742 N
Thrust per Engine	114,457 N
Mass Flow Rate	38.889 kg/s
Throat Pressure	28.22 bar
Throat Temperature	2909.09 K
Throat Area	0.01262 m ²
Throat Diameter	0.127 m
Throat Density	2.804 kg/m ³
Speed of Sound	1099.02 m/s
Chamber Volume	0.0151 m ³
Chamber Area	0.0505 m ²
Chamber Diameter	0.254 m
Chamber Length	0.300 m
Exit Area	0.37858 m ²
Exit Diameter	0.694 m
Exhaust Velocity	2943.18 m/s
Nozzle Length	0.83 m

Table 11: Engine parameters

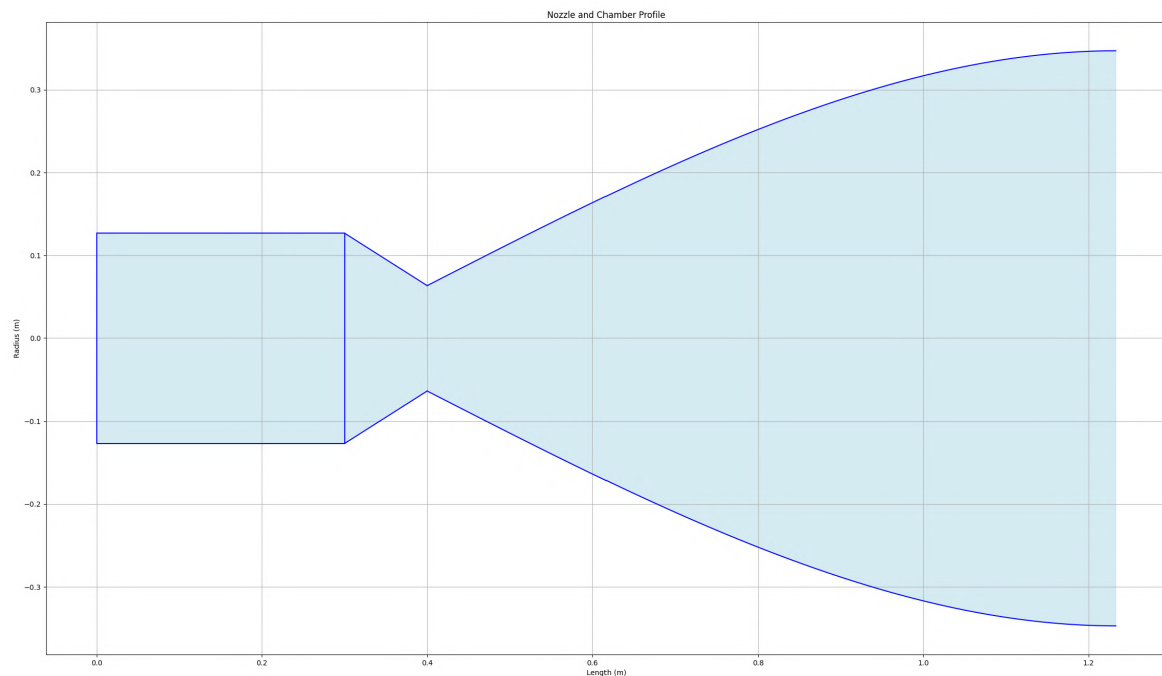


Figure 36: Engine geometry

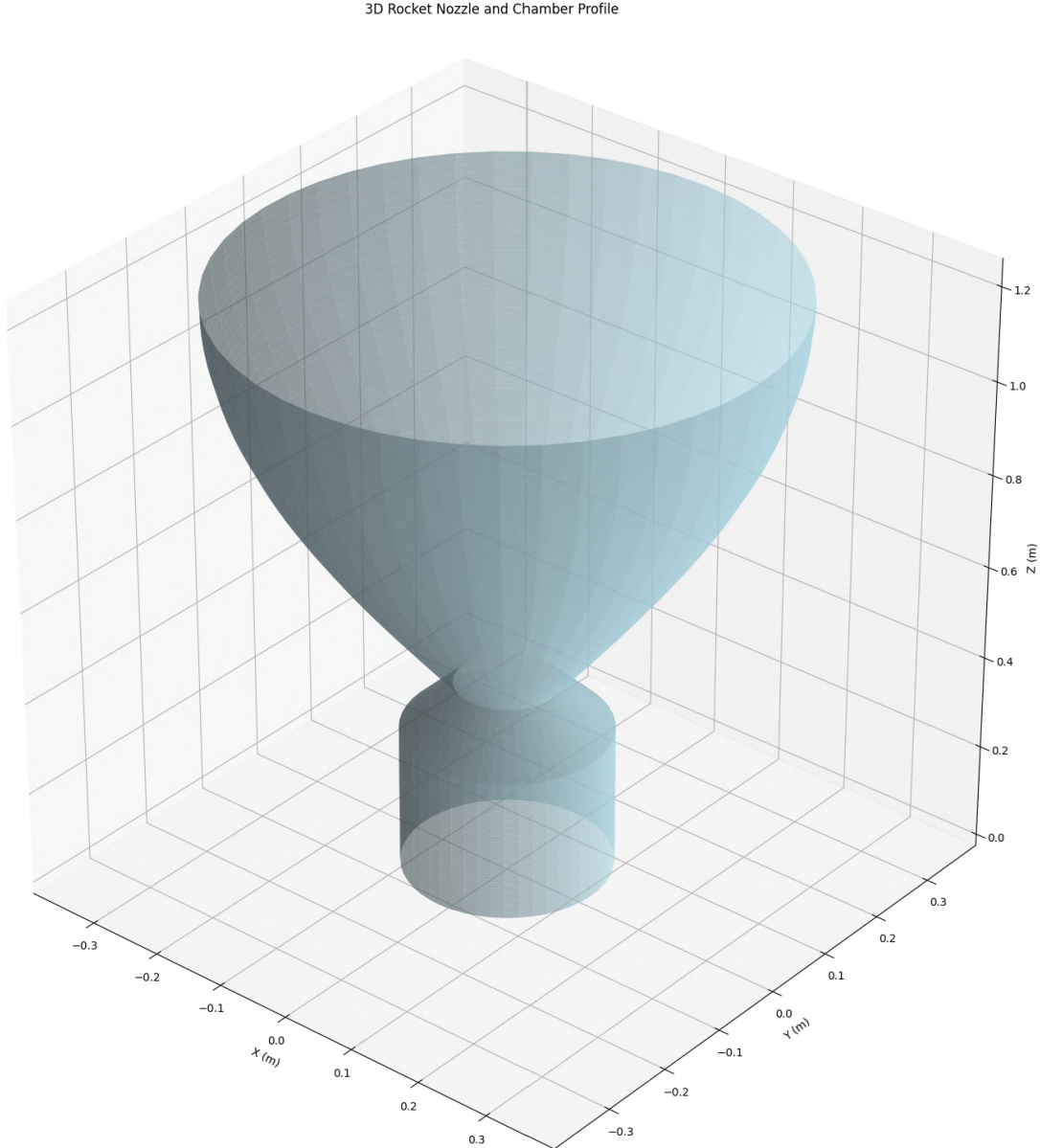


Figure 37: Engine 3D view

4.2 RCS Engine design

Using a similar approach to the main engines, the RCS engines are designed, with the required efforts of the subsystem in mind. As such, a maximum thrust of 400 N is set via trade-off in engine size, and we keep a 300s Isp as these thrusters are hot-gas in the spirit of minimising propellant feed complexity.

Setting a chamber pressure of 10 bars and an expansion ration $\epsilon = 15$, we obtain the following engine parameters and geometry:

Parameter	Value
Thrust per Engine	400 N
Mass Flow Rate	0.136 kg/s
Throat Pressure	5.64 bar
Throat Temperature	2727.27 K
Throat Area	0.00021 m ²
Throat Diameter	0.016 m
Throat Density	0.598 kg/m ³
Speed of Sound	1064.13 m/s
Chamber Volume	0.0001 m ³
Chamber Area	0.0009 m ²
Chamber Diameter	0.033 m
Chamber Length	0.050 m
Exit Area	0.00427 m ²
Exit Diameter	0.074 m
Exhaust Velocity	2943.18 m/s
Nozzle Length	0.22 m

Table 12: RCS Engine parameters

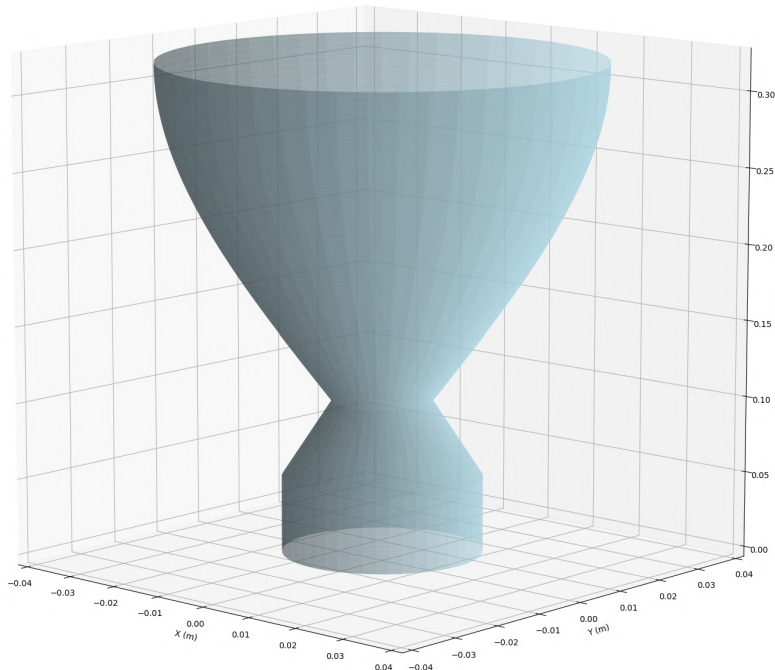


Figure 38: RCS Engine 3D view

We note that due the size of the engine, the ignitor and the injector should be slotted together for volume minimisation purposes.

4.3 Injectors

The showerhead configuration was chosen due to its straightforward design, well-characterized flow behavior, and compatibility with pressure-fed systems. To determine the number of injection holes in a showerhead-type injector, we use the following expression based on Bernoulli's equation and orifice flow theory:

$$\dot{m} = C_d \cdot N \cdot \pi R^2 \cdot \sqrt{2\rho\Delta P} \quad (23)$$

In this equation, \dot{m} denotes the total mass flow rate of the propellant. The coefficient C_d is the discharge coefficient (here 0.8), which accounts for inefficiencies due to orifice geometry and flow contraction. The variable N is the number of individual injection holes. Each hole has a radius R (0.9mm). ΔP is the pressure drop across the injector, estimated as a fraction of the chamber pressure. The pressure drop is estimated as:

$$\Delta P = 0.2 \cdot P_c = 10 \text{ bar} = 10^6 \text{ Pa} \quad (24)$$

Inserting the known values into Eq. 23, we compute the required number of holes:

$$N = \left\lceil \frac{\dot{m}}{C_d \cdot \pi R^2 \cdot \sqrt{2\rho\Delta P}} \right\rceil = 451 \quad (25)$$

This configuration yields 451 injection holes with a diameter of 1.8 mm. The injector plate is designed following a showerhead configuration, where individual injection holes are evenly distributed in a circular pattern. The design seeks to maximize propellant atomization while ensuring structural integrity through mechanical reinforcements.

The injector plate accommodates $N = 451$ holes of diameter $d = 1.8$ mm, distributed in concentric circular rows (rings) within an available radius R_{inj} . The available injector radius is defined by subtracting a safety margin δ from the combustion chamber radius R_c , that is, $R_{\text{inj}} = R_c - \delta$, with $\delta = 10$ mm. The radial spacing between rings Δr is chosen such that the total number of rings K satisfies:

$$K = \left\lceil \sqrt{N} \right\rceil, \quad \Delta r = \frac{R_{\text{inj}}}{K} \quad (26)$$

For each ring of radius $r_i = i \cdot \Delta r$, the number of holes is approximated by:

$$n_i = \left\lfloor \frac{2\pi r_i}{2.2d} \right\rfloor \quad (27)$$

where the factor 2.2 ensures a minimal spacing between holes to avoid structural weakening. To maintain the structural robustness of the plate, regions are intentionally left unperforated:

- Four radial sectors centered on $\theta = 0^\circ, 90^\circ, 180^\circ$, and 270° are excluded from perforation. Each exclusion covers an angular width of $\pm 10^\circ$.
- A concentric annular band centered at radius $R_{\text{ring}} = 50$ mm is kept hole-free to increase bending stiffness.

These reinforcements help to reduce stress concentration around hole patterns, maintain manufacturability with clear undrilled paths and prevent hole interaction near the chamber wall.

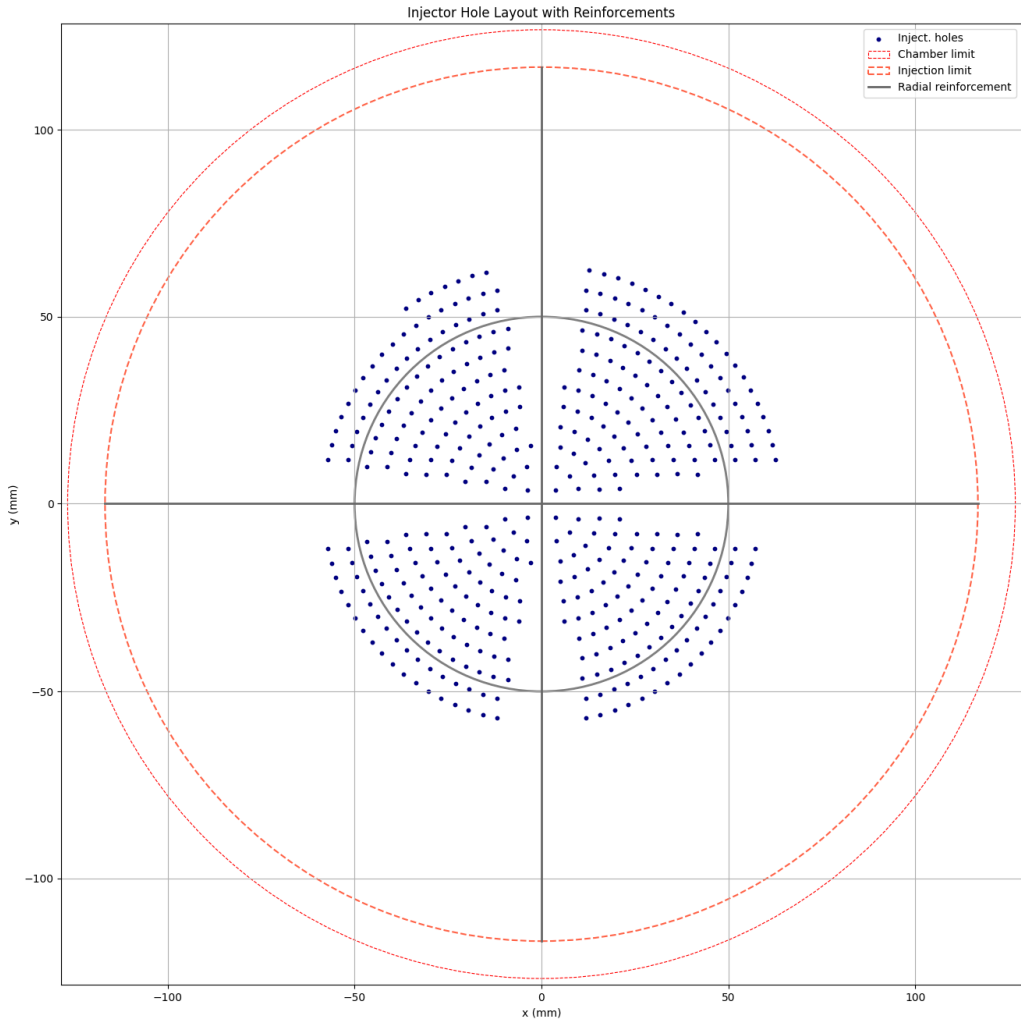


Figure 39: Top-view schematic of the injector plate

4.4 Ignitor

The ignition system relies on an acoustic ignitor concept, called SIFLET (Sonic Ignition For Liquid Engine Technology). This ignition system is inspired by the Hartmann-Sprenger principle, where a choked jet of propellant creates high-intensity pressure oscillations in a confined cavity. This phenomenon generates sufficient thermal energy to initiate the combustion process. A small portion of the total propellant mass flow is diverted to the ignitor:

$$\dot{m}_{\text{ignitor}} = \alpha \cdot \dot{m} \quad (28)$$

where α is the fraction allocated to ignition (here 0.5%). Assuming a converging nozzle with sonic conditions (i.e., choked flow at Mach 1), the required throat area is calculated from the compressible isentropic flow relation Sutton and Biblarz [2017]:

$$A^* = \frac{\dot{m}}{P_0} \cdot \sqrt{\frac{RT_0}{\gamma}} \cdot \left(\frac{\gamma + 1}{2} \right)^{\frac{\gamma+1}{2(\gamma-1)}} \quad (29)$$

Where, P_0 and T_0 are the stagnation pressure and temperature at the nozzle inlet. From the area A^* , the throat diameter is computed as:

$$D^* = 2\sqrt{\frac{A^*}{\pi}} \quad (30)$$

Based on empirical data from acoustic ignitor studies — [1973], Rocketdyne Engineering Division [1971], the ignitor cavity is defined using the following geometric relations:

$$D_{\text{exit}} = 1.6 \cdot D^* \quad (31)$$

$$L_{\text{tot}} = 4.5 \cdot D^* \quad (32)$$

$$\Delta = 2 \cdot D^* \quad (33)$$

$$r = \frac{D_{\text{exit}}}{5} \quad (34)$$

With Δ the spacing between throat and cone entrance. The cone length, with a gentle expansion angle $\theta = 10$, is then calculated as:

$$L_{\text{cone}} = \frac{D_{\text{exit}} - r}{2 \cdot \tan(\theta)} \quad (35)$$

The cavity acts as a quarter-wave resonator. The fundamental frequency is approximated as:

$$f = \frac{c}{4L} \quad (36)$$

with $c = \sqrt{\gamma RT_0}$ the speed of sound in the vapor. The resonator's acoustic power, governed by jet impingement, is sufficient to produce localized thermal ignition Rocketdyne Engineering Division [1971].

Ignitor Parameter	Value
Neck Area	$2.668 \times 10^{-5} \text{ m}^2$
Neck Diameter	0.006 m
Distance Neck / Channel	0.012 m
Channel Diameter (Cone)	0.009 m
Channel Length	0.026 m
Channel Diameter (Cylindrical)	0.002 m
Cone Length	0.014 m
Acoustic Resonance Frequency	5940.612 Hz

Table 13: Ignitor properties

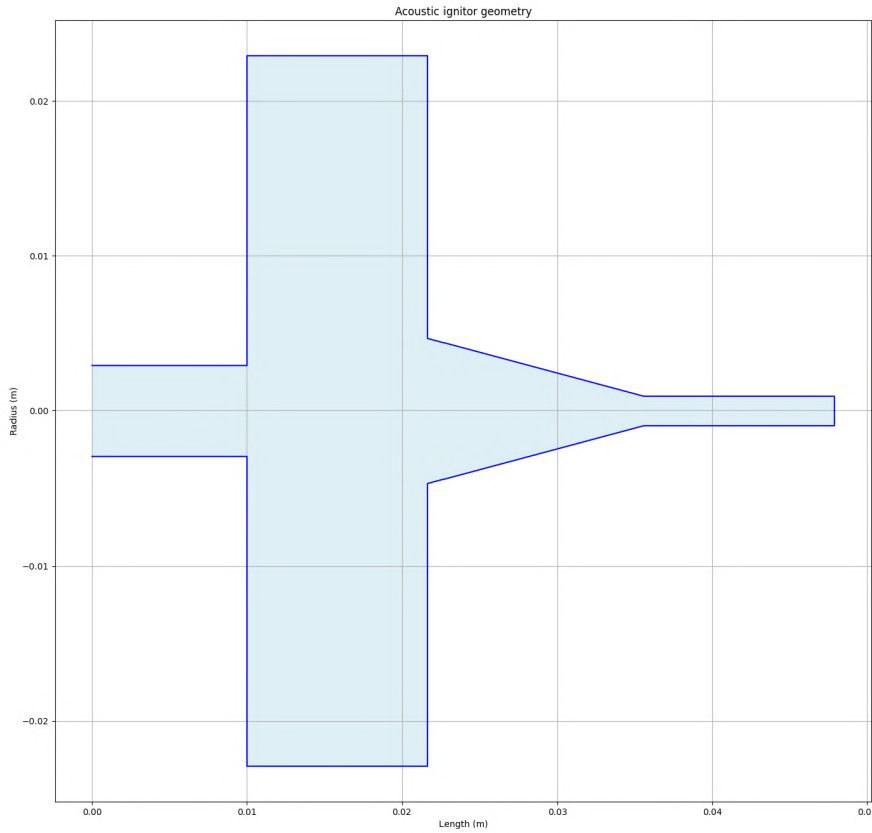


Figure 40: Acoustic ignitor geometry

The compact Hartmann-type ignitor offers high reliability, requires no moving parts, and provides sufficient thermal energy for flame initiation. The inlet sound speed ensures stable operation and prevents backflow. This ignitor can either be integrated into the injector assembly or implemented as an external system, depending primarily on thermal constraints and safety considerations. Placing the ignitor close to the combustion chamber can increase risks due to elevated temperatures and pressure fluctuations. However, in our design, we choose to integrate it within the injector manifold to maximize engine compactness. To mitigate thermal stress, a dedicated regenerative cooling channel is implemented around the ignitor region to prevent local temperature spikes.

4.5 Cooling system

The regenerative cooling system presented here is specifically designed for a pressure-fed rocket engine utilizing NOFBX (Nitrous Oxide Fuel Blend Experimental) as a premixed monopropellant. Given the favorable thermal stability and monopropellant characteristics of NOFBX, the design adopts a simplified cooling strategy by dedicating approximately 30% of the total propellant mass flow to regenerative cooling, while the remaining 70% is directly injected into the combustion chamber.

The regenerative cooling approach consists of 50 helically wrapped cooling channels surrounding the nozzle and combustion chamber. The cooling fluid (NOFBX propellant) enters the cooling circuit at the nozzle exit region (lowest thermal flux area) and grad-

ually flows upward toward the combustion chamber injector area (highest thermal load area). This ensures efficient heat transfer and manageable pressure drop. The geometrical parameters selected are:

Parameter	Value
Number of cooling channels	50
Axial pitch between channels	0.2
Target coolant flow velocity	5 m/s
Coolant mass flow rate	11.67 kg/s (30% of total engine mass flow)

Table 14: Cooling System Parameters

The diameter of each cooling channel is determined based on the required volumetric flow rate and desired coolant velocity:

$$d = \sqrt{\frac{4 \frac{\dot{m}_{cool}}{\rho}}{\pi N_{ch} V}} \quad (37)$$

In this equation, d is the diameter of each channel, ρ is the fluid density, N_{ch} the number of channels, and V the coolant velocity. The pressure drop along the regenerative cooling circuit is a critical parameter for ensuring sufficient injection pressure at the combustion chamber, especially in a pressure-fed engine. It is governed by the Darcy–Weisbach equation:

$$\Delta P = f \cdot \frac{L}{d} \cdot \frac{\rho V^2}{2} \quad (38)$$

The terms here include ΔP the pressure drop, f the friction factor and L the length of the cooling path. Lowering any of the terms L , V , or increasing d helps reduce the pressure drop, which is essential in pressure-fed engines.

In practice, achieving a target pressure drop requires a balanced approach, where channel diameter, total length, and velocity are selected to maintain both thermal efficiency and hydraulic feasibility. This trade-off is particularly critical in pressure-fed systems, where the pressure margin available from the tank is limited.

For a channel helically wrapped around the cylindrical surface of the engine, the total length L of one cooling channel can be expressed as:

$$L = n \cdot \sqrt{P^2 + (2\pi R)^2} \quad (39)$$

where n is the number of turns, P is the axial pitch, and R is the mean radius. This formula assumes that the channels follow a uniform helix along the chamber and nozzle outer wall. The total number of turns n can be obtained by dividing the total axial length of the cooling section by the pitch P .

Assuming N_{ch} channels are uniformly distributed around the circumference of the engine, the angular spacing between adjacent channels (center-to-center) is given by:

$$e = \frac{2\pi R}{N_{ch}} \quad (40)$$

To compute the effective material thickness between channels, the channel diameter d is subtracted:

$$e_{\text{eff}} = e - d \quad (41)$$

This effective spacing must remain large enough to ensure mechanical integrity under pressure and thermal stress, while maximizing the surface area available for heat transfer.

The following equations gives us an other approach to verify our results. The convective heat flux from hot combustion gases to the engine wall is estimated using the Bartz correlation Bartz [1957]:

$$\dot{q} = 0.026 \frac{\mu^{0.2} c_p}{Pr^{0.6}} \frac{P_c^{0.8} T_c^{0.6}}{D_t^{0.1} A_t^{0.9}} \left(\frac{D_t}{D} \right)^{0.5} \quad (42)$$

In this equation, \dot{q} is the heat flux in W/m^2 , μ is the dynamic viscosity of the combustion gas ($2e - 5 \text{ Pa} \cdot \text{s}$), c_p is its specific heat capacity ($2500 \text{ J/kg} \cdot \text{K}$), and Pr the Prandtl number (0.7). The parameters P_c and T_c represent the chamber pressure and temperature, while D_t is the throat diameter, A_t is the throat area, and D is the local diameter at the point of interest.

The coolant mass flow rate required to absorb the thermal load is calculated by the energy balance equation:

$$\dot{m}_{\text{cool}} = \frac{\dot{Q}}{c_{p,\text{cool}} \Delta T} \quad (43)$$

Here, \dot{m}_{cool} is the coolant mass flow rate in kg/s , \dot{Q} is the total thermal power to be absorbed, and ΔT is the allowed temperature increase.

Given the thermal stability of NOFBX (approximately up to 250–300 °C according to NASA technical studies Mungas et al. [2012]), preliminary calculations indicate the propellant temperature increase in the cooling channels is maintained below this critical limit (around 200 K rise), thus preventing decomposition or boiling upstream of injection. The pressure-fed configuration with a tank pressure of approximately 100 bar ensures an adequate margin (estimated 5 bar pressure drop through cooling channels), well within operational limits to sustain stable combustion chamber injection at 50 bar.

Overall, using 30% of the flow for cooling—as opposed to traditional 3–8% values—is justified here by the simplicity and robustness it brings: fewer but larger channels, better thermal margin, and easier fabrication.

This regenerative cooling strategy, enabled by the thermal properties of NOFBX, offers a robust and simplified rocket engine thermal management. We obtain the following design :

Cooling Parameter	Value
Channel Diameter	0.0081 m
Flow Rate (Primary Cooling)	11.667 kg/s
Volume Flow Rate	0.013 m ³ /s
Circumferential Spacing (e)	0.017 m
Number of Turns	22.66
Channel Length	18.945 m
Pressure Drop (ΔP)	5.246 bar
Wall Area (Bartz)	0.946 m ²
Heat Flux (Bartz)	1.165×10^6 W/m ²
Total Heat Load (Bartz)	1.101×10^6 W
Needed Flow Rate (Bartz)	3.061 kg/s

Table 15: Cooling system characteristics

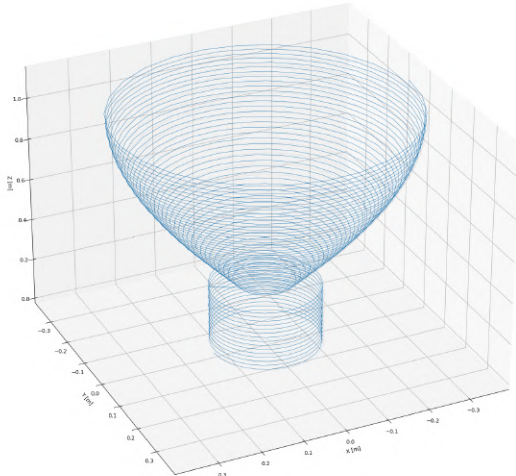


Figure 41: Cooling system with 1 channel

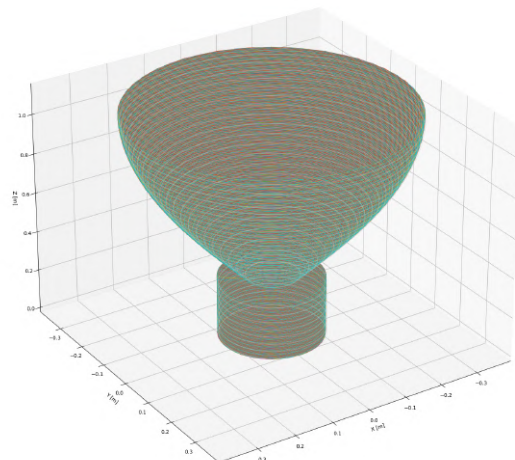


Figure 42: Cooling system with 50 channels

4.6 Gimballing

The engine must be capable of angulation to enable thrust-vector control of the vehicle, particularly in critical phases such as inclination changes, reentry or hover flip. Most turbopump-fed engine systems incorporate gimbals, which function as universal joints. These gimbals are typically mounted between the vehicle interface and the engine. Beyond allowing angular movement, the gimbal must also transfer engine thrust and all associated loads to the vehicle. This angulation is achieved through the use of bearing surfaces within the gimbal.

4.6.1 Choice of architecture

Two main gimbal architectures exist :

- Gimballed thrust-chamber nozzle: the nozzle is directly vectored by actuators attached to its side (via individual pads or a circumferential ring), such as can be

found on the Ariane 5 and Ariane 6 solid booster engines. Although this architecture allows for a faster response time and reduced mechanical complexity, by effectively "pulling" on the sides of the nozzle, it induces additional mechanical stress, increases propellant feed complexity and limits the available vectoring range. It is commonly used for solid propellant thrusters, where no propellant ducts are needed.

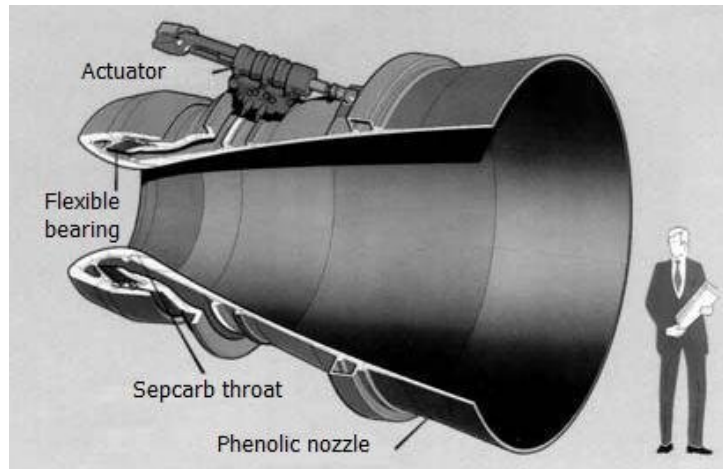


Figure 43: Ariane 5 TVC geometry Turner [2009]

- Gimballed thrust chamber/engine assembly : the entire engine assembly is mounted on a gimbal joint. Actuators (one each in the pitch and yaw plane) make the whole assembly tilt for thrust vectoring. This architecture provides better structural integrity, more control authority, easier integration of propellant feed lines and ensures a more efficient load transmission from the engine to the vehicle. It is more commonly used for liquid propellant thrusters.

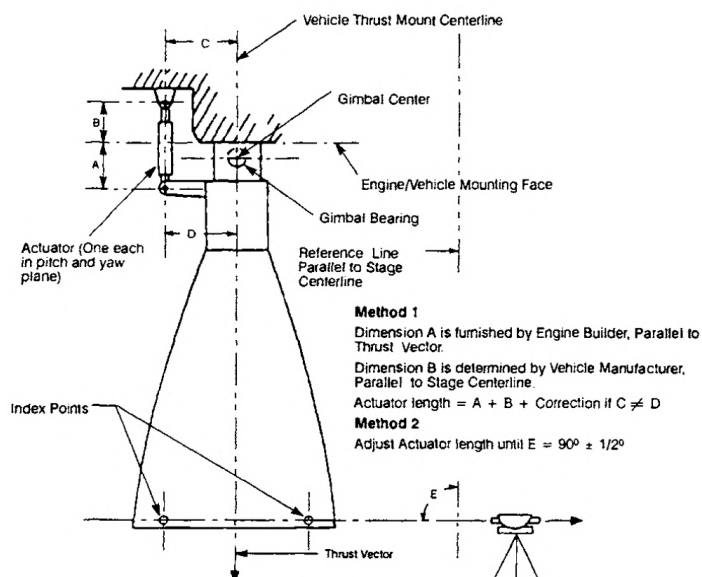


Figure 44: Gimballed engine assembly architecture Huzel and Huang [1992]

As such, our choice of gimbal architecture is logically the engine assembly architecture, as we use a liquid propellant thruster and we require the least possible structural stress to ensure reusability and the most efficient load transmission possible. Control considerations must also be made.

4.6.2 Design considerations

In designing the gimbal, custom dictates the following design considerations Huzel and Huang [1992]:

- Angulation: The engine assembly or thrust chamber must be able to pivot for thrust-vector control, typically within a range of $\pm X$ degrees.
- Thrust Alignment: The gimbal-engine interface must allow for lateral offset adjustments to ensure proper thrust alignment with the engine centerline, usually within a range of ± 0.10 to ± 0.4 inches.
- Load Transmission: The gimbal must accommodate side loads and moments as dictated by engine thrust requirements and configuration, ensuring proper load transfer to the vehicle.
- Operational Life: A typical gimbal must endure approximately 1,000 full cycles at maximum angulation—such as a total 40-degree movement for a 10-degree gimbal angle. Reusable engines demand even higher cycle durability.
- Bearing Surfaces: Designs should minimize deflection in bearing surfaces and provide sufficient bearing area to prevent damage.
- Propellant-Duct Integration: Some gimbal designs must accommodate a propellant duct passing through them.
- Maintenance: Certain gimbals require periodic lubrication of bearing surfaces, while others incorporate antifriction bearings or maintenance-free bearing inserts. Gimbal boots may be necessary to shield bearings from dust, water, and debris.
- Weight Efficiency: The use of high-strength, lightweight materials helps reduce the overall weight impact on the vehicle.

In our design, we make considerations for bearing surfaces, angulation, load transmission and operational lifetime.

4.6.3 Mount

We now consider the type of gimbal mount that would be adapted to the engine. There are three main types of mounts :

- Ring-type gimbal mount: designed for a low-thrust, upper-stage engine. The design has a closed-yoke, flow-through, ring-type gimbal with plain-bearing pivot joints. This configuration allows the main oxidizer duct to pass through the assembly in the longitudinal axis to the thrust-chamber dome. The gimbal mount was designed to connect the vehicle on one interface and the engine thrust-chamber dome on the

other interface. The lower support of the gimbal mount provides an adjustment mechanism for thrust vector alignment.

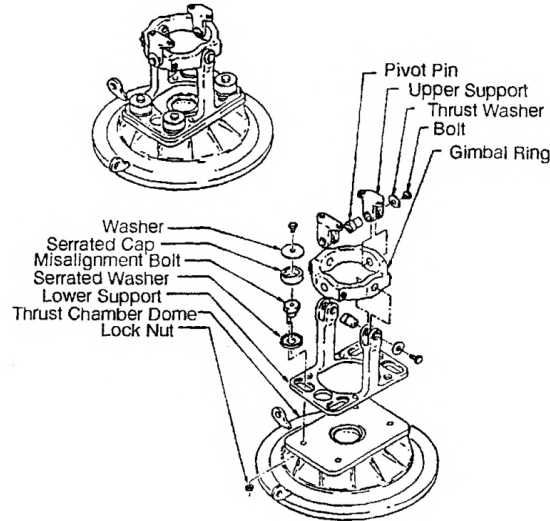


Figure 45: Ring-type Gimbal Mount Huzel and Huang [1992]

- Cross-type gimbal mount: the gimbal mount secures the engine assembly to the vehicle thrust frame and is mounted to the thrust chamber dome and elbow assembly. It consists of a cross-shaped unit incorporating bearing surfaces, upper and lower gimbal-bearing blocks, upper and lower retainers, and thrust-vector-aligning slides. This mount is typically used for medium-thrust engines.
- Spherical-type gimbal: similar designs have been used on engines with high thrusts. The gimbal is bolted to the vehicle on one side and to the engine powerhead on the other. The unit consists of a lower body with a spherical protrusion and an upper seat with a spherical socket. A center block and shaft transmit side and torsional loads. Spherical bearing surfaces receive the engine-thrust load.

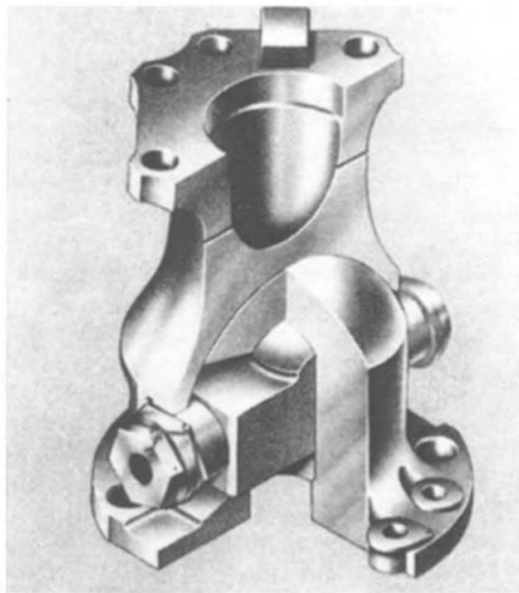


Figure 46: Spherical Gimbal Mount Huzel and Huang [1992]

By virtue of the thrust magnitude of the engine, the obvious choice of mount is the spherical type. A spherical gimbal mount is particularly advantageous in rocket thrust vector control systems due to its compactness, strength, and full-range angular flexibility. Unlike traditional dual-axis gimbals, it allows smooth, continuous motion in all directions from a single pivot point. Its centralized design provides a direct and efficient load path, minimizing bending stresses and enhancing structural integrity. Additionally, the spherical configuration reduces overall system mass and volume—critical in aerospace applications—and simplifies the mechanical layout by eliminating multiple joints. It also offers better alignment control and can accommodate thermal expansion more effectively. However, this type of mount can be more complex to manufacture and may require advanced materials, precision tolerances, and specialized solutions for routing propellant lines through or around the joint. We will not make considerations for these constraints in this study.

4.6.4 Design of the gimbal

4.6.4.1 Gimbal angle

The gimbal angle must be consequent enough in order to comfortably make the hover and reentry maneuvers. Gimbal angles for existing missions are given below:

Spacecraft	Gimbal angle
Space Shuttle	10° (pitch) 8.5° (yaw)
Starship	15°
SLS	20°
Hermes (estimated)	6-8°
Orion Capsule	7.5°

Table 16: Mission gimbal angles

We note the large angles for the Starship and SLS rocket, which correspond to the stringent mission constraints and vehicle capacity. We note that although our vehicle's mission trajectory is very similar to the Starship's, particularly upon landing, our mass and dimensions are sensibly smaller and as such, we won't need such a large angle.

We arbitrarily fix 10° and verify by a rapid analysis that it will be sufficient for the most stringent maneuver, the hover.

We assume the engines all gimbal together, in the same direction. This means the system behaves almost like a rigid-body gimballed engine, similar to how Space Shuttle's three SSMEs were gimballed in coordination.

We can calculate the lateral force generated by the gimballed engine:

$$F_{\text{lat}} = T_{\max} \sin(\theta) = 119244N \quad (44)$$

Assuming the effective lever arm r (distance from thrust vector to vehicle CG) is 2.5 m:

$$\tau = r F_{\text{lat}} = 298111Nm \quad (45)$$

We can calculate the moment of inertia around the yaw and pitch axes assuming a cylindrical architecture:

$$I = \frac{1}{12} M(3r^2 + h^2) = 812500kg.m^2 \quad (46)$$

We can now deduce the resulting angular acceleration, following Newton's second law for rotation:

$$\alpha = \frac{\tau}{I} = 0,37rad/s = 21,1^\circ/s \quad (47)$$

We obtain quite a high angular authority; we check how much time it would take to make a $\beta=90^\circ$ rotation (worst-case hover flip maneuver):

$$t = \sqrt{\frac{2\beta}{\alpha}} = 2,92s \quad (48)$$

We would obtain the desired angle under 3s, which is largely acceptable for such a maneuver, given that the Starship should make its flip in 14 seconds. We do note that this is just an estimate, and that a more rigorous study considering drag, wind, angular speed and velocity profiles would give a more realistic idea of the necessary gimbal angle.

4.6.4.2 Frame and actuators

Much like can be found in the Space X Merlin engines or in most literature concerning thrust vector control (TVC), we find that the use of a quadrupod frame with actuators is perhaps the most mechanically practical solutions.

A quadrupod gimbal frame offers a lightweight and mechanically efficient solution for thrust vector control. Using two actuated struts, it provides two degrees of freedom (pitch and yaw) without requiring large rotational bearings, which reduces mechanical complexity and maintenance needs. The load is distributed across four legs, improving structural stiffness and redundancy compared to traditional two-axis gimbals. Though it lacks full 6DOF like a hexapod, it delivers sufficient angular authority (typically $\pm 5^\circ$ to $\pm 15^\circ$) in pitch and yaw for engine vectoring during maneuvers. Its relatively simple control logic (compared to hexapods) still requires coordinated actuator motion to avoid

binding or overconstraint, but this trade-off is often worthwhile in terms of mass, cost, and compact integration near hot engine zones.

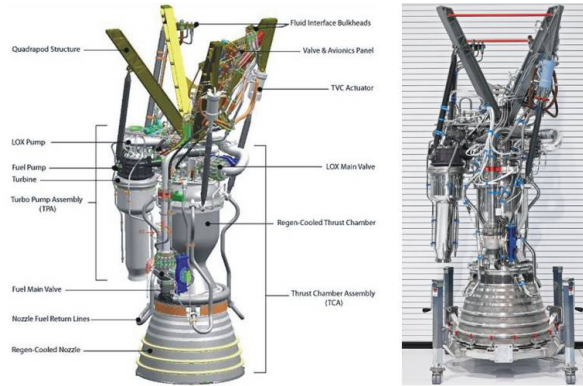


Figure 47: Merlin Engine Gimbal Frame the Space Techie [2020]

We develop a simplified version of the gimbal frame, inspired by the RETALT VTVL launcher design Krammer et al. [2022], utilizing electromechanical actuators. These actuators are particularly well-suited for gimbal applications due to their high precision, rapid response, and ease of integration with digital control systems. Unlike hydraulic or pneumatic systems, they eliminate the complexity of fluid management, reduce maintenance demands, and ensure clean, leak-free operation—benefits that are especially valuable in reusable or autonomous launch systems.

The actuators are connected to the nozzle via a dedicated ring mount near its upper section, minimizing local deformation while ensuring effective force transmission. This mounting location results from a trade-off: although attaching actuators to the combustion chamber would reduce stress on the nozzle itself, it would significantly increase the required actuator force due to reduced mechanical leverage. The selected configuration balances structural integrity, actuator sizing, and control authority effectively.

2D and 3D schematics of the mount, ring and actuators are presented below.

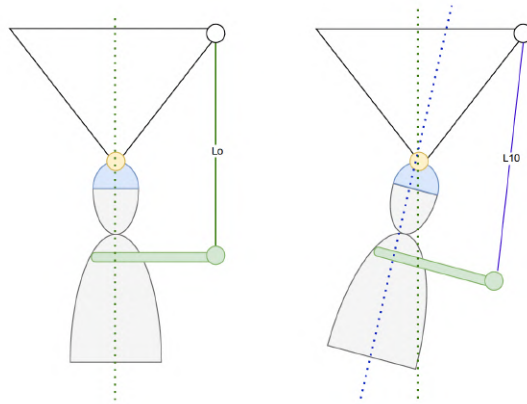


Figure 48: Gimbal frame 2D schematic

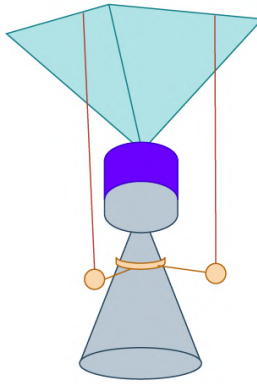


Figure 49: Gimbal frame 3D schematic

We now calculate the required actuator force to gimbal the engine. Computations are made assuming a full shuttle and engines thrusting at maximum capacity.

We can calculate the torque generated by gimbaled engine thrust that will need to be counteracted by the actuators, using the lever arm from the engine thrust application point to the actuators':

$$T_t = T_{\max} \cdot L \cdot \sin(\theta) \quad (49)$$

And deduce the required actuator force from the actuators' mounting distance:

$$F = \frac{T_t}{R} \quad (50)$$

The actuator stroke length is given by:

$$S = 2R \sin(\theta) \quad (51)$$

From these equations we compute the frame and actuators' characteristics, resumed in the table below.

Frame dimensions	
Parameter	Value
Frame height	0.6 m
Frame width	1.56 m
Gimbal mount height	0.2 m
Frame leg length	1.36 m
Ring mount length	0.352 m

Table 17: Gimbal frame characteristics

From these computations, we obtain quite a large frame, which is due to the necessary mount length for the actuator to push against the top of the nozzle. Considerations would need to be made for the available room between the combustion chamber feed and the propellant tank, but the data was not available at the time of the sizing.

Actuator characteristics	
Parameter	Value
Lever arm	1.2 m
Mounting length	0.5 m
Required Actuator Force	17 kN
Stroke length	0.1 m
Set time to reach 10°	2 s
Required speed	0.05 m/s
Required Power	880 W

Table 18: Gimbal frame characteristics

We obtain a quite high actuation required force for a quite short stroke length, indicating that the actuator as it is mounted will need a lot of help to push the load efficiently. Although the gimbal principle is quite well-documented, there is little resource on the actuators used for gimbaling. Industrial actuators are found (SOURCE) delivering similar values in thrust, but there is little documentation to confirm the reliability of the sizing. As such, it is considered preliminary.

We note, however, that a tradeoff was made with a gimbal mount at the top of the combustion chamber, which was found to require a 40kN magnitude of thrust from the actuators and a much larger frame mount.

We note additionally that the required speed of 0.05 m/s and the 2-second set time to reach 10° of motion suggest that the system is optimized more for torque than for rapid movement.

For a more detailed and accurate actuator sizing, it is important to account for the combustion chamber feed system, as gimbaling introduces the need for flexible or specially adapted piping to accommodate the engine's motion without compromising flow or structural integrity.

4.7 Tank design

4.7.1 NOFBX tank design

The propellant tank is designed to store a total of 12 tonnes of premixed NOFBX monopropellant at an internal pressure of 100 bar and ambient temperature. Given the density of NOFBX, taken here as $\rho = 900 \text{ kg/m}^3$ Mungas et al. [2012], the total required volume is:

$$V_{\text{tot}} = \frac{m_{\text{prop}}}{\rho} = \frac{12\,000}{900} = 13.33 \text{ m}^3 \quad (52)$$

A ullage volume of 1.5% is considered to accommodate pressurant gas and account for expansion, giving:

$$V_{\text{ullage, initial}} = 0.1 \cdot V_{\text{tot}} = 1.33 \text{ m}^3 \quad (53)$$

The main tank is implemented as a sphere body, depending on the optimal internal radius. The total volume of such a geometry is defined as:

$$V = \frac{4}{3}\pi r_{tank}^3 \quad (54)$$

where r_{tank} is the internal radius. A spherical tank is favored due to superior structural efficiency and lower mass. The required wall thickness is derived from the thin-wall approximation:

$$t = \frac{P \cdot r_{tank}}{\sigma_{adm}} \quad (55)$$

where $P = 100$ bar is the internal pressure, r is the radius, and $\sigma_{adm} = 900$ MPa is the allowable stress for carbon/epoxy composite materials McLaughlan et al. [2011], Kumar et al. [2022]. The structural mass is then calculated based on the wetted surface area and composite density $\rho_{struct} = 1600$ kg/m³.

4.7.2 Pressurant System

Autogenous pressurization has been discarded for this design due to significant long-term losses. Indeed, pressurant mass losses were estimated at 1–2% every 2 hours due to redissolution or thermal contraction, potentially leading to unacceptable inefficiencies over long coasting phases. In our case the shuttle should be able to stay inactive during a long time in space. For this reason, a classic inert gas system is chosen.

Helium is used as the pressurant due to its low molar mass, chemical inertness, and favorable storage properties at high pressures. To pressurize the ullage volume from 1.33 m³ to 13.33 m³ at 100 bar, we use the ideal gas law:

$$n_{He} = \frac{P_{tank} \cdot \Delta V}{RT} \quad (56)$$

Assuming an isothermal process at $T = 300$ K, the required helium quantity is computed from the volume expansion of the ullage. Since the propellant tank is initially filled at 98.5% and the ullage grows from 1.5% to 100% of the total volume, the net expansion is $\Delta V = V_{total} - V_{ullage}$.

The corresponding helium mass is deduced with the following equation ($M_{He} = 0.004$ kg/mol):

$$m_{He} = n_{He} \cdot M_{He} \quad (57)$$

We choose to store this amount of gas at 400 bar for mass and volume reasons. the total volume required is:

$$V_{He, tot} = \frac{P_{usage} \cdot \Delta V}{P_{storage} - P_{usage}} \quad (58)$$

The helium is stored in multiple composite overwrapped pressure vessels (COPV) with cylindrical geometry and hemispherical ends, each of fixed length $L = 2$ m. The radius r of each tank is computed numerically from the volume expression:

$$V = \frac{4}{3}\pi r^3 + \pi r^2 L \quad (59)$$

The corresponding structural thickness is:

$$t = \frac{P_{\text{storage}} \cdot r}{\sigma_{\text{adm}}} \quad (60)$$

We obtain the following result for our tank configuration. We choose 4 Helium tanks in order to maintain the pressure inside the main tank.

Tank Parameter	Value
Tank volume	13.5333 m ³
Tank radius (spherical)	1.478 m
Tank type	Spherical
Cylinder length	0.0000 m
Tank wall thickness	0.0118 m
Tank area	27.4634 m ²
He tank radius	0.3881 m
He tank volume	1.1111 m ³
He tank thickness	0.0120 m
He tank surface area	6.5021 m ²
Total tank height	2.9567 m

Table 19: Main propellant and helium tank dimensions

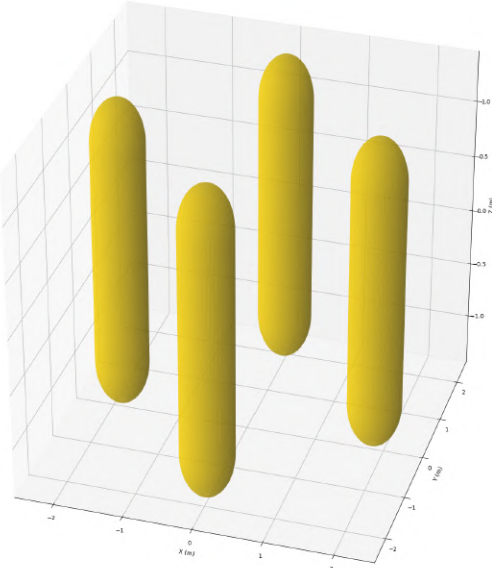


Figure 50: He Tanks

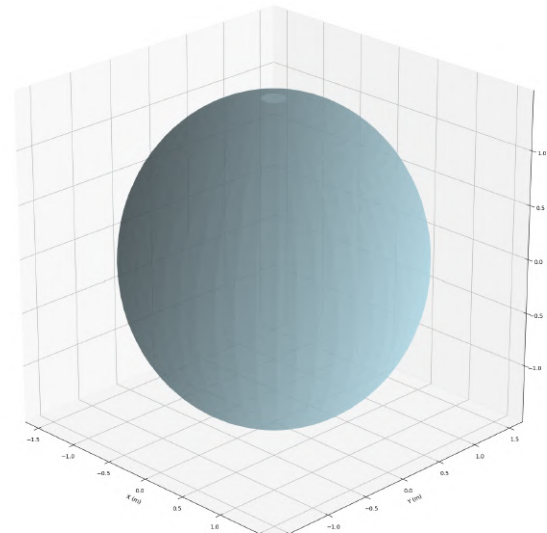


Figure 51: NOFBX tank

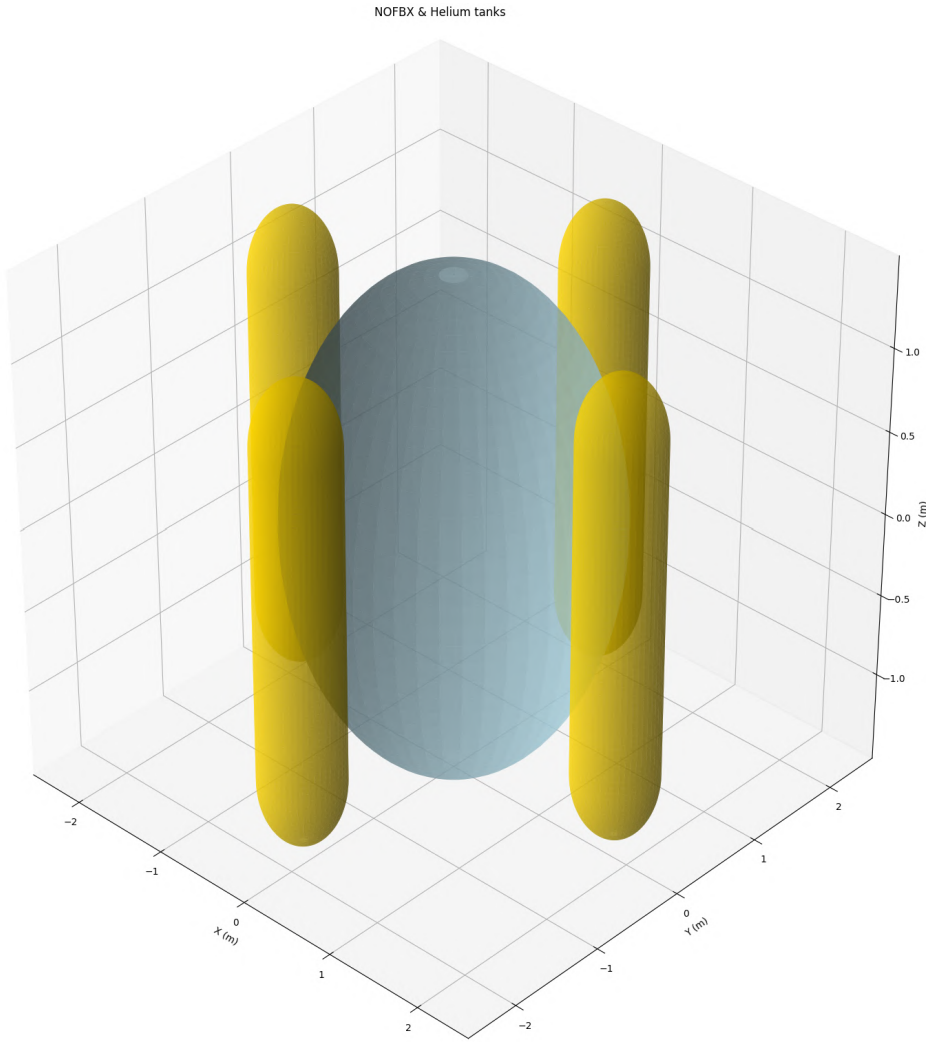


Figure 52: NOFBX + He tanks architecture

4.8 Mass budget

The total propulsion-related mass budget includes the propellant, its storage system, the helium pressurization system, and the engines. All tanks (both for propellant and helium) are implemented as COPVs (Composite Overwrapped Pressure Vessels). These consist of an internal liner made of aluminum 6061-T6 for impermeability and chemical compatibility with NOFBX, and a structural overwrap made of T700 carbon fiber impregnated with epoxy resin.

The composite material used is assumed to consist of 65% T700 carbon fiber by volume, which offers good mechanical properties with a conservative design stress of $\sigma_{\text{adm}} = 900 \text{ MPa}$ after applying a safety factor of 2. The following parts describe the mass estimation of each component.

The main propellant tank is modeled as a sphere. Its thickness is determined using thin-wall theory and the allowable stress of the composite overwrap. The corresponding mass is denoted as:

$$m_{\text{tank, prop}} = \frac{t_{\text{tank}} \cdot \rho_{\text{struct}} \cdot S_{\text{tank}}}{r_{\text{tank}}} \quad (61)$$

The helium storage tanks are assumed to be cylindrical with hemispherical ends, providing a good balance between structural efficiency and integration compactness. For each tank, the total outer surface is given by:

$$S_{\text{He}} = 4\pi r^2 + 2\pi r L \quad (62)$$

The structural mass of a single helium tank is:

$$m_{\text{tank, He}} = \frac{t \cdot \rho_{\text{struct}} \cdot S_{\text{He}}}{r} \quad (63)$$

Summing over the N helium tanks gives the total pressurant storage structure mass:

$$m_{\text{press}} = m_{\text{He}} + N \cdot m_{\text{tank, He}} \quad (64)$$

Each engine includes three main structural contributors: the combustion chamber, the nozzle, and the propellant feed lines (tuyauteerie). The chamber and nozzle wall thicknesses are computed from hoop stress considerations using a conservative allowable stress $\sigma_{\text{adm, engine}} = 250 \text{ MPa}$ for Inconel 718. The chamber wall thickness is:

$$t_{\text{chamber}} = \frac{P_c r_c}{\sigma_{\text{adm, engine}}} \quad (65)$$

and the nozzle throat thickness is:

$$t_{\text{throat}} = \frac{P_t r_t}{\sigma_{\text{adm, engine}}} \quad (66)$$

The chamber structural volume is given by:

$$V_{\text{chamber}} = \pi(r_c + t_{\text{chamber}})^2(L_c + 2t_{\text{chamber}}) - \pi r_c^2 L_c \quad (67)$$

And the nozzle structural volume is:

$$V_{\text{nozzle}} = \pi \left(\left(\frac{D_t + D_e}{2} + t_{\text{throat}} \right)^2 - \left(\frac{D_t + D_e}{2} \right)^2 \right) L_n \quad (68)$$

Multiplying each volume by the structural density $\rho_{\text{engine}} = 8250 \text{ kg/m}^3$ yields the mass of each part:

$$m_{\text{chamber}} = V_{\text{chamber}} \cdot \rho_{\text{engine}}, \quad m_{\text{nozzle}} = V_{\text{nozzle}} \cdot \rho_{\text{engine}} \quad (69)$$

The propellant is routed from the storage tank to the combustion chamber through a high-pressure piping system. In this preliminary design, we assume that the piping is made of stainless steel or high-strength alloy with a density of $\rho = 8000 \text{ kg/m}^3$ and an allowable stress of $\sigma_{\text{adm}} = 130 \text{ MPa}$. The internal operating pressure is taken as 100 bar, matching the propellant tank conditions. A single pipe segment of length $L = 2 \text{ m}$ and internal diameter $D = 0.05 \text{ m}$ is considered. The mass of the propellant feed lines is obtained via pipe pressure design, using:

$$t_{\text{wall}} = \frac{P_{\text{tank}} D_{\text{tuy}}}{2\sigma_{\text{tuy}}} \quad (70)$$

$$V_{\text{tuy}} = \pi \left(\left(\frac{D_{\text{tuy}}}{2} + t_{\text{wall}} \right)^2 - \left(\frac{D_{\text{tuy}}}{2} \right)^2 \right) L_{\text{tuy}} \quad (71)$$

$$m_{\text{tuy}} = V_{\text{tuy}} \cdot \rho_{\text{tuy}} \quad (72)$$

The total mass of one engine is:

$$m_{\text{engine}} = m_{\text{chamber}} + m_{\text{nozzle}} + m_{\text{tuy}} \quad (73)$$

And the total for all N_{engines} is:

$$m_{\text{engines}} = N_{\text{engines}} \cdot m_{\text{engine}} \quad (74)$$

The complete propulsion system mass including tanks, helium, and engines is then:

$$m_{\text{storage}} = m_{\text{propellant}} + m_{\text{tank, prop}} + m_{\text{press}} \quad (75)$$

$$m_{\text{total}} = m_{\text{storage}} + m_{\text{engines}} \quad (76)$$

With the chosen parameters, the propulsion-related mass is:

Component	Mass (kg)
Chamber mass	30.640 kg
Nozzle mass	50.918 kg
Pipes mass	22.307 kg
Engine mass (1 engine)	103.865 kg
Total engine mass (6 engines)	623.191 kg
Main propellant tank mass	351.531 kg
Helium mass	213.829 kg
Helium tanks structural mass	1331.622 kg
Tank + Propellant + Helium	13 896.983 kg
Total propulsion system mass	14 520.174 kg

Table 20: Mass breakdown of the propulsion system

The propulsion system mass budget presented in Table 20 shows that the total mass remains below 40% of the shuttle's total wet mass (40 tonnes). This margin is satisfactory considering that the propulsion system includes all main components: combustion chambers, nozzles, piping, propellant tanks, helium pressurization system, and six engines.

However, it is important to note that the estimated engine mass of 103.9 kg per unit may be underestimated. While the chamber and nozzle structural masses are rigorously derived from geometric and material assumptions, real flight-qualified engines typically include additional subsystems such as actuators, valves, instrumentation, thrust vector control mounts, and thermal protection layers. Taking this into account, a more realistic engine mass would likely be around 200 kg, which would raise the total propulsion mass by approximately 570 kg. This still remains within acceptable margins.

Further improvements to the mass estimation could be made by refining the modeling of the pipework system. At present, pipe mass is estimated using average parameters. In future iterations, the full flow architecture could be studied using dedicated fluid mechanics software (e.g., ANSYS Fluent or OpenFOAM) to simulate pressure losses, flow velocities, and optimize diameters and wall thicknesses. This would also help evaluate pressure drops in the injector manifolds and regenerative cooling circuit with greater precision.

5 AOCS

The Attitude and Orbit Control System (AOCS) of a space shuttle or any spacecraft is the subsystem that ensures that the vehicle maintains or changes its orientation and trajectory as required during various phases of the mission. For the StarCheap space shuttle, which must operate across orbital insertion, flight, rendez-vous, docking, debris capture reentry, and landing phases, the AOCS will have particularly stringent requirements.

The AOCS system design of a space shuttle encompasses six key aspects. First, it provides full 3-axis attitude control (pitch, yaw, roll) using thrusters, engine gimbals, and aerodynamic surfaces, depending on the flight phase. AOCS also handles trajectory and orbital control via its main propulsion system and the reaction control system (RCS) for tasks such as orbit insertion, rendezvous, docking, and deorbiting. The system relies on a suite of sensors to determine the shuttle's orientation and position - these sensors must be aptly chosen to answer precision and availability needs. AOCS requires on-board guidance, navigation and control software (GNC), integrates sensor data and computes commands to control the shuttle's motion. The system must include redundancy and fault-tolerant designs to ensure reliability, with multiple backups and fault detection protocols. Lastly, AOCS operates in distinct modes tailored to each mission phase—launch, orbit, reentry, landing, and safe mode—each with specific control strategies and actuator usage.

5.1 AOCS requirements

The specific requirements for the AOCS subsystem are resumed in the table below:

Table 21: StarCheap GNC Subsystem Requirements

Requirement ID	Description
GNC-REQ-001	The shuttle must control and maintain its orientation in space with minimal drift, especially during delicate operations like docking or debris capture.
GNC-REQ-002	The system must ensure sufficient accuracy for nominal operations.
GNC-REQ-003	The system must be able to precisely acquire, determine and predict the spacecraft's position and velocity in orbit, considering orbital dynamics and external influences.
GNC-REQ-004	The AOCS must include redundancy to ensure mission success in case of failures.
GNC-REQ-005	The system must support rendezvous with a space station or debris, ensuring accurate trajectory calculations and adjustments during approach.
GNC-REQ-006	The system should be 80% reusable.

Continued on next page

Requirement ID	Description
GNC-REQ-007	The mass of the system must represent 4% of the total mass of the shuttle.
GNC-REQ-008	System must be fully autonomous.
GNC-REQ-009	Components must resist to the specified temperature, radiations, particles, micrometeoroids, debris... to ensure the shuttle's nominal operation under the mission conditions.
GNC-REQ-010	System must ensure the shuttle follows optimal fuel or time efficient trajectories for the different mission phases.
GNC-REQ-011	Must ensure precise knowledge of the shuttle's attitude.
GNC-REQ-012	The system should be capable of adjusting and maintaining the spacecraft's orbit, including orbit circularization, rendezvous, and deorbit maneuvers.
GNC-REQ-013	The system must be able to detect potential collisions and autonomously avoid them in real-time.
GNC-REQ-014	The system must support rendezvous with a space station or debris, ensuring accurate trajectory calculations and adjustments during approach.
GNC-REQ-015	The system must be able to detect, track and identify debris in space.
GNC-REQ-016	The system must ensure controlled re-entry, managing the spacecraft's orientation and velocity to achieve proper aerodynamic behavior and safe descent through the atmosphere.
GNC-REQ-017	The system shall enable precise control of the descent phase, adjusting the spacecraft's orientation and flight path for an accurate and safe landing.
GNC-REQ-018	The system should ensure real-time, high-precision navigation to support mission-critical operations like rendezvous, docking, debris capture and landing.
GNC-REQ-019	System should be able to receive information of debris localization and perform avoidance maneuvers if necessary.
GNC-REQ-020	The IMU shall be positioned at the center of mass of the shuttle.

5.2 System choices

The choice of attitude control means is highly dependent on the shuttle's architecture. With a Starship-like blunt shape with little to no aerodynamic glide surfaces and such a large system mass, the choice of control means are in fact quite limited for such a vehicle.

Considering traditional attitude control means, reaction wheels and control moment gyroscopes (CMGs) offer precise, propellant-less attitude control through angular momentum exchange. These systems are commonly employed in small-to-medium spacecraft require-

ing high pointing accuracy and low-disturbance environments. However, their scalability to a shuttle-class vehicle is limited by mass, mechanical complexity, and diminished effectiveness in high-inertia platforms. Furthermore, their inability to generate rapid or large-angle maneuvers, combined with saturation issues and the need for desaturation mechanisms, significantly limits their utility in high-dynamic or large spacecraft applications.



Figure 53: ISS Control Moment Gyroscopes Charles Gurrissi and Ferguson [2009]

On the ISS for instance, large CMGs are used for maintaining and adjusting the attitude without consuming propellant. Each CMG consists of a high-speed spinning rotor mounted on a gimbal, which, when rotated, induces a reaction torque that changes the station's orientation. CMGs are ideal for the ISS due to their ability to provide continuous, precise three-axis control necessary for solar array alignment, docking, and scientific operations, all without expelling mass. When the system accumulates excess angular momentum, it is desaturated using thrusters from visiting vehicles or the Russian segment Charles Gurrissi and Ferguson [2009]. Such a system for the shuttle would impose a large mass, power budget and necessary room to accomodate the gimbal engine. Angular velocity response and requirements would also probably require large dimensions for the CMG, as well as an array of thrusters to desaturate, rendering the utility of the CMG questionable.

Although our main propulsion system is equipped with thrust vector control (TVC), it achieves limited attitude regulation by gimbaling the main engines, thereby altering the direction of the thrust vector relative to the vehicle's center of mass. This method provides high control authority and rapid response during powered flight phases, including vertical landing burns. For shuttle-class vehicles, TVC of the engines is an integral part of the launch and landing control strategy. However, TVC is only operable when the engines are active (which is only the case for short and precise durations imposed by the mission analysis and propulsing sizing) and is thus unsuitable for fine attitude adjustments during coasting or quiescent phases. Additionally, the use of main engine gimbaling for small adjustments is inefficient and potentially thermally taxing. We note particularly that the propellant mass budgets for the main propulsion system did not account for attitude

control.

Aerodynamic surfaces, including body flaps and fins, are responsible for attitude control during atmospheric flight phases. These surfaces utilize aerodynamic forces to generate control moments, enabling pitch, yaw, and roll adjustments through modulation of drag and lift vectors. On a vehicle such as the Starship, these control surfaces are critical during reentry, particularly during the high-drag belly-flop configuration and the subsequent pitch-up maneuver prior to landing. While effective in denser atmospheric regimes, these surfaces offer no functionality in vacuum, and their actuation systems add mass, require significant structural integration, and introduce mechanical failure modes. As such, their applicability is confined to atmospheric flight.

Given the stringent flight conditions upon reentry and the bluntness of the body, considering a reentry purely based upon propulsion capacities and the lift and drag generated by the body would be considering a fast and risky ballistic reentry, particularly when considering the hover flip maneuver and landing. Not capitalising on the possibility of slowing down the shuttle with aerodynamic surfaces would be a rather bold assumption and would put further stringent performance criteria on the propulsion system. Considerations for the available propellant at this stage, not only for the main propulsion system but also the RCS, should be made and any solutions that would alleviate the risk of running out of fuel and minimising propellant means should be taken.

RCS thrusters provide three-axis attitude control through the generation of differential torque using discrete, strategically located nozzles (often around the nose, tail and midsection). RCS thrusters are essential for maneuvering during orbital flight phases, reorienting between burns, and alignment for reentry and more complex rendezvous phases. However, the use of high-energy propellants introduces system complexity, thermal management requirements, and finite propellant limitations that can restrict mission duration and maneuverability. The choice of hot-gas, cold-gas, or vent-gas thrusters is key in dimensioning system complexity. For a shuttle-class vehicle operating in space, an RCS using propellant commonality with the primary propulsion system would be the most efficient. This integration simplifies storage and feed system design while optimizing mass efficiency.

It is noteworthy that the space shuttle used a total of 38 primary RCS engines and 6 vernier RCS engines, for all phases of flight. Divided between the FRCS (Front RCS) and the OMS pods (situated at each side of the vertical empennage), they delivered thrust from 3 to 100 kN, allowing docking maneuvers, satellite capture (with the Canadarm) and fine corrections. BLEVINS and HOHMANN [1975]

Given the stringent reentry conditions and fine corrections necessary for the shuttle's mission, the choice of a blend of an RCS and aerodynamic surfaces seems most appropriate for the StarCheap shuttle.

5.3 System efforts dimensioning

Control over the pitch, yaw and roll axes requires knowledge of how much torque and force would be necessary to move the shuttle in every mission phase.

This next part dimensions the necessary angular accelerations for each phase required for maneuvering and attitude corrections, and deduces the necessary torque and thrust.

We assume a vehicle with 5m of diameter, a height of 15 m and at full mass (40 tons) in order to size the requirements in the worst case.

Assessing every phase of the mission not only ensures knowledge of the system efforts to produce, but will also help assess ΔV and propellant required for the attitude system. Assumptions are made for angular maneuvers and corrections based on a visual and data-based analysis of an array of missions using various spacecraft, all performing maneuvers similar to the shuttle's preisional operations Belair et al. [2024] Santiago et al. [2009] Goodman [1988] Gibson and Humphries [1988]. Assumptions are made for the time to execute the maneuver depending on available information and phase criticity or level of danger. Obtained torques and forces may sometimes seem quite low for such a vehicle, but by imposing low rotational rates or execution times, the required force to move the vehicle allows for a lower control authority in some cases.

For comprehension purposes, the rotational axes of the vehicle are designated as in the schematic below, with x the roll axis, z the pitch axis and y the yaw axis.

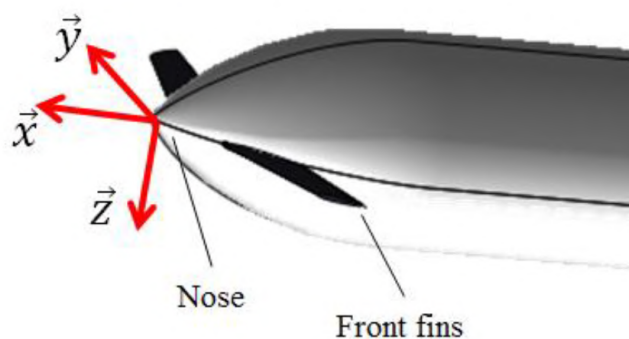


Figure 54: Shuttle Axis Denotation

5.3.1 Human factors

The acceptable rotational velocity and acceleration of the shuttle is first and foremost limited by the passengers on board. Exceeding acceleration limits can significantly impair human performance and cause injury, thereby threatening mission success and crew survival.

The NASA-STD-3001, Volume 2, Revision D outlines these limits, designed to prevent disorientation, motion sickness, and other adverse effects on the crew during sustained rotations, and also in translational accelerations.

The limits are resumed in the table below:

Axis	Max Acceleration	Max Duration (s)	Resulting Max Velocity
X (Fore-Aft)	39.2 m/s ²	5	196 m/s
Y (Lateral)	19.6 m/s ²	5	98 m/s
Z (Vertical)	39.2 m/s ²	5	196 m/s
Pitch	1.5°/s ²	0.67	1.0°/s
Yaw	1.5°/s ²	0.67	1.0°/s
Roll	1.5°/s ²	0.67	1.0°/s

Table 22: Maximum nominal translational and rotational accelerations and resulting velocities for crewed vehicle operations.

In the subsequent sections, we strive to size shuttle efforts under these limits with the highest possible margins in order to ensure crew safety and still ensure nominal operations and maneuvers. We note that translational maneuvers were not considered as they are heavily dependent on precise knowledge of the trajectory and subsequent maneuvers, and implied highly estimated assumptions for acceleration and deceleration control.

5.3.2 Reentry & Atmospheric flight

We consider moving the vehicle from orbital flight to atmospheric flight (belly flop) in nominal conditions.

In nominal flight, the only attitude maneuvers are:

- A pitch re-orientation in order to make the deorbitation/reentry burn at the right angle of attack
- A roll re-orientation to ensure the heat shield is Earth-facing
- A yaw re-orientation to ensure correct flight path to the landing site.
- In-flight corrections on each axis, particularly during stringent reentry conditions

We estimate the angular deviations in terms of nominal flight and then worst case scenario (i.e. the shield is opposite its nominal position at reentry, the shuttle presents its engines forward instead of its nose, is facing away from the flight path).

In terms of yaw, we want to move from a prograde inclined circular orbit, to a North-South reentry trajectory. To align a shuttle in a circular inclined orbit (up to 60°) with a north-south ground track for reentry and landing, a reorientation in the yaw axis is required. Initially, the vehicle's longitudinal axis is aligned with the orbital velocity vector, which lies tangential to the inclined orbital path. However, to transition from this eastward-leaning trajectory to a descent along a meridional (north-south) ground track, the vehicle must yaw away from the orbital prograde direction. The required yaw angle is approximately given by:

$$\theta = \arccos(\sin(i)) \quad (77)$$

This angle represents the deviation between the orbital ground track and a line of longitude. If we think of the orbital velocity vector as having components in the east-west and north-south directions, the sine of the inclination gives the north-south component of

that vector relative to the Earth's surface. To align the shuttle with the pure north-south direction, it must yaw so that its heading matches that component. In the case of a 40° inclined orbit, the yaw maneuver to be made is approximately 50°. In the case of a 60° inclination, the yaw maneuver to be made is approximately 30°. As the shuttle should not deviate from 40-60° in inclination for its orbits as it does not have the necessary available propellant to do so, we can assume yaw maneuvers will only have to be made between those values.

For the pitch maneuver, assuming a pitch angle of 0° for orbital flight, the swing to be made should match the desired angle of attack for reentry; i.e. 70° (in reality the angle of attack is variable during reentry, but we consider the highest value for sizing purposes).

Assuming no particular controlled orientation of the heat shield during orbital flight, a median value of the shield's position could be at a 90° angle from the Earth-facing position. We consider this the nominal maneuver case.

Axis	Nominal maneuver	Worst-case maneuver
Pitch	70°	180°
Yaw	30°	50°
Roll	90°	180°

Table 23: Reentry & Descent angular maneuvers

We also estimate the small angular corrections to be made during the flight. We note that the most stringent control is to be made on the yaw axis. During a flat-body descent, the vehicle is oriented at a high angle to the oncoming airflow to maximize aerodynamic drag and reduce terminal velocity. While this configuration provides inherent pitch stability due to symmetric pressure distribution about the lateral axis, it is directionally unstable in yaw. In the absence of vertical stabilizers or other passive restoring mechanisms, any small yaw deviation can lead to asymmetric aerodynamic loading across the vehicle's surface. This asymmetry generates a yawing moment that reinforces the initial deviation rather than damping it, creating a divergent dynamic response. If uncorrected, this can induce coupled motion across yaw, pitch, and roll axes, ultimately leading to a flat spin or tumbling behavior. As such, we assume higher yaw deviations during flight than can be expected (up to 5°), as we want to ensure maximum correction capacity.

Axis	Minimum expected correction	Maximum expected correction
Pitch	2°	5°
Yaw	1°	15°
Roll	2°	10°

Table 24: Reentry & Descent angular corrections

We now estimate the required time to make these corrections based on the criticality of the phase.

Small corrections should be made as quickly as possible, particularly on the yaw and roll axes. For example, a misorientation of the heat shield could be very problematic for the

integrity of the shuttle and its passengers. Tolerances on the pitch angle are larger as we have inherent pitch stability due to symmetric pressure distribution about the lateral axis.

Positionning the shuttle for reentry is typically done gradually on vehicles such as the Space Shuttle or the Starship, in order to avoid structural loads or instability. Maneuver time is evaluated at a few minutes in nominal conditions.

Axis	Maneuvers			
Pitch	Nominal	90 s	Worst	200 s
Yaw	Nominal	90 s	Worst	180 s
Roll	Nominal	120 s	Worst	200 s
Axis	Corrections			
Pitch	Time for smallest correction	5 s	Time for largest correction	10 s
Yaw	Time for smallest correction	5 s	Time for largest correction	20 s
Roll	Time for smallest correction	5 s	Time for largest correction	12 s

Table 25: Maneuver and Correction Timings for Reentry & Descent

From the angle to correct and time to correct we can derive the necessary angular accelerations from :

$$\alpha = \frac{2\theta}{t^2} \quad (78)$$

Maneuvers				
Pitch	Nominal Acc	0.0173 °/s	Worst case Acc	0.009 °/s
Yaw	Nominal Acc	0.0074 °/s	Worst case Acc	0.0031 °/s
Roll	Nominal Acc	0.0125°/s	Worst case Acc	0.009 °/s
Corrections				
Pitch	Acc for min correction	0.1 °/s	Acc for max correction	0.16 °/s
Yaw	Acc for min correction	0.075 °/s	Acc for max correction	0.08 °/s
Roll	Acc for min correction	0.1389 °/s	Acc for max correction	0.16 °/s

Table 26: Maneuver and Correction Required Accelerations for Reentry & Descent

Making a cylindircal approximation for the shape of the shuttle, we can estimate the moment of inertia, which depends on spacecraft geometry and mass distribution on each axis.

$$I_{\text{roll}} = \frac{1}{2}mr^2, \quad (79)$$

$$I_{\text{pitch}} = I_{\text{yaw}} = \frac{1}{12}m(3r^2 + h^2) \quad (80)$$

Using the moment of inertia we can determine the necessary torque from the angular acceleration using Newton's Second Law for Rotation:

$$\tau = I\alpha \quad (81)$$

We make assumptions as to the placement of the control systems in order to deduce lever arms in order to estimate the necessary force to produce the required torque.

Maneuvers				
Pitch	Nominal Torque	302 Nm	Worst case Torque	157 Nm
Yaw	Nominal Torque	129 Nm	Worst case Torque	54 Nm
Roll	Nominal Torque	109 Nm	Worst case Torque	79 Nm
Corrections				
Pitch	Torque for min correction	2793 Nm	Torque for max correction	1745 Nm
Yaw	Torque for min correction	1396 Nm	Torque for max correction	1309 Nm
Roll	Torque for min correction	1396 Nm	Torque for max correction	1212 Nm

Table 27: Maneuver and Correction Required Torque for Reentry & Descent

- We place the center of mass at coordinates [5;0;0]
- Roll : at the edges of the bottom of the shuttle, coordinates [0;2,5;0]
- Pitch/Yaw: Placed around the top of the shuttle to ensure maximum lever arm and pitch control, coordinates [13;2,5;0]

We obtain the following lever arms:

$$L_{\text{roll}} = 5m \quad (82)$$

$$L_{\text{yaw/pitch}} = 8m \quad (83)$$

The required force is deduced from:

$$F = \frac{\tau}{L} \quad (84)$$

Maneuvers				
Pitch	Nominal Force	38 N	Worst case Force	20 N
Yaw	Nominal Force	16 N	Worst case Force	7 N
Roll	Nominal Force	22 N	Worst case Force	16 N
Corrections				
Pitch	Force for min correction	349 N	Force for max correction	218 N
Yaw	Force for min correction	175 N	Force for max correction	164 N
Roll	Force for min correction	279 N	Force for max correction	242 N

Table 28: Maneuver and Correction Required Force for Reentry & Descent

In the following sections the calculations will not be detailed, only the results and hypotheses will be exposed.

5.3.3 Hover flip

The hover flip maneuver typically refers to the process where the vehicle transitions from a horizontal descent orientation to a vertical landing position. This maneuver is most commonly performed at low altitude (typically below 10 km) and involves significant angular changes, especially in pitch, with small deviations in yaw and roll as the spacecraft transitions to a stable vertical position.

The spacecraft starts in a belly-first orientation with a pitch angle near 90° (horizontal flight). During the flip, the pitch angle changes dramatically from 90° to 0° (nose-up) as the spacecraft rapidly rotates around the pitch axis. The attitude control system does not handle the burden of this flip, it is the main propulsion system that handles the majority of the flip with its gimballed engines. In this scenario we only consider corrections, which should range from $1\text{--}2^\circ$. The maneuver should not exceed 10s in duration.

Yaw primarily affects lateral (left-right) orientation. During a hover flip, small deviations in yaw may occur due to asymmetric forces from aerodynamic surfaces or engine thrust vectors. Expected deviations range from $\pm 5^\circ$ to $\pm 10^\circ$.

Roll axis will experience minimal motion during the hover flip, as the spacecraft primarily rotates around the pitch axis. Expected roll deviation range from $\pm 2^\circ$ to $\pm 5^\circ$ at most during the maneuver.

Axis	Minimum angle	Maximum angle
Pitch	1°	2°
Yaw	5°	10°
Roll	2°	5°
Axis	Required torque	Required Torque
Pitch	8727 Nm	2793 Nm
Yaw	1745 Nm	1551 Nm
Roll	3879 Nm	2424 Nm
Axis	Required force	Required force
Pitch	1091 N	349 N
Yaw	218 N	194 N
Roll	776 N	485 N

Table 29: Hover Flip Required Efforts for correction

Pitch and yaw corrections should be made very fast in order to not destabilise or delay the maneuver.

The necessary angular corrections, correction times, accelerations, torques and forces are resumed in the table below.

5.3.4 Orbital flight

The Reaction Control System (RCS) is not used for primary propulsion or long-distance orbital maneuvers like transfers between orbits or rendezvous points. Those maneuvers are handled by the main engines.

However, attitude control is necessary in two instances, firstly for burn alignment and secondly for attitude corrections along the flight.

Assuming nominal $[0^\circ; 0^\circ; 0^\circ]$ orientation in yaw, pitch and roll during flight in the orbital plane, we can estimate necessary changes and corrections.

Alignment for a burn induces maneuvering on the yaw and pitch axis.

For a prograde burn (i.e. with no out-of plane maneuvering), pitch and yaw are adjusted so vehicle nose points along the velocity vector (orbital track). This should be the case if the vehicle is placed on an orbit of same inclination as the station.

For a burn including inclination change (such as when the shuttle leaves the station to rendezvous with the debris), the burn must be made at a node and the direction includes a component perpendicular to the orbital plane — called the normal direction. If the burn is made at a node, we align with the new composite vector; this would only indicate only a pitch change. A burn outside of a node would indicate also a yaw change, which could be quite significant depending on the misalignment with the burn vector.

The shuttle and the mission are sized for a 10° inclination change at most. In the nominal case, we would have a 10° pitch change and a 0° yaw change if the maneuver is made at a node. In the worst-case scenario—making a 10° inclination change away from the nodes, such as at mid-orbit (90° from a node)—the required burn vector is nearly perpendicular to the orbital velocity vector, meaning the spacecraft must rotate its nose 80° – 90° upward from prograde to align with the thrust direction. This results in a pitch change of ≈ 80 – 90° and a yaw change of maximum 30° .

In this spirit, the necessary efforts for orbital maneuvering are sized and resumed in the following table.

Axis	Minimum angle	Maximum angle
Pitch	10°	90°
Yaw	0°	30°
Axis	Required torque	Required Torque
Pitch	96.96 Nm	218.17 Nm
Yaw	0 Nm	72.72 Nm
Axis	Required force	Required force
Pitch	12.12 N	27.27N
Yaw	218 N	9.09 N

Table 30: Orbital Flight Required Efforts for Maneuvering

We assume no roll correction is necessary for thermal control, but note we must keep as true as possible on this axis so as to not disorientate astronauts in orbit. Small RCS adjustments in the range of 0.5° to 1.5° may be applied as needed to counter drift, with peak corrections not exceeding around 2° .

During orbital flight, pitch and yaw corrections are small and used to maintain the spacecraft’s planned nominal orientation. These adjustments range from 0.5° to 2° , made through brief RCS thruster pulses to counteract gradual drift or to align with specific targets or reference points.

5.3.5 Rendezvous

Rendezvous maneuvers comprise a series of orbital adjustments that gradually bring a spacecraft into the same orbit and position as a target vehicle, without entering the final docking phase. These include phasing burns to match orbital periods and close longitudinal distance, height adjustment maneuvers to raise or lower the orbit for timing alignment, plane change burns (if needed) to match orbital inclination, and coelliptic burns to circularize the orbit near the target.

Throughout the process, the spacecraft performs attitude maneuvers—adjusting pitch, yaw, and occasionally roll—to orient correctly for burns, tracking, and communication.

Axis	Minimum angle	Maximum angle
Pitch	0.5°	2°
Yaw	0.5°	2°
Roll	0.5°	2°
Axis	Required torque	Required Torque
Pitch	174.53 Nm	2792 Nm
Yaw	174.53 Nm	2792 Nm
Roll	87.26 Nm	1396 Nm
Axis	Required force	Required force
Pitch	21.82 N	349 N
Yaw	21.82 N	349 N
Roll	17.45 N	279.25 N

Table 31: Orbital Flight Required Efforts for correction

The goal is to arrive in a matching orbit within close proximity (typically a few kilometers) of the target, aligned in velocity and plane, ready to begin approach and docking if needed.

Pitch remains the most actively used axis during rendezvous as it is critical for aligning the spacecraft with burn vectors during phasing, plane alignment, or coelliptic burns, and for reorienting relative to Earth and the target. In nominal operations, pitch changes of 10°–30° are typical, taking 15–60 seconds, especially when switching from one burn attitude to another. Worst-case pitch demands—like aligning for a complex off-nominal burn or mid-rendezvous correction—can require up to 90°, taking 1–3 minutes. Small pitch corrections for drift or attitude trim stay around 0.5°–2° and are made frequently in 5–10 second bursts.

Yaw becomes more active than before due to the changing orbital geometry between chaser and target. It's used to adjust the spacecraft's heading toward the target during coasting phases or when positioning for lateral components of burns (like radial-in or out). Nominal yaw maneuvers stay within 10°–25°, taking up to 60 seconds, especially when transitioning between burn geometries or re-targeting the spacecraft's nose. Worst-case yaw could reach 30°–45°, such as when correcting a large lateral misalignment or if the target's orbital plane differs slightly. Like pitch, small yaw corrections of 0.5°–2° are frequent and fast, done for stability and alignment.

Roll is kept as steady as possible to prevent disorientation and ensure predictable sensor or antenna alignment. Nominal roll corrections are minimal—±1° to ±2°, made with short pulses. Worst-case roll reorientations, such as if the vehicle must “right itself” after drifting out of plane or rotating for thermal/sensor alignment, could reach 10°–15°, typically resolved in 30–60 seconds. But frequent or aggressive roll is generally avoided until final approach or docking.

Axis	Minimum angle	Maximum angle
Pitch	30°	90°
Yaw	25°	45°
Roll	2°	15°
Axis	Required torque	Required Torque
Pitch	291 Nm	218 Nm
Yaw	242 Nm	109 Nm
Roll	87 Nm	73 Nm
Axis	Required force	Required force
Pitch	36 N	27 N
Yaw	30 N	14 N
Roll	17 N	15 N

Table 32: Rendezvous Required Efforts for maneuvers

Axis	Minimum angle	Maximum angle
Pitch	0.5°	2°
Yaw	0.5°	2°
Roll	0.5°	2°
Axis	Required torque	Required Torque
Pitch	698 Nm	698 Nm
Yaw	698 Nm	698 Nm
Roll	349 Nm	349 Nm
Axis	Required force	Required force
Pitch	87 N	87 N
Yaw	87 N	87 N
Roll	70 N	70 N

Table 33: Rendezvous Required Efforts for corrections

5.3.6 Docking

During the docking phase, spacecraft must adhere to stringent attitude control requirements to ensure safe and successful mating. The International Docking System Standard (IDSS) Program [2022] specifies precise limits for rotational rates and misalignments across all three axes:

- The combined pitch and yaw misalignment must not exceed 4.0 degrees, with a maximum rotational rate of 0.2 degrees per second for the vector sum of pitch and yaw rates. These constraints ensure that the spacecraft aligns accurately with the docking port, minimizing the risk of structural stress or misalignment during contact.
- Roll misalignment is also limited to 4.0 degrees, with a maximum rotational rate of 0.2 degrees per second. Maintaining roll within these parameters is crucial for proper alignment of docking mechanisms and to prevent undue torque upon connection.

These stringent requirements necessitate precise and controlled attitude adjustments during the final approach to docking. Docking spacecraft employ fine-tuned thruster firings

or reaction control systems to achieve the necessary alignment, often taking 30 to 90 seconds for final orientation maneuvers, depending on the initial misalignment.

Based on the standard, we establish that the docking phase should only be subjected to corrections, as the rendezvous phase should have ensured the final alignment. We base the maximal corrections to be applied on the maximum rotational rate, as the worst case scenario.

Axis	Minimum angle	Maximum angle
Pitch	1°	4°
Yaw	1°	4°
Roll	0.5°	4°
Axis	Required torque	Required Torque
Pitch	1396 Nm	349 Nm
Yaw	1296 Nm	349 Nm
Roll	970 Nm	698 Nm
Axis	Required force	Required force
Pitch	175 N	44 N
Yaw	175 N	44 N
Roll	194 N	140 N

Table 34: Docking Required Efforts for corrections

5.3.7 Debris capture

The capture of a debris using a net involves complex maneuvers and precise attitude adjustments across all three rotational axes. These maneuvers ensure the shuttle's alignment with the target, successful capture and stabilisation post-capture and during storage procedures.

Pitch is the most actively used axis during a net-based debris capture maneuver, particularly because the net deploys from the ventral (belly) side of the shuttle.

To ensure proper alignment of the net toward the incoming debris, the shuttle must pitch its nose upward or downward depending on the relative position of the target.

In nominal scenarios, pitch maneuvers range from 15° to 35°, taking 30 to 120 seconds to complete at a rate of 0.2° to 0.5° per second. These changes occur during the final alignment phase when the debris is within visual or sensor tracking range.

In worst-case conditions—such as large initial misalignments or last-minute trajectory changes from the debris—pitch adjustments of up to 60° may be required, potentially taking 3 to 5 minutes for a smooth and safe maneuver.

After capture, smaller pitch trims of 0.2° to 2° may be used to dampen induced oscillations or residual angular momentum.

Yaw is essential for lateral alignment between the shuttle and the debris. Because orbital debris may not always follow a purely head-on approach vector, the shuttle must yaw to align the net's deployment axis with the debris path.

Under nominal conditions, yaw adjustments typically fall within 10° to 25°, requiring 20 to 90 seconds of maneuver time at moderate rates of 0.2°/s. These adjustments are

generally made during the approach phase to fine-tune targeting.

In more challenging cases—such as an angled intercept trajectory or if the shuttle needs to realign for a second net attempt—yaw corrections may rise to 45°, requiring up to 4 minutes of controlled rotation.

Small yaw corrections, usually under 2.5°, are frequently made in the final seconds before deployment to maintain tracking accuracy.

Axis	Minimum angle	Maximum angle
Pitch	35°	60°
Yaw	25°	45°
Roll	10°	20°
Axis	Required torque	Required Torque
Pitch	85 Nm	23 Nm
Yaw	108 Nm	27 Nm
Roll	86 Nm	24 Nm
Axis	Required force	Required force
Pitch	11 N	3 N
Yaw	13 N	3 N
Roll	17 N	5 N

Table 35: Debris Capture Required Efforts for maneuvers

While roll is used less dynamically during net capture operations, it plays a critical role in ensuring the correct orientation of the net deployment plane. Since the net deploys from the belly of the shuttle, maintaining a level roll attitude ensures that the net is aligned properly with the target’s flight path. Maintaining accurate roll orientation is particularly important to avoid skewed or ineffective net deployment, which could compromise the mission.

Nominal roll corrections range from 5° to 10°, taking 15 to 45 seconds at rates between 0.1° and 0.3° per second. These maneuvers are made just before net deployment to fine-tune horizontal alignment.

In worst-case scenarios—such as unanticipated roll drift or a rotated debris orientation—larger roll adjustments of 15° to 20° may be needed, typically over 1 to 2 minutes.

Once the debris has been captured in the net, the shuttle-debris system may experience residual angular momentum, especially if the debris was tumbling or asymmetrical. This can lead to induced pitch, yaw, and roll oscillations, estimated in the 10° to 20° range. Stabilization following net capture may require coordinated thruster activity across all axes and could take anywhere from 5 to 15 minutes, depending on the severity of the induced motion and the responsiveness of the shuttle’s control systems. The maneuvers should not be made too quickly in order to not induce a swing motion in the tether, that may bring the debris crashing into the shuttle’s side. As they are made slowly over time, their necessary thrust will not be of high magnitude and is thus not sized.

Axis	Minimum angle	Maximum angle
Pitch	0.2°	2°
Yaw	0.2°	2.5°
Roll	0.5°	2°
Axis	Required torque	Required Torque
Pitch	70 Nm	19 Nm
Yaw	70 Nm	18 Nm
Roll	87 Nm	22 Nm
Axis	Required force	Required force
Pitch	9 N	2 N
Yaw	9 N	2 N
Roll	17 N	4 N

Table 36: Debris Capture Required Efforts for corrections

5.3.8 Orbital insertion

Upon detachment from a launch vehicle (such as a booster or upper stage), a shuttle must perform rapid stabilization and re-orientation maneuvers to establish safe, autonomous control and prepare for orbital insertion. The initial seconds after separation are typically pre-programmed but require real-time corrections due to slight imbalances or off-nominal forces from the separation mechanism.

In this section, we assume corrections after nominal positionning are the same as orbital flight.

Pitch is the primary axis used to orient the shuttle's prograde vector during insertion. Immediately after detachment, pitch corrections of 5° to 20° are estimated to transition from the separation trajectory to the orbital insertion attitude. These maneuvers occur over 30 to 90 seconds. In a worst-case scenario such as unexpected angular drift or slight booster misalignment, corrections of up to 35° may be required, potentially taking 2 to 3 minutes.

Yaw corrections help the shuttle align with its orbital plane and correct any sideways drift imparted by asymmetrical staging forces. Nominal yaw corrections are 5° to 15°, performed within 20 to 60 seconds at rates around 0.2°/s. Worst-case yaw corrections can reach 25°, taking up to 2 minutes, especially if staging occurred slightly off-target or if multiple small errors compounded during ascent.

Roll control ensures the shuttle is upright relative to the local vertical, both for attitude control, passenger orientation and potential thermal balance. Roll corrections range from 2° to 10°, requiring around 15 to 60 seconds. In rare cases, such as a rotating separation event, roll corrections may extend to 15°–20°, handled over 1–2 minutes.

5.3.9 Failure scenarios

In the event of a general failure — such as a loss of attitude reference, actuator fault, RCS misfire, or structural imbalance — the shuttle must perform rapid, large-scale corrective maneuvers to regain stability. These failures can result in uncontrolled rotations, misalignment with orbital trajectory, or unsafe orientations for crew or systems. Recovery depends on the magnitude and axis of the deviation, the responsiveness of onboard

Axis	Minimum angle	Maximum angle
Pitch	20°	35°
Yaw	15°	25°
Roll	10°	20°
Axis	Required torque	Required Torque
Pitch	48 Nm	38 Nm
Yaw	65 Nm	15 Nm
Roll	48 Nm	24 Nm
Axis	Required force	Required force
Pitch	6 N	5 N
Yaw	8 N	2 N
Roll	10 N	5 N

Table 37: Orbital Insertion Required Efforts for corrections

systems, and the availability of RCS propellant.

In tumbling scenarios, coordinated pitch control becomes essential to regain forward flight orientation and prevent further instability. Pitch can be severely impacted if the shuttle tips forward or backward due to off-axis thrust or sensor errors. The shuttle may enter a nose-up or nose-down attitude with pitch errors reaching 30° to 90°. Correcting such deviations typically requires 2 to 6 minutes.

Yaw disturbances are common if the shuttle's control systems misread inertial cues or if asymmetric thrust (or venting) occurs. Yaw corrections in failure scenarios often range between 25° and 60°, requiring 1.5 to 4 minutes for full recovery, depending on initial angular velocity. If not corrected quickly, yaw drift can lead to large deviations in orbital track or loss of navigation lock, complicating mission continuation.

Roll instability is especially dangerous in failure cases as it can lead to disorientation, sensor blind spots, or even system shutdowns if spinning exceeds design tolerances. Roll errors in failure events may escalate to 90°–360° of unintentional rotation and must be corrected within a few minutes.

Axis	Minimum angle	Maximum angle
Pitch	30°	90°
Yaw	25°	60°
Roll	90°	360°
Axis	Required torque	Required Torque
Pitch	73 Nm	24 Nm
Yaw	108 Nm	36 Nm
Roll	48 Nm	36 Nm
Axis	Required force	Required force
Pitch	9 N	3 N
Yaw	13 N	5 N
Roll	07 N	7 N

Table 38: Recovery Required Efforts for maneuvers

5.3.10 Hardware approach

Control system hardware requirements can be specified based on minimum and maximum torque capability rather than a specific number of thrusters with specific locations and orientations. This allows hardware designers to design the system based on availability of hardware, available space on the vehicle, and other mechanical design considerations. A Space Shuttle heritage criteria can be applied for defining acceptable control authority of an shuttle control system Hall et al. [2023]. This design criteria requires the control torque to exceed all known disturbance torques by a factor of two. From the rotational equations of motion, this criteria is written as:

$$T_c > 2[\max(\omega \hat{x} J \hat{\omega}) + \max(T_{\text{ext}})]$$

where T_c is the required control torque, ω is the body rate, J is the inertia tensor, and T_{ext} is the summation of external disturbance torques.

Worst case values are computed for each term and summed together to generate a peak disturbance value. Note the gyroscopic coupling effect from the Euler equations of motion is included and is a function of the desired rotational maneuver rate, meaning if higher maneuver rates are desired, larger control authority is required. Disturbances to consider are generally a function of the orbit and attitude. For low Earth orbits, gravity gradient is often the primary environmental disturbance torque.

This torque sizing model provides a conservative first-order estimate but comes with several limitations that reduce its suitability for detailed design. It assumes worst-case conditions by summing maximum gyroscopic and environmental disturbance torques, which may not occur simultaneously or in the same direction, leading to overly conservative and potentially oversized actuator requirements. The model also treats torques as scalar magnitudes rather than vectors, ignoring the directional nature of torque and the complexities of control allocation. Additionally, it does not account for actuator dynamics such as saturation, slew rate, or bandwidth, and assumes a rigid body with constant inertia, neglecting flexible components or shifting mass distributions.

With numerical applications, we find $5.656 \times 10^6 \text{ Nm}$ control torque, which is of uncomparable magnitude with the rest of the study. As such, we confirm the unsuitability of the criteria and disregard it for the sizing of the control authority.

5.3.11 Obtained System Limits

The maximum and minimum obtained force and torque requirements are assembled in the table below.

We note the limitations of this sizing, which imposes the lever arm on the system's design and constrains the placement of the control authority and subsequent shuttle structure design. It also assumes constant accelerations and bases maneuvering purely on estimates and found practices. We note however that all computed rotational accelerations and velocities remain well below the NASA 3001 Standard.

Thorough sizing of the efforts would require in-depth knowledge of the shuttle's trajectory and required maneuvers, which were not available for this study.

Required Efforts	Min.	Max.
Torque		
Pitch	19 Nm	8727 Nm
Yaw	15 Nm	1745 Nm
Roll	24 Nm	3879 Nm
Force		
Pitch	3 N	1091 N
Yaw	2 N	218 N
Roll	4 N	776 N

Table 39: Minimum and Maximum Required Shuttle Efforts

5.4 Design of the control means

This section will focus on the design of the required control means for the attitude (in pitch, yaw, roll axes) in all mission phases considering previously computed required efforts. The means for trajectory control are considered sufficient with the main gimballed propulsion system.

5.4.1 Reaction Control System

This section serves to size the RCS of the StarCheap Shuttle.

The Reaction Control System (RCS) is the most efficient and practical method for attitude control in shuttle-like vehicles to its ability to operate effectively in the vacuum of space, where aerodynamic control surfaces are useless. By expelling gas through small thrusters positioned around the vehicle, the RCS generates torque that allows for precise control over pitch, yaw, and roll.

This system provides immediate and fine-tuned maneuverability, which is essential for operations such as docking, orbital adjustments, and re-entry alignment. Additionally, the RCS operates independently from the main propulsion system, offering better fuel efficiency and control for minor adjustments without the need to engage larger engines. Its design should be modular, to allow for easy replacement of engines between flights, and include built-in redundancy, ensuring that the spacecraft remains controllable even if some thrusters fail.

The sizing approach to the RCS was done bearing in mind necessary efforts for rotational control and assuming translational control needs based on the translational acceleration capacities of existing spacecraft of comparable maneuvering capacity. Assuming 0.01 to 0.1 m/s^2 capacities, we size the thrust need per axis as:

- **X-axis (fore-aft)**: 2000 N
- **Y-axis (lateral)**: 1000 N
- **X-axis (vertical)**: 1000 N

5.4.1.1 Thrust Assessment & Axis Control

Placement of the engines is key in assessing the thrust requirements of the system, and ensuring both rotational and translational needs are met in both individual and simultaneous fashion.

Placement should be made considering the set lever arms in the previous section; in reality a trade-off would be required between the structure, mass budget, thermal requirements and pointing requirements, but this study was not able to reach iterative sizing loops.

To achieve effective pitch and yaw control using a Reaction Control System (RCS), four thrust centers spaced 90° apart around the spacecraft are necessary to provide balanced and symmetrical control authority. By positioning these centers at equal intervals the system can generate torque in both positive and negative directions along the pitch and yaw axes. This configuration ensures that for every desired movement, there is a corresponding set of thrusters that can fire in opposition to produce the required rotational force without introducing unintended translations.

It also provides redundancy—if one center fails, others can compensate to maintain control. The symmetrical placement eliminates asymmetrical thrust issues, making the system more stable and predictable, which is essential for precision maneuvers.

Using two thrust centers placed 180° apart at the bottom of the shuttle is key for effective roll control. By positioning these thrust centers on opposite sides of the vehicle, they can generate opposing forces that create torque around the shuttle's roll axis. When one center fires in one direction and the other fires in the opposite direction, the shuttle rotates around its central axis without causing translation or affecting pitch and yaw. The 180° separation maximizes the moment arm, making roll control more efficient.

The roll RCS thrusters should be housed under the propulsion system's skirt in order to be effective. Considerations should be made for the thermal protection of these thrusters as they coexist in the same space as the main engines and could be subject to consequent thermal loads and potential offgassing from the engine plumes. Gimballing considerations should also be made, but were not reached in this study.

In order to deliver pure translational thrust, we assume reliance on the initial thrust centers for pitch and yaw at the top of the shuttle. In order for the thrust to be purely translational, we have to place a second thrust center further down the side of the shuttle. We want to produce pure translational thrust, using two opposing thruster clusters placed at different distances from the center of mass. To do that, the torques from each cluster must cancel each other out, even if their distances (lever arms) aren't equal.

We can compute the required torque on each center of thrust as:

$$\tau_{\text{front}} + \tau_{\text{aft}} = 0 \quad (85)$$

$$T_f L_f + T_a L_a = 0 \quad (86)$$

Knowing the lever arms and the total required thrust on the translational axes (1000 N) we can deduce :

- $T_f = 272.7 \text{ N}$

- $T_a = 727.3 \text{ N}$

For purely translational movement along the roll axis, using four thrust centers spaced 90° apart around the aft of the vehicle ensures balanced, efficient, and disturbance-free translation. This configuration allows for pairs of thrusters to fire directly opposite each other, producing linear thrust along the x-axis without introducing unwanted rotational moments (torque). If only one or two thrusters were used asymmetrically, the shuttle would experience both translation and rotation, making precise maneuvering difficult. By having four equally spaced clusters, opposing thrusters used in pairs cancel out torque while producing clean, straight-line motion.

The question remains whether or not we are able to deliver both rotational and translational movement simultaneously. In spacecraft design, particularly for crewed or precision-guided vehicles like shuttles or landers, it is both realistic and common to require simultaneous translational and rotational movement. This need arises during operations such as docking, rendezvous, or stationkeeping, where the spacecraft must reposition itself in space while continuously adjusting its attitude to align with a target or maintain stability.

The key to achieve this is by ensuring that the sum of the forces results in the desired linear acceleration, while the sum of the torques creates the desired angular acceleration, and any unintended forces or torques cancel out. This is known as vector decoupling.

Assuming we want a 1,000 N translation in Z and a pitch-up torque of 1,100 Nm. We find a thrust distribution allowing for such a movement :

Thruster	Location	Lever Arm (m)	Thrust Output (N)
T1	Nose - Top Left	8.0	400
T2	Nose - Bottom Right	8.0	100
T3	Rear - Top Left	3.0	300
T4	Rear - Bottom Right	3.0	200
Total	—	—	1,000

Table 40: Sample thrust allocation for simultaneous +Z translation and pitch rotation. Lever arms are distances from the center of mass relevant to pitch torque.

In reality, it is the role of the GNC OBC to make these differential calculations in real time and allocate thrust accordingly.

In accordance to the stated control authority needs and allocated margins, the placement of the thrust centers for the RCS are as follows:

Location	Number of thrust centers	Spacing	Max required thrust
Front	4	90°	1200 N
Aft	4	90°	1000 N
Bottom (rotation)	2	180°	800 N
Bottom (translation)	4	90°	2000 N
Total	—	—	1,000

Table 41: Thrust Center Allocation

5.4.1.2 Engine Choice

Since the main propulsion system utilizes NOFBx, it is mass-optimal to adopt the same propellant for the RCS, as this enables the use of a common propellant tank, feed system, and pressurization infrastructure. This approach reduces system mass and complexity, simplifies integration, and improves overall vehicle efficiency.

While cold gas thrusters inherently offer finer thrust resolution and rapid response characteristics—making them well-suited for precise attitude adjustments—they are limited by low specific impulse and the need for high-pressure storage, which imposes significant mass penalties.

In contrast, NOFBx, as a high-performance monopropellant, provides substantially higher specific impulse and thrust density, making it more suitable for both primary and secondary propulsion roles Davidson [2012]. The primary limitation lies in achieving fine impulse control at the 1-5 N level, as combustion-based systems introduce challenges such as minimum impulse bit constraints and thermal transients. However, with appropriately designed fast-acting valves, precise pulse modulation, and rigorous control algorithms, we assume we will be able to achieve the required thrust granularity.

The trade-off ultimately favors NOFBx, as the performance and mass advantages outweigh the increased control complexity associated with hot gas operation.

Further iterations could include a blend of hot-gas NOFBx RCS engines and cold gas engines in order to ensure all magnitudes of thrust, but this was not addressed in this study.

With different levels of thrust required for different allocated thrust centers, we might assume different engines will be required to be designed in order to meet the different thrust levels. However, due to modularity wishes, we decide to use the same engine for all RCS thrusters.

Standardizing the RCS engines simplifies design, qualification, and testing processes, reducing non-recurring engineering costs and minimizing the risk of integration errors. It allows for common spare parts, streamlined maintenance procedures, and consistent performance modeling, which is particularly beneficial in multi-engine spacecraft architectures where attitude control authority is distributed. From a mass and volume standpoint, a uniform engine architecture enables shared mounting structures, thermal interfaces, and harness designs, leading to further reductions in complexity and potential failure points. Additionally, identical thrusters across clusters allow for redundancy and fault tolerance, as any unit can be substituted or re-tasked without reconfiguration.

Using the same approach as the design of the main engines, a trade-off is made between the number of engines in each cluster and the delivered thrust for each engine. A final balance is found with 400 N thrusters allocated as such:

- Front clusters : 3 engines
- Aft clusters : 3 engines
- Bottom rotational clusters : 2 engines
- Bottom translational clusters : 2 engines

The design of the engines are included in the propulsion section. The design of the feeding system, cooling system, tanks, ignitors and all other system considerations is not covered

in this study.

For safety and redundancy considerations, we double the number of thrusters in every cluster.

Configurations of the engines for every cluster is suggested in the schematics below. Configurations are assumed the same for front and aft clusters, but we note that modifications may have to be made for the front RCS clusters, as their lever arm at 8m above the CoM puts them at the same level as the provisional windows for the cabin module. A slanted mount is considered a possibility that may be advantageous for pitch control but is not designed.

We also note a necessity of positioning the front and aft clusters at a 45° angle from the flaps in order to not be blocked by their folded position in orbit.

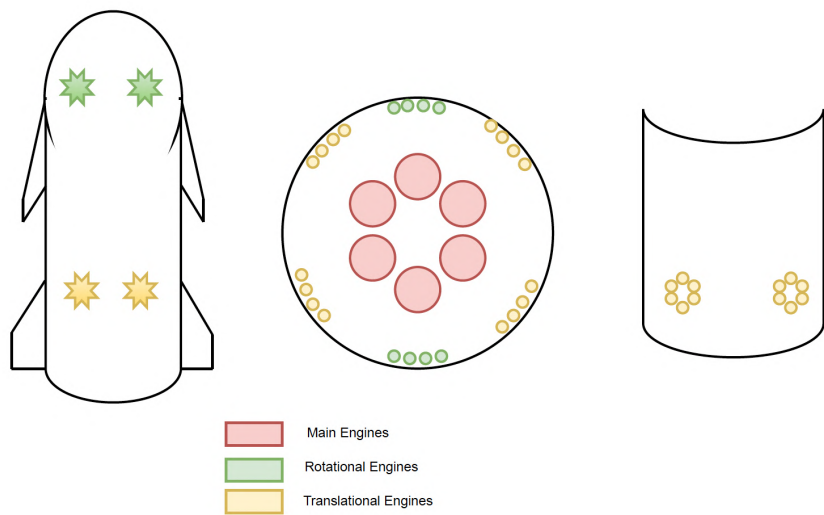


Figure 55: Schematics of RCS placements

Integration of the RCS thrusters within the structural envelope of the shuttle requires careful consideration, particularly on the ventral (belly) side, which is protected by the thermal protection system (TPS). While the thruster assemblies are relatively compact — approximately 7 cm in diameter — their presence must not compromise the integrity or uniform performance of the heat shield during atmospheric reentry. Localized geometric discontinuities or material heterogeneities introduced by the thruster interfaces can lead to thermal gradients, flow separation, or hot gas impingement, potentially resulting in overheating or delamination. Therefore, thruster integration must ensure both aerodynamic conformity and thermal continuity, possibly requiring recessed mounting, dedicated ablative or high-temperature insulation around the nozzles, and computational fluid dynamics (CFD) validation of flow and heat flux behavior.

5.4.2 Flaps

This section will serve to size the aerodynamic surfaces referred to as flaps.

We note that the use of flaps for aerobraking and attitude control in a blunt-body shuttle requires leveraging fundamental principles of fluid dynamics and control theory and optimizing both deceleration and maneuverability in a planetary atmosphere.

Flaps function by modifying the local airflow around a vehicle, thereby altering the distribution of aerodynamic forces. In the context of aerobraking, flaps increase the effective cross-sectional area and disrupt the laminar flow, greatly increasing the coefficient of drag (C_d). This augmentation in drag force, as described by

$$F_D = \frac{1}{2} \rho V^2 S C_d \quad (87)$$

where ρ denotes atmospheric density, S the drag cross-section, and V the velocity of the vehicle, converts a portion of the shuttle's kinetic energy into thermal energy, aiding in deceleration without expending fuel.

Attitude control via flaps is made possible by exploiting asymmetric lift and drag forces across the vehicle's body. By actuating flaps independently or in specific coordinated patterns, differential forces and moments are generated, allowing for precise control of pitch, yaw, and roll. For instance, extending a flap on one side of the shuttle increases drag and potentially creates a rolling or yawing moment, depending on its placement relative to the center of mass.

In a high-angle-of-attack regime typical of atmospheric entry, these moments are amplified due to the high dynamic pressures and large aerodynamic lever arms, enabling rapid attitude corrections and stability augmentation. This method provides a mechanically elegant and mass-efficient solution, minimizing reliance on the RCS which is limited by onboard propellant reserves and most particularly towards the end of the mission.

In spacecraft designed for multiple entries or high-mass payloads, such as the StarCheap shuttle, flap-based systems must be engineered to withstand extreme thermal and mechanical loads. Due to time and iteration constraints, the proper assessment of the durability of the flaps was unable to be assessed in this study.

The sizing of the StarCheap shuttle flaps is done based on the ballistic reentry data obtained with PSIMU (see Mission Analysis). Ordinarily, the preliminary sizing should be done considering a computed aerobraked trajectory and its key aerodynamic events (boost glide, hover flip), however an exact velocity, altitude and acceleration profile was unable to be obtained. We consider the ballistic trajectory as a worst-case preliminary case study.

The sizing approach is made considering flaps first and foremost as aerobraking devices and then testing their compatibility as attitude control surfaces.

5.4.2.1 Required aerobraking surface

From the PSIMU velocity profile as a function of altitude, we are able to extract the velocity data at various altitudes along the reentry trajectory. Using the drag force equa-

tion, we are able to plot the variation of drag force with respect to altitude.

The PSIMU software sets the drag and lift coefficients C_L and C_D as constants. In reality, these coefficients vary and are strongly dependent on the angle of attack and the shape of the vehicle, but PSIMU does not make these considerations. To illustrate the potential variation in drag at different angles of attack, we include a study estimate of the drag and lift coefficients for the Starship Reentry trajectory. D. [2022]

Star Ship Aerodynamics Estimate

Hypersonic through supersonic CD at AoA = 90, Hoerner 16-16	$C_{D90} := 1.28$
CD as a function of AoA:	$C_D(\alpha) := .07 + 1.28 \cdot \sin(\alpha)^3$
CL as function of AoA:	$C_L(\alpha) := C_{D90} \cdot \sin(\alpha)^2 \cdot \cos(\alpha)$
	$C_D(0) = 0.07 \quad C_D(90\text{deg}) = 1.35$
	$\alpha_a := 5\text{deg}, 6\text{deg}, 135\text{deg}$

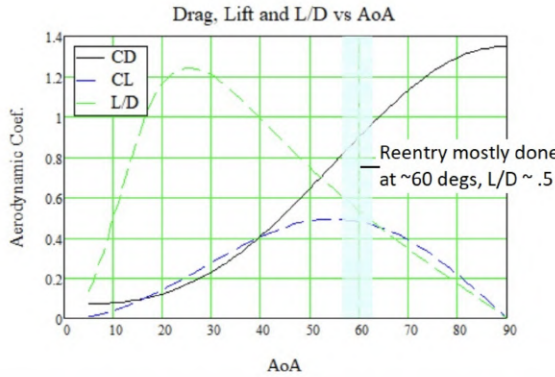


Figure 56: Starship Aerodynamics Estimates

We must first estimate the cross-section surface of the shuttle. Considering a simple approximation with a cylinder and a partial sphere, we can deduce the corresponding surface.

The cylinder cross section is a rectangle 12 m long and 5 m wide.

The nose's cross section is obtained considering the radius of curvature knowing the height and diameter:

$$R = \frac{h}{2} + \frac{d^2}{8h} \quad (88)$$

and the arc angle θ is given by:

$$\theta = 2 \arcsin\left(\frac{d}{2R}\right) \quad (89)$$

We deduce the area of the nose curve :

$$A_{\text{nose}} = R^2 \arccos\left(1 - \frac{h}{R}\right) - (R - h) \sqrt{R^2 - (R - h)^2} \quad (90)$$

The total drag cross section area is approximately 73 m^2 .

Using the PSIMU atmospheric density plots based on the US76 atmospheric model, we obtain the following drag force variation with respect to altitude:

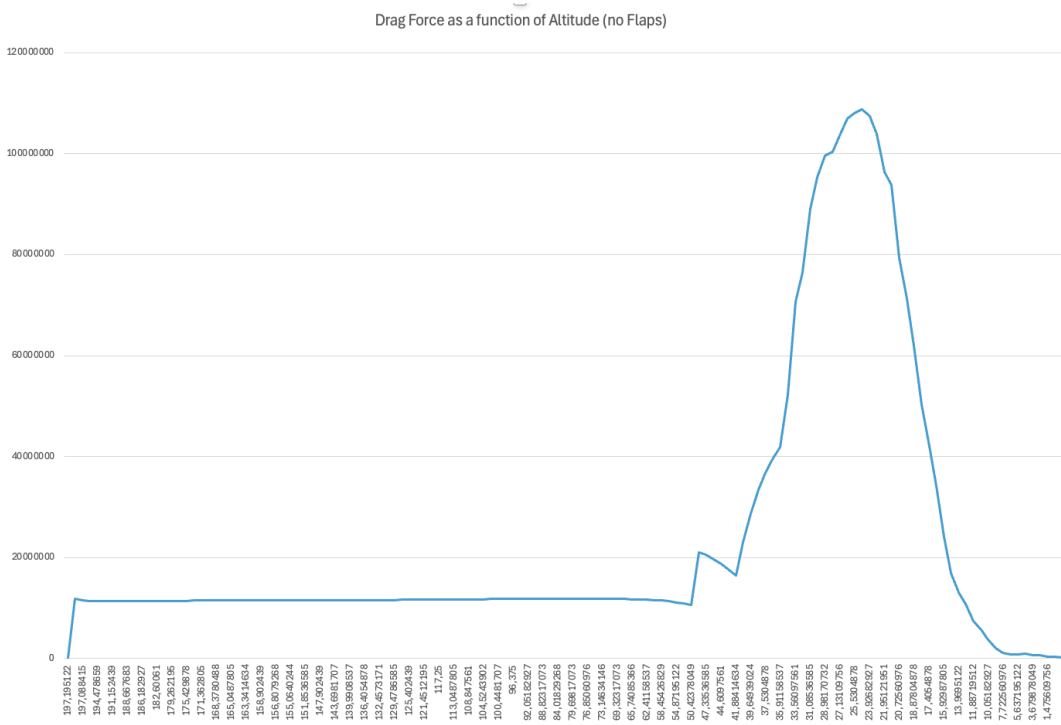


Figure 57: Estimated drag force upon ballistic reentry

We observe a significant increase in the generated force beginning around 60 km, due to the significant increase in atmospheric density at this altitude. We now know that above this altitude, there is no use in deploying any aerodynamic surfaces as they will not be effective.

We compute the resulting drag acceleration, and plot this acceleration with curves considering a 30-70 % increase in drag.

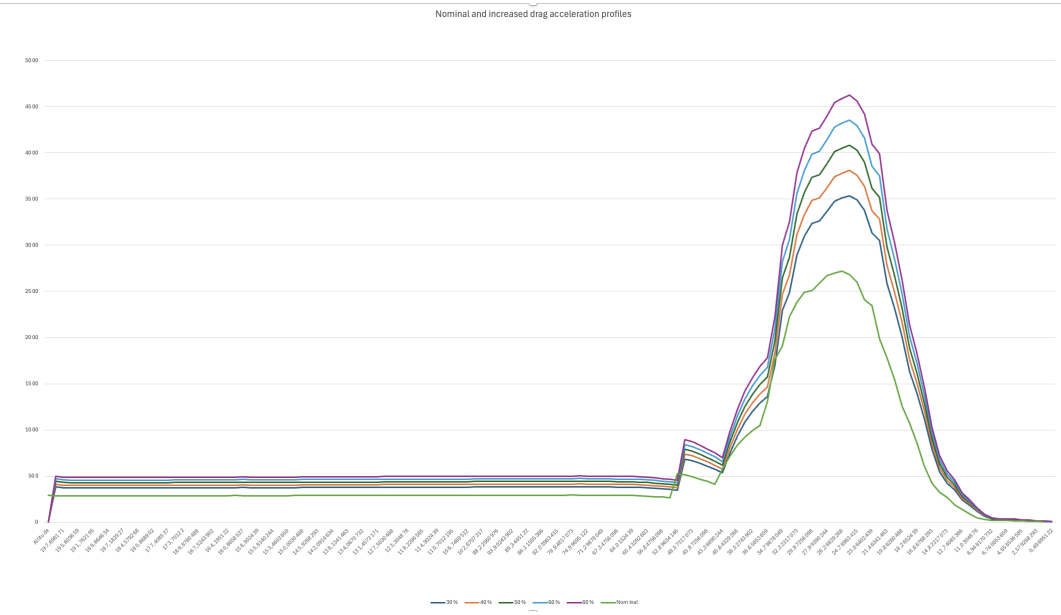


Figure 58: Estimated drag acceleration with increased profiles

At peak drag acceleration, we compute the additionnal surface required to achieve the increase in acceleration from:

$$A_{\text{flaps}} = \frac{2a_D m}{C_D \rho V^2} - A_{\text{body}} \quad (91)$$

Obtained results are synthesized in the table below:

Drag increase	Required flap surface	Flap/Body Ratio	Total Drag cross section
30	22,009 m^2	0.3	95,3760
40	29,346 m^2	0.4	102,712
50	36,683 m^2	0.5	110,04
60	44,02 m^2	0.6	117,39
70	51,356 m^2	0.7	124,722

Table 42: Drag increase resulting surface characteristics

We find a direct correlation between drag increase and surface increase. It is noteworthy to consider that maintaining a balanced ratio between flap surface area and body drag cross section ensures the aerodynamic forces remain manageable, the structural loads are within material limits, and the control authority remains precise and predictable.

Geometric estimations for the Starship vehicle yield a 25 % flap to body ratio. As flap technology for blunt bodies on reentry is a relatively novel concept, staying within reasonable bounds of these proportions is key to ensuring stability and controllability throughout the descent phase. Exceeding this ratio may lead to non-linear aerodynamic responses, increased thermal and mechanical stress, and potential loss of control authority under dynamic atmospheric conditions.

By adhering to established ratios such as the estimated 25 % flap-to-body area guideline observed in Starship, we can better manage trade-offs between aerodynamic efficiency, structural integrity, and guidance responsiveness. This conservative approach provides a

margin of safety while the field continues to mature through empirical testing and high-fidelity simulations.

As such, given the considered flap to body ratio, we set the acceptable bounds within 5% of the Starship's ratio, at 30%.

Using the PSIMU data for newtonian gravitational acceleration, we can estimate the resulting acceleration for reentry in the nominal case and with the dimensioned flaps.

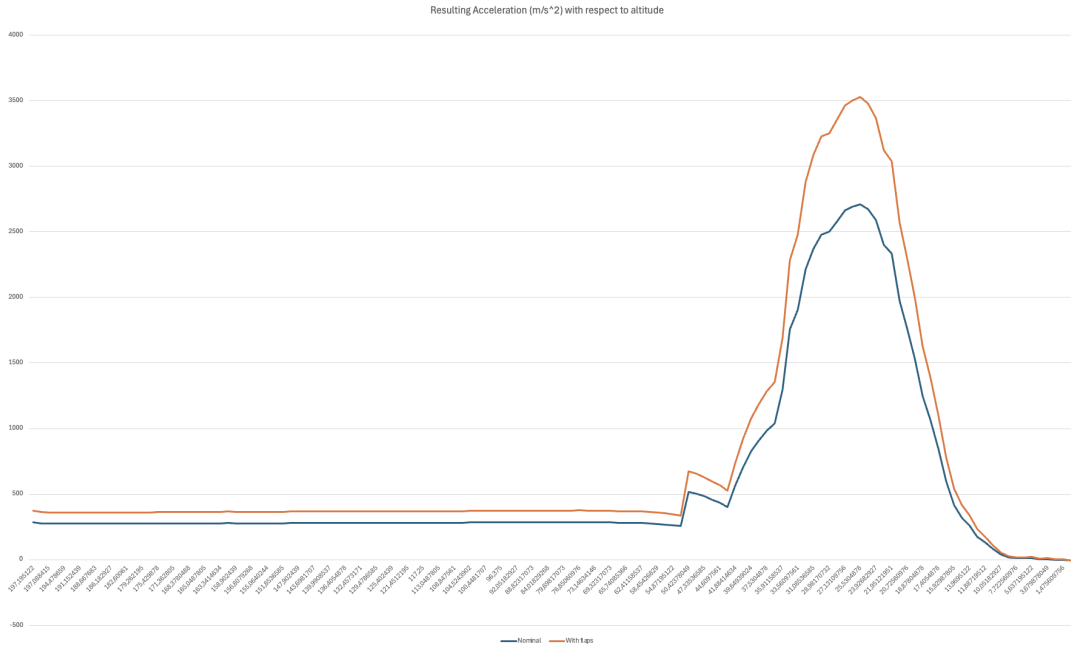


Figure 59: Resulting accelerations for reentry with and without flaps

We obtain a significant increase in acceleration, except at low altitude below 2 km where the gravitational acceleration is significantly overwhelming. We note that this is not relevant to the shuttle study case as the real trajectory will have made a boom glide and be preparing or executing the hover flip.

We acknowledge the limitations inherent in the presented results, as the analysis primarily relies on relative velocity and relative acceleration plots, which offer a simplified view of the vehicle's dynamic behavior. This approach does not fully account for the anisotropic nature of aerodynamic drag—specifically, how drag forces vary along each principal axis of the shuttle (longitudinal, lateral, and vertical). By not decomposing the drag effects along these individual axes, the analysis may overlook critical asymmetries in force distribution that can significantly influence vehicle attitude, stability margins, and control surface effectiveness during reentry. A more comprehensive model would require axis-specific drag coefficients and force breakdowns to capture the true aerodynamic environment experienced by the vehicle.

For our predesign we retain the final aerodynamics surface for the flap sizing as **22.009 m²**.

5.4.2.2 Validation of Control Authority

We now wish to see if we have enough surface to generate the required torque for the

sized efforts of the shuttle.

Considering the flaps placed at the side of the shuttle, we consider that moving them up or down will generate a lifting force. From the lifting force, we can derive the control torque as :

$$\tau = \frac{1}{2} \rho V^2 S C_L \quad (92)$$

We consider a front and rear flap configuration, such as the STarship does. Front and rear flaps are both necessary to provide full aerodynamic control during reentry, especially in pitch and roll. In the belly-flop orientation, the vehicle lacks natural stability, so the front flaps balance the aerodynamic moments generated by the rear flaps, allowing precise attitude control. Together, they help maintain the correct center of pressure, adjust descent trajectory, and execute maneuvers like the landing flip. Without both sets, the vehicle would lose critical control authority, compromising stability and maneuverability during descent.

Using the flap surface, we decide on an arbitrary $\frac{2}{5} / \frac{3}{5}$ split between the front and rear flaps.

Using the calculated lever arms of the following section, we compute the generated torque based on the initial velocity profile along the reentry trajectory. We find a maximum torque generated at 9.9×10^6 Nm for the front flaps and 9.66×10^6 Nm for the rear flaps. The magnitude of the generated torque far exceeds the required torque for effort, so we can say we possess the necessary control authority by a significant margin.

We note that at lower altitudes, we don't meet the maximum required torque, but at these altitudes we should be making the hover flip and will be able to be assisted by the RCS.

If the actuated torque is significantly higher than the required control torque, it can complicate attitude control by making the system overly sensitive and difficult to regulate precisely. High torque levels lead to rapid angular accelerations, which may cause the vehicle to overshoot its desired orientation or introduce oscillations, especially in low-damping environments like thin upper-atmosphere conditions. This reduces control precision and can destabilize the vehicle.

The current sizing would require extremely precise and controlled actuation of the flaps in order for them to also work as control surfaces. During reentry, actuators must operate reliably at high temperatures and withstand large mechanical stresses, while still providing fine angular resolution within fractions of a degree. The study of this is not pushed further, but the limits of using the currently sized flaps as control surfaces is noted.

5.4.2.3 Flaps geometry

In practice, flap geometry is often refined through CFD simulations and wind tunnel testing to optimize performance across reentry conditions. As we have neither precise reentry conditions nor CFD capabilities at this stage of the sizing, approximations are made using general rules of thumb derived from rocket fin design provides a practical and physically grounded starting point.

These empirical methods, based on decades of flight-proven configurations, offer reliable estimates for achieving sufficient aerodynamic control authority. Rocket fins and reentry flaps share similar functional goals—stabilizing and steering a body in a dynamic, high-

speed flow—so leveraging their geometries allows for a preliminary design considering hypersonic velocity regimes.

The hypersonic regime presents significant aerodynamic challenges due to extreme conditions such as intense heating, shockwave formation, and nonlinear flow behavior Kaushik [2019]. At speeds greater than Mach 5, airflow becomes highly compressed and ionized, leading to severe thermal dissociation and unpredictable aerodynamic forces. Shockwaves are stronger and more complex, interacting with the vehicle's surfaces in ways that can destabilize the flight path or create excessive drag. Additionally, the boundary layer becomes turbulent and prone to flow separation, while the high temperatures create extreme aerodynamic heating, demanding specialized thermal protection.

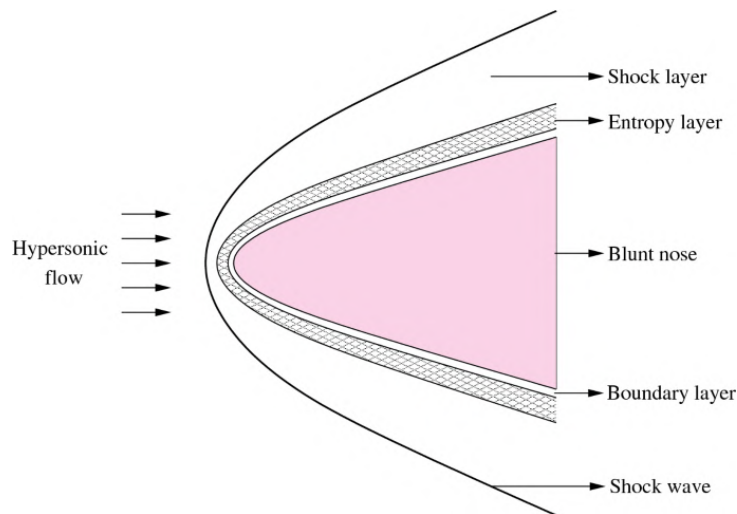


Figure 60: Hypersonic flow representation Kaushik [2019]

PSIMU's initial assessment of the reentry trajectory shows a velocity regime up to Mach 28 - although quite high due to the ballistic assumption, the Starship's flight was evaluated at Mach 25. So considering this regime in the case of StarCheap's flight is not far off from reality.

In the following study, choices are made in order to minimise instability due to hypersonic flow and leverage a maximum control authority given geometrical practices. It may seem counter-intuitive to want to minimise wave drag or impact of shockwaves, as the main objective of the flaps is to increase aerodynamic surface and drag effect, yet doing so without careful shaping would lead to uncontrollable pressure loads, increased thermal stress, and inefficient force generation. Therefore, the geometries are selected not simply to maximize drag, but to modulate it in a controlled, predictable, and structurally sustainable way, ensuring the flaps remain effective throughout the reentry envelope.

Many studies have been conducted on the subject of fins or flaps in hypersonic flows for blunt or ballistic bodies. The general consensus, such as can be found in the study conducted by Ukirde et al. [2023] , is that the tapered swept and delta clipped geometries are the most appropriate in hypersonic regimes..

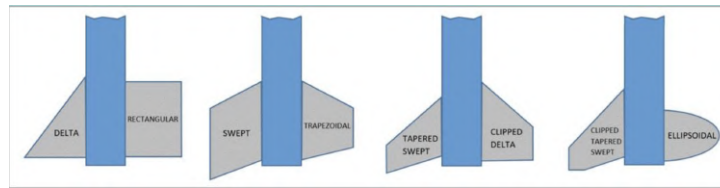


Figure 61: Existing flap geometries NAKKA [2024]

These considerations are even more pertinent as these are the geometries found on the Starship.

We make the choice of a tapered swept geometry for the front flaps and a clipped delta for the bottom flaps, in order to optimize both aerodynamic efficiency and structural resilience under extreme conditions. NAKKA [2024]

For the front flaps, the tapered swept geometry is ideal because it helps manage high-speed flow interactions effectively. The swept design naturally aligns with the airflow at hypersonic speeds, reducing shockwave intensity and improving the distribution of pressure along the flap. This minimizes aerodynamic loads and ensures smooth airflow, in order to maintain stability and control at high Mach numbers. Additionally, the tapered shape helps delay boundary layer separation, which enhances lift-to-drag ratios and keeps the vehicle stable during high-speed maneuvers. The front flaps, being in the leading portion of the vehicle, benefit from the sleek, aerodynamic characteristics of the swept geometry to maintain efficiency and control while minimizing drag.

For the bottom flaps, the clipped delta geometry is better suited because it offers enhanced structural robustness, which is essential for the high aerodynamic loads experienced during reentry. The broad base of the clipped delta provides strong structural integration near the hinge line, ensuring that the flap can withstand the immense forces acting on it during descent. The delta shape's reduced spanwise bending moments further improve mechanical resilience. This is particularly important for bottom flaps that need to handle large forces and potential high heating, as they will likely face more intense aerodynamic pressures during reentry due to the vehicle's orientation and interaction with the airflow.

The general geometry of the flaps is resumed in the figure below:

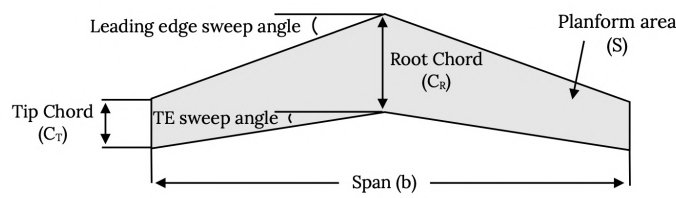


Figure 62: General Flap geometry denomination III [2021]

In hypersonic regime, certain practices in terms of ratios and coefficients are to be considered III [2021].

The aspect ratio is a measure of how long and slender a wing is from tip to tip.

$$AR = \frac{b^2}{S} \quad (93)$$

In supersonic and hypersonic regimes, we want the aspect ratio to be minimised. The reduced span leads to lower bending moments, which allows for thinner airfoils that are more suited for high-speed flight. Additionally, it offers better maneuverability due to reduced inertia, while a longer chord length provides small advantages in drag and flow characteristics.

The geometry of the flaps involves a subtle trade-off. While taller fins generate less normal force than wider fins and don't offer the highest control authority, the aspect ratio in the hypersonic regime calls for the opposite approach. However, since we've established that the control authority significantly exceeds what is actually required, we believe we can afford to sacrifice some of it in this trade-off.

In the hypersonic regime, the taper ratio—defined as the ratio of the tip chord to the root chord of a wing or control surface—should generally be minimized, meaning the tip is much narrower than the root.

$$T = \frac{c_t}{c_r} \quad (94)$$

A low taper ratio (narrow tip, broad root) helps align the flap surface more closely with the local hypersonic flow, especially near the root where shockwave strength is greatest. This minimizes oblique shock interactions and prevents flow separation, contributing to smoother, more predictable aerodynamic behavior. The root of the flap is structurally integrated and can support more robust thermal protection, while the tip, being more exposed and slender, benefits from reduced surface area to limit local heating. A wide root also offers a stronger moment arm and better load-bearing capacity, reducing torsional and bending stresses near the hinge line. A minimized taper ratio reduces bending moments toward the tip, improving flap stiffness and resistance to aeroelastic deformation. In hypersonic regime, we find in practice values between 0.1 and 0.3 for this ratio (source hypersonique).

Considerations must also be made for the leading edge sweep angle. At high hypersonic velocities, the vehicle generates strong oblique shockwaves at leading edges. A high sweep angle ensures that the leading edge remains encompassed in the local flow direction, even while the freestream is hypersonic. This significantly reduces the strength of the shockwaves and lowers wave drag, which is a dominant source of aerodynamic instability at these speeds. By aligning the surface more closely with the flow, the sweep delays the onset of high-pressure zones and reduces the intensity of shock-boundary layer interactions Allen and Eggers [1958].

Using the generale rule of thumb, at Mach numbers close to 25, we obtain a Mach cone opening of less than a few degrees. In practice though, we find that the hypersonic Mach cone is alleviated with rounded vehicle noses (Source), which we know will be the case for the shuttle.

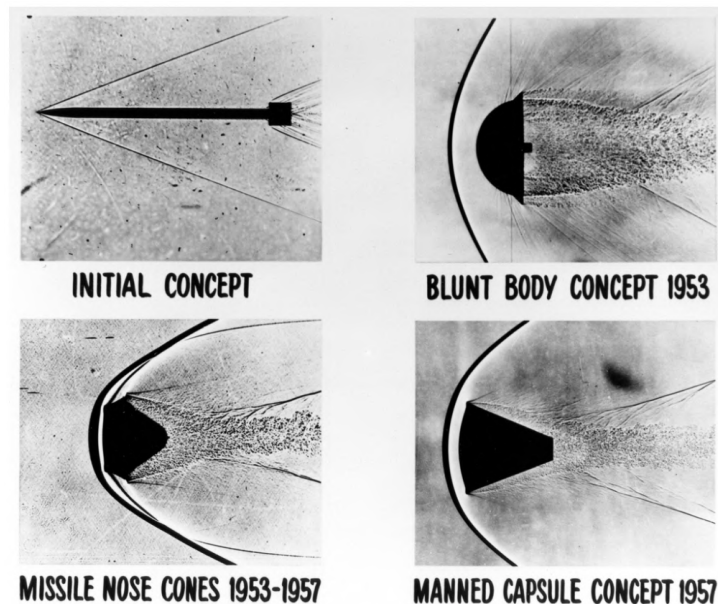


Figure 63: Impact of nose shape on the hypersonic shock wave Allen and Eggers [1958]

As such, we see the necessity of having a high sweep angle in order to minimise shockwave impact and wave drag on the flaps. Typical values for hypersonic vehicles vary from 60 to 75°.

Also, considering moving the flaps backwards from the nose of the shuttle allows for better protection from the shockwave and reduces mechanical complexity. This rearward placement positions the flaps in a more stable flow region, behind the primary bow shock, where aerodynamic loads are less extreme and more predictable III [2021]. Additionally, it simplifies thermal protection requirements and reduces exposure to intense stagnation heating, thereby improving the durability and longevity of the control surfaces during hypersonic flight.

With these design parameters in mind, we iterate around sweep angle, taper ratio and aspect ratio values in order to find an aerodynamic sweet spot, bearing in mind maximisation of the lever arms for control and the necessity of being able to fold the flap against the side of the shuttle when out of aerobraked flight. The front flaps are implemented from the bottom of the nose cone (at about 12 m from the base) and the aft flaps are implemented from the very bottom of the shuttle.

Obtained geometries for each flap are resumed in their respective tables.

Forward flap	
Geometrical parameter	Value
Geometry	Tapered Swept
Root Chord	4.012 m
Tip Chord	0.6 m
Sweep Angle	70°
Leading edge	3.63 m
Half Span	1.24 m
Mean chord	2.3 m
Lever arm	5.85 m

Table 43: Obtained Forward Flap Geometry

Aft flap	
Geometrical parameter	Value
Geometry	Clipped Delta
Root Chord	3.76 m
Tip Chord	1.13 m
Sweep Angle	60°
Leading edge	3.04 m
Half Span	1.52 m
Mean chord	2.45 m
Lever arm	3.77 m

Table 44: Obtained Aft Flap Geometry

A visual rendering of the flaps' geometry and attachment to the shuttle side is included below. CAD implantation of the flaps on the shuttle structure is included in the Structure part of this report.

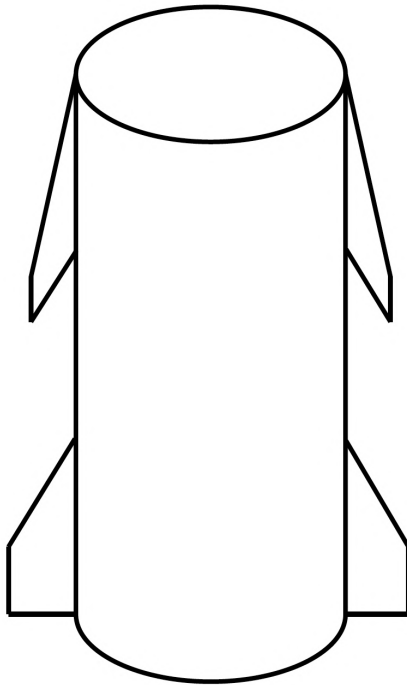


Figure 64: Flaps geometry and implantation schematic

Assumption is made for flap implementation at strictly 180° separation around the shuttle body. Further considerations with CFD studies should yield optimal placement of the flaps around the body with control surface angulation.

Flaps should also ideally be airfoiled rather than flat plates to improve their aerodynamic efficiency and control authority, especially in hypersonic regimes where flow separation and stability are critical concerns. An airfoiled shape, such as the symmetric NACA 0010, provides smoother pressure distribution, reducing shock-induced separation and improving lift-to-drag characteristics. Unlike flat plates, which can cause abrupt flow detachment and unsteady forces, airfoiled flaps generate more predictable and controllable aerodynamic responses, essential for precise attitude control during reentry.

5.5 Sensors Design

The shuttle requires a diverse array of sensors to ensure precise navigation and attitude determination throughout its mission. These sensors provide critical data on position, velocity, and orientation, enabling the shuttle to maintain stability, execute maneuvers, and interact with other spacecraft or celestial bodies. By continuously tracking motion and external reference points, they help correct errors, compensate for drift, and ensure accurate alignment for tasks such as orbital adjustments, docking, debris capture and reentry.

A set of sensors was determined for each operational phase, ensuring that the AOCS system has the sufficient data to maintain control of the shuttle, keeping the payload and other actors safe. Hybridisation of measurements was particularly considered.

Sensors particular to the docking and debris capture phases are omitted and detailed in their respective sections.

5.5.1 Navigation

Navigation sensors provide the data necessary to determine the position, velocity, and altitude of the space shuttle during different phases of flight—launch, orbit, and reentry. These sensors must work across multiple environments (e.g., atmospheric flight, low Earth orbit, reentry), requiring redundancy and complementarity.

5.5.1.1 GNSS (Global Navigation Satellite System)

GNSS receivers, including GPS, GLONASS, and Galileo, are critical for high-precision absolute position and velocity determination during the shuttle's ascent, orbital, and reentry phases. These receivers utilize time-of-flight measurements from multiple satellites in the system to triangulate the shuttle's position and velocity vectors with meter-level accuracy. GNSS is particularly effective in open-sky conditions, where line-of-sight to multiple satellites is available, offering a robust solution for navigation during phases such as launch, cruise, and reentry.

The GNSS receiver's multi-frequency operation enables the estimation of differential corrections for mitigating atmospheric delay errors and improving accuracy.

However, GNSS signals degrade in areas with low satellite visibility, such as polar orbits or during high-dynamics maneuvers. As such, GNSS is often supplemented by inertial navigation systems (INS), particularly during periods of signal loss (e.g., eclipse conditions or high-speed descent), where continuous and reliable position and velocity updates are required for precision guidance and control.

5.5.1.2 Inertial Measurement Unit (IMU))

The IMU provides relative position and velocity estimation by measuring specific force, angular rate, and magnetic field using a combination of accelerometers and gyroscopes. These devices operate based on the principle of inertial navigation, or dead-reckoning navigation, where the initial state is integrated over time to compute the current position, velocity, and orientation.

IMUs typically use high-performance ring laser gyroscopes (RLGs) or fiber-optic gyroscopes (FOGs), which are highly stable and accurate over short durations. While IMUs offer low-latency, real-time estimation of shuttle motion, they are subject to drift over time due to errors in the gyroscopes (e.g., bias instability or scale factor errors). This drift accumulates as a function of time, which introduces position and velocity errors in the absence of external updates. To counteract this, IMUs are calibrated and periodically corrected using absolute sensors (such as GNSS or star trackers), allowing the system to maintain high accuracy throughout the mission, even in GNSS-denied environments.

5.5.1.3 Altimeters (Radar or Laser)

Altimeters, either radar-based or laser-based, are used to measure the altitude of the shuttle relative to the Earth's surface. Radar altimeters work by emitting microwave sig-

nals and measuring the time-of-flight for the return signal, providing continuous altitude readings regardless of lighting or weather conditions. Laser altimeters, on the other hand, utilize laser pulses to achieve higher precision and finer resolution than radar altimeters, especially in terms of measuring surface elevation. Both altimeter types are critical for terminal descent, docking, and landing phases, where the shuttle must approach a target with high precision. During the final approach to landing, altimeters, when fused with LiDAR and IMU data, offer real-time vertical state estimates, enabling precise navigation and obstacle avoidance.

5.5.1.4 Light Detection and Ranging (LiDAR)

LiDAR utilizes laser pulses to measure the time-of-flight to a surface, providing highly accurate range and elevation data. LiDAR systems typically operate in the near-infrared spectrum, and their precise distance measurement capabilities enable the creation of detailed 3D maps of the shuttle's environment. This capability is particularly valuable during close-quarters operations such as docking, rendezvous, or landing.

LiDAR is independent of lighting conditions, allowing it to function effectively in both daylight and night. It can provide highly accurate terrain-relative navigation by measuring elevation differences with respect to a known reference (e.g., the lunar or Earth surface). During rendezvous or docking with a space station, LiDAR assists in relative positioning by delivering millimeter-level accuracy in the shuttle's proximity. Furthermore, its use in autonomous landing ensures obstacle detection, enabling safe operation in environments where GPS signals or visual references may be unavailable.

5.5.2 Attitude

Attitude sensors are used to measure the orientation of the spacecraft relative to inertial space or reference frames such as Earth or stars. This information is critical for flight control, communication pointing, and payload operations.

5.5.2.1 IMU

In the context of attitude determination, the IMU provides angular velocity and acceleration data, which can be integrated to derive the shuttle's orientation over time. Typically employing high-precision gyroscopes and accelerometers, the IMU facilitates short-term attitude propagation by measuring changes in the spacecraft's orientation.

However, over extended periods, errors in the gyroscopes (such as drift and bias instability) result in attitude inaccuracies. These errors accumulate through integration, leading to misalignment between the estimated and actual spacecraft orientation. To mitigate this, the IMU is typically used in conjunction with absolute attitude sensors, such as star trackers, to correct drift and provide accurate attitude estimates. The IMU offers high-frequency updates and low-latency response, making it ideal for rapid attitude control during maneuvering or in-between periodic updates from external references.

5.5.2.2 Star tracker

Star trackers are the gold standard for absolute attitude determination in space applications. They rely on optical imaging of stars in the sky and use algorithms to match the ob-

served star field with an onboard star catalog, yielding high-precision, three-dimensional attitude data.

The accuracy of star trackers is typically in the range of arcseconds (e.g., $<0.01^\circ$), making them suitable for tasks that require extremely fine attitude control, such as payload pointing and science experiments. Star trackers are highly robust to external disturbances like the Earth's magnetic field or gravitational anomalies, providing reliable orientation information even in high-dynamics scenarios.

However, their effectiveness can be reduced if the stars are obscured by sunlight intrusion, spacecraft structure, or planetary bodies, necessitating the use of other sensors (such as the IMU or Earth horizon sensor) during such conditions.

5.5.2.3 Earth Horizon Sensor

The Earth horizon sensor provides a coarse attitude estimate by detecting the position of the Earth's limb relative to the shuttle. It operates by detecting the edge of the Earth's atmosphere or surface and comparing it to the shuttle's frame of reference.

The Earth horizon sensor is particularly useful in low Earth orbit, where the Earth's curvature is clearly visible. Its primary function is as a redundant or backup attitude sensor in scenarios where star trackers are not operational, such as during sun-blocked conditions or if the sensor is temporarily obstructed.

While the Earth horizon sensor cannot match the accuracy of star trackers, its passive nature and low computational demand make it a reliable sensor for maintaining basic orientation knowledge during non-critical phases of the mission.

5.6 Integration and Rendundancy considerations

Spacecraft operations, such as orbital insertion, rendezvous, docking, attitude control, and landing, require continuous, real-time updates on the shuttle's position and orientation to ensure both mission success and crew safety. The shuttle's ability to perform these operations hinges on the seamless interaction of multiple sensor types, each providing specific insights into the spacecraft's state. The navigation sensors—such as GNSS, IMUs, LiDAR, and altimeters—collect position, velocity, and altitude data, while the attitude sensors—including IMUs, star trackers, and Earth horizon sensors—provide critical orientation information.

To synthesize the data from these diverse sensors and create accurate, real-time estimates, sensor fusion algorithms are applied. These algorithms, particularly Kalman filters, play a pivotal role in filtering out noise and correcting for errors in the sensor measurements. Kalman filters are recursive estimation algorithms that optimize the combination of sensor data based on a dynamic system model and the inherent uncertainty in each sensor's readings. By leveraging the complementary capabilities of each sensor, the Kalman filter continuously combines information from, for example, GNSS for absolute position and IMUs for short-term relative motion, to provide consistent, accurate estimates of the shuttle's state (both attitude and navigation) across all phases of flight. This fusion process not only improves the accuracy of individual sensor measurements but also mitigates errors caused by sensor limitations or temporary failures, such as GNSS signal loss or IMU drift over time.

The system's resilience should be further enhanced by the incorporation of redundant sensors. The use of not only duplicate sensors but also backup sensors, such as the Earth horizon sensor, is an essential aspect of maintaining high system reliability. While star trackers provide highly accurate attitude data under ideal conditions, they may be temporarily unavailable due to sunlight interference, spacecraft blockage, or other environmental factors. In these situations, the Earth horizon sensor can take over to provide a coarse estimate of the shuttle's attitude. Although less precise than star trackers, the Earth horizon sensor's ability to function in low-light conditions makes it a crucial failover system, ensuring that the shuttle retains critical attitude information even in challenging scenarios. This redundancy principle should be applied to all sensors in all scenarios to ensure the lowest risk of AOCS failure as possible.

6 Structure

The structural architecture of the spacecraft was divided into four major modules: the Propulsion Stage, the Cargo Module, the Pressurized Crew Capsule ("life module") and the abort system. Each of these elements was sized independently using analytical methods derived from thin shell theory, local buckling criteria, and axial stiffness estimation.

The structural sizing process was guided by load and stiffness constraints defined in the project specifications. These include internal pressurization, inertial accelerations from launch and reentry, dynamic pressure during ascent (Max-Q), and minimum eigenfrequencies to avoid structural resonance. A minimum wall thickness of 5 mm is applied to all primary elements to ensure manufacturability and interface robustness. For the crew capsule, a safety factor of 1.5 is additionally applied on all thicknesses due to the critical nature of the system.

The structural methodology adopted in this report is based on the techniques and formulas taught in the Aerospace Structures course at Politecnico di Milano pol [2023], and validated through simplified analytical tools. Two distinct approaches were followed for the structural design of the modules: the propulsive and crew modules were sized using analytical formulations derived from pol [2023], while the cargo module was dimensioned following the methodology presented in the Space Mission Analysis and Design handbook Wertz and Larson [2011]. The material properties and design requirements used throughout the structural analysis are summarized in Table 45.

Table 45: Requirements and Material Properties

Requirements	
Load Factors	Axial: 6.0 (launch), Lateral: 3.0 (reentry)
Axial Stiffness	First axial mode frequency > 25 Hz
Lateral Stiffness	First lateral bending mode frequency > 10 Hz
Internal Pressure	1 atm = 101,325 Pa
Factor of Safety	2.0 (1.5 for capsule)
Structure Mass < 20%	
Carbon Composite Material Properties	
Young's Modulus E	$150 \times 10^9 \text{ N/m}^2$
Poisson's Ratio ν	0.3
Density ρ	1600 kg/m^3
Ultimate Tensile Strength σ_u	$600 \times 10^6 \text{ N/m}^2$
Aluminium 7075-T6 Material Properties	
Young's Modulus E	$71 \times 10^9 \text{ N/m}^2$
Poisson's Ratio ν	0.33
Density ρ	$2.8 \times 10^3 \text{ kg/m}^3$
Ultimate Tensile Strength F_{tu}	$524 \times 10^6 \text{ N/m}^2$
Yield Tensile Strength σ_y	$448 \times 10^6 \text{ N/m}^2$

6.1 Propulsive module

The structural layout of the propulsive stage was modeled as a cylindrical shell made of carbon-fiber, reinforced by aluminum longitudinal stiffeners (stringers) and transverse stiffening rings. In the structural design of the propulsion stage, a minimum wall thickness of 5 mm is imposed on all structural elements. This constraint is not driven by mechanical requirements, but rather by manufacturing and assembly considerations.

6.1.1 Carbon shell

The axial load due to the upper modules and tanks was distributed between the carbon shell (40%) and the aluminum stringers (60%). The carbon shell thickness was dimensioned accordingly from axial stress (40% of the shuttle mass):

$$t_{\text{carbon}} = \frac{F_{\text{axial,carbon}}}{2\pi r_{\text{outer}} \sigma_{\text{adm,carbon}}} \quad (95)$$

6.1.2 Reinforcement rings

To ensure skin buckling stability between rings, a target critical stress σ_{cr} of 100 MPa was imposed. Using a simplified local buckling criterion for cylindrical shells supported by rings, the minimum ring thickness is given by:

$$t_{\text{ring}} = \sqrt{\frac{\sigma_{\text{cr}} \cdot R \cdot s}{\pi^2 E_{\text{Al}}}} \quad (96)$$

where R is the mean cylinder radius and s is the spacing between rings. The ring shape is square area of side t_{ring} .

6.1.3 Reinforcement stringers

The axial structural load is partially supported by aluminum stringers (longerons) distributed along the inner wall of the cylindrical shell. In the present design, 60% of the total axial force is assigned to the longerons, while the remaining 40% is carried by the carbon shell. The total axial force applied to the structure is:

$$F_{\text{longerons}} = m_{\text{total}} \cdot g_0 \cdot 0.6 \quad (97)$$

Assuming a uniformly distributed load over $n_{\text{longerons}}$ stringers, the required cross-sectional area for each longeron is calculated from the allowable stress $\sigma_{\text{adm,Al}}$ as:

$$A_{\text{longeron}} = \frac{F_{\text{longerons}}}{n_{\text{longerons}} \cdot \sigma_{\text{adm,Al}}} \quad (98)$$

In order to represent the section of each stringer in the model, we assume a square cross-section of side t_{longeron} such that:

$$t_{\text{longeron}} = \sqrt{A_{\text{longeron}}} \quad (99)$$

6.1.4 Thrust ring

The total thrust generated by the propulsion system is transmitted to the structural frame through a dedicated thrust support ring, positioned at the base of the stage. This structural element is dimensioned to carry the full thrust load generated by the engines.

We consider the total thrust force F_{thrust} to be distributed uniformly over the cross-sectional area of the ring, which is an annular surface of external radius R and thickness t_{ring} . The admissible stress of the material, denoted σ_{adm} , determines the minimum required cross-sectional area:

$$A = \frac{F_{\text{thrust}}}{\sigma_{\text{adm}}} \quad (100)$$

This area corresponds to the annular region between the outer radius R and the inner radius $R - t_{\text{ring}}$:

$$A = \pi R^2 - \pi(R - t_{\text{ring}})^2 = \pi(2Rt_{\text{ring}} - t_{\text{ring}}^2) \quad (101)$$

Solving for t_{ring} gives the expression:

$$t_{\text{ring}} = R - \sqrt{R^2 - \frac{F_{\text{thrust}}}{\pi\sigma_{\text{adm}}}} \quad (102)$$

In the final geometry, the thrust ring is not located at the lowest axial position of the vehicle. Instead, it is elevated slightly above the engine plane. This configuration allows the lower portion of the propulsion stage structure to serve as a protective engine skirt. This skirt surrounds the engines and provides aerodynamic shielding during ascent.

The elevated ring is connected to the launch vehicle via a set of explosive bolts located along the outer diameter of the skirt. These separation devices are designed to ensure a clean separation from the lower stage.

6.1.5 Structural mass

The total structural mass of the propulsion stage is composed of the three main elements:

- Carbon shell :

$$m_{\text{carbon}} = \pi(R_{\text{outer}}^2 - (R_{\text{outer}} - t_{\text{carbon}})^2) \cdot h \cdot \rho_{\text{carbon}} \quad (103)$$

- Longerons :

$$m_{\text{longerons}} = n_{\text{longerons}} \cdot A_{\text{longeron}} \cdot h \cdot \rho_{\text{Al}} \quad (104)$$

- Reinforcement rings :

$$m_{\text{rings}} = n_{\text{rings}} \cdot [\pi(R^2 - (R - t_{\text{ring}})^2) \cdot t_{\text{ring}} \cdot \rho_{\text{Al}}] \quad (105)$$

- Thrust ring :

$$m_{\text{thrust}} = \pi R^2 \cdot t_{\text{thrust}} \cdot \rho_{\text{Al}} \quad (106)$$

The combined structural mass is thus:

$$m_{\text{structure, total}} = m_{\text{carbon}} + m_{\text{longerons}} + m_{\text{rings}} + m_{\text{thrust}} \quad (107)$$

6.1.6 Verifications

Now we can verify that the structure sustains the vibrational loads using simplified spring-mass approximations. For axial vibrations:

$$f_{\text{axial}} = \frac{1}{2\pi} \sqrt{\frac{k}{m}}, \quad \text{with} \quad k = \frac{E_{\text{eq}} \cdot A_{\text{tot}}}{L} \quad (108)$$

where A_{tot} is the total axial cross-section and E_{eq} the effective modulus combining carbon and aluminum contributions.

For radial vibration modes (mode 2,1), the frequency was estimated with:

$$f_{\text{radial}} = \frac{1}{2\pi} (n^2 - 1) \sqrt{\frac{D}{\mu R^4}} \cdot 10^2 \quad (109)$$

with $D = \frac{Et^3}{12(1-\nu^2)}$ the bending stiffness, $\mu = \rho t$ the surface density, and ν the Poisson ratio.

Results:

- Estimated axial natural frequency: 52.5 Hz (target: ≥ 25 Hz)
- Estimated radial natural frequency: 11.2 Hz (target: ≥ 10 Hz)

The maximum dynamic pressure was taken as:

$$q = \frac{1}{2} \rho v^2 = \frac{1}{2} \cdot 0.5 \cdot 700^2 = 122,500 \text{ Pa} \quad (110)$$

This produces a hoop stress in the cylindrical shell:

$$\sigma_\theta = \frac{q \cdot r}{t} \quad (111)$$

Results:

- Dynamic pressure: 122.5 kPa
- Circumferential stress: 61.2 MPa
- Carbon admissible stress: 800 MPa

The carbon shell withstands both the axial loads and the dynamic pressure at Max-Q with significant margin. Vibrational modes are above required thresholds. We obtain the following geometry for the propulsion module.

Parameter	Value
Outer cylinder radius r_{outer}	2.50 m
Inner cylinder radius r_{inner}	2.485 m
Cylinder height h	5.00 m
Carbon shell thickness t_{carbon}	5.0 mm
Number of stringers	8
Stringer cross-section area A_s	96 mm ²
Stringer estimated thickness	9.8 mm
Number of stiffening rings	8
Ring thickness t_{ring}	15 mm
Ring spacing s	0.625 m
Thrust ring thickness t_{thrust}	34.2 mm
Total structural mass $m_{\text{structure}}$	1783 kg

Table 46: Main geometric parameters of the propulsive stage

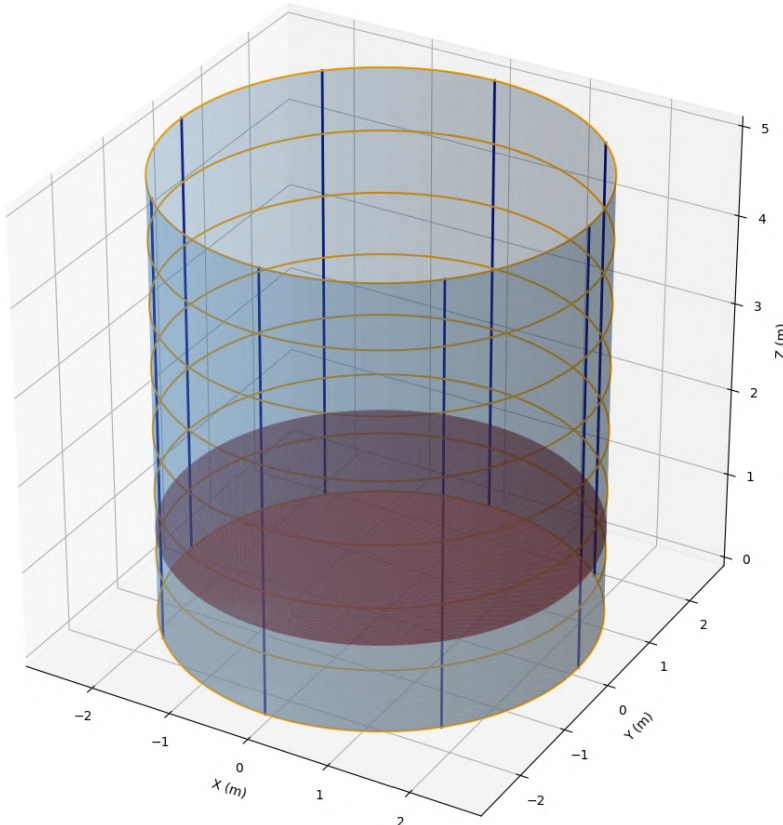


Figure 65: Propulsive module

6.2 Cargo Module

The Cargo Module is idealized as a pressurized cylindrical shell and sized independently to withstand its own inertial loads and internal pressurization. This represents a reasonable starting point for initial structural sizing and stiffness estimation of the module itself, without including loads from adjacent modules.

The module is equipped with a large side door to enable debris capture operations using a net; consequently, local reinforcement and magnetic shielding of the surrounding walls are required to mitigate the effects of the high-intensity magnetic fields generated by magnets during retrieval.

The structure must resist internal pressurization, inertial loads from launch acceleration, and aerodynamic lateral loads during atmospheric reentry. Furthermore, the structure must exhibit sufficient axial and lateral stiffness to maintain acceptable deflections and dynamic performance under launch conditions.

Design assumptions and specifications are summarized in Table 47.

Geometry	
Cylinder Length	6.0 <i>m</i>
Cylinder Diameter	5.0 <i>m</i>
Distributed Mass	12.0 <i>tons</i>

Table 47: Cargo Module Specifications

Material Utilization

The carbon composite shell is primarily responsible for resisting internal pressure and providing the required axial and lateral stiffness to meet vibration frequency constraints. Aluminium 7075-T6 structural reinforcements (rings and stringers) are employed to enhance buckling resistance, improve global bending stiffness, and distribute localized loads around structural openings, such as the large side door. The design will be aligned with the approach taught in the SMAD Wertz and Larson [2011].

6.2.1 Shell sizing

The first sizing step consists of determining the required shell thickness based on internal pressure and dynamic stiffness requirements.

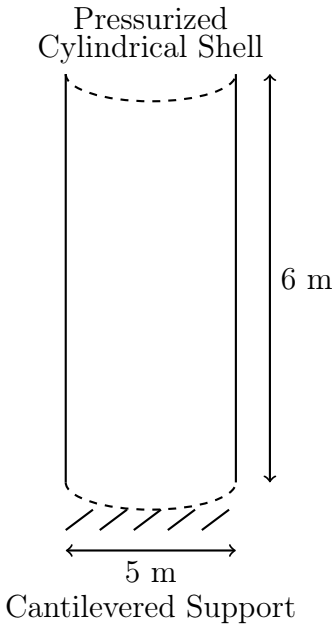


Figure 66: Structure idealization of the Cargo Module

The axial natural frequency $f_{nat,axial}$ for a uniform cantilevered cylinder is given by:

$$f_{nat,axial} = 0.250 \sqrt{\frac{AE}{mL}}$$

Rearranging for the minimum cross-sectional area A :

$$A = \left(\frac{4f_{nat,axial}^2 mL}{E} \right) = \frac{4 \times 25^2 \times 24,000 \times 6.0}{150 \times 10^9} = 400 \text{ mm}^2$$

The lateral natural frequency $f_{nat,lateral}$ for bending is given by:

$$f_{nat,lateral} = 0.560 \sqrt{\frac{EI}{mL^3}}$$

Rearranging for the minimum area moment of inertia I :

$$I = \left(\frac{f_{nat,lateral}^2 mL^3}{0.3136E} \right) I = \frac{10^2 \times 24,000 \times 6.0^3}{0.3136 \times 150 \times 10^9} \approx 11,000 \text{ cm}^4$$

The shell cross-section must satisfy simultaneously:

$$\pi(r_0^2 - r_i^2) \geq A \quad \text{and} \quad \frac{\pi}{4}(r_0^4 - r_i^4) \geq I$$

We solve for the internal radius r_i based on both constraints:

From the section area:

$$r_i = \sqrt{r_0^2 - \frac{A}{\pi}} = \sqrt{2.5^2 - \frac{0.0004}{\pi}} \approx 2.499975 \text{ m}$$

Thus, thickness due to axial stiffness:

$$t_{section} = r_0 - r_i \approx 2.5 - 2.499975 \approx 0.025 \text{ mm}$$

This is extremely thin, as expected: axial stiffness usually does not govern.

From the bending inertia:

$$r_i = \left(r_0^4 - \frac{4I}{\pi} \right)^{1/4} = \left(2.5^4 - \frac{4 \times 0.011}{\pi} \right)^{1/4} \approx 2.4984 \text{ m}$$

Thus, thickness due to lateral bending:

$$t_{bending} = 2.5 - 2.4984 \approx 1.6 \text{ mm}$$

The structure must also resist internal pressurization due to the 1 atm (101,325 Pa) environment inside the module.

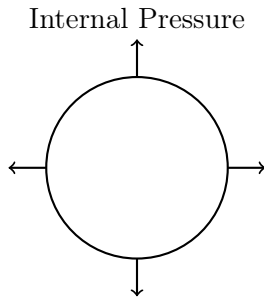


Figure 67: Hoop stress on the Cargo Module

The hoop stress in a thin-walled pressurized cylinder is given by Barlow's formula:

$$\sigma_h = \frac{Pr_0}{t} = \frac{101,325 \times 2.5}{0.0016} = 158.32 \text{ MPa}$$

The allowable tensile strength for the carbon composite is: $F_{tu} = 600 \text{ MPa}$ and considering a factor of safety of 2.0: $F_{allowable} = \frac{600}{2} = 300 \text{ MPa}$.

Since $\sigma_h = 158.32 \text{ MPa} < 300 \text{ MPa}$, the shell thickness of 1.6 mm is sufficient to withstand the internal pressure.

Thus, the final preliminary thickness remains:

$$t_{final} = 1.6 \text{ mm}$$

ensuring compliance with both dynamic stiffness and internal pressure resistance.

6.2.2 Reinforcements Sizing

We consider a simplified structural architecture in which the primary load-carrying elements of the Cargo Module are composed solely of an aluminium 7075-T6 lattice structure. The lattice includes longitudinal stiffeners (stringers) and transverse hoops (rings) with no load-bearing contribution from the composite skin. The objective is to determine the optimal number and sizing of these reinforcements to:

- Resist axial launch loads and lateral aerodynamic loads during reentry,
- Prevent local panel buckling,
- Minimize the total structural mass.

The equivalent axial load considering bending effects is:

$$M_{bending} = P_{lateral} \times L = 12,000 \times 9.81 \times 3.0 \times 6.0 ,$$

$$P_{eq} = P_{axial} + \frac{2M_{bending}}{R} = 12,000 \times 9.81 \times 6.0 + \frac{2 \times 2,118,960}{2.5} = 2,401,488 N$$

Applying a factor of safety, the ultimate load is then:

$$P_{ult} = 1.25 \times P_{eq} = 3,001,860 N$$

The presence of stringers and rings subdivides the skin into small rectangular panels that must be checked against local buckling. A skin thickness of $t = 1.6 mm$ is adopted from the previous analysis. The critical buckling stress for the panel is calculated using:

$$\sigma_{cr} = \frac{k\pi^2 E}{12(1-\nu^2)} \left(\frac{t}{b}\right)^2$$

where $k = 80$ from the graph in Figure 68 and $b = \text{circumferential bay width} = \frac{\pi D}{n_{stringers}}$.

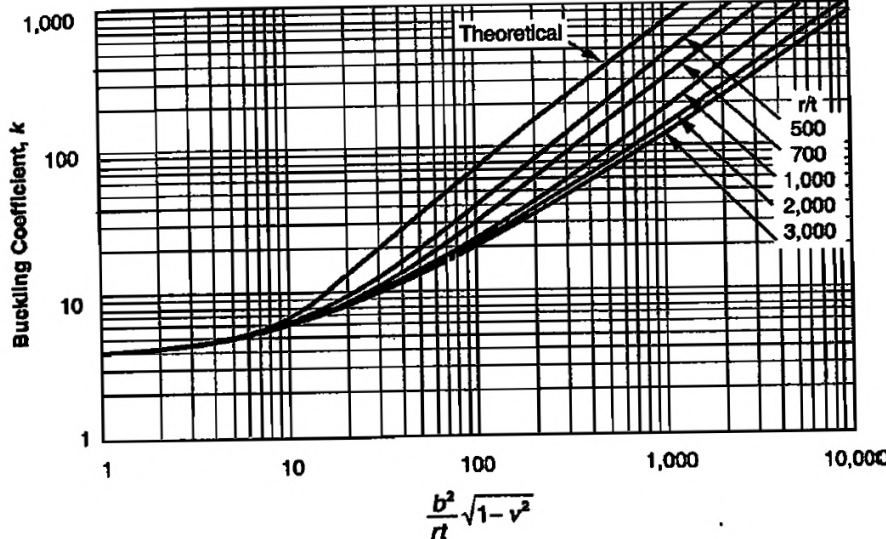


Figure 68: Coefficients of Axial Compressive Buckling for Long Curved Plates

The panel buckling load is:

$$P_{cr} = \sigma_{cr} \times (b \times h)$$

where $h = \frac{L}{n_{rings}}$ is the axial bay height.

The margin of safety on panel buckling is defined as:

$$MS = \frac{P_{cr}}{P_{ult}} - 1$$

Only configurations satisfying $MS \geq 0$ are retained.

Each stringer and each ring must carry a portion of the total axial-bending load:

$$\text{Force per stringer} = \frac{P_{ult}}{n_{stringers}} \Rightarrow A_{stringer} = \frac{\text{Force per stringer}}{\sigma_{yield}}$$

$$\text{Force per ring} = \frac{P_{ult}}{n_{rings}} \Rightarrow A_{ring} = \frac{\text{Force per ring}}{\sigma_{yield}}$$

The total mass is calculated considering the contributions of all stringers and rings. The optimization process explored various numbers of stringers and rings to minimize total structural mass while ensuring stability. A Python script was developed to sweep through all admissible combinations of:

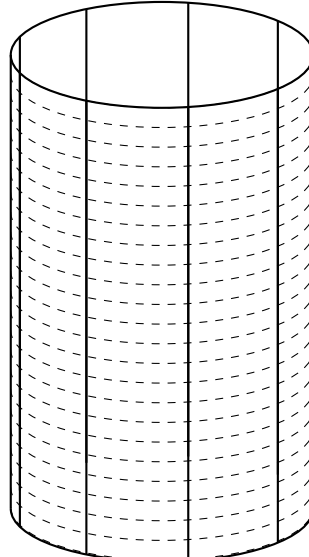
- $n_{stringers} \in [8, 40]$
- $n_{rings} \in [8, 40]$

The optimal configuration found is:

Parameter	Value
Number of Stringers	9
Cross-sectional Area per Stringer	4.82 cm^2
Number of Rings	23
Cross-sectional Area per Ring	1.89 cm^2
Total Mass	263.5 kg
Margin of Safety (Panel Buckling)	+0.03

Table 48: Optimized Structural Reinforcements for Cargo Module

This result ensures sufficient buckling resistance and structural capacity with minimal added mass, using a realistic layout of longitudinal and circumferential reinforcements.



Stringer-Ring Layout: 9 Stringers, 23 Rings

Figure 69: Stringer and Ring Arrangement for the Cargo Module

6.2.3 Large Opening Door

The Cargo Module features a large access double door covering half of the circumference over a longitudinal extent of 5.0 m. This opening significantly impacts the structural behavior by:

- Interrupting the load paths in the shell,
- Concentrating axial and hoop loads around the door frame,
- Locally reducing global stiffness and stability.

To mitigate these effects, structural reinforcements are implemented:

- Reinforced rings above and below the door to bridge the opening,
- Vertical posts along the door edges to redistribute hoop and axial loads,
- Increased stringer density adjacent to the opening to maintain stiffness.

A preliminary mass penalty of approximately +10% of the baseline reinforcement mass (+26 – 30 kg) is expected due to these adaptations.

Component	Mass (kg)
Carbon Composite Shell	113
Stringers and Rings Reinforcements	263.5
Additional Reinforcements (Door Region)	30
Total Structural Mass	406.5

Table 49: Cargo Module Preliminary Mass Budget

6.2.4 Preliminary Verification

A preliminary finite element analysis on Abaqus was conducted to verify that the composite shell thickness determined analytically could withstand the internal pressurization without exceeding material limits. The results are summarized in Table 50.

Input	Finite Element Results	Analysis Results
<p>Shell thickness: 1.6 mm</p> <p>Internal pressure: 1 atm</p>		<p>Maximal stress: ≈ 182 MPa</p> <p>Material: Composite Ultimate tensile strength: 600 MPa</p> <p>Status: Sized</p>

Table 50: Preliminary Verification of the Shell under Internal Pressure

6.3 Crew module

To prevent local skin buckling of the carbon shell between stiffening rings, a simplified analytical approach is used based on classical thin shell stability theory. Although the upper part of the capsule is conical, the following analysis assumes an equivalent cylindrical behavior with a correction factor to account for the cone inclination. This assumption is acceptable for a first-order structural sizing with an appropriate safety factor. Due to the criticality of the pressurized capsule structure and its role in crew protection, a safety factor of 1.5 is applied to all thicknesses.

6.3.1 Carbon shell

The primary structure of the capsule consists of a carbon-fiber shell, designed to withstand both the internal pressurization and a share of the axial structural load. The pressure differential between the inside and outside of the capsule is defined as:

$$P_{\text{diff}} = P_{\text{internal}} - P_{\text{external}} = 0.7 \text{ bar} - 0.1 \text{ bar} = 0.6 \text{ bar} = 60000 \text{ Pa} \quad (112)$$

Additionally, a fraction of the axial load (40%) is supported by the shell, leading to an axial stress. The required shell thickness is deduced as follow:

$$t_{\text{carbon}} = \frac{P_{\text{diff}} \cdot r}{\sigma_{\text{adm,carbon}}} + \frac{F_{\text{axial,carbon}}}{2\pi r \sigma_{\text{adm,carbon}}} \quad (113)$$

The total mass of the carbon shell (including the cylindrical and conical portions) is:

$$m_{\text{carbon}} = \rho_{\text{carbon}} \cdot (V_{\text{cyl}} + V_{\text{cone}}) \quad (114)$$

$$V_{\text{cyl}} = \pi (r_{\text{outer}}^2 - (r_{\text{outer}} - t_{\text{carbon}})^2) \cdot h_{\text{cylinder}} \quad (115)$$

$$V_{\text{cone}} = \frac{1}{3}\pi (r_{\text{outer}}^2 - (r_{\text{outer}} - t_{\text{carbon}})^2) \cdot h_{\text{cone}} \quad (116)$$

6.3.2 Reinforcement rings

the upper half of the capsule is a conical shell. Buckling in conical shells typically occurs at lower critical loads due to the inclination angle θ of the surface with respect to the vertical. This reduces the effective load-bearing capacity in the axial direction. To account for this effect the critical stress is reduced by the cosine of the cone angle:

$$\sigma_{\text{cr,cone}} = \sigma_{\text{cr}} \cdot \cos(\theta) \quad (117)$$

This leads to an extended cylindrical formula for the required ring thickness in the conical region:

$$t_{\text{ring,cone}} = \sqrt{\frac{\sigma_{\text{cr}} \cdot \cos(\theta) \cdot R \cdot s}{\pi^2 E_{\text{Al}}}} \quad (118)$$

The total length of rings includes both the cylindrical and conical regions. For each region, the circumference is computed and multiplied by the square cross-sectional area:

$$V_{\text{rings}} = \sum_{i=1}^{n_{\text{rings}}} C_i \cdot t_{\text{ring}}^2 \quad (119)$$

The corresponding mass is:

$$m_{\text{rings}} = V_{\text{rings}} \cdot \rho_{\text{Al}} \quad (120)$$

6.3.3 Reinforcement stringers

Aluminum stringers are used to reinforce the capsule structure and provide axial load-carrying capacity. A total of $n = 15$ stringers are placed symmetrically along the circumference. The design assumes that 60% of the total axial force is supported by the stringers. The required cross-sectional area for each stringer, considering the conical inclination angle θ , is:

$$A_{\text{stringer}} = \frac{F_{\text{axial, stringers}}}{n \cdot \sigma_{\text{adm, Al}} \cdot \cos(\theta)} \quad (121)$$

A square cross-section is assumed, with an equivalent thickness given by:

$$t_{\text{stringer}} = \sqrt{A_{\text{stringer}}} \quad (122)$$

The length of each stringer spans the cylindrical height plus the slant height of the cone:

$$L_{\text{stringer}} = h_{\text{cyl}} + \sqrt{h_{\text{cone}}^2 + r_{\text{outer}}^2} \quad (123)$$

The total mass of the stringers is then computed by multiplying the area, length, number of stringers, and material density.

6.3.4 Separation ring

The interface between the capsule and the lower cargo module is ensured by a structural separation ring designed to withstand internal pressure and the force transmitted by the crew system (3 tons). This annular aluminum bulkhead is dimensioned for the combination of both load types:

$$t_{\text{sep}} = \left(\frac{P_{\text{diff}} \cdot r}{\sigma_{\text{adm, Al}}} + \frac{F_{\text{sep}}}{2\pi r \cdot \sigma_{\text{adm, Al}}} \right) \quad (124)$$

The design assumes a full annular plate of radius r and thickness t_{sep} , with the resulting volume and mass given by:

$$V_{\text{sep}} = \pi r^2 t_{\text{sep}} \quad ; \quad m_{\text{sep}} = \rho_{\text{Al}} \cdot V_{\text{sep}} \quad (125)$$

6.3.5 Verification

To ensure the structural integrity of the capsule during ascent and operation, two verifications are performed: the natural frequencies of the structure, and its resistance to dynamic aerodynamic pressure.

6.3.5.1 Vibrational modes The capsule is modeled as a spring-mass system to estimate the first axial mode. The effective axial stiffness k combines contributions from the carbon shell and aluminum stringers:

$$E_{\text{eq}} = \frac{E_{\text{Al}} \cdot n_{\text{stringers}} \cdot A_{\text{stringer}} + E_{\text{carbon}} \cdot 2\pi r_{\text{outer}} \cdot t_{\text{carbon}}}{A_{\text{axial, total}}} \quad (126)$$

$$k = \frac{E_{\text{eq}} \cdot A_{\text{axial, total}}}{L_{\text{total}}} \quad (127)$$

$$f_{\text{axial}} = \frac{1}{2\pi} \sqrt{\frac{k}{m_{\text{capsule}} + m_{\text{structure}}}} \quad (128)$$

The resulting axial frequency was found to be $f_{\text{axial}} = 96.8 \text{ Hz}$, well above the requirement of 25 Hz.

The shell is approximated as a cylindrical thin-walled structure. The fundamental radial frequency (mode 2,1) is estimated using classical shell theory:

$$D = \frac{E_{\text{carbon}} \cdot t_{\text{carbon}}^3}{12(1 - \nu^2)} \quad (129)$$

$$\mu = \rho_{\text{carbon}} \cdot t_{\text{carbon}} \quad (130)$$

$$\omega_{\text{radial}} = (n^2 - 1) \cdot \sqrt{\frac{D}{\mu \cdot R^4}} \cdot 10^2, \quad \text{with } n = 2 \quad (131)$$

$$f_{\text{radial}} = \frac{\omega_{\text{radial}}}{2\pi} \quad (132)$$

The natural radial frequency is calculated as $f_{\text{radial}} = 162.2 \text{ Hz}$, exceeding the minimal threshold of 10 Hz.

6.3.5.2 Dynamic Pressure The capsule is subject to peak aerodynamic pressure during transonic flight, typically around Mach 1 and 10 km altitude. A conservative estimate assumes:

$$\rho = 0.5 \text{ kg/m}^3, \quad v = 700 \text{ m/s} \quad (133)$$

$$q_{\text{dyn}} = \frac{1}{2} \rho v^2 = 122.5 \text{ kPa} \quad (134)$$

This pressure induces a circumferential stress in the shell:

$$\sigma_{\theta} = \frac{q_{\text{dyn}} \cdot r_{\text{outer}}}{t_{\text{CFRP}}} \quad (135)$$

With the computed shell thickness, the resulting hoop stress is $\sigma_{\theta} = 40.8 \text{ MPa}$, far below the CFRP allowable stress $\sigma_{\text{adm}} = 800 \text{ MPa}$.

At the end we obtain the following results for the life module design :

Table 51: Main geometric and mass parameters of the capsule structure

Element	Value
Outer radius (capsule)	2.50 m
Cylindrical height	1.00 m
Conical height	3.00 m
CFRP shell thickness	0.0075 m
Number of stringers	15
Stringer area	0.000020 m ²
Estimated stringer thickness	0.0100 m
Stringer length	3.91 m
Number of rings	15
Ring thickness	0.0218 m
Average spacing (cylinder)	0.143 m
Average spacing (cone)	0.429 m
Separation ring thickness	0.0100 m
CFRP mass	376.4 kg
Stringer mass	4.2 kg
Ring mass	242.2 kg
Separation mass	549.8 kg
Total structural mass	1172.6 kg
Inner radius (capsule)	2.493 m

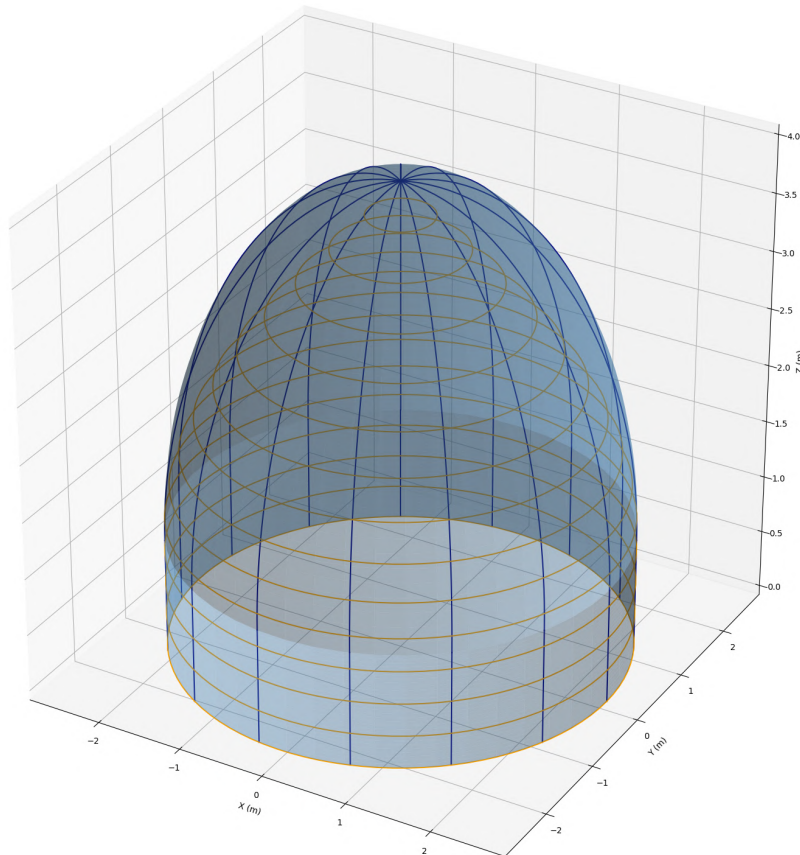


Figure 70: Life module

6.4 Computer Aided Design

The complete shuttle was modeled in 3D using PTC Creo, providing a comprehensive view of the internal and external structures, as well as the integration of major subsystems. This CAD model supports preliminary structural studies, propulsion layout, and system interfaces.

The structure of the shuttle consists of a lattice framework. The frame follows a quasi-geodesic pattern that allows load distribution and is compatible with thermal shielding tiles and structural panels.

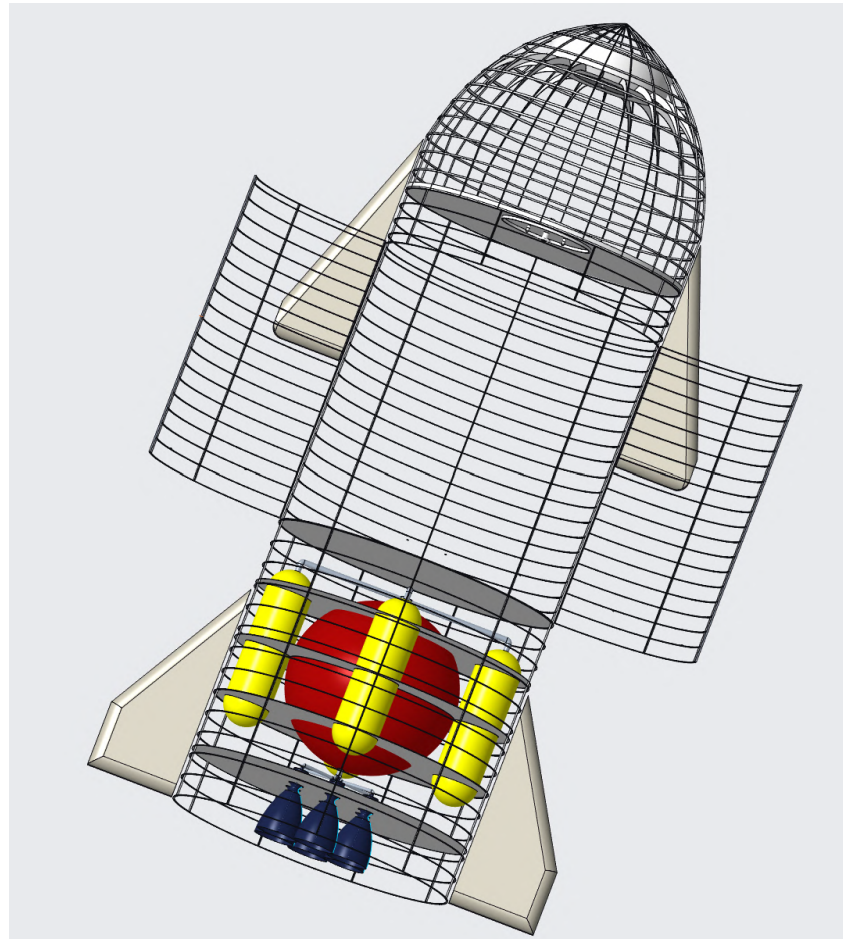


Figure 71: Structural frame

The propulsion subsystem is centered around a large spherical NOFBX tank (red), surrounded by multiple high-pressure helium Composite Overwrapped Pressure Vessels (yellow) for pressurization. The engines are located at the base of the system, with feed lines connecting the tanks and thrusters through a series of manifolds.

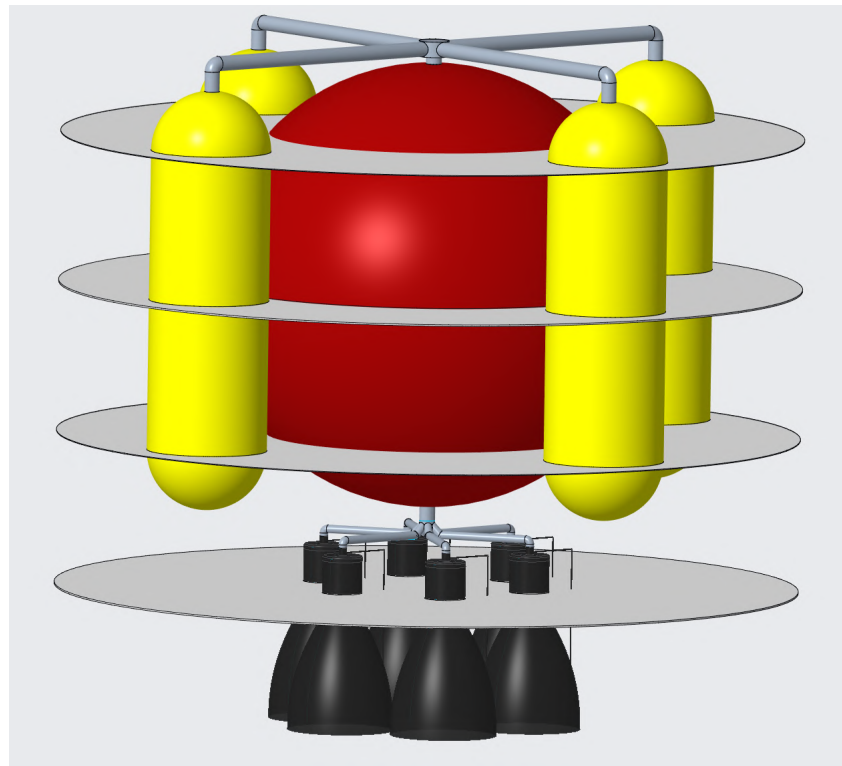


Figure 72: Propulsion layout

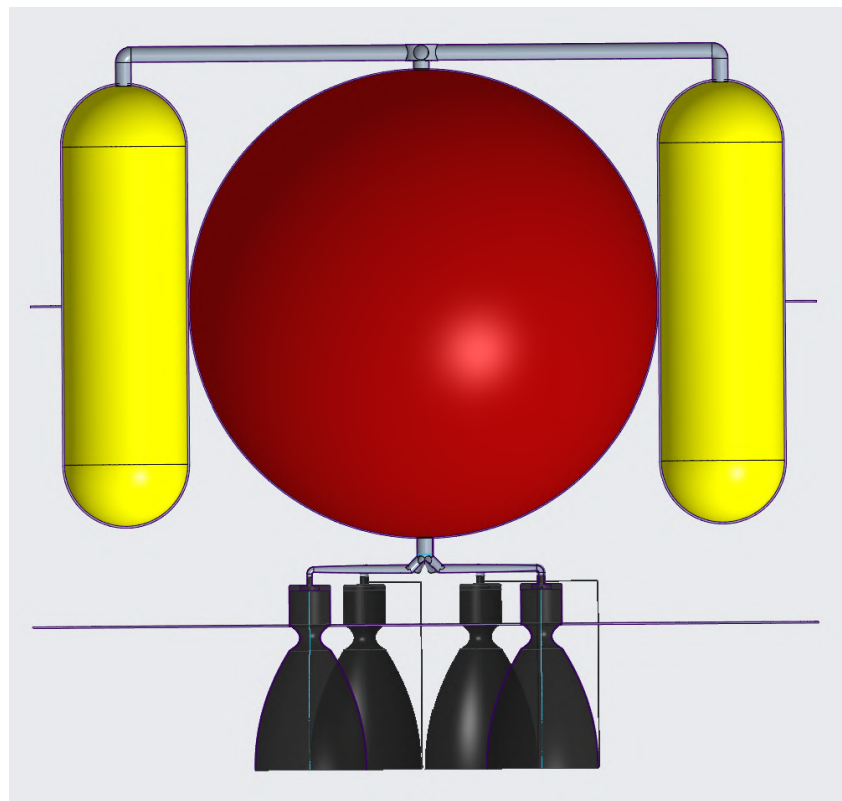


Figure 73: Propulsion section

The docking port has been modeled with the interface chosen in the docking part. The

hatch mechanism includes a pressurized airlock chamber with both open and closed configurations visualized below.

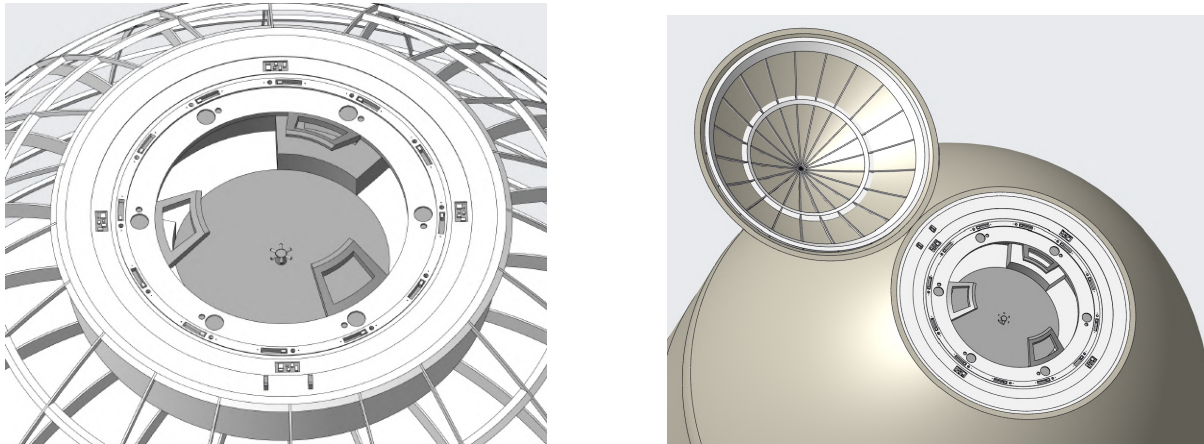


Figure 74: Detail of the docking interface

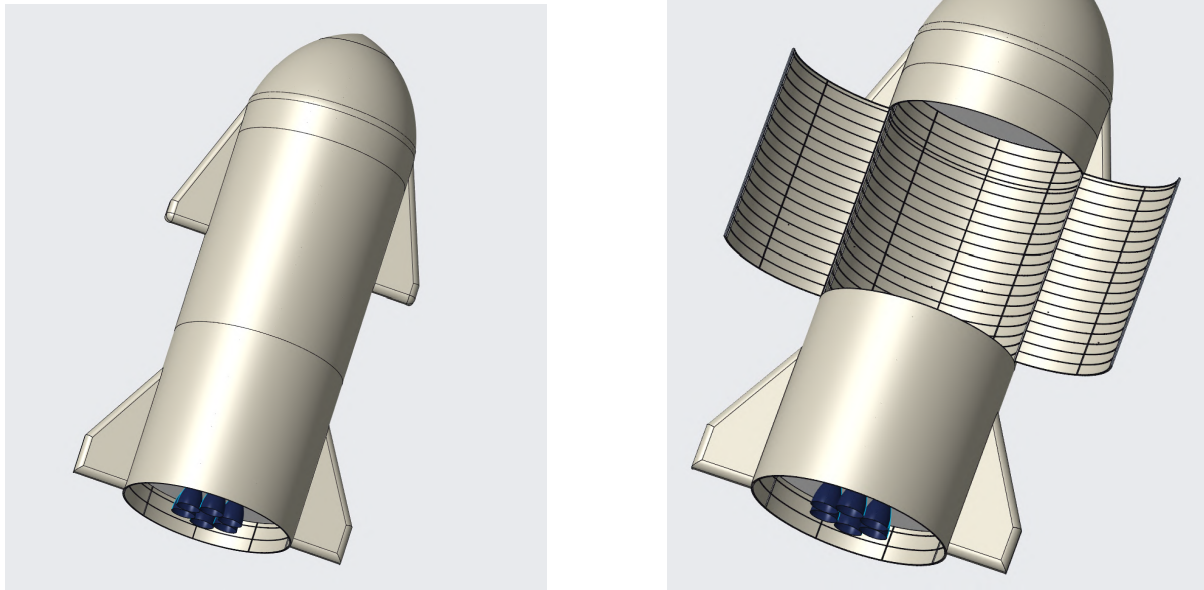


Figure 75: Cargo hatch in open and closed positions

The shuttle model also includes aerodynamic control surfaces (flaps). Detailed modeling was performed for critical components such as the engine injector and ignitor, which are shown in the following figures. The final capsule geometry, including the pressurized structure and hatch mechanisms, is also depicted to provide a complete overview of the spacecraft.

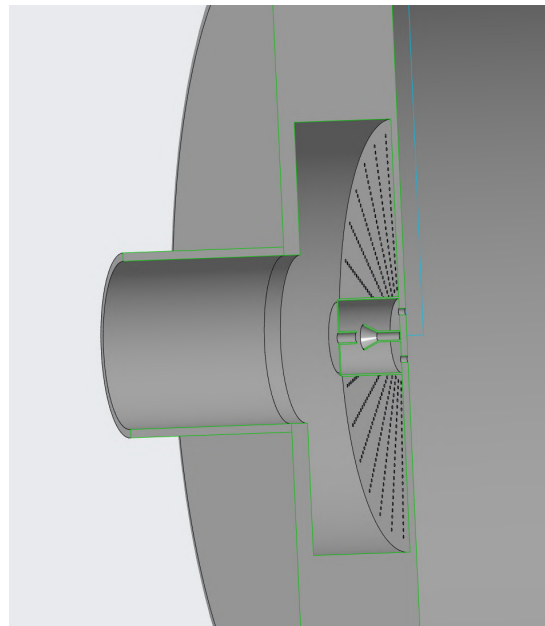


Figure 76: Engine injector and ignitor

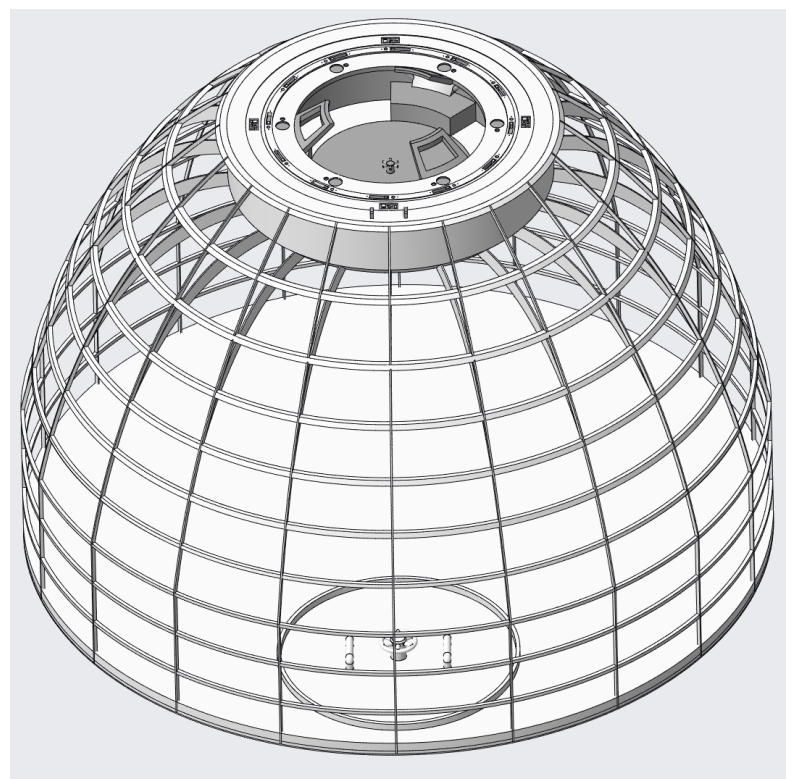


Figure 77: Capsule layout

This CAD effort enables future Finite Element Analysis (FEA), thermal path validation, and mass estimation.

6.5 Abort system

To ensure crew safety in all critical situations, the spacecraft is equipped with an integrated emergency escape system designed to function during the launch and landing phases.

In the event of a critical failure during launch, explosive bolts allow rapid separation from the launch vehicle. Immediately after separation, all main engines of the shuttle are activated to ensure sufficient thrust for safe distancing. Once a safe distance is reached, a retropropulsive maneuver is executed to decelerate the shuttle and initiate a controlled return trajectory. This sequence allows the capsule to perform a safe landing, preserving astronaut integrity.

In the event of a catastrophic failure during landing, an individual ejection system (100 kg) is provided for each astronaut (as demonstrated by the Russian emergency procedures during the Soyuz program). Above each seat, a canopy is installed to provide situational awareness. If necessary, explosive bolts shatter the canopy, allowing for ejection. Each seat, based on the Martin-Baker ejection system Martin-Baker Aircraft Company Limited [2025], is equipped with integrated retro-rockets to propel the astronaut away from the structure. A personal parachute, embedded in the seat, is automatically deployed to ensure a safe and independent descent.



Figure 78: Martin Becker seat

Note: Ejecting with a Martin-Baker seat grants you a complimentary tie.

6.6 Conclusion

The structural design of the spacecraft rely on classical analytical approaches to satisfy mechanical strength and stiffness. The propulsion and crew modules were sized using a load-sharing strategy between a carbon-fiber shell and aluminum reinforcements, while the cargo module adopted a stiffened shell approach with optimized reinforcements to minimize mass. The total structural mass of the spacecraft is approximately 3700 kg, which remains well below the 20% mass budget requirement. However, this estimation does not yet account for several subsystems such as the heat shield, flaps and thermal insulation. A second iteration will be required to refine the mass estimate and verify compliance with all constraints under a more complete configuration.

All structural elements meet the minimum stiffness and strength requirements under axial, lateral, and pressurization loads, with verified safety margins. Preliminary vibrational analysis confirms that natural frequencies remain above critical thresholds, avoiding potential resonance issues. Furthermore, the integration of CAD models provides a detailed visualization of the structure and will support future Finite Element Analysis (FEA).

7 Communication

7.1 Requirements

Requirement ID	Description
COM-REQ-01	Ensure telemetry (TM) transmission to ground.
COM-REQ-02	Ensure telecommand (TC) reception from ground.
COM-REQ-03	Ensure continuous real-time communication (voice + video) during Rendezvous and Docking phases.
COM-REQ-04	Maintain a direct communication link with the Station during docking (voice + sensor data).
COM-REQ-05	Provide secure communication with encryption and authentication.
COM-REQ-06	Include an emergency UHF beacon for backup communication.
COM-REQ-07	Ensure redundancy for all critical communication links.

Table 52: StarCheap Communication Subsystem Requirements

7.2 Needs Analysis

Throughout all mission phases, a continuous real-time communication link with ground control is mandatory. This link must carry telemetry and telecommand data, as well as crew voice communications. The telemetry flow, comprising housekeeping data such as system statuses, temperatures, pressures, and voltages, is expected to require approximately 100 kbps under nominal conditions. In parallel, voice transmission from the crew to ground control, using efficient compression techniques, will require an additional 16 to 32 kbps. Consequently, the permanent real-time TT&C channel must support a total data rate of approximately 132 kbps.

During critical operations, such as rendezvous with debris and docking maneuvers, real-time video transmission becomes essential. To enable proper supervision and validation of these phases, a compressed video stream must be transmitted continuously to the ground. A typical operational video feed, providing moderate resolution and frame rate, will require a data rate between 500 kbps and 1.5 Mbps.

Simultaneously, during docking with the Station, a direct communication link must be established to exchange voice communications and relative navigation sensor data independently from relay satellite coverage. This link must be capable of handling a combined data rate of 72 kbps. The modest bandwidth has to ensure reliable transmission with sufficient margin even in degraded conditions.

Finally, an emergency communication capability must be continuously active. In case of failure of the primary communication links, a simplified backup channel must allow transmission of critical telemetry and beacon signals to ground control.

7.3 Communication Strategy

7.3.1 Continuous Link with Relays

Due to the low altitude of StarCheap (500 km), the shuttle travels at approximately 7.6 km/s and completes an orbit in about 90 minutes. Each ground station only provides a visibility window of 5 to 10 minutes per pass.

To achieve true continuous coverage only with ground stations would require approximately **80 ground stations** distributed uniformly across the Earth's surface. This is impractical in terms of cost, logistics, and coordination.

To ensure a real-time continuous link during critical phases, different relay options were considered:

Relay System	Technology	Remarks
TDRSS (NASA)	S/Ku/Ka	High datarate, not for commercial projects
EDRSS (ESA)	Laser/Ka	Requires laser terminal, high complexity
O3b mPOWER (SES)	Ka	High datarate, flexible access

Table 53: Relay Options Trade-Off

Selected solution: The SES O3b mPOWER system has been selected for the StarCheap mission to guarantee continuous communication for TM/TC, voice, and video throughout all mission phases, with high reliability and commercial flexibility.

7.3.2 Direct Link with Ground

In addition to relayed communication through satellite relays, direct communication with ground stations is possible whenever the StarCheap passes over a ground station within line of sight.

Primary use of the direct link is to download non-critical housekeeping telemetry and specific mission data. However, the direct S-band link with ground stations is also fully capable of handling TT&C and voice communications when there is a visibility opportunity. Thus, the StarCheap can switch dynamically to direct TT&C and voice operations through the ground station, either to increase link robustness or as a backup path in case of relay unavailability.

To ensure these capabilities, it is necessary to select a network of ground stations meeting specific operational and technical criteria. Stations must be located at latitudes that allow frequent visibility windows given StarCheap's orbital inclination of approximately 50 degrees and be equipped with S-band transmitters and receivers.

Based on these criteria, the following ground stations from the ESTRACK network have been selected:

Station	Latitude	Longitude	Diameter (m)	Efficiency	Gain Command (dB)	Gain Telemetry (dB)	Transmit Power (dBW)	Noise Temp (K)
Redu	50.0° N	5.17° E	2.5	0.6	48.16	48.95	40	200
Kourou	5.16° N	52.65° W	15	0.6	48.16	48.95	40	200
Maspalomas	27.77° N	15.58° W	15	0.6	48.16	48.95	40	200
New Norcia	30.95° S	116.19° E	35	0.6	55.52	56.31	40	50

Table 54: Summary of ESTRACK Ground Stations Selected

These stations are strategically distributed across Europe, South America, and Oceania, ensuring that the StarCheap can maintain regular contact opportunities across multiple orbital revolutions.

To validate the viability of direct communication with ground stations, a visibility analysis was conducted using the Satorb orbital simulation software. The analysis simulated StarCheap's access opportunities to each selected ground station over several orbital periods during one week (01/01/2030 → 08/01/2030), considering a minimum elevation angle of 5 degrees.

The results are summarized in the table below:

Station	Number of Passes	Mean Duration per Pass (min)	Total Time (min)	Average Time per Day (min)
Kourou	27	7.45	201.15	28.74
Maspalomas	35	7.52	263.20	37.60
New Norcia	42	7.29	306.18	43.74
Redu	7	7.94	55.58	7.94

Table 55: Access Summary Results per Ground Station (Satorb Analysis)

Figures below illustrate the access opportunities calculated for each ground station:

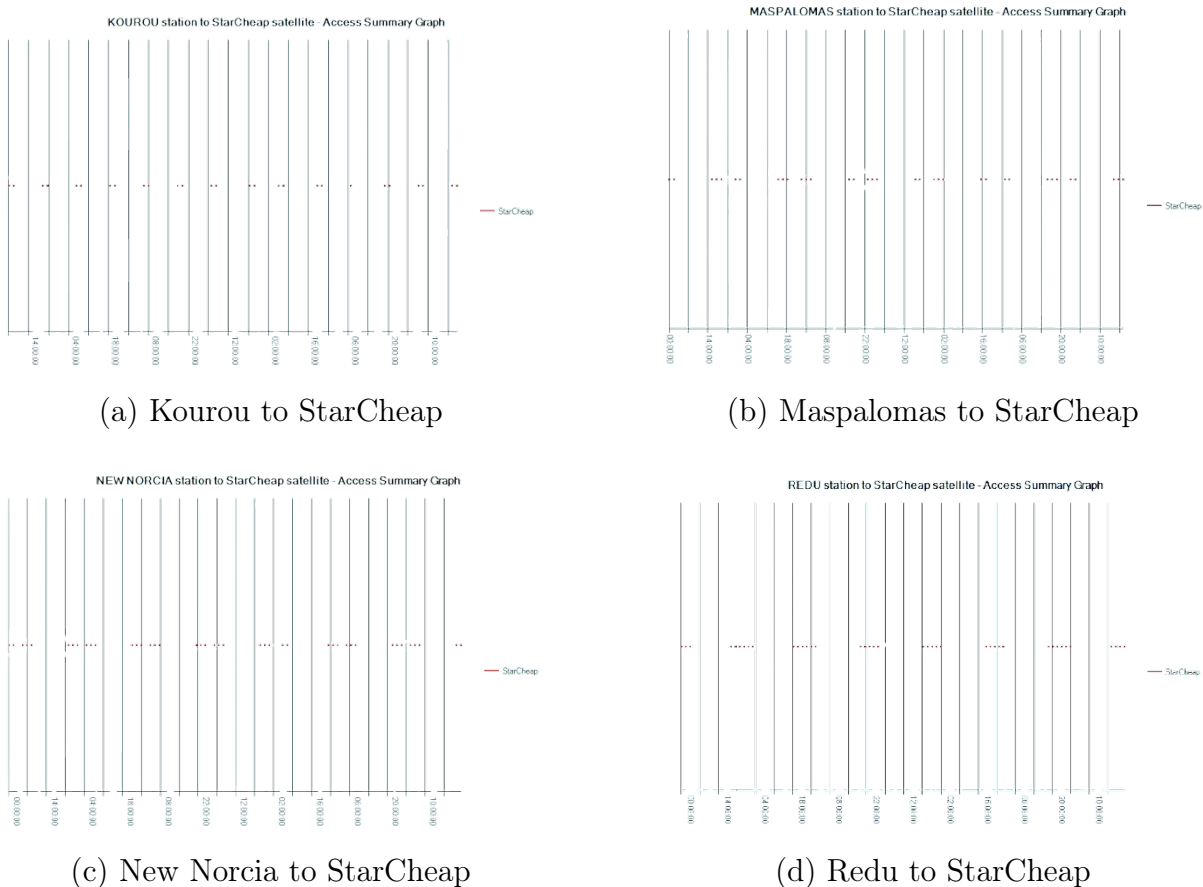


Figure 79: Access Windows between StarCheap and Ground Stations (Satorb Analysis)

The simulation confirms that direct communication windows with ground stations occur frequently throughout StarCheap’s orbital period. The average access duration per pass is approximately 7.4 minutes with an average total access duration per day of approximately 2 hours. Considering all ground stations combined, the average time between two communication opportunities remains acceptable for opportunistic housekeeping data transmission.

7.3.3 Direct Link with Station

For docking and close-proximity operations with the Station, the StarCheap establishes a direct communication link, allowing us to remain fully autonomous during safe approach maneuvers, independent from any relay satellite infrastructure. The use of S-band around 2.2 GHz is motivated by its favorable propagation characteristics in LEO, offering good resistance to atmospheric effects and the use of relatively compact antennas.

To ensure interoperability, the communication system has been interfaced and harmonized with the design of both the Station and the partnering OSIRIS Shuttle. This alignment guarantees compatibility of the transmission parameters and communication protocols.

The direct communication link is activated at the S_0 rendezvous point, corresponding to an approach distance of approximately 30 km from the station, with the StarCheap

positioned 30 degrees below the Station in its local orbital frame.

The modulation scheme selected for this link is Staggered QPSK (SQPSK), following the current state of the art for proximity links in space applications. SQPSK provides increased robustness against multipath and Doppler effects, while maintaining high spectral efficiency.

7.3.4 Global Architecture

The following figure illustrates the global communication architecture, showing the various links established between the StarCheap, relay satellites, ground stations, and the Station:

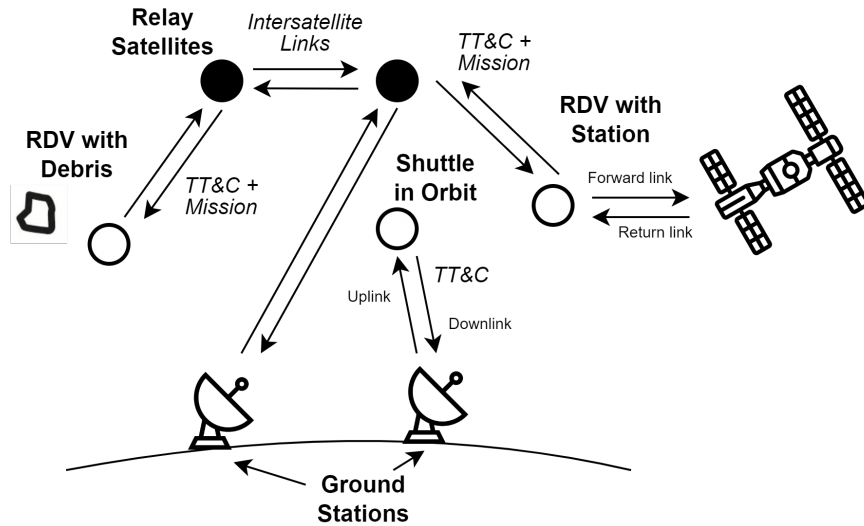


Figure 80: Communication Architecture

A summary of the different communication links, their corresponding frequency bands, and transmission media is provided in Table 56:

Link	Band	Medium
TT&C + Voice	Ka-Band	SES O3b mPOWER Relay or Direct Ground
Mission Data (Video)	Ka-band	SES O3b mPOWER Relay
Specific Telemetry	S-band	Direct to Ground Stations
Docking Link	S-band	Direct to Target Station
Emergency Beacon	UHF	Direct to Ground

Table 56: Summary of Communication Links for StarCheap

For the different communication links, the selection of radio parameters is performed in compliance with the Radiocommunication Regulations established by the International Telecommunication Union (ITU).

The key characteristics considered for each type of link are summarized below:

Link	Frequency	Data Rate	Bandwidth	Modulation
Relays	Uplink: 27.5–31.0 GHz Downlink: 17.7–21.2 GHz	1.7 Mbps		QPSK / 8PSK
Ground	Uplink: 2.2 GHz Downlink: 2 GHz	132 kbps	100 kHz	BPSK
Station	Forward link: 2.2 GHz Return link: 2.2 GHz	72 kbps	100 kHz	SQPSK / BPSK

Table 57: Summary of Link Parameters

7.4 Links budget calculation

7.4.1 Communication with Relay - SES O3b mPOWER

We are going to calculate the link budget for our downlink between the shuttle and the O3B relay satellites located at an altitude of 8,000 km. We make several assumptions, in particular the maximum distance between a satellite in the constellation and the shuttle is 14,412 km. Furthermore, since the shuttle will be picking up debris at 896 km, we're assuming a maximum shuttle altitude of 1000 km.

Link	StarCheap (Patch Antenna)	O3b mPower (Patch Antenna)
Frequency: 21.2 GHz	Max depointing: $\Delta\gamma_{max} = 5^\circ$	$G_r/T_s : 26.5 \text{ dB}$
Bit Error Rate (BER): 10^{-8}	Antenna efficiency: $\eta_s = 0.6$	Antenna efficiency: $\eta_{gs} = 0.6$
Modulation: QPSK	Line Loss: $L_{ls} = 3 \text{ dB}$	$G_r : 54.26 \text{ dB}$
Rate: 1.7 Mbps	Power Amplification Ratio: $\eta_{amp} = 0.2$	$T_s : 597.026 \text{ K}$
Demodulator degradation: $L_d = 1.5 \text{ dB}$		
Pointing Loss: $L_\theta = 3 \text{ dB}$		
Link Margin: $LM = 5 \text{ dB}$		

Table 58: Downlink data from StarCheap to O3B mPower satellites

The link budget can be expressed by the following formula:

$$EIRP = C/N_0 - \frac{Gr}{T_s} - \sum L_i - 10 \log_{10}(k)$$

$$EIRP = P_t + L_{ls} + G_t$$

$$C/N_0 = E_b/N_0 + 10 \log_{10}(R_b) + LM$$

Where : EIRP the effective isotropic radiated power in dBw, C/N_0 the carrier-to-noise-

density-ratio in dB, E_b/N_0 is the ratio of received energy-per-bit to noise-density in dB, G_t is the transmit antenna gain in dB, G_r is the receive antenna gain in dB, L_i are losses in dB, L_{ls} is the transmitter-to-antenna line loss. k is Boltzmann's constant = $1.380 \times 10^{-23} \text{ J/K}$, R_b is the data rate.

For the modulation QPSK at BER of 10^{-8} , the required E_b/N_0 is 12 dB.

Thus, the Carrier-to-noise density ratio is:

$$C/N_0 = 12 + 10 \log_{10}(1.7 \times 10^6) + 5 = 12 + 62.3 + 5 = 79.3 \text{ dB}$$

In our case, we consider the free-space loss, pointing loss, demodulation loss and line loss.

$$\sum L_i = L_{FSPL} + L_d + L_\theta + L_{ls} = 202.14 + 1.5 + 3 + 3 = 209.64 \text{ dB}$$

The free-space loss:

$$L_{FSPL} = 20 \log_{10} \left(\frac{3 \times 10^8}{4\pi \times 14412 \times 10^3 \times 21.2 \times 10^9} \right) \approx -202.14 \text{ dB}$$

Now we compute the gain of the antenna on our space shuttle. We assume a the maximum vertical angle between the StarCheap and th O3B constellation is $\theta = 5$. Also we have $\theta_{3dB} = 45$.

$$G_{t, max} = 10 \log_{10} \left(0.6 \times \left(\frac{70\pi}{45} \right)^2 \right) = 14.32 \text{ dB}$$

$$G_t = G_{t, max} - 12 \left(\frac{5}{45} \right)^2 \approx 14.18 \text{ dB}$$

Finally, the required transmitted power:

$$P_t = 79.3 - 14.18 - 26.5 + 209.64 - 228.6 = 16.66 \text{ dBw}$$

Converted to Watts :

$$W = \frac{10^{16.66/10}}{\eta_{amp}} \approx 46.35 \text{ W}$$

Thus, the required transmitted power is approximately **46.35 W** to maintain the down-link under nominal conditions.

Link	StarCheap (Patch Antenna)	O3b mPower (Patch Antenna)
Frequency: 31 GHz	Max depointing: $\Delta\gamma_{max} = 5^\circ$	Antenna efficiency: $\eta_{gs} = 0.6$
Bit Error Rate (BER): 10^{-8}	$G_r/T_s : 12.8 \text{ dB}$	$G_t : 53.84 \text{ dB}$
Modulation: QPSK		Line losses $L_{ls} : 0.5 \text{ dB}$
Rate: 1.7 Mbps		Antenna efficiency: $\eta_s = 0.6$
Miscellaneous losses: $L_d = 1.5 \text{ dB}$		
Pointing Loss: $L_\theta = 3 \text{ dB}$		
Link Margin: $LM = 5 \text{ dB}$		

Table 59: Uplink data from O3B to StarCheap

Following the parameters summarized in Table 59, and considering the carrier-to-noise density ratio $\left(\frac{C}{N_0}\right)$ target for the backup command link, the required Effective Isotropic Radiated Power (EIRP) from the O3B constellation acting as a relay is approximately 56.54 dBW.

The following antenna corresponds to the Ka-band uplink and downlink link budget. The antenna is configured with 2 Transmit Subarrays (20 x 40 cm) and 6 Receive Subarrays (45 cm x 34 cm). The array weights 11 kg for the Rx and 7 kg for the Tx. This phased array antenna stands out for its ability to generate multiple independently steerable beams, providing enhanced flexibility and precision. With the distribution of active components, this antenna benefits from high reliability, reducing the risk of failure. However, it has notable drawbacks, such as high cost and weight, as well as increased losses in the feed distribution system. Despite these challenges, it achieves a high equivalent isotropically radiated power (EIRP: 49 dBW at boresight and 46.8 dBW at 45° elevation) by combining

signals from many small transmitters, a technique known as space combining. This feature makes it a preferred choice for applications requiring high performance and extensive coverage. In addition, this antenna can achieve a transmission power of 430 W, enabling us to increase the data rate to 130 Mbits.



Figure 81: Ka-Band Antenna - BAE Systems



Figure 82: SWIFT-X KTRX Transceiver

Characteristic	Value
Tx Frequency	20.2 - 21.2 GHz / 24 - 27 GHz
Rx Frequency	30 - 31 GHz
RF Modulation	BPSK / QPSK / OQPSK / 8PSK / 16APSK
Error Correction	LDPC / BCH / Reed Solomon / Convolutional
Bandwidth	Tx: 250 MHz / Rx: 200 MHz
Peak Throughput	> 1 Gbps
Tx Power	Up to +35 dBm
Receiver Sensitivity	Minimum -117 dBm
Frequency Accuracy	± 1.5 ppm
Power Consumption	Tx: 50 W / Rx: 20 W (Total: 60 W)
Weight	< 1 kg

Table 60: Characteristics of the SWIFT-X KTRX Transceiver.

The SWIFT-X KTRX transceiver, is an ideal component for the design of our spacecraft, especially when paired with the previously described antenna, considering the addition of SMA connection cables to the mass budget.

7.4.2 Direct Communication with Ground

Link	StarCheap (Patch Antenna)	Redu Station (Parabolic Antenna)
Frequency: 2.2 GHz	Max depointing: $\Delta\gamma_{max} = 5^\circ$	Antenna diameter: $d_{gs} = 2.5 \text{ m}$
Bit Error Rate (BER): 10^{-6}	Antenna efficiency: $\eta_s = 0.6$	Antenna efficiency: $\eta_{gs} = 0.6$
Modulation: BPSK	Line Loss: $L_{ls} = 1 \text{ dB}$	Noise Temperature: $T_{gs} = 200 \text{ K}$
Rate: 132 kbps	Power Amplification Ratio: $\eta_{amp} = 0.2$	
Demodulator degradation: $L_d = 1.5 \text{ dB}$		
Atmospheric/rain loss: $L_a = 0.2 \text{ dB}$		
Link Margin: $LM = 5 \text{ dB}$		

Table 61: Downlink data from StarCheap to Ground Station (Redu)

We will now calculate the required transmitted power, antenna gains, and other parameters to achieve the desired signal quality and data rate for the downlink from StarCheap to ground.

The link budget can be expressed by the following formula:

$$P_t = C/N_0 - G_t(\theta) - G_r + 10 \log_{10}(T_r) + \sum L_i + 10 \log_{10}(k)$$

Where:

- P_t : Required transmitted power [dBW]
- C/N_0 : Carrier-to-noise density ratio [dBHz]
- G_t : Gain of the transmitting antenna [dB]
- G_r : Gain of the receiving antenna [dB]
- T_r : System noise temperature [K]
- L_i : Total link losses (transmission, rain, degradation) [dB]
- k : Boltzmann constant = 1.380649×10^{-23} J/K

First, the receiver gain (Redu Station) is computed using:

$$G_r = 20 \log_{10} \left(\frac{\pi \times d}{\lambda} \right) + 10 \log_{10}(\eta)$$

where:

$$\lambda = \frac{c}{f} = \frac{3 \times 10^8}{2.2 \times 10^9} = 0.136 \text{ m}$$

Thus:

$$G_r = 20 \log_{10} \left(\frac{\pi \times 2.5}{0.136} \right) + 10 \log_{10}(0.6) = 44.4 \text{ dB}$$

For the modulation BPSK at BER of 10^{-6} , the required E_b/N_0 is 10.8 dB.
Thus, the Carrier-to-noise density ratio is:

$$C/N_0 = 10.8 + 10 \log_{10}(132000) + 5 = 10.8 + 51.2 + 5 = 67 \text{ dB}$$

Now, for the spacecraft patch antenna:

The half-power beamwidth (HPBW) is computed from the minimum elevation of 5° :

$$\theta_{3dB} = 2 \times (\arcsin(\cos(5^\circ)) \times \frac{R_e}{R_e + h}) + \Delta\gamma_{max} \approx 128.9^\circ$$

Thus, the maximum transmit antenna gain is:

$$G_{t, max} = 10 \log_{10} \left(0.6 \times \left(\frac{70\pi}{128.9} \right)^2 \right)$$

$$G_{t, max} \approx 2.42 \text{ dB}$$

We now have the transmitter gain:

$$G_t = G_{t, \max} - 12 \left(\frac{\arcsin(\cos(5^\circ) \times \frac{R_e}{R_e+h})}{128.9} \right)^2 \approx -0.13 \text{ dB}$$

The slant range is computed with the Law of Cosines:

$$d = \sqrt{(R_e + h)^2 + R_e^2 - 2(R_e + h)R_e \cos(90^\circ - \Delta\gamma_{\max} - \theta_{3dB}/2)}$$

where $h = 1000$ km the highest debris altitude we target, $R_e = 6378$ km.

Thus:

$$d \approx 2643.6 \text{ km}$$

The free-space loss:

$$L_{FSPL} = 20 \log_{10} \left(\frac{4\pi \times 2643.6 \times 10^3}{0.136} \right) \approx 167.8 \text{ dB}$$

Additional losses considered:

- Transmission losses: 1 dB
- Atmospheric/rain loss: 0.2 dB
- Demodulator degradation: 1.5 dB

Total link losses:

$$\sum L_i = 1 + 0.2 + 1.5 + 167.8 = 170.5 \text{ dB}$$

Finally, the required transmitted power:

$$P_t = 67 + 0.13 - 44.4 + 23.01 + 170.5 - 228.6$$

$$P_t = -12.36 \text{ dBW} = 17.64 \text{ dBm}$$

Converted to Watts:

$$W = \frac{10^{-12.36/10}}{\eta_{amp}} \approx 0.29 \text{ W}$$

Thus, the required transmitted power is approximately **290 mW** to maintain the down-link under nominal conditions at 1000 km altitude.

Link	StarCheap (Patch Antenna)	Redu Station (Parabolic Antenna)
Frequency: 2 GHz	Gain: -0.13 dB	Antenna diameter: $d_{gs} = 2.5$ m
Bit Error Rate (BER): 10^{-6}	Noise Temperature: $T_s = 450^\circ K$	Antenna efficiency: $\eta_{gs} = 0.6$
Modulation: BPSK		Losses: $L_{gs} = 2$ dB
Rate: 50 kbps		
Miscellaneous losses: $L_{mis} = 1.5$ dB		
Atmospheric/rain loss: $L_a = 0.2$ dB		
Link Margin: $LM = 5$ dB		

Table 62: Uplink data from Ground Station (Redu) to the StarCheap

Following the parameters summarized in Table 62, and considering the carrier-to-noise density ratio (C/N_0) target for the backup command link, the required transmitted power from the ground station is approximately **11.2 W**. Thus, the backup uplink for command transmission ensures a sufficient link margin and robustness, even under nominal worst-case slant range conditions.

7.4.3 Communication with Station

The communication parameters for both the forward link (Shuttle to Station) are summarized below:

Link	StarCheap / Station (Patch Antenna)
Forward Frequency: 2,2005 GHz	Max depointing: $\Delta\gamma_{max} = 5^\circ$
Bit Error Rate (BER): 10^{-6}	Antenna efficiency: $\eta_s = 0.6$
Modulation: SQPSK	Line Loss: $L_{ls} = 5 \text{ dB}$
Rate: 72 kbps	Noise Temperature: $T_s = 450^\circ K$
Demodulator degradation: $L_d = 1 \text{ dB}$	Power Amplification Ratio: $\eta_{amp} = 0.2$
Link Margin: $LM = 5 \text{ dB}$	$G_{t, max} = 6.5 \text{ dB}$

Table 63: Direct link communication parameters between StarCheap and the Station

The link budget follows the standard form:

$$P_t = C/N_0 - G_t(\theta) - G_r + 10 \log_{10}(T_r) + \sum L_i + 10 \log_{10}(k)$$

The StarCheap is located at approximately 30 km of the station during S0 approach.

A 5° maximum depointing error is considered, leading to a total beam coverage requirement corresponding to a HPBW of approximately 130° .

Here are the main computations:

- Patch antenna gain with HPBW = 130° :

$$G_t = G_{t, max} - 12 \left(\frac{60}{130} \right)^2 \approx 3.94 \text{ dB}$$

- Required Carrier-to-noise density ratio (C/N_0) with SQPSK and BER 10^{-6} :

$$C/N_0 = 11 \text{ dB} + 10 \log_{10}(72 \times 10^3) + 5 = 11 + 48.57 + 5 = 64.57 \text{ dB}$$

- Free-space path loss over 30 km slant range:

$$\lambda = \frac{c}{f} = \frac{3 \times 10^8}{2.2005 \times 10^9} = 0.1363 \text{ m}$$

$$L_{FSPL} = 20 \log_{10} \left(\frac{4\pi \times 30 \times 10^3}{0.1363} \right) \approx 128.84 \text{ dB}$$

- Total link losses including degradations:

$$\sum L_i = L_{FSPL} + L_{ls} + L_d = 130.5 + 5 + 1 = 134.84 \text{ dB}$$

We obtain the final required transmitted power from the StarCheap antenna:

$$P_t = 64.57 - 3.94 - 3.94 + 26.53 + 134.84 - 228.6 \\ P_t = -10.54 \text{ dBW} = 19.46 \text{ dBm}$$

Converted to Watts:

$$W = \frac{10^{-10.54/10}}{0.2} \approx 442 \text{ mW}$$

Thus, the required antenna output power is approximately **442 mW** to maintain nominal communication conditions for the docking link.

The return link (Station to StarCheap) parameters are summarized below:

Link	StarCheap / Station (Patch Antenna)
Return Frequency: 2,03043 GHz	Max depointing: $\Delta\gamma_{max} = 5^\circ$
Bit Error Rate (BER): 10^{-6}	Antenna efficiency: $\eta_s = 0.6$
Modulation: BPSK	Line Loss: $L_{ls} = 5 \text{ dB}$
Rate: 72 kbps	Noise Temperature: $T_s = 450^\circ K$
Demodulator degradation: $L_d = 1 \text{ dB}$	Power Amplification Ratio: $\eta_{amp} = 0.2$
Link Margin: $LM = 5 \text{ dB}$	$G_{t, max} = 6.5dB$

Table 64: Return link communication parameters between the Station and StarCheap

The slant range and geometric configuration are identical to the forward link (30 km distance, 130° HPBW). There is a slight change in frequency between the forward and return links leading to a negligible difference in wavelength. As a result, the antenna gains remain effectively unchanged for both directions.

The modulation changes to BPSK, leading to a slightly higher E_b/N_0 requirement (13 dB for BER 10^{-6}). Thus, the Carrier-to-noise density ratio is:

$$C/N_0 = 13 + 10 \log_{10}(72 \times 10^3) + 5 = 13 + 48.57 + 5 = 66.57 \text{ dB}$$

The free-space loss and additional losses remain approximately the same:

$$\sum L_i = 134.14 \text{ dB}$$

The final required transmitted power from the Station is then:

$$P_t = 66.57 - 3.94 - 3.94 + 26.53 + 134.14 - 228.6 \\ P_t = -9.24 \text{ dBW} \approx 20.76 \text{ dBm}$$

Converted to Watts:

$$W = \frac{10^{-9.24/10}}{0.2} \approx 0.596 \text{ W}$$

Thus, approximately **596 mW** of output power is required for the return link to maintain nominal communication conditions during the docking phase.

7.5 Physical Layer Architecture

The hardware architecture of the Communication Subsystem is organized into multiple radio frequency (RF) chains, each dedicated to a specific link function. These chains are interfaced via a centralized **CDH Interface** module responsible for routing data and commands between the communication hardware and the StarCheap OBC. The figure below shows the full layout:

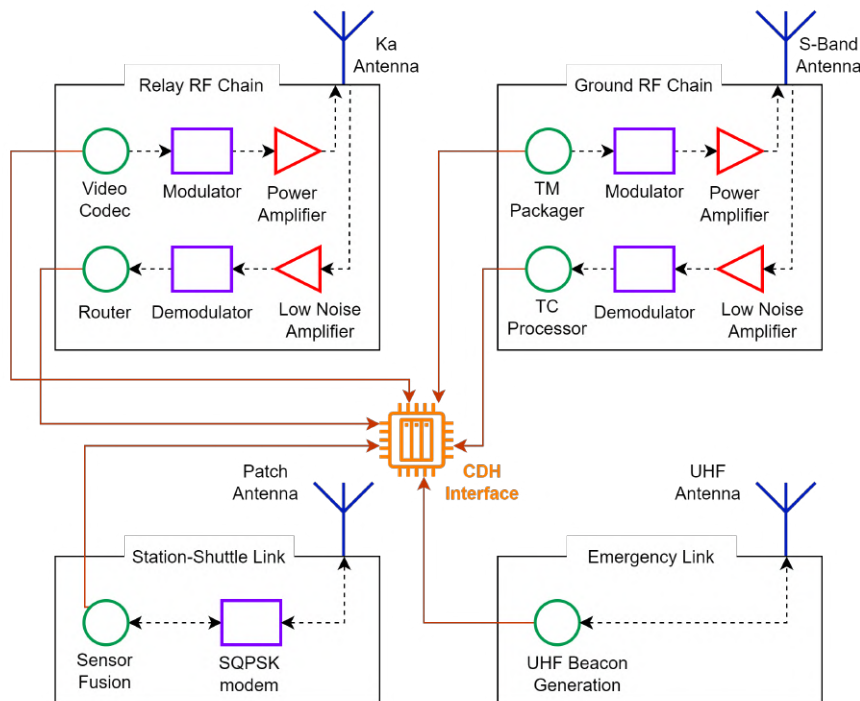


Figure 83: Communication Hardware Architecture of StarCheap

The diagram presents the following functional blocks: Relay RF Chain, Ground RF Chain, Station-Shuttle Link, Emergency Link and CDH Interface, that packages telemetry, decodes commands, and routes mission/video data to the appropriate RF chain.

The table below summarizes the estimated mass budget for all components, including redundancy and necessary margins.

Component	Unit Mass (g)	Quantity
S-band Patch Antenna	150	4 (2 per link \times 2 chains: Ground + Station)
Ka-band Phased Array (Relay)	1,000	2
UHF Antenna (Emergency)	120	1
Power Amplifier (S-band)	250	2
Power Amplifier (Ka-band)	600	1
Low Noise Amplifier (S-band)	150	2
Low Noise Amplifier (Ka-band)	300	1
Modulator	200	3 (Relay, Ground, Station)
Demodulator	200	3
Router + Video Codec	350	1
RF Cabling, Connectors	400	1 (lumped mass)
Mounting Structures + Margins	800	1 (structure + 20% margin)
Total Estimated Mass	5.62 kg	

Table 65: Estimated Mass Budget of the Communication Subsystem

7.6 Protocol, Packet, Safety

7.6.1 Protocol

In the development of our space shuttle, our decision to adopt the standards of the Consultative Committee for Space Data Systems (CCSDS) is driven by the need to ensure reliable and interoperable communication in space. The CCSDS standards are internationally recognized and used by major space agencies worldwide, ensuring that our shuttle can seamlessly integrate with existing and future infrastructures. By utilizing these standards, we benefit from robust and proven protocols that minimize technical and operational risks while enabling efficient data and communication management. Additionally, adopting CCSDS standards allows us to leverage the latest technological innovations while ensuring compatibility with the systems of our international partners.

7.6.2 Packet

The CCSDS Space Packet defined in Space Packet Protocol, CCSDS 133.0-B-1 is shown in the figure hereafter.

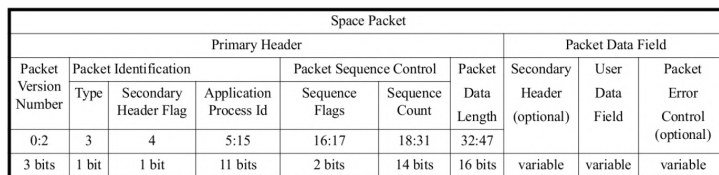


Figure 84: CCSDS Space Packet

The CCSDS Space Packet is one of several data units that can be transferred in Telecommand or Telemetry Frames. The CCSDS Packet Transfer Protocol packet is shown in the figure hereafter. The CCSDS standard is interoperable with our SpaceWire control bus, as described in the CDH (Command data handling) chapter.

	Target SpW Address	Target SpW Address
Target Logical Address	Protocol Identifier	Reserved = 0x00	User Application
CCSDS Packet (First Byte)	CCSDS Packet	CCSDS Packet	CCSDS Packet
CCSDS Packet	CCSDS Packet
CCSDS Packet	CCSDS Packet (Last Byte)	EOP	

Figure 85: CCSDS Packet Transfer Protocol packet

7.6.3 Safety

The CCSDS (Consultative Committee for Space Data Systems) protocol enables secure TT&C (Telemetry, Tracking, and Command) exchanges for space communications. The security of data exchanged between space and ground systems is ensured through the use of the AES (Advanced Encryption Standard) algorithm, recommended by the CCSDS as the sole symmetric encryption algorithm for all space missions. AES operates on 128-bit data blocks and can utilize keys of 128, 192, or 256 bits. The AES encryption process involves multiple repeated steps over a number of rounds, including adding a round key, byte substitution, row shifting, and column mixing, ensuring a complex and secure data transformation.

8 Power

8.1 Requirements

Requirement ID	Description
POW-REQ-001	Ensure that the shuttle functions nominally under all mission conditions.
POW-REQ-002	Operate fully autonomously without requiring external manual intervention during the mission.
POW-REQ-003	Should be fully reusable; if not feasible at 100%, it must be at least 80–90% reusable.
POW-REQ-004	Implement redundancy strategies in accordance with FDIR principles.
POW-REQ-005	The mass of the EPS shall not exceed 10% of the total shuttle mass.
POW-REQ-006	Deliver the power required by all onboard systems under all mission phases.
POW-REQ-007	The EPS must be dimensioned to ensure continuous power supply during eclipse periods.
POW-REQ-008	Provide efficient conversion and distribution of energy to all subsystems.
POW-REQ-009	Include protections against overvoltage, overcurrent, short circuits, and other electrical anomalies to ensure operational safety.
POW-REQ-010	Interface and utilize power from the station when docked.
POW-REQ-012	Include appropriate energy storage sized according to the selected power generation architecture.

Table 66: StarCheap Power Subsystem Requirements

8.2 Power Budget

The power budget, including margin, is provided for each operational phase and will be used to size the electrical power subsystem.

This power budget is an initial estimation based on preliminary assumptions and is not yet derived from detailed or measured figures. It represents a first iteration and will need to be refined in future phases of the project.

Equipment	Power Consumption [W]	Number	Margin	Peak Power Consumption [W]					
				Launch Mode (LM)	Rendez-vous (RV)	Docking Mode (DM)	Transfer Mode (TM)	Capture Mode (CM)	Landing Mode (LM)
AOCS	1940			0	1064.5	52.5	325.5	1924.5	724.5
Sensors (IMU, ...)	80		5.00%	0	84	0	84	84	84
Actuators (RCS)	150		5.00%	0	315	52.5	315	525	630
GNSS (receiver)	10	1	5.00%	0	10.5	0	10.5	10.5	10.5
Capture Sensors (lidar, cameras)	100		5.00%	0	0	0	0	105	0
Capture Mechanisms (net)	1000	1	20.00%	0	0	0	0	1200	0
Docking Sensors (cameras)	100		5.00%	0	105	0	0	0	0
Docking Mechanisms (berthing)	500		10.00%	0	550	0	0	0	0
Propulsion	270			0	21	21	741	21	741
Sensors	20		5.00%	0	21	21	21	21	21
Actuators	250		20.00%	0	0	0	720	0	720
Thermal	100			0	105	0	105	105	105
Heaters	20		5.00%	0	21	0	21	21	21
Radiators	80		5.00%	0	84	0	84	84	84
Communication	210			0	745.5	63	220.5	220.5	220.5
Antennas	150		5.00%	0	682.5	0	157.5	157.5	157.5
Transceivers	10		5.00%	0	10.5	10.5	10.5	10.5	10.5
Amplifiers	50		5.00%	0	52.5	52.5	52.5	52.5	52.5
CDH				210	210	210	210	210	210
On Board Computer	200	1	5.00%	210	210	210	210	210	210
ECLS	1850			1942.5	1942.5	1942.5	1942.5	1942.5	1942.5
Air revitalization	500		5.00%	525	525	525	525	525	525
Air control	300		5.00%	315	315	315	315	315	315
Emergency services	50		5.00%	52.5	52.5	52.5	52.5	52.5	52.5
Water management	500		5.00%	525	525	525	525	525	525
Waste management	300		5.00%	315	315	315	315	315	315
Lights & Control Panels	200		5.00%	210	210	210	210	210	210
Power	50			52.5	52.5	52.5	52.5	52.5	52.5
PCDU	50		5.00%	52.5	52.5	52.5	52.5	52.5	52.5
			Total	2205	4141	2341.5	3597	4476	3996
			Total + 20% Margin	2646	4969.2	2809.8	4316.4	5371.2	4795.2

Figure 86: Initial Estimation of the Power Budget

The nominal power is **3238.2 W**, and the peak power is **5371.2 W**. The nominal power consumption corresponds to the steady-state operation, while the peak consumption reflects maximum short-duration (15 minutes max) loads. This peak is reached during the capture mode of our shuttle. However, we also shouldn't neglect the rendez-vous mode as well as the landing mode which also consume a lot. These mode are critical, the power must ensure a nominal fonctionnement under any conditions.

8.3 Primary Energy Source Design

8.3.1 State of the Art

The NASA Space Shuttle employed fuel cells for its short missions. These three alkaline fuel cells combined liquid hydrogen and oxygen to generate electricity and potable water. While effective for short missions, fuel resupply would be impractical for longer ones. ?

Solar arrays are the preferred solution for extended missions. For example, Boeing's X-37B and Sierra Space's Dream Chaser use deployable solar arrays combined with battery storage. Radioisotope Thermoelectric Generators (RTGs) are excluded due to astronaut safety concerns.

System	Power Source	Mission Duration
Space Shuttle	Fuel Cells	7-16 days
X-37B	Solar Panels	900 days
Dream Chaser	Solar Panels	6 months

Table 67: Summary Table of the EPS technologies used

8.3.2 Technology Trade-Off

We are doing a decision matrix. Each criterion is weighted based on mission importance. Systems are rated from 1 (poor) to 5 (excellent).

- (A) Continuous power provision
- (B) Minimal mass
- (C) Long-term reliability
- (D) Low thermal dissipation and simplicity
- (E) Reliable operation during eclipses

Criterion	Weight	Fuel Cells	Solar Panels	Justification
A	5	5	3	FCs provide continuous power.
B	4	3	4	Batteries heavy; H ₂ tanks add weight.
C	5	4	3	FCs have predictable degradation.
D	3	3	5	Solar panels are passive.
E	4	5	3	FCs produce water.

Table 68: Decision Matrix of the Primary Energy Source

Fuel cells score better overall (**82 vs. 77**) due to continuous power provision and reliability, despite higher integration complexity.

8.3.3 Fuel Cell Design

A trade-off analysis between Proton Exchange Membrane Fuel Cells (PEMFC) and Alkaline Fuel Cells (AFC) was conducted to determine the most suitable technology for our mission requirements.

Criterion	PEMFC	AFC
Oxygen Form Used	Compressed gaseous O ₂ or Liquid O ₂ (LOX)	Compressed gaseous O ₂ or Liquid O ₂ (LOX)
Required Purity	Very high (tolerates some humidity and nitrogen)	Extremely pure (no CO ₂ allowed, purity \geq 99.999%)
Tolerance to Impurities	Low (can withstand some ambient air)	Very low (CO ₂ causes membrane damage by carbonate formation)
Storage Complexity	Standard (similar to rocket engines)	More demanding (requires CO ₂ filters), good weight-to-power ratio
Safety	Good, with thermal and pressure management	Good, but requires strict gas control
Operatin temperatures	60°C-90°C	70°C-120°C

Table 69: Comparison between PEMFC and AFC technologies for space applications

Based on the trade-off analysis, PEMFC technology was selected due to its greater tolerance to operational conditions and simpler storage requirements compared to AFC. Moreover, the PEMFC works at mean lower temperatures, enabling a liquid water recovery more efficient (less vapor) than with an AFC, making it a suitable choice for water generation (see 9 - Life Support section).

In a PEMFC, hydrogen gas H₂ is supplied to the anode where it is split into protons and electrons. The protons migrate through the proton exchange membrane to the cathode,

while the electrons travel through an external circuit, generating electricity. At the cathode, protons, electrons, and oxygen O_2 combine to form water.

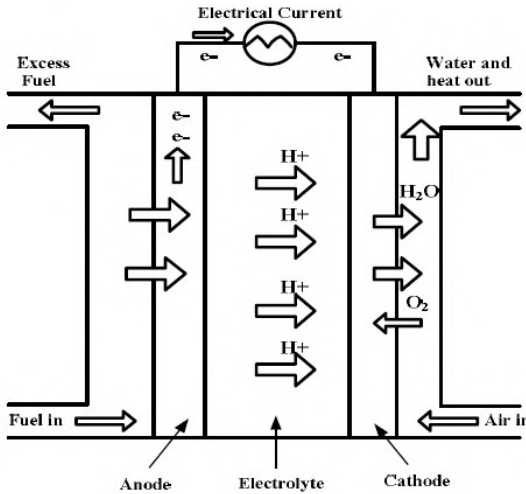
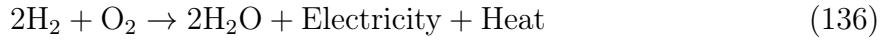


Figure 87: Schematic Diagram of PEMFC

The overall chemical reaction is:



The first operational use of PEMFCs was during the Gemini program (1965–1966), where fuel cells developed by General Electric delivered about 1 kW per stack for short missions (up to 14 days), with a lifetime of 200–350 hours. In the early 2000s, NASA and UTC Fuel Cells developed an advanced PEMFC prototype, delivering 4 kW with over 10,000 hours of lifetime, certainly designed for long-duration missions such as future galactic exploration Scott [2007].

The main mission parameters for the sizing are summarized below:

Parameter	Value
Mission Duration	96 hours
Average Power Consumption	3240 W
Fuel Cell Efficiency	50%
Power Margin	20%
Thermal Margin	5%
Structural Margin	3%

Table 70: Mission and design parameters for fuel cell sizing.

Considering the nominal output of a single PEMFC unit (4 kW), the system requires the integration of two fuel cells to ensure both nominal operation and redundancy. This configuration provides sufficient power margin to guarantees operational continuity even in case of minor degradation or single-unit failure.

First, the total electrical energy required over the mission duration by the fuel cell is calculated using the average power consumption, accounting for the power, thermal, and structural margins as well as fuel cell efficiency:

$$E_{input} = \frac{P_{avg} \times t_{mission} \times (1 + m_{power}) \times (1 + m_{thermal}) \times (1 + m_{structural})}{\eta_{FC}}$$

$$E_{input} = \frac{3240 \times 96 \times 1.2 \times 1.05 \times 1.03}{0.5} = 807,336 \text{ Wh}$$

8.3.4 Tank Design

The hydrogen mass necessary to supply the required energy is obtained by considering the gravimetric energy density of hydrogen (33,000 Wh/kg):

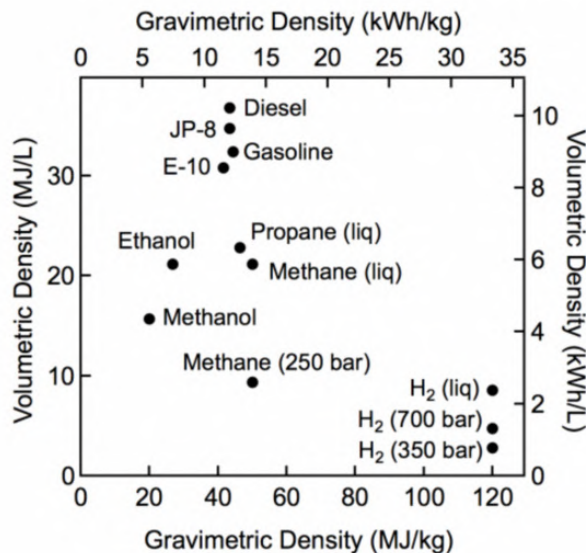


Figure 88: Gravimetric and volumetric energy densities of various fuels

$$m_{H_2} = \frac{E_{input}}{33,000} = 24.5 \text{ kg}$$

Thus, approximately 24.5 kilograms of hydrogen are required for the entire mission.

Assuming a hydrogen density of 0.0315 kg/L at 350 bar:

$$V_{H_2} = \frac{24.5}{0.0315} \approx 777.5 \text{ m}^3$$

We choose a spherical tank because it distributes internal pressure evenly in all directions. Assuming a hydrogen specific volume of 0.0318 m³/kg at 350 bar, the corresponding radius of a spherical tank is:

$$r = \left(\frac{3V}{4\pi} \right)^{1/3} = \left(\frac{3 \times 0.0318 \times 24.5}{4\pi} \right)^{1/3} \approx 0.57 \text{ m}$$

Material	Yield Strength (MPa)	Density (kg/m ³)	Cost (\$/kg)
Stainless Steel (316L)	290	8000	3
Aluminium 7075-T6	500	2810	5
Titanium	880	4430	35
Composite	2000	1800	60

Table 71: Properties of candidate tank materials

We selected Aluminium 7075-T6 for its good compromise between strength, mass, and cost. The required wall thickness is computed considering a safety factor of 2:

$$e = \frac{P \times r \times SF}{\sigma} = \frac{35 \times 10^6 \times 0.57 \times 2}{500 \times 10^6} = 0.08 \text{ m} = 8 \text{ cm}$$

Thus, the spherical hydrogen tank will have an internal radius of 0.57 meters and a wall thickness of 8 centimeters.

In LEO, pressurizing a hydrogen tank at 350 bar is technically challenging due to thermal fluctuations and microgravity. Several techniques are available: pre-pressurization on the ground, helium pressurization system, autogenous pressurization, or thermal pressurization. For this mission, which has a short duration, the chosen solution is to pre-pressurize the tank on the ground and use thermal pressurization as an emergency method to compensate for potential pressure drops caused by thermal cycles or minor leaks.

No dedicated oxygen tank is sized for the PEMFC operation. Instead, the oxygen required for the reaction – 195.7 kg – will be drawn from the life support system’s oxygen reserves, ensuring system integration and mass optimization.

In addition to electricity, the fuel cell system produces water as a by-product. For each kilogram of hydrogen consumed, 8.936 kg of water are produced by the fuel cell.

$$\dot{V}_{H_2O} = 8.936 \times P_{avg} \quad \text{m}^3/\text{s}$$

The architecture of the primary energy system is presented below. It illustrates the

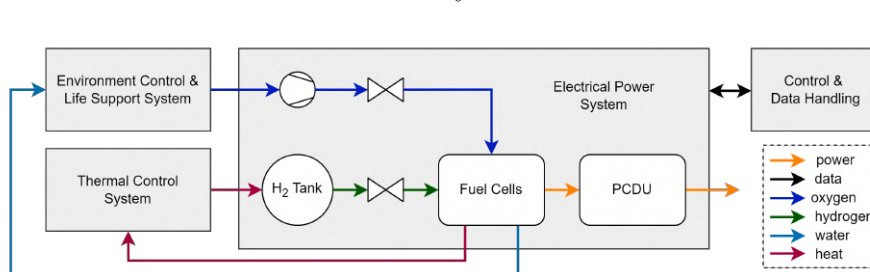


Figure 89: Schematic architecture of the primary energy source

The mass budget of the primary energy source system, composed of the fuel cells, reactants (hydrogen and oxygen), storage tanks, and other components, is detailed below.

Item	Mass (kg)
Fuel Cells (2 units)	230.0
Hydrogen (fuel)	24.4
Oxygen (oxidizer)	195.7
Hydrogen Tank (Al 7075-T6)	834.7
Other Components (15%)	159.9
Total	1444.7

Table 72: Mass budget of the primary energy source system

8.4 Secondary Source Design

8.4.1 State of the Art

For energy storage, it is preferred to rely on Li-Ion batteries due to their superior performance compared to older technologies like Ni-Cd or Ni-H₂ batteries. They offer higher energy density, enabling more compact systems, and a longer cycle life, ideal for extended space missions. Their faster charge and discharge rates also ensure a reliable power supply, particularly during eclipse phases where immediate and efficient energy delivery is critical.

8.4.2 Batteries Design

The battery subsystem is primarily designed to handle peak power demands that exceed the continuous fuel cell output capacity.

The key parameters considered for battery sizing are summarized below:

Parameter	Value
Peak Power Consumption	5380 W
Peak Mission Duration Ratio	10%
Battery Depth of Discharge (DoD)	80%
Battery Regulator Efficiency	90%
Battery Safety Margin	10%

Table 73: Battery design parameters

The system architecture includes two fuel cells, with only one operating under normal conditions to satisfy the average mission power. The second fuel cell is reserved for redundancy and is not active during standard operations.

Given that the operating fuel cell provides a nominal 4000 W, and peak mission power can reach up to 5380 W, the batteries must supply the deficit during peak periods.

The instantaneous power deficit is:

$$P_{\text{deficit}} = P_{\text{peak}} - P_{\text{FC}} = 5380 - 4000 = 1380 \text{ W}$$

Peak demand periods are expected to occur during 10% of the total mission duration:

$$t_{\text{peak}} = 0.10 \times 96 = 9.6 \text{ hours}$$

The required energy storage capacity to support peak phases is therefore:

$$E_{peak} = P_{deficit} \times t_{peak} = 1380 \times 9.6 = 13,248 \text{ Wh}$$

To determine the effective battery capacity needed, we include the battery safety margin, account for the Depth of Discharge (DoD), and the regulator efficiency:

$$E_{battery_real} = \frac{E_{peak} \times (1 + m_{battery})}{\text{DoD} \times \text{Eff}_{reg}}$$

Substituting:

$$E_{battery_real} = \frac{13,248 \times 1.10}{0.8 \times 0.9} = \frac{14,572.8}{0.72} \approx 20,240 \text{ Wh}$$

Thus, the batteries must store approximately **20.2 kWh**.

The SAFT VES100 lithium-ion cell is selected:

Cell electrical characteristics

Nominal voltage	3.6 V
Nominal capacity at C/1.5 rate at 4.1 V/3 V & 20°C	27 Ah
Maximum discharge current at 25°C	100 A (Continuous -2 s pulse)
Specific energy (minimum guaranteed)	118 Wh/Kg
Energy density	230 Wh/l

Cell mechanical characteristics

Diameter (max)	53 mm
Height (max)	185 mm
Mass (max)	0.81 kg

Cell operating conditions

Lower voltage limit for discharge	Continuous [0°C to +45°C] 2.57 V
Charging method	Constant current/constant voltage (CCCV)
Charging voltage (max)	4.1 V
Recommended continuous charge current	GEO/MEO C/10 LEO (20 % DoD) C/5
Operating temperature	Charge +10°C to +35°C Discharge 0°C to +40°C
Storage and transportation temperature	-40°C to +65°C

(a) Datasheet



(b) Li-ion Cell

Figure 90: SAFT VES100 Battery

The number of battery cells needed is:

$$N_{cells} = \frac{E_{battery_real}}{100} = \frac{202.4}{100} \approx 203 \text{ cells}$$

Given the nominal bus voltage of 28 V and individual cell voltage of 3.6 V, the number of cells in series is:

$$N_{series} = \left\lceil \frac{28}{3.6} \right\rceil = 8 \text{ cells}$$

Thus, the battery pack is organized with 8 cells in series, and:

$$N_{parallel} = \left\lceil \frac{203}{8} \right\rceil = 26 \text{ parallel strings}$$

resulting in a battery architecture of **8S26P** (8 in series, 26 in parallel).

The total battery mass is:

$$m_{battery} = 8 \times 26 \times 0.81 = 168.5 \text{ kg}$$

8.5 Power Control and Distribution

The Power Control and Distribution (PCD) is responsible for regulating, conditioning, and distributing electrical power from the primary (fuel cells) and secondary (batteries) sources to the spacecraft loads.

8.5.1 Power Control Strategy

A Direct Energy Transfer (DET) architecture was selected, complemented by a regulated main bus at 28V to ensure stability across all operating conditions.

A Battery Charge Regulator (BCR) and Discharge Regulator (BDR) manage battery charging and discharging operations, maintaining optimal battery health and performance.

All electrical loads are connected via controlled switches, with embedded protection mechanisms against overvoltage, undervoltage, and overcurrent conditions.

8.5.2 Power Distribution Topology

The system uses a single regulated DC bus at 28V:

- Local DC/DC converters provide specific voltages for sensitive equipment.
- A DC/AC inverter supplies necessary AC loads.

Essential loads (such as life support and avionics) are prioritized and permanently connected, while non-essential loads (e.g., capture payload) can be load-shed if necessary.

The PCDU is designed to be fully compatible with Ground Support Equipment (GSE) during pre-launch operations. It allows safe external power injection, battery charging, and system testing via dedicated GSE interfaces compliant with space industry standards (MIL-STD-1540).

Additionally, the PCDU ensures compatibility with space station docking ports, enabling external power transfer upon docking. Automatic reconfiguration mechanisms are implemented to prioritize external station power over internal sources when docked, ensuring a seamless transition without power interruption.

8.5.3 Fault Tolerance

Redundancy is integrated at multiple levels:

- Redundant fuel cell available in cold standby.

- Battery architecture organized in parallel strings to maintain functionality in case of string failure.
- Redundant DC/DC converters for critical systems.

Fault isolation through smart load switching ensures that electrical faults can be contained without propagating to the entire system.

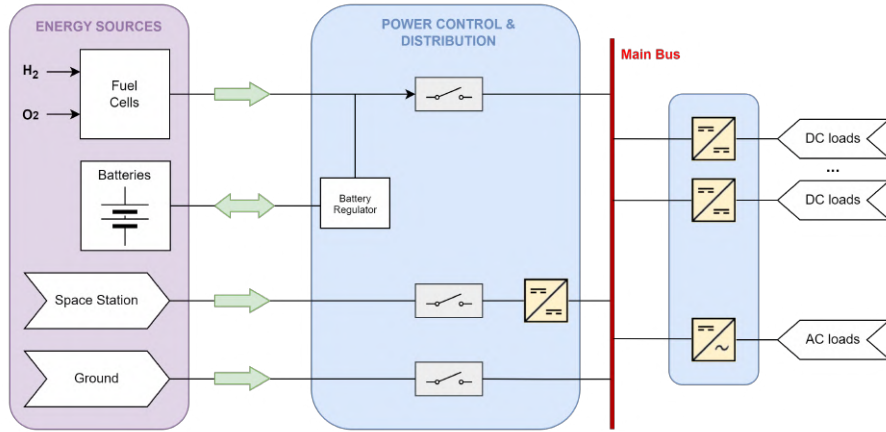


Figure 91: Final architecture of the Electrical Power System (EPS)

8.6 Environmental Considerations

Proper electrical and mechanical design practices are implemented throughout the Electrical Power System (EPS) to ensure reliability in the space environment.

Electrostatic discharge (ESD) protection is achieved by bonding all conductive structures to a single-point ground tied to the spacecraft chassis. Harnesses are shielded and connector backshells are properly grounded to limit electromagnetic interference (EMI).

All EPS subsystems, including fuel cells, batteries, tanks, and power distribution units, use materials selected for:

- High conductivity and low-resistivity.
- Low outgassing (per ECSS-Q-ST-70-02C standards) to minimize contamination risk.
- Radiation resistance to maintain electrical insulation properties.

Special attention is given to thermal cycling durability and vibration resistance to survive launch, operation in orbit, docking or re-entry phases.

8.7 Lifespan and Reusability

The EPS is designed to support multiple mission cycles over a minimum operational life of 10 years. To enable reusability and long-term reliability, the following strategies are applied:

- **Modularity:** Components such as fuel cells, regulators, and battery packs are modular and replaceable without major system redesign.
- **Derating of Components:** All electrical components operate below 70% of their rated maximum limits (voltage, current, temperature) to extend lifetime.
- **Health Monitoring:** Integrated telemetry continuously monitors key parameters (voltage, current, temperature) for preventive maintenance and early fault detection.
- **Serviceability:** Interfaces are designed to allow inspection, servicing, and replacement during ground turnaround or docking operations.

These provisions ensure that the EPS remains operational despite environmental stressors, component aging, and multiple launch-recovery cycles.

It would be relevant to reassess the architecture with a new iteration of the power budget to validate the consistency of the sizing. However, the power margins integrated into this model are designed to absorb potential variations in consumption and ensure sufficient system robustness at this stage.

9 Life Support

The Life Support subsystem ensures the habitability and survival of the crew throughout the mission. It manages the essential functions for human life in space.

For each ECLSS equipment, based on our mission phases, we consider a 5 days for sizing purpose and autonomy designs. This duration take in account 1 day for launch and docking, 3 days for autonomy and one additional day for margin. Also the docking phase with a duration of 5 months between day 1 and day 2 (start of the autonomy design) must be taken into account.

9.1 Requirements

In this section, the requirements for the life support system are presented to define its operational boundaries and performance expectations.

- **LS-REQ-001 – Oxygen Supply:** The system must maintain a breathable atmosphere by ensuring a continuous supply of oxygen ($20.9\% \pm 0.5\%$).
- **LS-REQ-002 – Carbon Dioxide Removal:** The system must ensure efficient removal of carbon dioxide to maintain acceptable levels below 0.5%.
- **LS-REQ-003 – Oxygen Regeneration:** The system should integrate a regenerative loop capable of recycling up to 70% of oxygen to reduce resupply needs.
- **LS-REQ-004 – Pressurization:** Cabin pressure must be maintained between 70 and 101 kPa under nominal conditions, and emergency support must last over 20 minutes. Leak detection must be included.
- **LS-REQ-005 – Temperature:** Temperature must be regulated within the habitable module between 15°C and 29°C.
- **LS-REQ-006 – Humidity:** Humidity must be controlled within the range of 30–70%, as per NASA LSS handbook recommendations.
- **LS-REQ-007 – EVA Support:** The system must support EVA by providing pressurized separation and autonomous air supply.
- **LS-REQ-008 – Fire Control:** A gas safety system must activate in less than 1 minute, and a suppression system must ensure fire extinction.
- **LS-REQ-009 – Pressure Maintenance:** In case of depressurization, emergency air masks and tanks must be available.
- **LS-REQ-010 – Air Filtering:** The air must be filtered continuously to remove particulates and microorganisms.
- **LS-REQ-011 – Mass:** The life support system must represent no more than 5% of the total shuttle mass (approx. 2000 kg).
- **LS-REQ-012 – System Autonomy:** The system must be fully autonomous in operation.

- **LS-REQ-013 – Reusability:** The system must be reusable for at least 10 missions or a total lifetime of 5 years.
- **LS-REQ-014 – Food Support:** The system must ensure storage, preparation, consumption, and waste handling of food for the crew.
- **LS-REQ-017 – Hygiene:** The system must provide access to hygiene facilities including water for cleaning, personal hygiene kits, and waste fluid management.
- **LS-REQ-018 – Fault Tolerance:** The system must be designed to tolerate faults and ensure continued operation during anomalies.
- **LS-REQ-019 – Redundancy:** Critical components of the LSS must be redundant to allow continued function in case of failure.
- **LS-REQ-020 – Waste Management:** The system must handle waste (solid and liquid), isolate it safely, and dispose of it properly.
- **LS-REQ-021 – CO₂ and O₂ Exchange During Docking:** The life support subsystem must allow for CO₂ and O₂ transfer with the docking station.
- **LS-REQ-022 – Air Circulation:** Air must be continuously circulated in all habitable areas to ensure uniform conditions.
- **LS-REQ-023 – Water Distribution:** The system must provide reliable water access for drinking, hygiene, and cooking.
- **LS-REQ-024 – Waste Water Treatment:** Wastewater (e.g., urine, sweat) must be processed and recycled into usable water.
- **LS-REQ-025 – Medical Necessities:** A complete medical kit must be provided for routine and emergency treatments, including basic medications and advanced tools.
- **LS-REQ-026 – Health Monitoring:** The crew's vital signs must be continuously monitored with appropriate sensors.
- **LS-REQ-027 – Solar Flares Prevention:** The shuttle must be equipped with alert systems and procedures to protect astronauts from solar flares within 10 minutes of detection.

In the case of off-nominal conditions, such as a system failure or crew health emergency, the Life Support System must provide backup solutions and maintain survival parameters for a minimum of 24 hours. This includes emergency oxygen supply, basic temperature control, and pressure stabilization until either system recovery or external intervention is possible. The goal is to guarantee that the crew is not endangered during unexpected scenarios, even in the absence of immediate ground support.

9.2 Environment

The regulation of the environment of the crew module of the shuttle ensures the habitability and safety of the passengers. This is ensured by the ECLSS (Environmental Control and Life Support System), which serves to regulate essential physical parameters to ensure comfort and safety, but also managing byproducts of human presence which must be removed to prevent harmful buildup.

Key aspects to consider are the cabin pressurisation, temperature, humidity and CO₂ removal, oxygen supply, air filtration and circulation and fire control.

9.2.1 State of the art & Design Considerations

Designing the ECLSS for the StarCheap shuttle comprised of assessing the needs and requirements for the ECLSS, as well as surveying the existing technology.

All sizing is done assuming 5 days of autonomous flight (including margins), with 3 people in the shuttle including one woman and two men.

The goal is to minimise the consumable components in the ECLSS system in order to respect the reusability requirements; the ideal case is to only have to re-load the consumables in the system and replace defective components between missions.

A survey of ECLSS technologies on-board the ISS, CrewDragon capsule and Orion capsule is made below. We note that although a lot of the environment systems produce water for usage onboard, the approach for the StarCheap shuttle was to separate water production from the environment subsystem.

9.2.1.1 ISS ECLSS

The ISS Environmental Control and Life Support System (ECLSS) integrates multiple subsystems to maintain a habitable environment for long-duration missions. Carbon dioxide is removed using regenerable zeolite beds and further processed via ESA's Advanced Closed Loop System (ACLS), which recycles CO₂ into water and oxygen through the Sabatier reaction and electrolysis. Oxygen is generated by the Oxygen Generation Assembly (OGA) from water electrolysis, with hydrogen reused in the Sabatier process to close the loop. Air is circulated and filtered through intermodular and intramodular ventilation systems and Common Cabin Air Assemblies, while the Atmosphere Revitalization system removes contaminants with activated carbon beds, catalytic oxidizers, and LiOH filters. Fire safety relies on smoke detection, automatic shutdowns, and portable extinguishers, with the ability to isolate and depressurize modules. The pressurized environment is actively monitored, with pressure equalization valves facilitating hatch operations. Temperature and humidity are regulated through the Temperature and Humidity Control (THC) system and a two-loop Active Thermal Control System (ATCS), ensuring heat dissipation and water recovery. NASA [2024]

9.2.1.2 Orion ECLSS

Orion's ECLSS emphasizes regenerative, low-maintenance operation suitable for lunar missions Mera et al. [2023]. Its Carbon Dioxide and Humidity Control (CHC) system uses dual-bed, amine-based adsorption to continuously remove CO₂ and water vapor with minimal consumables. Oxygen is supplied via high-pressure gaseous oxygen tanks

with flow controllers to maintain breathable cabin conditions, as the spacecraft does not generate oxygen in-flight. Air is circulated and filtered by the Air Revitalization System (ARS), which includes both cabin and suit ventilation loops to manage temperature, trace contaminants, and particulates. The Trace Contaminant Control System (TCCS) combines charcoal filters and catalytic oxidation to eliminate harmful gases such as CO and hydrogen. Fire safety involves smoke and combustion gas detection with CO₂-based extinguishers. Thermal control is managed through ARS integration, providing consistent crew-selected comfort throughout missions.

9.2.1.3 CrewDragon ECLSS

Crew Dragon's ECLSS is designed for short-duration missions, relying on simple, reliable components. CO₂ is scrubbed using non-regenerative lithium hydroxide cartridges, with enough capacity for typical mission durations. Oxygen is stored in high-pressure tanks and distributed to both the cabin and suit loops, with redundant systems for fault tolerance. The air sanitation system removes contaminants via activated carbon and HEPA filters, supported by ammonia filters and dehumidifiers with Nafion membranes that vent humidity to space. Air is circulated by redundant cabin and suit fans, with flapper valves and check valves ensuring consistent airflow and gas mixing. Thermal control is phase-dependent: in orbit, radiators on the trunk dissipate heat; during launch and reentry, a vapor compression system using refrigerants and external ambient air ensures temperature regulation. Fire suppression is achieved with nitrogen-based systems that displace oxygen without leaving harmful residues, maintaining air quality in a closed environment. Silverman et al. [2023]

9.2.2 System Design

Considering the state of the art and design considerations, design choices for the ECLSS of the StarCheap shuttle were made in the spirit of reusability and safety.

At the time of the design, no cabin design had been produced, and as such, the ventilation system is not addressed.

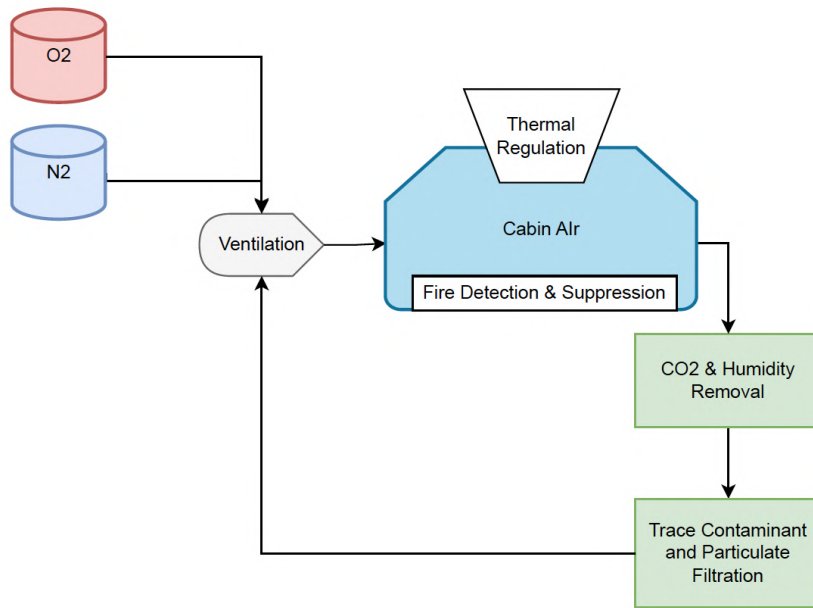


Figure 92: ECLSS Architecture

9.2.2.1 Cabin Atmosphere Composition and Pressure Control

As the mission duration is short, onboard oxygen generation via electrolysis is deemed unnecessary. Electrolysis systems (such as Solid Polymer Electrolyte [SPE] or Alkaline Electrolyzers) require significant power, water mass, and subsystem support (e.g., gas-water separators, compressors), adding unnecessary mass, volume, and complexity for limited-duration missions. Instead, storing pre-filled gases is simpler, lighter, and more reliable in the short term.

To ensure a habitable and safe cabin environment, the spacecraft maintains a sea-level-like atmospheric composition—approximately 101.3 kPa (1 atm) total pressure. This avoids the need for crew pre-breathing protocols or decompression adaptation and supports standard physiological functions. The mix includes ≈ 21 kPa of oxygen, closely matching Earth's partial pressure, to ensure adequate alveolar oxygen exchange without inducing hyperoxia. Nitrogen (N₂) constitutes the balance ($\approx 78\text{--}80$ kPa) and acts as an inert diluent, maintaining pressure without interfering with respiration. A higher oxygen fraction would increase fire hazard and oxygen toxicity risk, especially in pure O₂ or reduced-pressure environments, hence the choice of a mixed-gas atmosphere at ambient pressure.

Nitrogen is physiologically inert and not consumed metabolically, so losses should only be due to cabin leakage. While spacecraft are designed to minimize leakage (often <0.1 percent /day), conservative sizing assumes a higher nominal leak rate (≈ 1 percent/day of total volume) to ensure robustness. Over a 5-day mission, this implies ≈ 5 percent N₂ loss, but a buffer of $\approx 20\text{--}25$ percent is included to account for uncertainties, operational venting, or rapid depress events.

We calculate the number of moles and mass of N₂ required:

Using the ideal gas law:

$$PV = nRT \quad (137)$$

With:

- P = 79.3 kPa
- V = 20 m³
- R = 8.314 J/mol.K
- T = 293K (room temperature ≈ 20°C)
- M = 28,0134 g/mol (nitrogen molar mass)

We obtain :

$$n = \frac{PV}{RT} \approx 652 \text{ moles} \quad (138)$$

$$m = nM \approx 18,4 \text{ kg} \quad (139)$$

Considering leak losses and buffer volume, we choose to omit the leak losses for simplification, but a true sizing on the necessary N₂ mass would have to include the leak factor not only for the in-flight time, but also for the time spent docked to the station. As no nitrogen was included in the exchanges between the shuttle and the station, we choose not to consider them in this presizing so as to not unnecessarily constrain the mass budget. We calculate the total mass considering a 25 percent buffer:

$$m_{\text{tot}}^{\text{N}2} = m \times 1.25 = 22,8 \text{ kg} \quad (140)$$

Oxygen, in contrast, is metabolized by the crew, which means not only must the mass budget consider the fill of the cabin, but it must also include compensation of consumption during the flight, as well as potential leakage losses. As oxygen can be supplied by the station, they are considered in this sizing.

For the initial cabin fill, we calculate the number of moles and mass of O₂ required. Using the ideal gas law with:

- P = 21 kPa
- V = 20 m³
- R = 8.314 J/mol.K
- T = 293K (room temperature ≈ 20°C)
- M = 31,999 g/mol (O₂ molar mass)

We obtain:

$$n = \frac{PV}{RT} \approx 173 \text{ moles} \quad (141)$$

$$m_{\text{init}} = nM \approx 6,9 \text{ kg} \quad (142)$$

Per NASA STD 3000 requirements, the metabolic consumption rate is $\approx 0.84 \text{ kg/day/person}$. Rounding up for buffer purposes, we assume 1 kg/day/person . For a 5 day mission, the metabolic consumption mass is:

$$m_{\text{met}} = 1 \times 3 \times 5 = 15 \text{ kg} \quad (143)$$

Considering the same rate losses as nitrogen, we have about 5 percent of losses over total flight time. We don't consider losses while docked, as the cabin is not supposed to be in use or inhabited except during flight. Should there be need for use of the cabin whilst the shuttle is docked, the oxygen supply (including losses), will be carried by the station. So leakage loss mass over 5 days can be estimated as:

$$m_{\text{loss}} = 0.05 \times 6,9 = 0,34 \text{ kg} \quad (144)$$

which we round to 0.4 kg for buffer.

Total required oxygen mass considering an additional 25 percent buffer given the criticality of the oxygen supply yields :

$$m_{\text{tot}}^{\text{O}_2} = (m_{\text{loss}} + m_{\text{met}} + m_{\text{init}}) \times 1.25 = 27.8 \text{ kg} \quad (145)$$

We note that upon launch, we only need 1/5 of the provisional supply, as we only have 1 day of flight to the station. The required loaded oxygen on the ground is thus 5.56 kg.

To ensure supply, both gases should be stored in high-pressure form using composite overwrapped pressure vessels (COPVs), selected for their high strength-to-weight ratio and proven aerospace use. Storing gases as high-pressure rather than cryogenic liquid reduces thermal control demands and simplifies tank design.

The sizing approach used is described in the water tank sizing section. For simplicity and considering the necessary quantities for a 5-day mission, the tanks are assumed spherical and non-COPV but have pressurisation set to COPV standards. Their characteristics are resumed in the tables below:

Input Parameters	Value
Ullage (%)	5%
O ₂ volume desired (m ³)	0.014
Ullage volume (m ³)	0.0007
Tank pressure (bar / Pa)	300 bar / 30,000,000 Pa
Material	Stainless Steel 304
Safety factor (SF)	2
Chosen thickness	1 mm
Steel volume (m ³)	0.0000272
Output Dimensions	
Total volume (m ³)	0.0147
Tank weight (empty, kg)	0.213 kg
Radius (m)	0.167

Table 74: O₂ tank sizing parameters and results

Input Parameters	Value
Ullage (%)	5%
N2 volume desired (m ³)	0.1586
Ullage volume (m ³)	0.00793
Tank pressure (bar / Pa)	100 bar / 10,000,000 Pa
Material	Stainless Steel 304
Safety factor (SF)	2
Chosen thickness	1 mm
Steel volume (m ³)	0.000349
Output Dimensions	
Total volume (m ³)	0.16653
Tank weight (empty, kg)	2.74 kg
Radius (m)	0.376

Table 75: N2 tank sizing parameters and results

An automated gas management system regulates the injection of O₂ and N₂ using sensors and valves, maintaining cabin pressure and composition. Such systems are standard in crewed spacecraft and reduce manual workload while ensuring rapid response to any pressure or leak anomalies.

9.2.2.2 Carbon Dioxide and Humidity Control

Considering a dual system able to handle CO₂ removal and dehumidification such as flown on the Orion capsule offers optimal balance between efficiency, reusability, and integration.

The system adsorbs CO₂ and H₂O vapor on one amine bed while the other is regenerated via vacuum desorption, enabling continuous operation without expendable canisters.

This eliminates the need for consumables such as lithium hydroxide, aligning with the goal of reusability.

For a 3-person crew, we consider the following produced humidity and CO₂ levels. Levels are considered with approximately 20 percent margins (based on NASA STD 3001 NASA [2023]).

- CO₂ produced : 3 crew x 1.2 kg/day x 5 days : 18 kg
- Metabolic water production : 3 crew x 0.5 kg/day x 5 days : 7.5 kg

The total adsorbate load over five days is 25.5 kg.

The sorbent used is a solid-state amine-functionalized material capable of adsorbing both CO₂ and H₂O vapor simultaneously. Based on data from Orion's CHC system Mera et al. [2023] and comparable sorbents such as BASF's SorbeaBASF [2023], we conservatively assume adsorption capacities :

- 110 g of CO₂ per kg of sorbent
- 300 g of H₂O per kg of sorbent

At a combined capacity of \approx 0.41 kg adsorbate per kg sorbent, a total of approximately 62.2 kg of sorbent is required. This is rounded to 64 kg for operational margin and longevity.

The sorbent is divided evenly across two beds, each containing 32 kg, with a target bulk density of 0.5 g/cm³.

This corresponds to 64 liters per bed, increased to 75 liters per bed to account for structural housing, internal void space, and airflow channels.

To regenerate the saturated sorbent, each bed must be exposed to vacuum for desorption of CO₂ and H₂O. Regeneration occurs via direct venting to space vacuum (\approx 10⁻⁴ torr), using electromechanical vacuum isolation valves.

Each vacuum line is sized with an internal diameter of approximately 25 mm, sufficient to evacuate the desorbed gas mass (up to 12.75 kg per bed) over a 20–30 minute cycle without creating significant backpressure.

This requires 2 vacuum valves rated for full 1-atmosphere pressure differential, with vacuum-rated materials and seals (e.g., perfluoroelastomer).

Vacuum lines are connected to a vacuum manifold, sized to accommodate flow from one bed at a time, with check valves to prevent re-entry of ambient gas and ensure fault isolation. All lines are thermally insulated to prevent condensation of water vapor in cold space environments during regeneration.

Cabin air is drawn through the active bed via a low-pressure-drop manifold. To maintain proper contact time with the sorbent, the system must sustain a flow rate of \approx 100–150 L/min, based on crew metabolic output and Orion CHC analogues.

Assuming a linear velocity of \approx 2 m/s and low Reynolds number for laminar flow to reduce erosion of sorbent, the cabin air manifold is sized at 50 mm diameter. An inline EC brushless fan provides the motive force, controlled to balance flow rate with thermal conditioning needs.

The return ductwork ensures even distribution of scrubbed air into the cabin volume. Redundant fans or two-fault-tolerant fan arrays are included to ensure reliability.

Each bed requires two gas flow control valves: one for cabin air inlet and one for outlet to the vacuum system. In total, four high-cycle-rated valves are used for the dual-bed configuration. These valves must be electrically actuated, capable of switching every 15–30 minutes, and constructed for high vacuum compatibility with minimal leakage (leak rates $< 10^{-6}$ sccs He).

A bypass valve is optionally included for fault tolerance and isolation. To regulate airflow and ensure correct switching timing, mass flow controllers or variable-speed drive fans are placed upstream of the beds, providing closed-loop control via pressure and flow sensors. Flow is monitored continuously to avoid stalling or insufficient exchange.

A dedicated CHC controller unit manages the bed switching cycles, monitors pressure, humidity, and temperature, and interfaces with the spacecraft's avionics.

The controller follows a fixed or adaptive cycle strategy (e.g., 20 minutes adsorption, 20 minutes desorption), but should be capable of responding dynamically to crew metabolic rate variations.

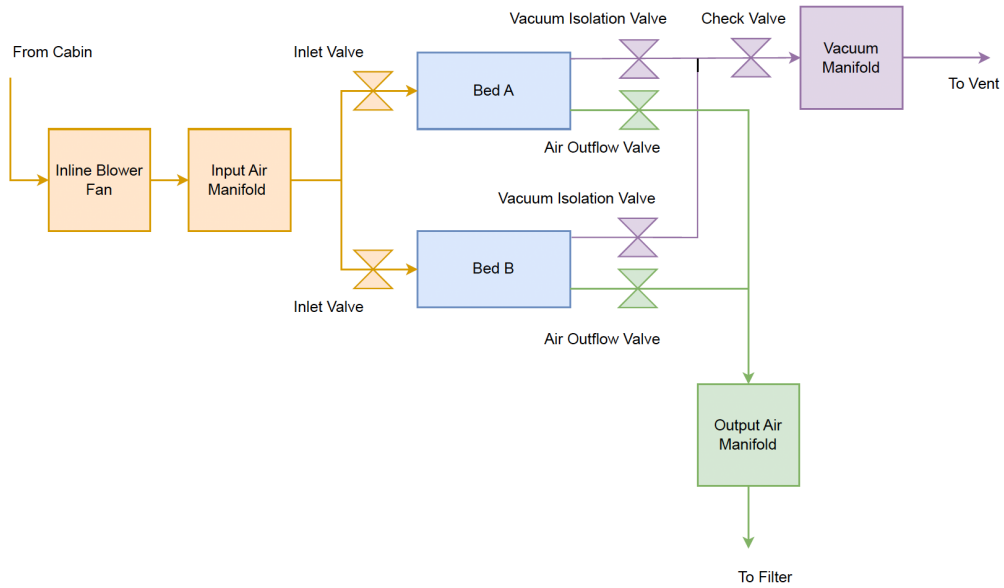


Figure 93: CO₂ and Humidity Removal System Architecture

This system simplifies integration by handling both moisture and CO₂, reducing subsystem mass and complexity.

In future iterations, desorbed water vapor could be condensed and recovered for grey-water reuse, although water recycling is not strictly necessary for a 5-day mission with storable water

9.2.2.3 Trace Contaminant and Particulate Filtration

To preserve air quality and protect downstream components, the ECLSS includes a modular air sanitation assembly comprising a multi-layer filter pack: activated carbon media for trace volatile organic compounds (VOCs) and chemical off-gassing products, a catalytic oxidizer to neutralize CO, MOF fiber mats for hazardous gases and a downstream HEPA filter for particulates.

In a sealed spacecraft environment, trace chemical contaminants can accumulate from human metabolism, material offgassing, cleaning agents, and operational equipment. These compounds, though often present in low concentrations (ppm or ppb), pose risks to crew health and sensitive electronic systems. Volatile organic compounds (VOCs) such as acetone, isopropanol, formaldehyde, benzene, and toluene are emitted from breath, skin, disinfectants, adhesives, and plastics.

Activated carbon media is an excellent solution for removing trace volatile organic compounds (VOCs) and chemical off-gassing products due to its high surface area-to-volume ratio, enabling efficient adsorption in a compact form factor. It is highly effective across a broad range of organic molecules. From a reusability perspective, activated carbon can be thermally regenerated or replaced as modular filter elements between missions, minimizing waste.

Carbon monoxide (CO), an accumulate in spacecraft primarily due to incomplete com-

bustion or degradation of onboard materials, and is particularly a concern during anomalies or specific operations. Given the enclosed nature of spacecraft and limited air exchange with the external environment, even small sources can lead to hazardous CO concentrations if not properly mitigated.

A catalytic oxidizer neutralizes carbon monoxide (CO) by converting it into carbon dioxide (CO₂) through a surface-catalyzed oxidation reaction :



This process typically uses a noble metal catalyst, palladium, which facilitates the reaction at relatively low temperatures by lowering the activation energy required. CO and oxygen molecules adsorb onto the catalyst surface, where the CO reacts with atomic oxygen to form CO₂, which then desorbs and re-enters the cabin air stream. This method is highly efficient, does not rely on consumable materials, and operates continuously without producing harmful byproducts.

Although the risk of microbial growth is lower in space due to rigorous cleanliness protocols, biological contaminants such as bacteria, fungi, and viruses can still be introduced through the crew or surface contamination. These organisms can produce volatile metabolic byproducts (e.g., acetic acid) and pose infection risks during long missions.

To counter this, the air filtration systems uses a silver-based anti-microbial surface. Its ions provide broad-spectrum antimicrobial action without the need for external activation (like UV light). Silver-based materials are passive and reusable, with no need for reapplication or manual activation between missions. They also exhibit low off-gassing, making them safe for use in closed atmospheres.

The surface is introduced in the caging of the filtration box, giving a maximum of surface for the biological contaminants to be neutralised.

Maintaining relative humidity within acceptable limits is also key to suppressing microbial propagation.

Particulate contamination arises from various sources within the spacecraft, including human biological shedding (skin flakes, hair), textile fibers, equipment wear debris, and crystallized residues from outgassing. These particles not only affect air quality but can interfere with sensors, optics, and ventilation systems.

To mitigate this, a high-efficiency particulate air (HEPA) filter is used to capture particles down to 0.3 μm with high efficiency. The filters is placed downstream of the trace contaminant scrubbers to protect them from mechanical fouling and serve to trap any foreign object debris (FOD) released during cargo operations or maintenance activities.

Leaks of spacecraft fluids such as propellants or coolants are rare but serious events that require filtration capabilities. Potentially hazardous gases include hydrazine or monomethylhydrazine (MMH) from propulsion systems, ammonia from thermal control loops, and hydrofluorocarbon (HFC) refrigerants used in air conditioning. These compounds can be toxic or act as asphyxiants and must be detected and removed rapidly. Metal-organic frameworks (MOFs) are implemented into the filtering system. As a class of materials known for their extremely high surface area and porosity, they are highly efficient at adsorbing various gases, including hydrazine, MMH, ammonia, and HFCs. Li et al. [1998]

To ensure the efficient removal of hydrazine, MMH, ammonia, and HFCs, a combination of UiO-66 (zirconium-based) for hydrazine and ammonia, ZIF-8 (zinc-based) for HFC refrigerants), and MIL-101(Cr) (chromium-based) for ammonia removal are selected. These MOFs are tailored for the specific requirements of air filtration in space environments. The MOFs are incorporated as MOF-coated substrates, in fiber mats. This approach offers the ideal balance of high surface area, selective adsorption, and integration flexibility. The mesh or fiber mat structure allows for uniform distribution of the MOFs across a large surface area, while still ensuring efficient airflow with minimal pressure drop.

These components are included in an air sanitation box architecture, with a design emphasis on reusability and ease of replacement between flights.

The filter architecture is resumed in the following figure:

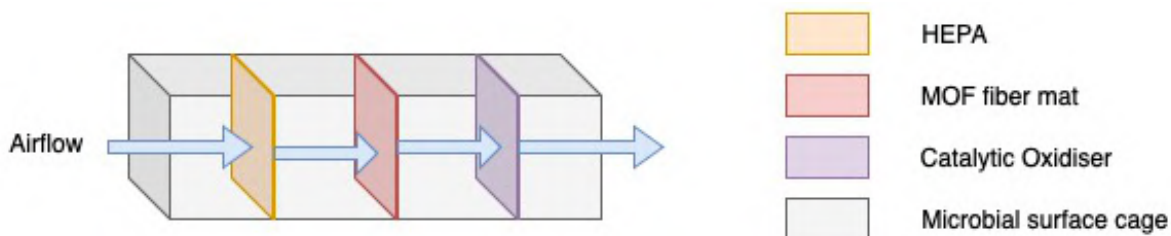


Figure 94: Air Filtration Architecture

The filter box should be positioned within the airflow path of the air regeneration system so that all cabin air passes through the filtration process. Integrating the filter box here allows for continuous filtration of both trace contaminants and particulates, ensuring that the air is constantly scrubbed of harmful gases, VOCs, and particulates during circulation. The filter box should be placed after the CO₂ and humidity removal system to ensure that air entering the fine filtration stages (like MOFs and activated carbon) is free of moisture and large particulates, allowing for more efficient adsorption of hazardous gases and trace chemicals. This also prevents clogging and maximizes the lifespan and effectiveness of the filtration media in the filter box.

Since the air regeneration system is integral to maintaining the overall atmosphere of the spacecraft, having the filter box within this system means that any issues with the filtration media (e.g., saturation or clogging) should be easily addressed without disturbing other critical systems. A modular design to the filters also facilitates this process.

For this mission duration, these filters are expected to last beyond a single flight cycle and be refurbished or swapped during ground servicing based on in-flight cabin metrics.

9.2.2.4 Thermal and Humidity Regulation

Temperature is managed via a two-stage thermal control system: an internal closed-loop air circuit exchanges heat with a liquid coolant loop, which is in turn thermally coupled to external radiators for heat rejection. This approach uses a vapor-compression refrigeration cycle on the ground and an external radiator-based thermal management system in orbit.

The internal loop uses a water/glycol mixture due to its favorable thermal properties and low toxicity.

Humidity is also passively removed through Nafion membrane dehumidifiers, exploiting cabin-air partial pressure differentials against vacuum; this eliminates moving parts and consumables while protecting sensitive electronics from condensation. The dehumidified air is recirculated via cabin fans, ensuring uniform thermal and compositional distribution.

The redundancy in dehumidification systems is sized so that the amine system handles the metabolic load (e.g., exercise-induced humidity, group presence), whereas the Nafion dehumidifier acts as a steady-state stabilizer that maintains dew point and protects systems from condensation, especially during uncrewed docked periods, partial power, or during amine bed regeneration cycles.

9.2.2.5 ECLSS Mass Budget

Although all subsystems are not thoroughly designed, an estimate of the mass budget required for each is made :

Environment Mass Budget	
Subsystem	Total weight (kg)
O2/N2 Supply	50
CO2 + Humidity Control	70
Trace Contaminant & Particulate Filter	10
Thermal Control	17
Ventilation	8
Total (kg)	162 kg

Table 76: Environment Mass Budget

9.3 Safety Procedures

9.3.1 Solar flares procedures

Depending on the phase of the mission, we propose different solutions to protect our astronauts against solar flares. We distinguish 2 phases: the docking phase and the capture phase. Since we can predict a solar flare within 1 to 3 days, we must adapt our mission to protect our crew.

If the solar flare occurs during the docking phase, our astronauts will be protected by the dedicated module of the station.

On the other hand, if we already left the station to capture the debris and a solar flare is coming, our astronaut will be exposed. To avoid designing and deploying a solar flare protection module while still ensuring our astronauts' safety, we will deorbit and land on Earth within a day.

9.3.2 Fire Detection and Suppression

In the event of a fire, the system uses a gaseous nitrogen-based suppression system, which acts by displacing oxygen locally without introducing reactive residues or impairing downstream filtration. This method is compatible with the cabin's inert diluent gas nitrogen,

avoids chemical extinguishants, and is appropriate for microgravity environments. The system includes both fixed nozzles and portable delivery units, offering redundancy.

Backup systems are available for the crew, with handheld portative extinguishers. For our space shuttle with a 5-day mission duration and following our atmosphere composition, the preferred composition of handheld portable fire extinguishers is pressurized carbon dioxide. CO₂ is effective in microgravity as it displaces oxygen to smother flames, is non-conductive, leaves no residue, and poses minimal risk to sensitive spacecraft systems. Although high local concentrations of CO₂ can be hazardous, the short exposure duration and the capability of the environmental control and life support system (ECLSS) to remove excess CO₂ mitigate this risk. The extinguisher design typically includes a tethered, conical nozzle to ensure safe deployment without recoil, and a pressurized canister delivering approximately 2–5 kg of CO₂ per unit.

A distributed array of smoke and combustion gas sensors, integrated into cabin airflow ducts, provides real-time fire monitoring.

Electrical shutoffs and local airflow isolation are also automatically triggered upon fire detection.

9.4 Food management

Eating in space face challenges as the closed environment of the spacecraft and the absence of gravity. The food system must ensure that every astronaut receives enough calories to stay healthy and perform tasks efficiently. It must also be safe (avoid contamination), easy to store, simple to prepare, and adapted to microgravity.

9.4.1 Astronauts Needs

Each crewmember has specific caloric needs depending on their age, weight, height, and activity level. Thus, each meals are prepared individually for each crew members. According to NASA [2023], the estimated energy requirement (EER) is calculated using standard equations with an activity factor of 1.25. Thus, we used the equation below for a crew composed of two men and one women.

- For men (above 19 years old) :

$$\text{EER (kcal/day)} = 622 - 9.53 \times \text{Age} + 1.25 \times (15.9 \times \text{Body Mass [kg]} + 539.6 \times \text{Height [m]}) \quad (147)$$

- For women (above 19 years old) :

$$\text{EER (kcal/day)} = 354 - 6.91 \times \text{Age} + 1.25 \times (9.36 \times \text{Body Mass [kg]} + 726 \times \text{Height [m]}) \quad (148)$$

- If an astronaut performs an EVA, the system provides an additional 837 kJ (200 kcal) per hour.

Based on the crew profiles and the mission duration (5 days), we computed the totals needs of our crew. We also took into account the EVA possibility if needed. Thus,

we consider one EVA per day of 6 hour maximum and perform by only one crew member. Focusing on a pre-design methodology, we only perform the food budget based on the calories needed and assume that each meals are prepared with the right amount of macronutrients and micronutrients.

The EVA considerations impose the needs detailed below :

EVA additional kca /h	200 kca
Nb EVA hour/day	6 h
Kca/EVA	1200 kca
Additional water needed/day	611,67 ml
For 5 days mission	6000 kca

Table 77: EVA considerations

The crew needs are evaluated with the formulas detailed previously. We take into account the EVA by dividing the EVA calories per day between the 3 crew member to simplify calculations. However, this doesn't imply that every crew member will perform an EVA if necessary.

Crew needs per day	Member 1	Member 2	Member 3
Sex	Women	Men	Men
Mass (kg)	60	70	70
Height (m)	1,65	1,75	1,75
Age	30	30	30
Kcal needed	2346,75	2907,725	2907,725
Extra kca for EVA	400	400	400
Margin (%)	10	10	10
Total with margin	3020,6825	3638,4975	3638,4975
Total for crew/day	10297,6775		

Table 78: Crew needs per day (3 members)

9.4.2 Food distribution & storage

Food storage and distribution are carefully designed to ensure efficiency, safety, and ease of use during the mission. The food consumed is freeze-dried reducing the weight and volume of the food, which is essential to reduce mass and storage in our shuttle. It also extends the shelf life and prevents microbial growth, meeting safety and stability requirements. Thermostabilized meals are heat-treated to ensure they remain safe without refrigeration. These types of food are easy to prepare by simply adding hot water, fulfilling the requirement for minimal preparation. All meals are individually packaged to avoid contamination.

The food repartition for one day and one crew member is organised following the table below :

Meals	kcal	Weight (g)	Water needed (ml)
Breakfast	430	100	120
Lunch	506,67	120	293,33
Diner	506,67	120	293,33
Snack	250	50	25
Dessert	250	50	25
Total	1943,33	440	756,67

Table 79: Meals organisation and needs

Storage System

The food pouches are securely stored in dedicated compartments to prevent them from floating around. Each compartment is organized based on meal types (breakfast, lunch, dinner, and snacks) to make selection easier for the crew. The storage system also includes a labeling system to help astronauts quickly identify their meals since each meal have a specific composition for each crew member.

Food Preparation and Distribution

To prepare a meal, astronauts use the hot water dispenser and adds the necessary amount of hot water to the freeze-dried pouch. Once rehydrated, the pouch is gently kneaded to ensure even moisture distribution. Astronauts eat directly from the pouch using a spoon or a straw, preventing crumbs or spills that could float in the cabin.



Figure 95: Example of water dispenser to rehydrate the meals

9.4.3 Food and mass budget

We finish our food system design by suming up the food needs and the associated water and weight. The water estimation will be take as an input in the water budget, here we doesn't consider the weight associated to the water distribution, this will be describe in the water section.

The mass budget for the food system is based on the crew caloric needs, the EVA consideration and the water needed to rehydrate the meals. The weight considered for food is the weight of the freeze-dried meals.

Per day	kcal	Water (ml)	Weight (g)	Packaging (g)
Crew (3 CM)	10297,6775	4009,55821	2331,549623	78
Margin %	already included	10	5	-
Total /crew with margin	10297,6775	4410,514703	2448,127104	-
Total for mission (5 days)	51488,3875	22052,57351	12240,63552	390
Total weight (kg)			34,7	

Table 80: Food and mass budget for the crew during 5 days missions

9.5 Medical Necessities

We pre-design a medical systems onboard to ensure the health and safety of the crew, during our autonomy mission. As in the other section, we still consider a 5 days mission for dimensionning. With this duration, the risk of serious medical events is relatively low. However, if a health problem or injury occurs, the consequences can be significant. Under normal conditions, the impact of the medical system on onboard resources is limited. But in the event of an emergency, the system must be ready to respond quickly and effectively without putting other systems or crew members at risk.

The medical system on board must consider unique spaceflight constraints such as microgravity, limited volume, mass, power, and available crew time. Unlike Earth-based systems, space medical care must be compact, efficient, and usable by all crew members, including non-physicians as explained in the NASA-STD-3001. The design must also include options for emergency treatment and situations involving biological hazards, such as blood or body fluids, that must be safely contained and disposed of.

NASA's medical classification system defines five levels of care. For missions lasting less than eight days, such as Low Earth Orbit (LEO) operations, the expected medical needs are limited. The system must be able to provide: space Motion Sickness management, Basic Life Support (BLS), first aid, response to allergic reactions (Anaphylaxis) and finally private audio communication with medical personnel on the ground.

Also, according to NASA-STD-3001, we must respond to the following requirements :

- A minimum of 0.5 kg of potable water shall be available for eye irrigation in case of particulate events (e.g., dust or foreign object exposure).
- A minimum of 5 kg of water shall be available per medical contingency event, such as chemical exposure or skin burns.
- There must be enough volume and surface area to treat a patient and to allow access for the caregiver and necessary equipment.
- Medical equipment must be usable by any trained crew member.
- Biological hazards, such as blood, must be contained and disposed of to prevent contamination.
- The spacecraft must have a protocol for handling the body of a deceased crew member in a respectful and safe way.

Thus, the following elements must be defined for our shuttle medical system :

- A designated medical area : this space should allow for proper access to the patient and storage of all necessary materials.
- A medical computer and health monitoring system to support diagnosis and treatment.
- An equipment list adapted for short-duration missions
- A mass budget of the medical system

9.5.1 TASTrain recommendations

Working closely with TASTrain to prepare the astronauts to operate our shuttle, they gave us recommendations regarding the medical necessities. Thus, we have a list of element requirep splitted in categories : Medications and Treatments, Basic Medical Equipment and First Aid. Still considering a 5 days mission for a crew of 3 astronauts, we defined a mass for each of these equipement. We obtained the following table.

Item	Estimated Mass (g)
Antibiotics (Amoxicillin, Ciprofloxacin)	150
Antivirals (Oseltamivir)	150
Painkillers (Paracetamol, Ibuprofen)	100
Antihistamines (Diphenhydramine, Loratadine)	80
Antacids (Omeprazole, Ranitidine)	100
Anti-nausea (Ondansetron)	70
Wound Care (Hydrocortisone cream, antiseptic creams)	250
Medications for Headaches (Aspirin, Paracetamol)	100
First Aid Supplies (Bandages, Sterile Gauze)	300
Medications for Sleep Disorders (Melatonin, Zolpidem)	50
Cough Syrup	100
Vitamins and Supplements (Vitamin D, Vitamin C)	100

Table 81: Medications and Treatments – Estimated Mass per 5 Days for 3CM

Item	Estimated Mass (g)
Thermometer	100
Blood Pressure Monitor	500
Stethoscope	100
Pulse Oximeter	100
Glucometer	100
Defibrillator	2500
Bandages, Gauze, and Compresses	300
Sterile Gloves	150
Scissors	100
Masks for Emergency Situations	200
Portable Diagnostic Kit	500
Sutures and tissue repair kit	100

Table 82: Basic Medical Equipment – Estimated Mass per 5 Days for 3CM

Item	Estimated Mass (g)
Urinary Infection Test	100
Wound Dressings and Bandages	300
Antiseptic Gel	100
Burn Cream	100
Cold and Hot Packs	100
Stress Management Tools	100
Vitamins and Mineral Supplements	100
Psychological Follow-up File	100

Table 83: Diagnostic Instruments and First Aid – Estimated Mass per 5 Days for 3CM

9.5.2 Procedures classification

Thus, for our health system we will rely on the TASTrain list and on the NASA recommendations previously quoted. We will not have any advanced medical system, in case of emergency we will have to quickly land on Earth and abort the mission. The table below from the Chen et al. [2022] describes the procedures depending on the class of the medical event.

Characteristics	Examples	Response
Class I		
Mild Symptoms	Gastrointestinal Distress	
Effects Performance Minimally	Headache	
No Threat to Life	Mild Ulcer	
Prognosis Is Self-Limited	Laceration of Abrasion Sprains and Strains	
Class II		
Moderate to Severe Symptoms	Urinary Infection or Inflammation Respiratory Irritation	Self Care
Marked Effect on Performance	Allergy, Conjunctivitis, or, Dermatitis DCS Air Embolism	
Potentially Life Threatening	Arrhythmia Partial Circulatory Blockage Ulcer Respiratory Distress	Prompt adequate diagnosis and treatment
Could Be Protracted	Toxic Inhalation Exposure Chemical burns Stones Diverticulitis Appendicitis	
Class III		
Symptoms Immediate and Severe	Explosive Decompression	
Incapacitating	Complicated Heart Malfunction	
Life Threatening If Not Immediately Fatal	Overwhelming Infection Crush Injury	Evaluate Promptly and Transport or; Take Measures to Store, Return, or Destroy the Body
Crewmember Won't Survive If Not Treated Promptly	Brain Surgery Burn > 40% of Body Surface Area	

Figure 96: Illness Classification from NASA/TP-2015-218570

9.5.3 Crew Health Monitoring

During the 5-day autonomous mission, we will use real-time monitoring of the crew's vital signs. Ground teams will be able to remotely access physiological data and respond quickly in the event of anomalies or emergencies. Each astronaut will be equipped with a wearable biometric device continuously tracking heart rate, blood pressure, body temperature, oxygen saturation (SpO₂), and ECG data. Thus, we add the following elements to our equipment list :

- Wearable health monitoring patches (0.6 kg)
- ECG module with electrodes (0.4 kg)
- Data transmission module (0.5 kg)

9.5.4 Medical computer

To support health diagnostics and emergency response, we use a medical computer especially design for the health system. It allow the crew members to access medical protocols, record symptoms, and consult diagnostic tools onboard. It also provides remote

access to Earth-based medical teams, who can analyze real-time data and give instructions when needed.

The medical computer is defined by these key functions:

- Display of real-time biometric data from wearables
- Medical records of each crew member
- Access to medical protocols and first-aid procedures
- Secure communication with ground medical team and providing a private communication if needed.
- Connection to onboard diagnostic sensors (ECG, oximeter, etc.)

9.5.5 Medical Area

Due to the limited space available in the shuttle, the medical area must be compact and highly functional. Unlike the ISS, which includes a designated area for medical procedures, our shuttle does not have the volume to support a dedicated medical bay, thus the medical care is integrated into the cabin.

One of the existing crew seats is used for medical evaluation or intervention. The medical kit is stored close to the crew, in an accessible locker. The area includes a the medical computer connected to the wearable sensors that monitor vital signs in real-time. Although minimal, this setup ensures the crew can manage medical issues during the 5-day autonomous mission.

9.5.6 Medical Mass Budget

The total estimated mass for the medical subsystem is **10.7 kg**. This value includes all the necessary equipment and consumables required for a 5-day mission with a crew of three astronauts. The mass budget is given below.

Équipement / Consommable	Poids (g)
Water pouches (> already counted in water budget)	NA
Medical computer	2000
Health monitoring	
Wearable health monitoring patches	600
ECG module with electrodes	400
Data transmission module	500
TASTrain recommendations	
Thermometer	100
Blood Pressure Monitor	500
Stethoscope	100
Pulse Oximeter	100
Glucometer	100
Defibrillator	2500
Scissors	100
Antibiotics (Amoxicillin, Ciprofloxacin)	150
Antivirals (Oseltamivir)	150
Painkillers (Paracetamol, Ibuprofen)	100
Antihistamines (Diphenhydramine, Loratadine)	80
Antacids (Omeprazole, Ranitidine)	100
Anti-nausea (Ondansetron)	70
Wound Care (Hydrocortisone cream, antiseptic creams)	250
Medications for Headaches (Aspirin, Paracetamol)	100
First Aid Supplies (Bandages, Sterile Gauze)	300
Medications for Sleep Disorders (Melatonin, Zolpidem)	50
Cough Syrup	100
Vitamins and Supplements (Vitamin D, Vitamin C)	100
Bandages, Gauze, and Compresses	300
Sterile Gloves	150
Masks for Emergency Situations	200
Portable Diagnostic Kit	500
Sutures and tissue repair kit	100
Urinary Infection Test	100
Wound Dressings and Bandages	300
Antiseptic Gel	100
Burn Cream	100
Cold and Hot Packs	100
Stress Management Tools	100
Vitamins and Mineral Supplements	100
Total mass (kg)	10.7

Table 84: Medical necessities mass budget for a 5 days mission with 3 CM

9.6 Crew Module/Living Quarters

9.6.1 EVA

EVA en cas de truc à réparer -> on compte une eva de 6h max par jour -> demande des needs additonal en food et en water

EVA en cas d'urgence ? lesquelles ? Mass budget

9.6.2 Habitacle

9.6.3 Hygiene on board

Maintaining personal hygiene in microgravity is essential for the comfort and well-being of the crew. Since water cannot flow freely in space, hygiene routines must be adapted using water-free solutions when possible and specialized equipment.

Washing the Body

Astronauts clean themselves using a set of pre-packaged wipes designed for different hygiene needs:

- Soapy wipes for body cleaning
- Hand wipes for quick hand sanitation
- Dry wipes that can be moistened with water for additional cleaning

For the hair, we provide dry shampoo to use directly on the scalp and then wiped off. Since water is limited and must be carefully managed, no rinsing is required, and all used wipes are properly stored in waste containers.



(a) Karen Nyberg applying shampoo in the ISS



(b) Chris Hadfield wetting wipe in the ISS

Figure 97: Examples of hygiene means in the ISS

Brushing Teeth

For oral hygiene, astronauts use classic toothpaste and a damp toothbrush. Instead of spitting out excess toothpaste, they wipe it off with a towel to prevent floating particles. Water is used minimally, only to moisten the toothbrush and rinse if necessary.



Figure 98: Chris Hadfield brushing his teeth in the ISS

Non provided equipment

Since the autonomy phase lasts only 4 days (including one day margin), certain hygiene tasks are not included like shaving, nail cutting, haircuts, Showering (no water-based washing system) and laundry.

By simplifying hygiene needs, the shuttle ensures a clean, efficient, and practical environment for all crew members.

Mass budget

Having all this routines, we can define a mass budget for the hygiene equipment. We consider 5 day mission as the worst case : one day from launch to docking, 3 days of debris removal mission and one additional day for margin. We obtained the mass budget below for our 3 crew member :

For the entire mission and crew (3 CM)		
Equipment	Quantity	Total weight (kg)
Hygiene wipes	-	3,45
Weight of hygiene wipes packaging	-	0,075
Water (200ml pouches)	30	0,06
Water Packaging (200ml pouches)	30	0,42
Dry shampoo	1	0,015
Comb	1	0,04
Toothpaste	6	0,03
Toothbrush	6	0,06
Towel	6	0,24
Total for the entire mission and crew (kg)		4,39

Mission duration	5 days
Crew member	3 CM

Table 85: Mass budget for hygiene equipment (5 days mission for 3 CM)

9.6.4 Absence of Artificial Gravity and a Gym

Our spacecraft will stay in orbit around Earth for only 3 days. For such a short mission, there is no need for artificial gravity or a gym because the effects of microgravity on the human body happened in longer stay in space. Scientific studies show that muscle loss and bone weakening happen mainly during long missions in space. In just a few days, these changes are very small and do not affect the astronauts' health or ability to work.

Adding artificial gravity would require complex technology, more energy, and extra weight, making the spacecraft heavier and more expensive. A gym would also take up space and would not give real benefits in such a short time. Instead, we focus on making the best use of space and resources to ensure the crew's safety and comfort during the mission.

9.7 Water management

For a mission lasting up to five days, the water management system must ensure that clean, safe, and reliable water is available at all times for drinking, food rehydration, hygiene, and medical needs. Although the duration of this mission is short, the system must be autonomous and capable of supporting all planned operations.

The water system must be able to supply, store, distribute and monitor water quantity. Because of the short mission duration, complex water recovery or wastewater recycling systems are not necessary and would not be mass- or energy-efficient. Thus, we choose to not rely on recycling and to produce our water thanks to the fuel cells used in the power system.

According to NASA-STD-3001, we add the following requirement :

- At the point of crew consumption or contact, the total iodine concentration shall be less than or equal to 0.20 mg/L.
- The microbial content, measured in colony-forming units (CFUs), shall remain within the safe limits defined by health standards described below :

Table 3—Potable Water Microbiological Limits

Characteristic	Maximum Allowable	Units
Bacterial Count	50	CFU/ml
Coliform Bacteria	Non-detectable per 100 ml	-
Fungal Count	Non-detectable per 100 ml	-
Parasitic Protozoa, e.g., Giardia and Cryptosporidium	0	-

Figure 99: Potable water microbiological limits from NASA-STD-3001

- The system shall provide a minimum of 2.0 kg of potable water per crewmember per day for drinking and food rehydration.
- The water shall be dispensed at a rate compatible with the food system.
- The system shall provide an additional 240 mL of potable water per hour for each crewmember performing an EVA.
- Water must be available at different temperatures to support different needs (e.g., warm water for food or medical care, cool water for drinking).

9.7.1 Water Budget

First, we start our design by defining the water needs for our crew of three astronauts considering a 5 days mission. We established a water budget of the drinking water needed each day to ensure the necessary contribution to the different systems : Hygiene, food, medical, EVA and drinking.

Purpose	Q/CM-d (L)	Margin(%)	Q/3CM-d (L)	Temp (°C)	Availability
Drinking	2	5	6,3	15,6°C	All day
Food	1,470171568	include	4,410514703	68,3°C – 79,4°C	All day
Medical	2,166666667	20	7,8	18–28°C	Immediately
Hygiene	0,4	5	1,22	15,6°C	Twice a day
EVA	NA	include	1,44	15,6°C	All day
Total /crew/day = 21,1705147 L					

Table 86: Water budget per day for a crew of three astronauts

The necessary water for the food also include the eventuality of an EVA, while the mention "EVA" only concern the water consume during it. This table also showcase the different temperatures needed to distibute water, this will be detailed in later sections.

Applying margins, we obtained a total of **21,17 L per day** for our crew. This amount includes the regular water needs and exceptional water needs like water for medical and EVA activities. If not use, these two sources of water represent 9.8 L per day to manage.

9.7.2 Fuel cell water recovery

In the optic of performing automous missions, being able to produce water directly on board present a significant advantage. If we look at the past space missions such as Apollo and the Space Shuttle, Alkaline Fuel Cells (AFC) were used to produce water as a byproduct. This water was mainly recovered as vapor and required condensation and treatment before being used. More recently, Proton Exchange Membrane Fuel Cells (PEMFC) have been studied for water production purpose. In fact, they produce water in liquid form due to their lower operating temperatures (60 °C–90 °C), making water collection easier and more efficient. These fuel cells generate electricity through an electrochemical reaction between hydrogen and oxygen, and one of the main byproducts of this reaction is pure water (H_2O).

Although the water produced by PEMFC is chemically pure, it is not directly suitable for drinking. Pure water lacks essential minerals and may contain contaminants coming from the degradation of internal fuel cell components, such as metal ions. This can happen due to contact with electrode materials or corrosion inside the fuel cell.

The study "*Recovery and quality of water produced by commercial fuel cells*" perfom by Juan E. Tibaquirá, Kiril D. Hristovski , Paul Westerhoff and Jonathan D. Posner Tibaquirá et al., give us hints about what we need to implement to obtain drinkable wa- ter. They identify two key elements : the presence of metals such as nickel and aluminum in the water and the lack of mineral salts.

Thus, if we want to obtained drinkable water, we must :

- **Remove contaminants:** nickel and aluminum must be filtered or chemically removed.
- **Add essential minerals:** sodium (Na^+), chloride (Cl^-), calcium (Ca^{2+}), magnesium (Mg^{2+}), and potassium (K^+).

These treatments are required to comply with potable water standards, as defined by NASA and international health guidelines. Without this mineral content, the water can cause health issues if consumed regularly, since it does not support the body's electrolyte balance.

To ensure drinking water production from PEMFC, we must find a way to recover and purify the PEMFC output. We're going to implement the same recovery system as the one described in the study presented above. Their water collection system consists of a stainless steel drain trap (FA-150, Spirax Sarco) and a high-density polyethylene (HDPE) carboy. At the outlet of the PEMFC, the flow includes liquid water, water vapor, air, and unreacted hydrogen. This mixture enters the drain trap, where liquid water is separated and collected into a carboy. Thus, we're going to use the same collection system, except that the drain trap will directly lead to our water treatment system and finally to our tank for storage instead of the carboy. In addition, the remaining gases and vapor will be vented outside the spacecraft using a dedicated venting mechanism.

From pure water to drinkable water

Providing drinking water from our fuel cell implies a complete treatment chain to ensure water safety and quality for our astronauts (see below).

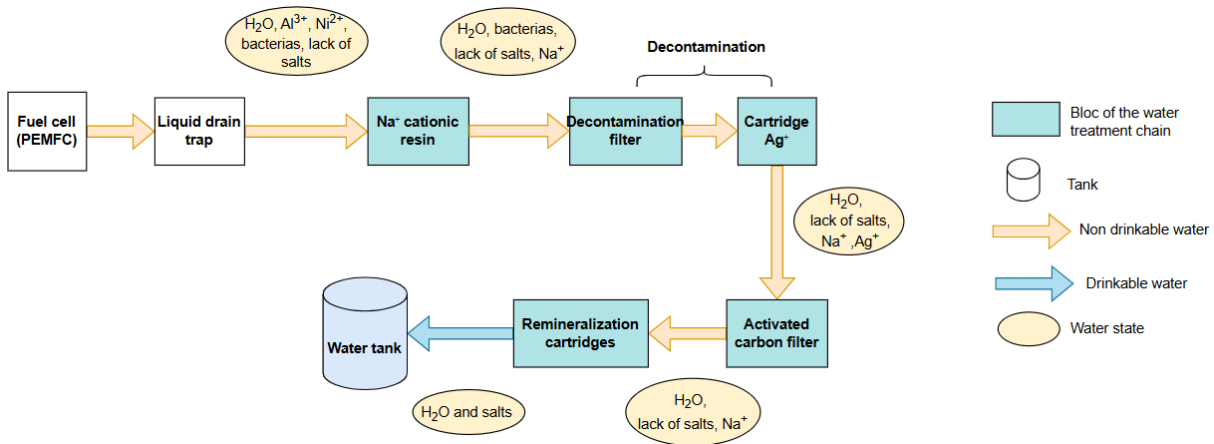


Figure 100: Diagram representing the drinkable water production chain

The treatment chain is composed of several stages:

- **Water Collection:** The water output from the fuel cell (a mix of liquid and vapor) is first directed to a stainless steel liquid drain trap as described previously.
- **Heavy Metals Removal:** The collected water, which contains aluminum and nickel, passes through a sodium cationic resin. This ion-exchange resin removes heavy metal ions and replaces them with sodium (Na^+), which is safe in small amounts for drinking.

- **Decontamination and Disinfection:** Even if water is chemically clean, microbiological contamination is possible. To ensure safety, the water passes through a 0.2 μm filter and then a silver ion (Ag^+) cartridge. The Ag^+ acts as a disinfectant and sterilizes the water. To avoid excessive silver concentration, an activated carbon filter is included to reduce the Ag^+ content below 0.1 mg/L and to absorb other possible impurities.
- **Remineralization:** Water produced by PEMFC and purified through decontamination steps lacks essential minerals. Therefore, the water is sent through remineralization cartridges containing mineral powders like NaCl , CaCO_3 , MgSO_4 , and KCl . These salts slowly dissolve, enriching the water with essential ions such as sodium, calcium, magnesium, and potassium. This process is passive and requires no additional energy.
- **Storage:** The final drinkable water is stored in a dedicated tank, ready to be used for drinking, food rehydration, hygiene, or medical purposes.

9.7.3 Water management along the mission

To ensure water autonomy, we assessed the total water needs of the crew and compared them with the water production rate from the fuel cells. This step is essential to confirm that our system can sustain the crew.

We calculated the average hourly water production from the fuel cells and compared it with the hourly consumption of the crew, based on the previous established water budget, which we must note, already include margin on the consumption. The water consumption analysis is based on a detailed budget, broken down by activity, with associated quantities and daily frequency.

Daily Activities and Water Needs

The table below summarizes the water usage throughout a typical mission day, including meals, hygiene, and critical needs like medical emergencies or EVA support. We recall that the water required for EVA includes extra drinking water and food hydration, and assumes one EVA per day, limited to one crew member for a maximum of 6 hours.

Medical water, although ideally unused, must always be available. As seen in the medical section, a minimum of 5 L should be accessible at any time to comply with mission safety requirements.

Hour of the Day	Purpose	Quantity (L)	Availability / day
7	Breakfast	1.10	1
12	Lunch	1.10	1
16	Snack	1.10	1
20	Dinner	1.10	1
NA	Drinking	6.30	24/24h
NA	Medical	7.80	24h/24H
8	Hygiene	0.61	1
18	Hygiene	0.61	1
NA	EVA	2.05	24h/24h

Table 87: Water consumption by purpose over one day for a 3-person crew.

This table help us ensuring sufficient water availability even during peak usage periods or in the case of unplanned events such as medical incidents or extended EVA operations.

Using this table, we check if the water produce by the fuel cells permit to be fully autonomous for the life support needs. The following inputs were used in our calculations:

Fuel cell water production rate	0.877 L/h
Total crew water consumption/day	21.17 L
Initial onboard water (launch)	4 L
Required medical water (always available)	5 L

Table 88: Daily water system input data

We plotted a graph which for each hour associate : the quantity produce by the fuel cell (L/h), the water quantity consumme per hour (L/h), the total consumption and the water quantity left (L) all along the day for our crew. We base this analysis on the previous established table listing the crew needs along the day. Concerning the needs that has to be available 24h/24h, we splitted them along the 24 hours of the day. We obtained the graph below :

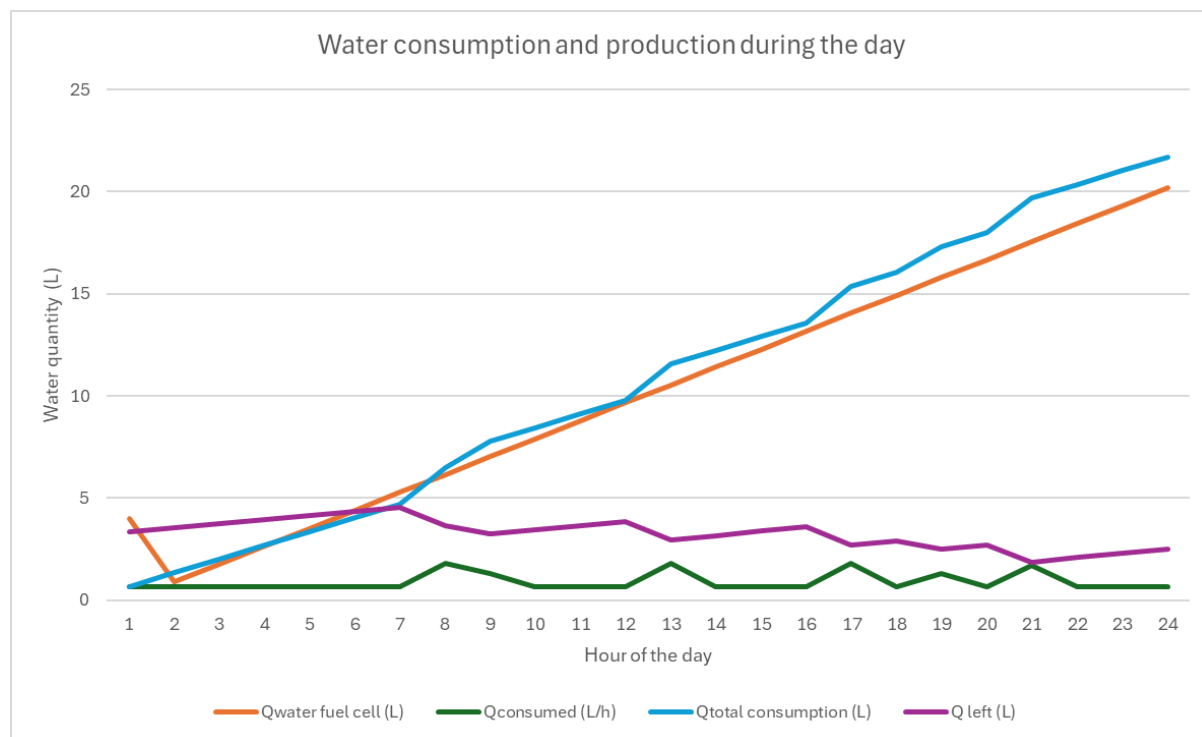


Figure 101: Water consumption and production during the day

We can see that the overall consumption (blue curve) is higher than what we produce with the fuel cell (orange curve). However, if we follow the violet curve, we still have water left. This is because we assumed that without an initial water reserve, the system would not meet the requirement of having 5 L of medical water instantly available at any time. Therefore, we included 4 L of pre-stored water at launch to reduce the initial deficit. Within one hour after launch, the fuel cells produce nearly 0.9 L, reducing the gap rapidly and assuming no water will be used for drinking, hygiene or food during this first hour.

At the end of the day, the system has an estimated minimum surplus of 2.5 L of water. This is significant, especially if medical reserves or EVA allocations were not fully used. Such excess must be considered in the sizing of the tank and surplus water management systems must be considered.

Finally, we confirm our autonomy by looking at the green curve which represents the water quantity consumed per hour, we see that we stay largely below the water produced (orange curve).

Managing the extra water

The extra amount of water will be managed by expanding the water tank to contain it. As the active thermal control wasn't properly sized, we consider that surplus water could be used to regulate the shuttle temperature. Using venting system, we could dissipate the spacecraft heat by sublimating water into space. We eliminate the possibility to use liquid water in the thermal control, this would require a closed loop system.

For the first day of the mission, the extra water will be given to the station using the docking port. For hygiene and health reasons, stagnant water must be avoided, thus we can't keep water on board during the docked phase. When leaving the station, as it is the case in the launch phase, we will embark 4 liters of water for medical reasons.

In case the produced water isn't potable, until we fix the issue, the system must be able to evacuate the unused water. For that, we integrate an external evaporation system inspired by the sublimator technology from the Apollo program. This system allows excess water to be safely ejected into space while also helping to dissipate heat from the spacecraft.

9.7.4 Storage : Tanks design

The water produced by the PEMFCs must be safely stored before distribution. Our design includes two tanks: one for storing potable water and one for nitrogen (N_2) used for pressurization of the water tank.

To ensure safety and efficiency, the potable water tank must meet several key requirements:

- It must not release any toxic particles or contaminants into the water.
- It must be compatible with common disinfectants such as iodine or ionic silver (Ag^+).
- It must resist temperature variations due to heating and cooling in the spacecraft.
- It must be lightweight to reduce the overall mass of the life support system.
- It must withstand vacuum and space radiation to prevent evaporation and material degradation.

The water tank is pressurized using nitrogen (N_2) gas to maintain a stable internal pressure of 4 bar, as required by docking and distribution systems. Maintaining positive pressure ensures a constant water flow, regardless of volume changes in the tank as it fills or empties.

Tank sizing

To achieve this, we size the water tank based on the mission's hydration needs, and then calculate the volume and pressure needed for the nitrogen tank. The nitrogen tank is pressurized to 8 bar. This pressure must remain higher than the water tank's pressure to ensure a consistent flow of water.

To properly size the potable water tank, we based our calculations on the predicted water usage during the mission and considered the worst-case scenario. This scenario is based on not using the water allocated for medical and EVA necessities, plus a 10% margin on the water budget (see previous section).

The mission includes a launch and docking phase on Day 0, a docking phase and four autonomy days (Day 1 to Day 4). The docking phase permit to release the extra water to the station and to leave with the necessary 4 liters for medical necessities. The table below shows the initial quantity of water onboard, the amount of water produced by the fuel cells daily, the total used quantity, and the remaining quantity in both nominal and worst-case conditions.

Quantity/Day	Day 0	Docking	Day 1	Day 2	Day 3	Day 4
Initial quantity (L)	4	0	4	12.452	20.904	29.356
Total used Q worst case (L)	11.727	0	11.727	11.727	11.727	11.727
Total left Q worst case (L)	12.452	0	12.452	20.904	29.356	37.808

Table 89: Worst case scenario for water consumption

Using the worst-case scenario, we decided to go with tank capacity of at least 38L to meet the crew needs, while ensuring a safety margin for the worst case consumption scenario, unexpected delays or higher consumption.

Water tank sizing

To determine the correct size and weight of the potable water tank, several input parameters were considered, including ullage, maximum water volume, internal pressure, material choice, and safety factor. A small ullage of 5% was included to account for gas expansion and avoid overpressurizing. The maximum volume of water planned for the mission is 38L, which leads to a total tank capacity of 39.9L when including the ullage. The tank is pressurized at 4 bar using nitrogen gas.

The material selected for the tank is stainless steel 304, known for its corrosion resistance, compatibility with disinfectants, and good mechanical properties. The minimum wall thickness was calculated using the thin-wall pressure vessel approximation for a cylindrical tank:

$$e = \frac{P \cdot r}{\sigma_{\text{adm}} \cdot SF}$$

Whith :

- P : internal pressure (Pa)
- r : radius (m)
- σ_{adm} : admissible stress for stainless steel (Pa)
- SF : safety factor (2)

The theoretical thickness obtained was very low ($\sim 4.67 \times 10^{-9}$ m), but for practical and manufacturing reasons, a thickness of 1 mm was chosen. Assuming a spherical shape with radius, we compute the stainless steel volume and obtained the empty mass of the tank :

$$m = \rho \cdot V_{\text{steel}} = 5.37 \text{kg}$$

Where $\rho = 7850 \text{ kg/m}^3$ (density of stainless steel).

We resume our computation and output in the table below.

Input Parameters	Value
Ullage (%)	5%
Water volume desired (L)	38
Ullage volume (L)	1.9
Total tank volume (L)	39.9
Tank pressure (bar / Pa)	4 bar / 400,000 Pa
Material	Stainless Steel 304
Safety factor (SF)	2
Chosen thickness	1 mm
Steel volume (m^3)	0.000684056
Output Dimensions	
Total volume (m^3)	0.0399
Tank weight (empty, kg)	5.37 kg
Radius (m)	0.233

Table 90: Water tank sizing parameters and results

Nitrogen tank sizing

The nitrogen (N_2) is dimensioned according to the water tank needs. We start by computing the necessary volume of nitrogen to presurize the water tank assuming a 8 bar pressure for nitrogen:

$$V_{N2} = \frac{P_{water} * V_{water}}{P_{N2,initial} - P_{water}} \quad (149)$$

Including an ullage of 5% and a safety margin of 10% added for the nitrogen gas volume, we obtained the tank volume : $V_{TankN2} = 0,04389m^3$.

The amount of nitrogen required is determined using the ideal gas law, with a fixed temperature of 348K equivalent to the ideal fuel cell temperature. Thus, given the pressure, temperature, and tank volume, we compute the number of moles (n) of nitrogen.

$$PV = nRT \Rightarrow n = PV/RT \quad (150)$$

Then, using the molar mass of nitrogen (28g/mol), we calculate the mass:

$$m = n \times M = 0.324 \text{ kg} \quad (151)$$

Like the water tank, we choose the stainless steel 304. The wall thickness is calculated based on the maximum stress allowed and a safety factor of 2. We obtained a wall thickness of 1.926 mm, so a rounded value of 2 mm was chosen. Finally, assuming a spherical tank, we computed the radius the empty mass of the tankWe sum up our results and inputs in the table below.

Input Parameters	Value
Ullage (%)	5%
Nitrogen gas volume + margin (m ³)	0.0418
Tank pressure (bar / Pa)	8 bar / 800,000 Pa
Temperature (K)	348
Number of moles (n)	11.56 mol
Mass of N ₂ (kg)	0.324 kg
Safety factor	2
Chosen thickness (m)	0.002
Material	Stainless Steel 304
Steel volume (m ³)	0.001404
Steel density (kg/m ³)	7850
Output Dimensions	
Tank volume (m ³)	0.04389
Radius (m)	0.241
Tank empty weight (kg)	11.03
Total tank weight (kg)	11.35

Table 91: Nitrogen tank sizing parameters and result

Material trade-off

Before choosing the stainless steel as our tank material, we also look at other materials such as carbon composite T700, which can withstand very high pressures and are extremely lightweight (around 2 kg for both tanks). The mass of the steel tanks is approximately 14 kg in total, which remains acceptable within the 2000 kg budget allocated for the life support system. We chose the stainless steel because it is much more cost-effective and easier to manufacture than carbon composites while still offering excellent corrosion and mechanical resistance.

Tank architecture

The water storage tank used in our shuttle is based on the architecture developed for the NASA Space Shuttle.

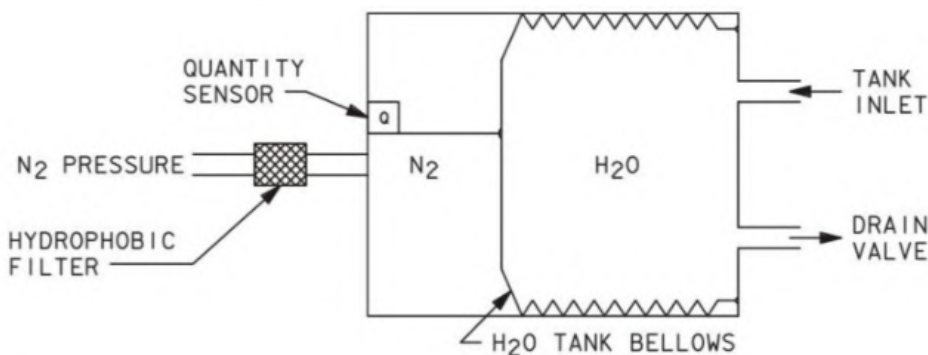


Figure 102: NASA's Space Shuttle water tank Unknown [2025]

The tank is divided into two sections: one for potable water and one for pressurizing nitrogen gas (N₂). The water compartment includes a flexible metallic bellows that separates the water from the nitrogen. As water is withdrawn, the bellows contracts, allowing

nitrogen to expand and maintain a constant pressure.

A hydrophobic filter is placed on the nitrogen inlet to let it out of the tank while preventing any liquid water or contaminants from entering the nitrogen line. The tank also includes a sensor that monitors the amount of water inside. Water is supplied through a tank inlet valve and distributed via a drain valve.

Nitrogen Recycling loop

Each time the potable water tank is refilled with water from the fuel cells, we must take care of the nitrogen output. To optimize efficiency and resource, we include a nitrogen recycling closed loop. This subsystem recaptures escaping nitrogen, filters it, and repressurizes it back into the tank. Although the detailed design of this system is not yet designed, it is based on principles similar to gas recovery systems used in closed-loop environmental control systems.

9.7.5 Water distribution

The water dispensing system is responsible for delivering water to different operational units of the spacecraft: food preparation, drinking, hygiene, and medical use. Based on the NASA-STD-3001, each application requires water at specific temperatures, as detailed in this table.

Purpose	Temp (°C)
Drinking	15,6°C
Food	68,3°C – 79,4°C
Medical	18–28°C
Hygiene	15,6°C
EVA	15,6°C

Table 92: Water temperature needed

Water is dispensed primarily using refillable flexible water pouches. This method is adapted from systems used aboard the ISS and earlier missions. These pouches are manually filled and serve to all the water needs detailed in the table. The crew is responsible for maintaining the number of filled pouches for each needs. The filled pouches for drinking and hygiene should be 5 degrees under the cabin temperature. Thus, they will be stored in colder environment while the medical pouches doesn't need any particular storage. However, they must be easily accessible in case of emergency. For food rehydration, the crew uses a gun-like tool to inject water directly into the pouch.

Our water tank will be maintained to approximately 20°C (cabin temperature). This temperature is chosen to avoid having too much temperature control in output. Thus, the medical water will be directly available. The drinking and hygiene water will only need a chiller and for the food, we will only need to heat the water 4 times a day. Thus, to ensure proper temperature control, the system integrates a water chiller and heater. This approach was inspired by the Apollo spacecraft, which featured a water chiller capable of cooling water and a heater.

Using the Apollo mission as a reference, our shuttle includes several interface points for water dispensing:

- Drinking water gun: manually operated dispenser connected via flexible tubing, providing cool water.
- Food hydration port: injection port for water delivery into freeze-dried food bags.
- Medical and hygiene port: to refill sterile water pouches.

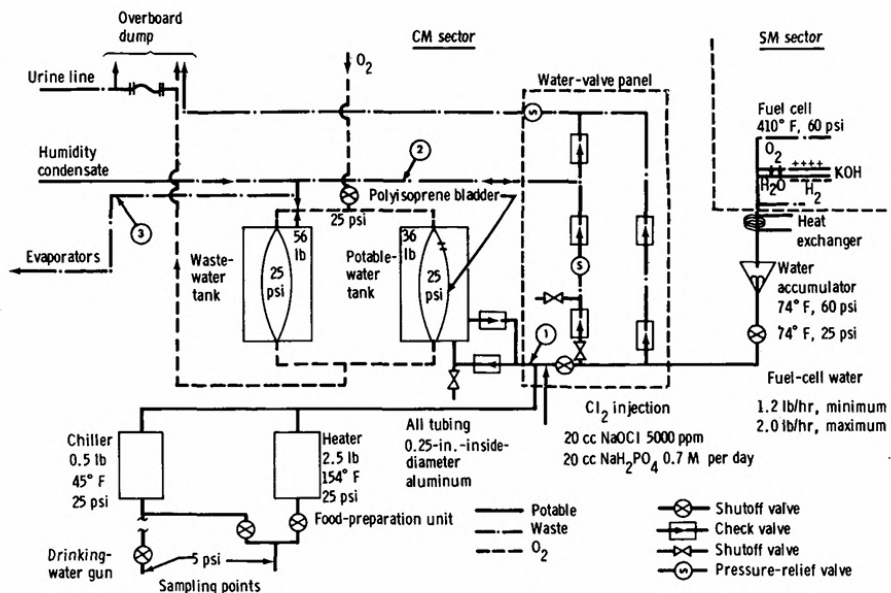


Figure 103: Schematic of the CSM management system in Apollo Sauer and Calley [1973] Wikipedia contributors [2025]

Design of the Water Pouches

The water pouches used in the shuttle are designed to be both functional and efficient. They are made from polyethylene, polyurethane, nylon, or Mylar, and utilize multi-layered materials to combine the benefits of different substances. This ensures that the pouches are durable, flexible, and able to withstand the demanding environment of space and the need for sterility and safety when storing water. These pouches come in different sizes (1L, 500mL, 200mL) depending on their specific use. They can be reusable, not directly during the mission but once return to Earth they will be cleaned and reuse for another mission.

The pouches used for drinking water are typically holding around 500 milliliters of water. These are designed for easy handling and are equipped with a straw or valve, allowing astronauts to drink without spilling or creating floating droplets in the microgravity environment. Pouches for hygiene purposes, such as those used for cleaning or washing have different spouts for easier control of the water flow. Finally, medical pouches reserved to water are sealed and often come in various sizes to meet the needs of different treatments or medical procedures in space.

We established the below table regarding the quantity of empty pouches needed. This will be used later in computation of the mass budget.

Water pouches for 5 days + 3 CM	1L	500ml	200ml
Drinking	-	60	-
EVA drinking	-	35	-
Food	-	45	-
Hygiene	-	-	30
Medical	10	20	100
Total	10	160	130

Table 93: Number of water pouches for 5 days mission and 3 crew members

Use of Membrane Pumps for water circulation

The circulation of water is managed using membrane pumps responsible to provide both hot and cold water as needed. Membrane pumps can move water efficiently without relying on gravity, which is essential in the microgravity environment of space. They use a flexible diaphragm to create pressure and move water through pipes and tubes.

The primary goal of this system is to distribute the water into pouche for different uses. These pouches are essential for hydration, hygiene, and medical needs. They ensure potable water distribution at any time and without spilling it or contaminate it. This system maintain a consistent flow and provides astronauts with the necessary resources for daily life in space.

9.7.6 Monitoring

To ensure optimal performance and crew safety, the entire water subsystem—responsible for water production, treatment, distribution, and storage—requires continuous monitoring. This includes both hardware-based measurements and software-based alerts to detect any anomalies. The following parameters are constantly monitored throughout the mission:

- **Water Levels:** storage tanks are equipped with sensors to track the volume of water and nitrogen (N_2) at any time.
- **Tank Pressures:** Both water and N_2 tanks are fitted with pressure sensors to ensure they remain within safety margins.
- **Water Temperature:** Temperature sensors are placed along the distribution circuit to confirm the heater and cooler efficiency.
- **Water Composition:** Sensors analyze the chemical composition of potable water, verifying that it meets required standards and is free of harmful contaminants. The system can detect the presence of disinfectants such as silver ions (Ag^+) and iodine.

This monitoring system provides data to astronauts and ground control, allowing them to anticipate shortages, detect contamination early, and ensure the water subsystem performs efficiently under the constraints of spaceflight.

9.7.7 Final architecture

We present the final design of our water system in the diagram below. To provide an efficient pre-design of our water system, we focus on the production, storage and distribution of drinkable water during a 5 days mission.

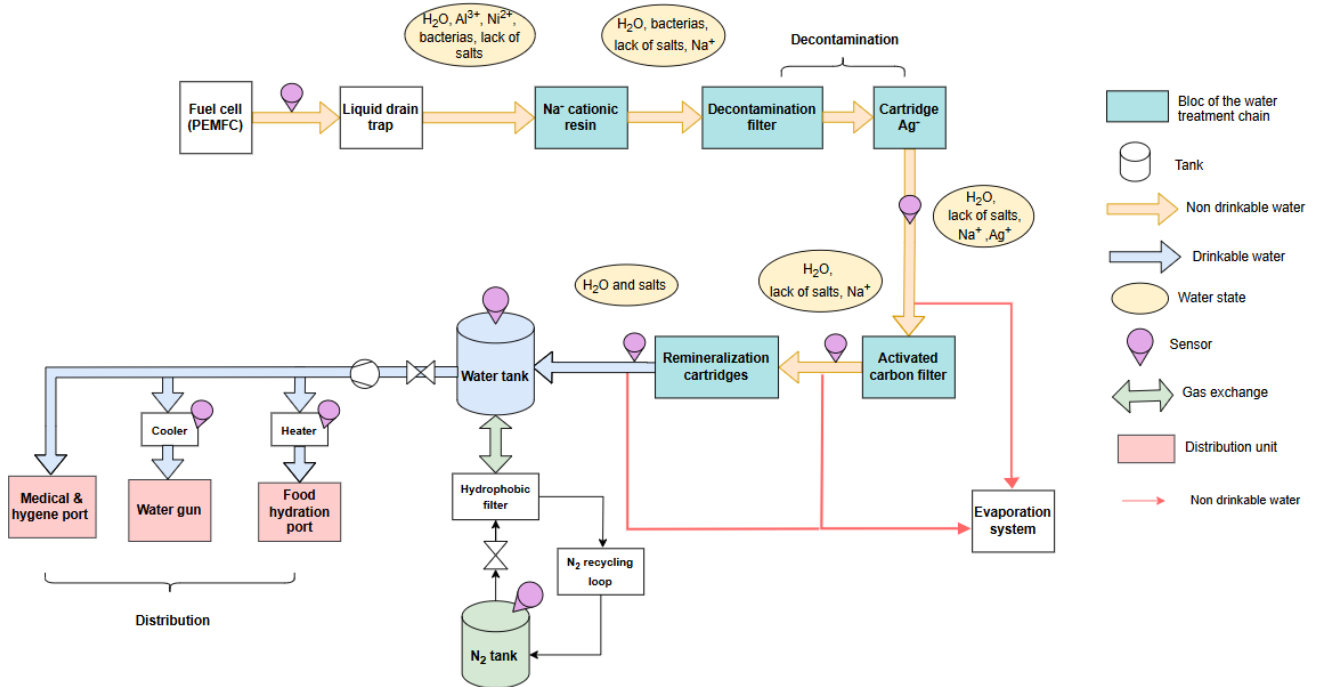


Figure 104: Water system architecture

9.7.8 Mass budget

In this section we present the associated mass budget.

Item	Weight (kg)
Water dispenser	8.8
Water treatment	11
Evaporation system	5.5
Water tank	5.37
N ₂ tank	11.02
N ₂ mass	0.32
Max water in tank (worst case)	37.8
Packaging pouches 1L	0.7
Packaging pouches 500mL	6,125
Packaging pouches 200mL	1.82
Total mass (kg)	88,47

Table 94: Mass budget of the water system

We add some precisions regarding the weight estimations :

- For the water dispenser, the water treatment and the evaporation system, their weight has been estimated based on historical data and current technological stan-

dards. The water dispenser system, which includes the drinking water gun, the food hydration port, medical and hygiene ports, as well as heating and cooling elements, is projected to weigh approximately 8.0 kg. This estimation aligns with similar systems used in past missions, such as the Apollo program's water dispensers.

- The water treatment system is more complex, since it has never been developed in space. The total mass for is estimated at 10.0 kg.
- Lastly, the evaporation system is estimated to have a mass of 5.0 kg. The design is inspired by the sublimator systems employed during the Apollo missions.
- For these three equipments, we add a 10% margin on their weight. The other items have already their margins included.

9.7.9 Limits of the drinkable water system design

While PEMFCs offer a promising method for water production in space, some challenges remain. The fuel cell components may degrade over time, especially under thermal stress, potentially releasing harmful substances into the water. Continuous monitoring and filtering systems are therefore necessary to ensure that the water remains safe during the mission.

Another limitation, is that the use of PEMFC fuel cells for water production in space is still experimental. Although ground-based studies show promising results, this technology has not yet been tested in real spaceflight conditions, and its performance and reliability in microgravity remain uncertain.

The current predesign is also limited regarding the water treatment chain which the assembly remains theoretical. Each component of the system would need to be properly dimensioned, tested for chemical compatibility, and validated to ensure that the complete process can produce safe, drinkable water in a space environment.

Regarding the water consumption, it is important to note that all values used in this study are part of a pre-design phase. The current estimations are based on simplified assumptions and ideal daily schedules. In future mission phases, detailed simulations and operational studies would be required to refine the real-time water needs, both on an hourly and daily basis. These refined analyses should take into account the actual activities of the crew, environmental variations, and stress-related hydration needs.

Moreover, the current water budget does not yet consider water usage for thermal control systems. As water may be used for heat transfer or cooling purposes, this additional consumption must be included in future calculations.

9.8 Waste Management System

Waste management play a key role in the crew health, hygiene, and overall habitability. Representing a non negligible weight, we must deliver a pre-deisgn of this system. We still consider a mission of five days for our three crewmembers. The waste management system should be designed to ensure safe collection, secure containment, and proper

disposal of body waste, while also offering privacy and ease of use for all crewmembers during the mission.

Following the NASA standards from the document NASA-STD-3001, the waste management system must comply with several key requirements:

- It shall be physically isolated from food preparation and consumption areas to ensure hygiene.
- The system shall ensure odor control, especially for biological and body waste.
- It must allow safe storage and later disposal of solid and liquid waste, including urine, feces, vomit, blood, and other body fluids.
- Trash management shall be integrated and able to handle packaging waste from food, water, medical supplies, and hygiene products.
- All components must be cleanable, sanitizable, and maintainable.

Thus, the architecture of the waste management system consists of:

- A suction toilet system
- A vacuum cleaner
- A urine tank connected to the toilet for liquid waste.
- A feces tank for solid body waste also connected to the toilets
- A general trash tank for dry waste (packaging, hygiene wipes, medical waste, etc.).

For this 5-day mission, recycling of urine is not considered necessary. Instead, all waste will be stored onboard and returned to Earth. Except for the first day of the mission. Once docked, we will only give our general trash to the station to avoid any contamination during the docked phase. However the urine and the feces will stay in during the docking phase. After this, during the autonomous mission, the onboard storage tanks will be used. All containers are hermetically sealed to prevent leaks and contamination in the cabin.

Odor Control Strategy

Odor control is a crucial element for crew comfort. Our system uses a two-level approach:

- Primary containment: All waste is stored in airtight containers to prevent gas dispersion.
- Passive odor filters: Charcoal-based odor control packs are installed in the vent lines of each waste tank. This approach is inspired by the Waste and Hygiene Compartment (WHC) on the ISS, which uses activated carbon and HEPA filtration to reduce odor and airborne contaminants.

These simple yet effective solutions reduce the need for powered ventilation, aligning with the short-duration mission.

9.8.1 Waste budget

Assuming these data from the NASA [2023] and the Chen et al. [2022] document :

Waste Type	Value (/CM-day)
Urine	1 L
Feces	2 events × 150 g
Food packaging waste	0.26 kg
Waste food adhered to packaging	0.10 kg
Hygiene wipes	0.23 kg
Water packaging (per 500 ml)	0.035 kg
Hygiene wipes packaging	0.005 kg
Miscellaneous waste	0.011 kg

Table 95: Daily waste generation per crew member

Using these data, we establish the following waste budget as depending on the day of the mission.

Sources	Unit	Day 0	Docking	Day 1	Day 4
Urine tank					
Urine	(L)	3	-	6	15
Feces tank					
Feces	(kg)	0.9	-	1.8	4.5
Feces bags	(kg)	0.18	-	0.36	0.9
Toilet paper	(kg)	0.075	-	0.15	0.375
Trash tank : Hygiene					
Miscellaneous waste	(kg)	0.033	-	0.033	0.132
Hygiene packaging	(kg)	0.099	-	0.099	0.396
Hygiene wipes	(kg)	0.69	-	0.69	2.76
Food					
Waste food adhered to packaging	(kg)	0.3	-	0.3	1.2
Food packaging	(kg)	0.78	-	0.78	3.12
Drinking					
Water packaging	(kg)	0.42	-	0.42	1.68
Medical					
Medical waste	(kg)	0.6	-	0.6	2.4
Medical water packaging	(kg)	0.56	-	0.56	2.24
EVA					
EVA support interface wastes	(kg)	0.02	-	0.02	0.08

Table 96: Total waste generation by all crew (3 CM) over 5 mission days

These wastes are split between three tanks : the urine tank, the feces tank and the trash tank. We precise that for the medical necessities and EVA, we computed the worst case, meaning we use all the resources. We also recall that on the first day (day 0), the trash will be given to the station. Thus, in the contrary of the two other tanks, these one will be empty at the beginning of the autonomy phase. Thus, we obtained the following quantity in each tank.

Day 0	Value	Margin (%)	Total
Total urine tank (L)	3	10	3.3
Total poop tank (kg)	1.155	10	1.2705
Total trash tank (kg)	3.502	10	3.8522
Autonomy mission	Value	Margin (%)	Total
Total urine tank (L)	18	5	18.9
Total poop tank (kg)	6.93	5	7.2765
Total trash tank (kg)	14.008	10	15.4088

Table 97: Tank waste estimates for Day 0 and a 4 day mission

9.8.2 Tank Dimensioning

From the value of the waste budget and base on the same methodology as the water tank dimensioning, the following tank capacities are proposed.

Urine tank	
$V_{\text{Max Waste}}$ (L)	18.9
V_{tank} (L)	19.845
V_{tank} (m^3)	0.0198
Rayon (m)	0.184
Weight (empty) (kg)	3.37
Feces tank	
Approximative density (kg/m^3)	1060
$V_{\text{Max Waste}}$	6.864
V_{tank} (L)	7.21
V_{tank} (m^3)	0.007
Rayon (m)	0.132
Weight (empty) (kg)	1.72
Trash tank	
Approximative density (kg/m^3)	200
$V_{\text{Max Waste}}$ (L)	77.1
V_{tank} (L)	80.90
V_{tank} (m^3)	0.081
Rayon (m)	0.295
Weight (empty) (kg)	8.6

Table 98: Tank dimensioning output for waste system

Again, like the water tank, stainless steel 304 was selected as the tank material due to its excellent corrosion resistance, mechanical strength, and compatibility with biological fluids. It is commonly used in medical and sanitary applications, which ensures it can

safely contain urine, feces, and other biological waste without degradation. Additionally, the tanks will be equipped with secure locking mechanisms and antibacterial coatings to ensure sanitation.

9.8.3 Toilet Architecture and Design

The space shuttle is equipped with a suction toilet system that operates using an airflow mechanism to ensure that waste is safely collected and does not float around. It consists of several key components to ensure proper waste collection and hygiene:

- Suction System: instead of relying on gravity, the toilet uses a strong airflow to pull waste into the correct storage areas.
- Urine Funnel: A special funnel is used, one for men and one for women. The urine is not recycled but is stored in the defined urine tank.
- Solid Waste Seat and Collection Bags: waste is collected in individual disposable bags, which are automatically sealed after each use.
- Storage Compartment: after use, waste bags are stored in a pressurized containment unit to control odor and maintain hygiene.

The toilet is positioned in a dedicated hygiene module, ensuring privacy and ease of access for all crew members. Additionally, a footrest and thigh straps help astronauts stay in position while using the toilet.



Figure 105: Picture of the urine funnel in the ISS

9.8.4 Vacuum cleaner

Due to the lack of gravity, any crumbs, dust, or miscellaneous body wastes can float freely and pose a risk to both the crew and the equipment. To address this, we use a vacuum cleaner specifically designed for space conditions. The vacuum is cordless, allowing for easy maneuverability. The vacuum is equipped with specialized filters to capture even the smallest particles, including crumbs from food and any debris generated by the crew's daily activities.

9.8.5 Mass budget

The estimation of the mass budget for the waste management system remains challenging due to the moderate level of pre-design currently achieved. Several assumptions were made based on available data from previous space missions including the Space Shuttle Waste Collection System and ISS-related components. We also used data from the NASA's Life support values and assumptions document. As a result, the provided values should be considered as approximations. All values fall within a reasonable order of magnitude, the goal was to ensure that the proposed system remains feasible within the overall constraints. Thus, the mass budget is detailed below :

Equipement / Consommable	Weight (kg)
Total urine waste	18.9
Total feces waste	7.2765
Total trash waste	15.4088
Urine tank	3.37
Feces tank	1.72
Trash tank	8.6
Feces bags	1.08
Toilet paper	0.375
Charcoal filter + venting	3
Toilet system	20
Vacuum cleaner	3
Total	82.7303

Table 99: Waste system mass budget

9.9 ECLSS Mass budget

The total mass of the ECLSS, excluding the habitat structure and EVA components, is estimated at {719.58 kg}. Each ECLSS subsystem was carefully dimensioned to match the needs of a 5-day mission with a crew of three astronauts.

Élément	Poids (kg)
Food	11.5
Water system	88.47213295
Waste system	82.7303
Hygiene	4.39
Medical necessities	10.7
Environment	155
Fire Suppression	7
Total (hors habitat et EVA)	359.7924329
Habitacle	
EVA	
Total final	719.5848659

Table 100: ECLSS mass budget

10 Thermal

The thermal subsystem is essential to ensure the safe and efficient operation of the shuttle in space. It is responsible for maintaining all components within their acceptable temperature ranges despite extreme external conditions such as solar exposure, eclipses, and reentry heating. This includes both passive and active thermal control methods. The system must provide protection during all mission phases, from launch to docking and reentry.

10.1 Requirements

The thermal control system of the shuttle must fulfill a set of functional and performance-based requirements to ensure mission success and vehicle safety. These requirements cover operational performance in space, environmental resistance, autonomy, energy efficiency, and reusability. They are defined as follows:

- **The-REQ-001 – Efficient thermal system:** The thermal system must ensure that the shuttle functions nominally under the mission conditions.
- **The-REQ-002 – Component resistance in space:** Thermal components must resist the specified temperatures, radiations, particles, micrometeoroids, and debris expected during the mission.
- **The-REQ-003 – System during docking:** The thermal system must remain operational during the docking phase.
- **The-REQ-004 – Power needs:** The thermal system must minimize the necessary energy to maintain the thermal conditions of the shuttle.
- **The-REQ-005 – System autonomy:** The thermal system must be fully autonomous.
- **The-REQ-006 – Passive thermal control:** The thermal system must rely as much as possible on passive thermal control solutions.
- **The-REQ-007 – Reusability:** The thermal system should be fully reusable. If 100% reusability is not possible, a target of 90–80% should be considered.
- **The-REQ-008 – Redundancy:** In accordance with FDIR principles, redundancy must be considered for active thermal control elements.
- **The-REQ-009 – Mass:** The mass of the thermal system must represent 8% of the total shuttle mass (approximately 3200 kg).
- **The-REQ-010 – Electronics protection:** The thermal system must protect and maintain the electronic components within their specified operating temperature range.
- **The-REQ-011 – Fault tolerance:** The thermal system must include fault-tolerant strategies and apply redundancy if needed.

- **The-REQ-012 – Heat shield:** The heat shield must be designed to perform efficiently during atmospheric reentry.
- **The-REQ-013 – Thermal structure:** The materials chosen for the thermal structure must ensure the resistance and performance of the shuttle under mission conditions.

10.2 Heat Shield design

During atmospheric re-entry, a spacecraft's heat shield (thermal protection system - TPS) is exposed to extreme thermal and mechanical loads. Designing an efficient heat shield is therefore a key aspect of mission safety and success.

Several physical phenomena must be considered when analyzing the thermal environment the spacecraft will face:

- Shock waves : Caused by the high-speed interaction between the shuttle and the atmosphere, generating intense compression and heating of the gas in front of the shuttle.
- Convection: Heat is transferred from the hot surrounding gases to the surface of the shuttle through conduction and convection.
- Radiation: At high temperatures, gases and the vehicle itself emit thermal radiation, which adds to the total heat flux received by the heat shield.
- Laminar and turbulent flow: The turbulent or laminar regime varies along the re-entry. Turbulent flow typically results in higher heat fluxes than laminar flow.

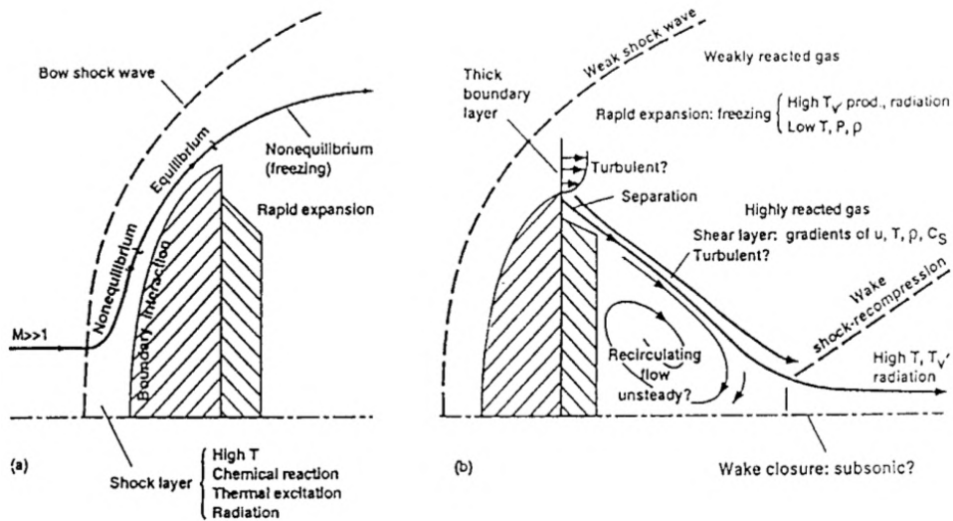


Figure 106: Representation of the different fluxes on a capsule during the re-entry, extract from MOULIN

The figure 106 present the different key phenomena during the re-entry experienced by a capsule. Even if the capsule re-entry is ballistic, in our case, we still experience the same phenomenon.

The design of the heat shield is closely linked to the re-entry trajectory. From this trajectory, a maximum heat flux (isoflux) can be determined. This value depends mainly on the velocity of the spacecraft and the atmospheric density, which itself changes with altitude. This maximum heat flux serves as a thermal limit that guides the selection of materials and shapes for the thermal protection system and influence the re-entry trajectory.

10.2.1 Objectives: Methodology for Heat Shield Design

We try to describe the standard approach to desing a heat shield in order to help us identifying the key element for a pre-design methodology. The standard approach includes:

1. **Definition of constraints:** The two primary constraints to consider are:
 - The maximum surface temperature (T_{\max}) the shuttle can withstand.
 - The total heat flux received, which is the sum of the convective heat flux and radiative flux from the surrounding hot gases.
2. **Mechanical constraints:** Include structural loads such as aerodynamic forces, pressure gradients, and vibrations experienced during descent. These loads need to be evaluated to ensure that the heat shield tile's will not crack under these conditions.
3. **Material selection:** Materials must be chosen based on the expected constraints and their location on the shuttle (e.g., nose, flaps, body), as exposure levels vary.
4. **Determination of thermal and aerodynamic fluxes:** This is typically done using Computational Fluid Dynamics (CFD) simulations.
5. **Calculation of thermal loads:** A thermal map is created to identify hot and cold zones over the vehicle's surface.
6. **Tile geometry design:** Using the CFD and the mechanical and thermal load values, the shape and dimensions of the heat shield tiles are optimized based on thermal distribution.

Pre-design Approach

Knowing that the main design drivers are the heat fluxes and heat loads, we defined a simplified methodology based on the previous one to follow a pre-design methodology for our heatshield. We focus on the core parameters: material, placement and tile shape. The approach is based on the concept of designing from a fixed isoflux while taking into account the maximum temperature and the mechanical loads.

An isoflux heat shield aims to ensure that the incoming thermal energy is uniformly distributed across the vehicle's surface. This is achieved by adjusting the tile properties (material, thickness, and thermal conductivity), so each tile dissipates heat at a similar rate, despite spatial variations in local heat flux. An isoflux condition is defined when the heat flux per unit area (W/m^2) remains constant over the protected surface.

Having this in mind, we defined our **pre-design methodology** :

1. Definition of the target isoflux.
2. Estimation of the maximum surface temperature.
3. Selection of appropriate materials.
4. Computation of the mechanical loads
5. Geometry definition for the tiles based on the mechanical loads.
6. TPS architecture on the shuttle

10.2.2 Application of the pre-design methodology

Step 1 : Target isoflux

Following the established pre-design methodology, we start by fixing an isoflux for our shuttle. For that, we will consider our shuttle during the atmospheric flight of the re-entry, the most dimensional phase. We can neglect the bellyflop and hover phases as they encountered much less constraints than in the atmospheric flight.

The isoflux serve as a thermal limit and can be approached by the Sutton-Grave equation at the stagnation point. This point represent the point where the fluid velocity is null and thus the static pressure is at maximum as well as the temperature and the thermal fluxes. This equation give us the convective flux, we use this flux in our isoflux approach because it is the dominant flux during the re-entry phase and also because it varies a lot depending on the geometry of the vehicle.

$$q = k * \left(\frac{\rho}{R}\right)^{\frac{1}{2}} * V^3 \quad (152)$$

Sutton-Grave equation at stagnation point

With :

- q : thermal convective flux (W/m^2)
- k = $1,83 * 10^{-4}$ (on Earth)
- ρ : atmospheric density (kg/m^3)
- R : effective radius of curvature (m)
- V : velocity (m/s)

The isoflux depend of the speed of the vehicle and the atmospheric density of the atmosphere (based on the altitude). Thus, we need the re-entry profile of our Shuttle to define the worst thermal case and apply the Sutton-Grave equation at this point. To define this dimensionning point, we use a study "Heat Transfer Analysis for a Winged Reentry Flight Test Bed" (see Viviani and Pezzella [year unknown]). This study, although it was done on a winged vehicle, give us a range for this critical point. Using the velocity profile of the vehicle and the convective heat flux as a function of time, we define different points

and compute their isofluxes in the case of our shuttle. Thus, the study only serve as an input to define our dimensionning point for our shuttle.

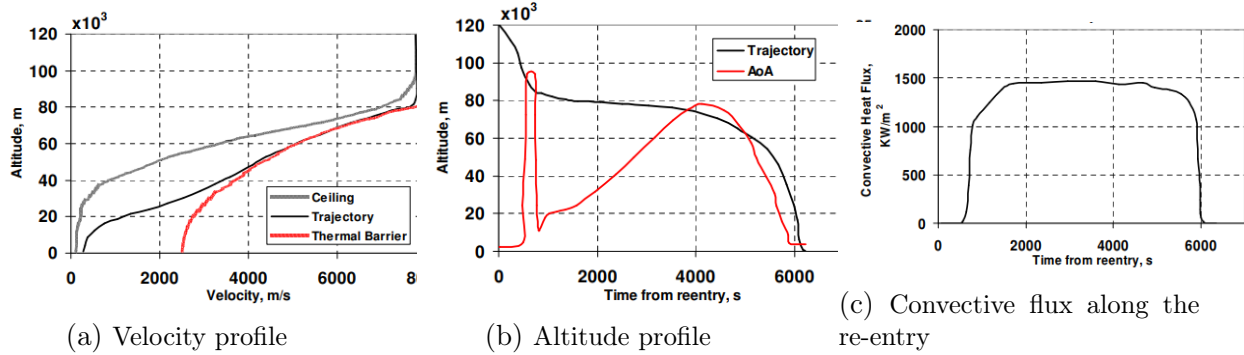


Figure 107: Graphics from the study of Antonio Viviani and Giuseppe Pezzella

Looking at their data, we see that the convective flux reach it maximum with a value of $15 \cdot 10^{-5} W/m^2$ for an altitude of 75km and a speed of approximatively 7000 m/s. Using this first input, we compute the maximum isoflux for our shuttle.

To perfom this caltung, we also define R , the effective radius of curvature use in the Sutton-Grave equation. The effective radius of curvature is describes how "sharp" or "blunt" a surface is. During atmospheric re-entry, this value help determining how the airflow interacts with the surface of the vehicle. We use a simplify model of our shuttle and compute the curvature radius using the oblique combined radius formula and with θ , the angle of attack :

$$R = \frac{R_{nose} * R_{body}}{R_{nose} * \sin(\theta)^2 + R_{body} * \cos(\theta)^2} \quad (153)$$

Having all the parameter of our Sutton-Grave equation, we perfom multiple iteration to determine the isoflux. We start with the value provided by the previous study and refine to obtained our corresponding values.

Parameter	Value
Altitude	80 km
Velocity	7300 m/s
Atmospheric density	$3,67 \cdot 10^{-5} kg/m^3$
Curvature radius	2,5 (m)
Isoflux	$3,33 \cdot 10^5 W/m^2$

Table 101: Isoflux condittion of StarCheap during the atmospheric flight

Step 2 : Maximum surface temperature

In order to design our TPS, it is also necessary to estimate the maximum surface temperature reached during the re-entry phase. In our simplified approach, we assume that the heat flux on the surface is uniformly distributed and corresponds to the concept of isoflux. We also still design our heat shield according to the atmospheric flight phase. This allows us to approximate the thermal environment using a steady-state energy balance at the surface.

We consider the convective flux as the dominant contribution to the surface heat load, and we neglect heat conduction and radiative heating from the surrounding gas. Under these assumptions, the incoming heat flux can be considered equal to the radiative heat loss from the surface:

$$q_{\text{net}} = q_{\text{conv}} = \varepsilon \cdot \sigma \cdot T^4$$

where:

- q_{conv} : convective heat flux (W/m^2) (obtained from the isoflux condition)
- ε : emissivity of the surface material of our heat shield
- σ : Stefan-Boltzmann constant ($5.67 \times 10^{-8} \text{ W m}^{-2} \text{ K}^{-4}$),
- T : surface temperature (K)

This method allows for a first estimation of the maximum surface temperature as a function of the chosen material emissivity and the applied isoflux. For now, we fixed an emissivity of 0.75 equivalent to the lower limit for our heat shiel materials. Thus we obtained a maximum temperature T_{max} of **1399°C** (1672 Kelvins).

Step 3 : Materials selection

Having the isoflux and the maximum temperature during re-entry, we consider different materials that can withstand extreme thermal environments based on our state of the art. We first compare two spacecrafts: the Space Shuttle (NASA) and the SpaceX Starship. Each of these vehicles uses different approaches and materials to ensure thermal protection and structural integrity during the re-entry phases.

Spacecraft	Isoflux W/m^2	Tmax (°C)
Starship	3.10^5	1427
NASA Space shuttle	$2, 25.10^5$	1260

Table 102: State of the art - Thermal conditions

In this table, the maximum temperature refers to the temperature whistand by the material during the re-entry. It depends of the materials and the encountered heat fluxes. The presented isofluxes come from different studies, but were not computed due to lack of informations. In order to efficiently choose our materials, we must look at what the Starship propose since we are closer to their thermal conditions than the space shuttle. However, the TPS configuration of both shuttle must be study to define our TPS architecture and the tiles placement.

In this optic, we will first focus on the most recent TPS materials used on the Space Shuttle. The different used materials are presented in the table below.

Material	Full Name	Type	Tmax (°C)
RCC	Reinforced Carbon–Carbon	Reinforcement	~1650
LI-2200	Low-Density Silica Tiles	Tile	~1260
LI-900	Ultra Low-Density Silica Tiles	Tile	~1200
FRCI-12	Felt Reusable Composite Insulation	Insulation	~1260
AFRSI	Advanced Flexible Reusable Surface Insulation	Insulation	~650

Table 103: Final TPS materials used on the Space Shuttle

The most interesting material for us are the RCC which was used on the nose and the wings edges as well as the LI-200 and the FRCI-12. The schematic below describe the clever repartition of the different material according to the heat fluxes along the shuttle during its re-entry. Thus, a smart tile placement could help optimizing our heat shield mass.

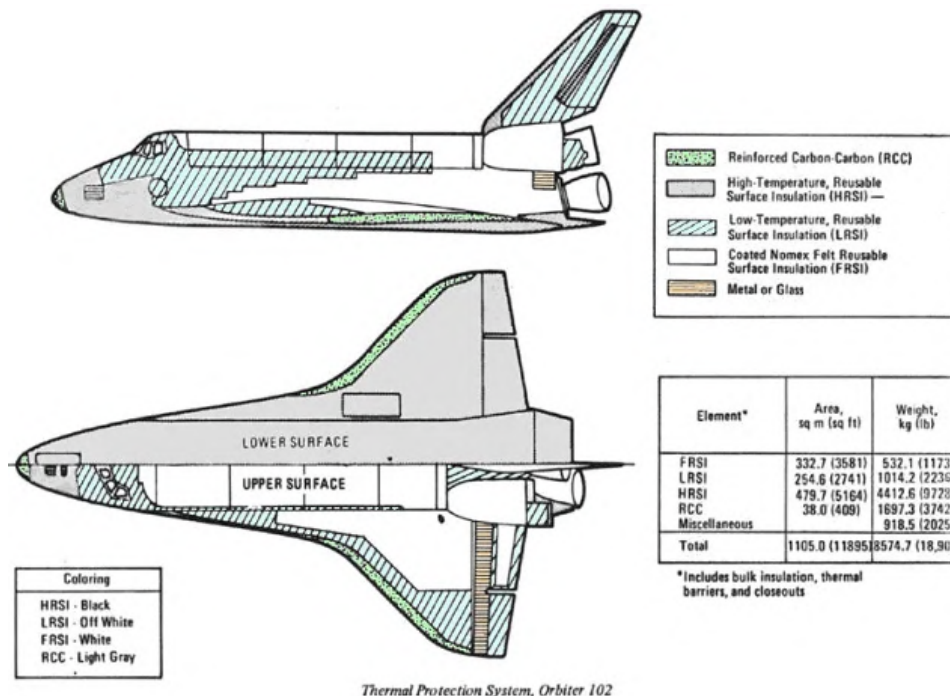


Figure 108: Material repartition on the NASA's space shuttle

On the other hand, SpaceX's Starship has a different TPS design philosophy, relying on layering with a high-temperature metallic structure as a first layer. The table below presents the different materials used and their characteristics.

Material	Description	Type	Tmax (°C)
TUFI	Ceramic Hexagonal Tiles	Tile & insulation	~1500
Stainless Steel	301/304L	Structural skin	~1100

Table 104: TPS materials used Starship

Regarding the Starship, what is interesting for us is the simplest architecture and the use of a new working configuration by utilizing a stainless steel structure and hexagonal ceramic tiles. The stainless steel body offers better heat resistance and structural

performance under high thermal loads. This design allows for potential full reusability with reduced maintenance, as the steel structure can endure more aggressive re-entry conditions.

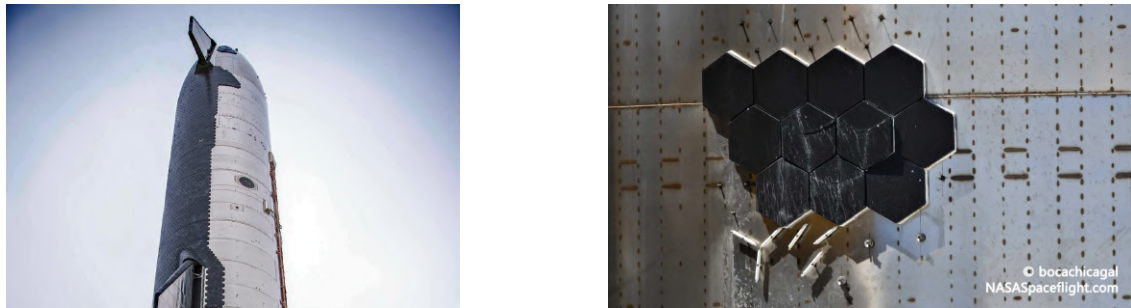


Figure 109: Heat shield structure of the Starship

Studying these two configurations, we can clearly see that there are two ways of thinking. Either we choose to put different materials on the spacecraft's surface regarding the faced heat fluxed, like in the NASA's space shuttle. This approach helps to reduce the heat shield mass by assigning specific tiles or insulations for each areas. The second approach is simpler to the detriment of the mass. Based on layering, the concept is based on one common layer (stainless steel structure) and an additional layer applied on the entire lower part of the spacecraft. Having this simple configuration does not take into account the heat flux variations over the spacecraft. The tiles are dimensioned for a global isoflux and not for local heat fluxes, thus adding more protection and more weight on part that could need less.

Following our pre-design mindset, we choose to use a configuration similar to the Starship one. It better align with our structure and our pre-design methodology where we have to make choices relying on the isoflux and the temperature. This configuration also offer a simpler design and avoid having to deal with too much materials on the surface but increase the mass of the heat shield.

Finally, our goal is to define:

- A material for our shuttle structure
- An insulating layer between the tiles and the structure
- Heat-resistant tiles for lower part

Tiles and insulators materials are hard to test, define and qualified. Our pre-design approach doesn't leave space to test new materials. Thus, we will choose the same tiles as the Starship one. TUFI tiles are made of a fibrous silica base material, which provides excellent insulation properties, and are coated with a tough outer black layer. They integrate both thermal insulation and surface protection in a single piece. The silica-based core acts as the insulator, while the glassy outer coating improves strength, toughness, and resistance to environmental conditions.

On the other hand, as described in the structure section, our shuttle is made of carbon fiber. Like the Starship we could go for an entire structure made of stainless steel, however, mass reduction is a critical objective. For this reason, we choose to keep the carbon

composite structure and add Inox 310S liner on top of it to protect the carbon layer since it suffer under the high re-entry temperatures.

The added liner contains 24–26% chromium and 19–22% nickel, which allows it to form a thin protective chromium oxide layer when exposed to high temperatures in an oxidizing environment. This process, begins above 800°C and so during the re-entry, the "cold" surface temperatures (in blue, see thermal map) will approach 1110°C . Thus, the 310S liner will oxidize slowly and form a stable oxide layer which acts as a thermal barrier and increases the surface emissivity, up to 0.90. This improves radiative cooling, which helps regulate surface temperatures. We determined the emissivity of this surface based on the Wien's Law :

$$\lambda_{max} = b/T \quad (154)$$

With :

- λ_{max} (m): peak wavelength of radiative emission
- $b = 2,8989.10^{-6}$ (m/K)
- T : Temperature (K)

We computed it with a worst-case surface temperature of 1672 K, and obtained $\lambda_{max} = 1730$ nm. This allows us to determine the emissivity (0.90) using the result of the study : *Pyrometric Method for Measuring Emittances at High Temperatures* by J. Ballestrí, J. Rodríguez , M. E. Carra1 , I. Cañadas , M. I. Roldan , J. Barbero and A. Marzo.

We resume our material choices in the table below :

Structure	Carbon T700 & Inox 310S
Insulator & tiles	TUFI (Toughened Uni-piece Fibrous Insulation)

Table 105: TPS materials used on our shuttle StarCheap

Step 4: Mechanical Loads Estimation

The TPS must not only withstand intense heat fluxes but also endure significant mechanical loads during atmospheric re-entry. These mechanical loads arise mainly from three sources: aerodynamic forces, pressure gradients, and vibrations. Understanding and estimating these loads is essential to inform the geometry and placement of heat shield tiles (as discussed in Step 5).

1. Aerodynamic Forces

The shuttle experiences high-speed flow during re-entry, generating dynamic pressure and shear forces on the surface. The aerodynamic pressure is given by the standard formula:

$$q = \frac{1}{2}\rho V^2 \quad (155)$$

Where:

- q : dynamic pressure (Pa)
- ρ : atmospheric density (kg/m^3)
- V : velocity of the shuttle (m/s)

2. Pressure Gradients

As the vehicle transitions from high altitudes to denser atmospheric layers, pressure gradients appear across the surface, especially between the stagnation point and the sides. These gradients cause differential mechanical loads between adjacent tiles. An approximation of the pressure differential over a distance L is (Bertin [1994]):

$$\Delta P \approx \frac{dq}{dx} \cdot L \quad (156)$$

- $\frac{dq}{dx}$: spatial variation of dynamic pressure (Pa/m)
- L : characteristic tile length (m)

3. Vibrational Loads

Re-entry generates significant vibrations due to turbulent unsteady flow and vehicle oscillations. These loads act on the tiles and can be approximated by (European Cooperation for Space Standardization [2010]):

$$F_{\text{vib}} = m_{\text{tile}} \cdot a_{\text{RMS}} \quad (157)$$

- F_{vib} : vibrational force on a tile (N)
- m_{tile} : tile mass (kg)
- a_{RMS} : root-mean-square acceleration (in m/s^2)

For the StarCheap, we consider a conservative estimate of $3g$ for the vibrational acceleration:

$$a_{\text{RMS}} = 3g = 3 \times 9.81 \text{m}/\text{s}^2 = 29.43 \text{m}/\text{s}^2$$

Estimated Mechanical Loads Table

Based on our re-entry conditions (altitude ~ 80 km, velocity ~ 7300 m/s, density $3.67 \times 10^{-5} \text{kg}/\text{m}^3$), we compute the following values:

Mechanical Constraint	Input Values (Assumptions)	Estimated Load
Dynamic Pressure	$\rho = 3.67 \times 10^{-5}$, $V = 7300$	$\sim 9770 \text{Pa}$
Pressure Gradient	$\frac{dq}{dx} \approx 1000 \text{Pa}/\text{m}$, $L = 0.2$	$\sim 200 \text{Pa}$
Vibrational Load	$m = 0.5 \text{kg}$, $a = 29.43 \text{m}/\text{s}^2$	$\sim 14.7 \text{N}$

Table 106: Estimated mechanical loads on TPS tiles during atmospheric re-entry

These mechanical loads will directly influence the tile design, which is discussed in the next step. In particular, they constrain the allowable tile size, bonding strategy, and placement scheme. Each tile must be sized to avoid failure under these loads, especially in the high-stress regions such as the nose.

Step 5: Tile Geometry Design

Once thermal and mechanical constraints are estimated, the geometry of the heat shield tiles must be defined. Our objective is to define a tile geometry that ensures tight and continuous surface coverage in order to prevent hot gas infiltration during re-entry. Additionally, manufacturability and ease of integration onto the shuttle's structure must be considered to facilitate production and maintenance.

Adoption of Hexagonal Tiles

Inspired by the SpaceX Starship design, we propose to use hexagonal tiles for the main heat shield of StarCheap. Unlike traditional rectangular or square tiles, hexagonal tiles present several key advantages:

- **Minimized gas leakage paths:** Rectangular tiles create linear seams that can act as channels for hot gas. In contrast, hexagonal tiles interlock more efficiently and reduce long continuous gaps, improving thermal sealing and protection.
- **Redundancy in load paths:** Each hexagon shares edges with six neighbors (versus four in square tiling), enabling more isotropic stress distribution and limiting the impact of a failed tile.
- **Improved alignment with curved surfaces:** Hexagons fits better on the complex curved geometries of a shuttle body compared to rectangular tiles.

Applicability to the StarCheap

Given our thermal and mechanical conditions ($\text{isoflux} \sim 3.33 \cdot 10^5 \text{W/m}^2$ and estimated dynamic pressure $\sim 9770 \text{Pa}$), we observe that our shuttle operates in a similar range to the Starship, as shown in Table 102. Therefore, the hexagonal tile approach is transferable. Since our TPS design relies on a homogeneous isoflux-based approach rather than a localized tile assignment strategy (as in the NASA Shuttle), a uniform tiling scheme is more relevant.

Based on the Starship design and our structural interface, we adopt a tile length of approximately 20 to 30 cm with interlocking hexagonal geometry.

The final design will still require optimization in terms of thickness and mass, but the hexagonal layout represents a robust and proven baseline for our reusable shuttle concept.

Step 6 : TPS repartion on the shuttle

Normally, engineers use advanced tools like Computational Fluid Dynamics (CFD) to calculate the heat and aerodynamic fluxes on the surface of the vehicle. This helps to

create a detailed thermal map of the spacecraft and identify the hot and cold zones.

However, following our pre-design approach, we do not run simulations, but instead rely on existing studies and past flight data to estimate the heat exposure. We make simple assumptions to choose the materials and place them correctly on the spacecraft.

Here, our goal is to define the TPS materials repartition along our shuttle. Using data from the Starship and the NASA's space shuttle. We make a rough approximation on the cold and heat points of our shuttle during it re-entry. We try to represent the difference of exposure during it re-entry to justify the heat shield architecture. Following the drawing below, we identify in red the hottest area, in orange hot areas and in blue "cold" areas. The colors are here to express the need of protection during this phase.

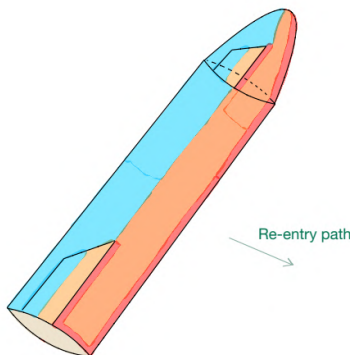


Figure 110: Thermal map of the StarCheap during it re-entry

Having this in mind, we can assigned our TPS materials to the different areas of our shuttle. This is resume in the table below.

layer	Area	Material
1st layer	Structure	Carbon T700 & Inox 310S
2nd layer	Flaps leading edge	RCC (Reinforced Carbon–Carbon)
	Belly	TUF Hexagonal ceramic tiles
	Top	NA - see section passive thermal control

Table 107: TPS materials repartition our shuttle StarCheap

The 1st layer is the structure of our shuttle. The TPS come on top of it with the 2nd layer. This layer consist of the TUF hexagonal tiles and are only applied on the belly, since it is the most exposed part, they resist to temperature up to 1870° (in single use). In addition, the flaps leading edges will also be exposed during the re-entry. We cannot apply the same tiles as in the belly of our shuttle, their are to rigid and could hinder the flaps in their movement. Thus, we use the same material as in the NASA's space shuttle to protect the particulary exposed leading edges of the wings, we use RCC. Finally, the top part of the shuttle isn't concern with a TPS 2nd layer, it material will be detailed in the next section.

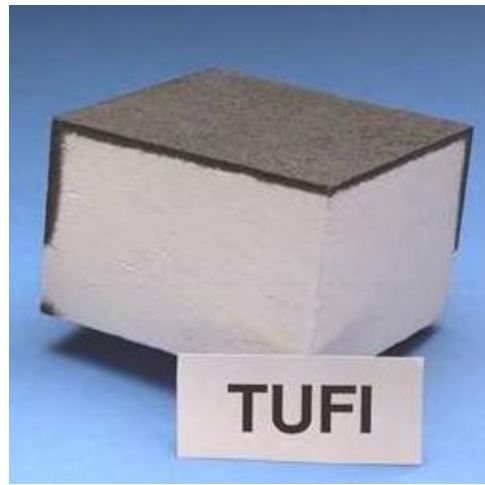


Figure 111: Picture of the TUFI material

10.2.3 Feasability & limits

The pre-design methodology presented allows for a first-order estimation of the heat shield requirements and configuration for our shuttle. By focusing on an isoflux-based approach and drawing from state-of-the-art systems such as the Space Shuttle and SpaceX Starship, we can define a feasible thermal protection system (TPS) within realistic constraints. However, several assumptions and simplifications inherent to this preliminary approach introduce limitations that must be acknowledged.

Feasibility

Our approach is feasible for early-phase design and comparison purposes:

- The estimated isoflux value ($3.33 \times 10^5 \text{ W/m}^2$) is consistent with values observed in comparable vehicles such as Starship, reinforcing the validity of our input parameters.
- Material choices are aligned with current standards, using a combination of ceramic tiles, insulating layers, and structural metals.
- The design of tile geometry and placement strategy is inspired by successful configurations, such as the hexagonal ceramic tiles of Starship, known for their effectiveness in minimizing hot gas leakage and mechanical stress.

Moreover, we have focused the heat shield design on the most critical phase of re-entry (the high-speed atmospheric flight) where convective heating is dominant and thermal constraints peak. This suppose that the TPS is robust under the most extreme conditions it will encounter.

Limitations and Assumptions

Despite its practicality, our methodology comes with limitations inherent to its simplified nature:

- **Absence of proper re-entry trajectory** Facing difficulties, no re-entry trajectory has been computed for our shuttle. Instead, a simplified trajectory profile was obtained from external literature sources in order to estimate the thermal dimensioning point. This approach allowed us to define a representative worst-case scenario for sizing the thermal protection system (TPS), but it does not reflect the exact flight conditions that our shuttle would experience. Future work should include a proper re-entry trajectory analysis to improve the accuracy of the TPS design and confirm the critical heating point.
- **Neglect of aerodynamic and structural interactions:** The mechanical loads and thermal environment are treated separately, whereas in reality, aerodynamic forces (especially during belly-flop and hover phases) interact with thermal stresses and can induce material fatigue or failure. A full CFD coupled with thermal-structural analysis would be required to fully capture these interactions.
- **Simplified isoflux estimation:** The isoflux was calculated using a fixed reference point and does not account for variations across different parts of the vehicle, especially high-gradient areas such as flap edges, where the radius of curvature is smaller and thus local heat fluxes are higher. Although our estimate falls within the right order of magnitude (validated against literature), it likely underestimates peak local heating.
- **No active cooling system considered:** Our design assumes only passive thermal protection. While this simplifies design and reduces mass, it limits reusability and may be insufficient for repeated high-load missions without maintenance. We could implement a thermal fluid cooling system under the TPS.
- **Material degradation and aging:** The docking phase due to its long duration may degrade TPS materials due to space radiation, micrometeoroid impacts, and atomic oxygen exposure. This has to be taken into account in the choosing material and maintenance plan during the docking phase.
- **Fatigue and reuse considerations:** The heat shield must endure thermal cycling across multiple re-entries. No fatigue analysis is performed, and material aging under cyclic thermal stress remains to be investigated.
- **Mechanical load estimation uncertainty:** The mechanical constraints (dynamic pressure, pressure gradients, and vibrational loads) are estimated using simplified assumptions. These do not guarantee identification of the worst-case scenario, particularly in critical zones such as the nose or flap edges. A high-fidelity structural analysis would be required to assess peak loads and failure risks.

Finally, this pre-design approach is suitable for early conceptual studies and provides a solid foundation to iterate from. It helps identify key drivers—such as isoflux thresholds, material capabilities, and tile geometry—that influence the final heat shield configuration. However, the assumptions made limit the precision and robustness of the results.

10.3 Shuttle thermal exposure in orbit

StarCheap will be exposed to four different environments :

- From launch to the station ASTROIKOS
- Station's circular orbit during the docked phase with an altitude of 500km and an inclination of 50°.
- Orbit debris removal which can go up to an altitude of 1100 km and varies with an inclination of $\pm 10^\circ$.
- From orbit to re-entry

Following the mission analysis, our shuttle will spend most of the time on the orbit station with the 5 months docking phase. In fact, the other phases only last few hours to 3 days, thus they will not be considered in this thermal pre-design. At the station's altitude, our shuttle will be exposed to a wide range of thermal temperatures. Since the periods is approximately 90 minutes, we have frequent transitions between sunlight and eclipse phases. These repeated thermal cycles cause alternative heating and cooling of the shuttle surfaces and thus threaten the shuttle integrity.

In addition to the heat fluxes receives from Earth's infrared emission and albedo, the shuttle is also exposed to solar radiation. In sunlight the surface can heat a lot, while during eclipse, the shuttle is shadowed from the Sun and the surfaces can cool down to very low temperatures. This thermal variations need to be take in to account for temperature-sensitive systems and, thus requires proper thermal control.

As explained in 3.3, the spacecraft is subject to atomic oxygen erosion, UV radiation, and thermal fatigue due to repeated expansion and contraction. These effects can degrade external materials and coatings over time and must be considered when selecting thermal protection solutions.

10.4 Thermal budget

This table summarizes the thermal operating ranges required by critical component of the shuttle. Each element must remain within the defined temperature range to ensure its proper functioning and reliability during the mission. This thermal budget is essential for the design of both active and passive thermal control systems. Thermal protection must be designed to avoid overheating sensitive electronics or equipement and to prevent freezing of critical fluids like water or propellants. We must note that we applied a $\pm 10^\circ$ margin on non-fixed temperature element, thus we obtained the table below.

Component	Subsystem	Ope. Range	Notes
Hydrogen Tank	Power	20°C	To maintain hydrogen pressure
Fuel Cell (PEMFC)	Power	70–80°C	Fuel cell operating range
Battery (Li-Ion)	Power	20°C	Avoid degradation & performance losses
Propellant Tank	Propulsion	10–60°C	Maintain usability of the propellant
Helium Tank (He)	Propulsion	10–60°C	Maintain helium gas stability
Waste Liquid Tank	ECLSS	10–60°C	To avoid freezing/boiling
Trash Tank	ECLSS	10–60°C	To avoid freezing/boiling
Waste Solid Tank	ECLSS	10–60°C	To avoid freezing/boiling
Water Tank	ECLSS	~20°C	Water distribution efficiency
Consumable Storage	ECLSS	20°C	Maitain at ambient temperature Food/Water/Medical items
N ₂ Tank	ECLSS	75°C	Maintain defined pressure by fixing temperature
Cabin	ECLSS	20°C	Crew thermal comfort and equipment stability
Oxygen Tank (O ₂)	ECLSS	20°C	Storage at stable temperature
N ₂ Tank (atmosphere)	ECLSS	20°C	Maintain tank pressure
Transceiver Ka	Comms	-20°C to +50°C	Ensure communication equipment remains operational

Table 108: Thermal Operating Ranges of StraCheap critical component

10.5 Passive Thermal Control System (PTCS)

The Passive Thermal Control System (PTCS) ensure the proper functioning and safety of the spacecraft by maintaining all components and areas within acceptable temperature ranges. In the space environment, where heat cannot be removed by convection, the spacecraft must rely mainly on radiation to reject excess heat and preserve thermal balance. The PTCS does not use mechanical or powered components to regulate temperature. Instead, it relies on the cleaver selection of surface coatings, with appropriate thermal properties, insulation, and the strategic placement of radiative surfaces.

10.5.1 Systema Analysis : Thermal context

We use Systema, a thermal analysis software developed by Airbus. Systema allows us to simulate the space environment, compute incoming heat fluxes (solar, Earth infrared, albedo), and analyze the thermal behavior of the shuttle in orbit.

The docked phase is the most dimensioning phase, thus we use this configuration for our study. The orbit is defined at an altitude of 500 km with an inclination of 50°. Additionally, we conduct the study for the worst cold case and the worst hot case associated.

Modelisation and mission definition

We start by designing our shuttle on Systema by reducing it to a simple model made of

a two half cylinder, two half cones and a disk, to follow the material repartitions as seen in table 107. We then apply the FEM on our model and obtained the node detailed in the table below.

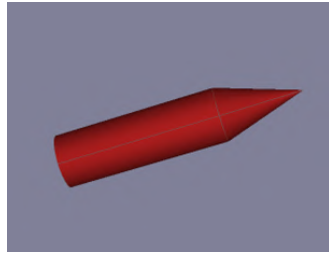


Figure 112: Systema modelisation of StarCheap

Node	Associated area
100	Top body (<i>facing deep space</i>)
200	Bottom body (<i>facing Earth</i>)
300	Bottom nose (<i>facing Earth</i>)
400	Top nose (<i>facing deep space</i>)
500	Bottom of the shuttle
9999	Deep space node

Table 109: Node association

Then, we defined the mission by adding the orbit trajectory and select the winter solstice for the hot and cold case, giving us 16 eclipse for a one day simulation.

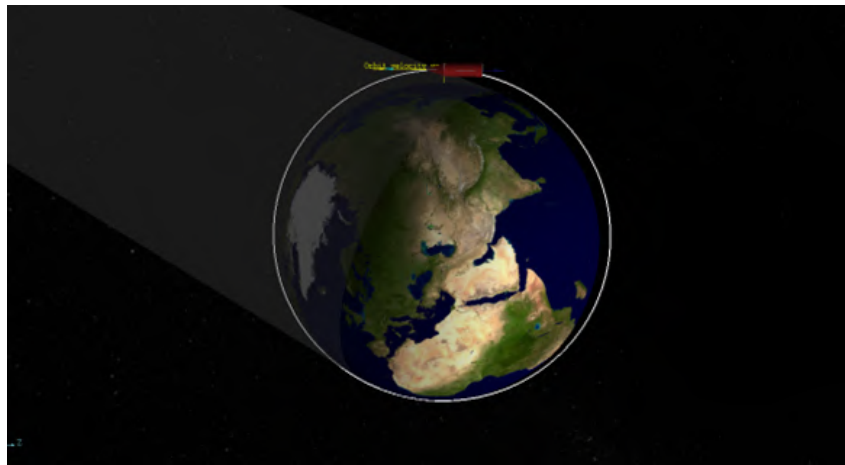


Figure 113: Trajectory definition on Systema

Having this define, we study our shuttle thermal behaviour under the worst hot and cold case.

Worst Hot case definition

The worst hot case occurs when the spacecraft receives the maximum thermal fluxes from its environment. To simulate the shuttle environment, we fix an albedo of 35% with an Earth's temperature of -9°C, and compute the solar and IR flux using Systema. For this case, we obtained the fluxes below.

Parameter	Value
Earth temperature	-9°C
Earth albedo	0.35
Node & Albedo flux	
100	93 W/m ²
200	4363 W/m ²
300	1096 W/m ²
400	247 W/m ²
500	297 W/m ²
Node & Solar flux	
100	2738 W/m ²
200	6845 W/m ²
300	458 W/m ²
400	774 W/m ²
500	3189 W/m ²
Node & IR flux	
100	319 W/m ²
200	2730 W/m ²
300	685 W/m ²
400	836 W/m ²
500	174 W/m ²

Table 110: Worst hot case Conditions

Worst Cold case definition

The worst cold case occurs when the shuttle receives minimal thermal fluxes. Here, we fixed an albedo of 0.15 and a temperature of -29°C to simulate this case.

Parameter	Value
Earth temperature	-29°C
Earth albedo	0.15
Node & Albedo flux	
100	402 W/m ²
200	1870 W/m ²
300	469 W/m ²
400	106 W/m ²
500	127 W/m ²
Node & Solar flux	
100	2738 W/m ²
200	6845 W/m ²
300	458 W/m ²
400	774 W/m ²
500	3189 W/m ²
Node & IR flux	
100	233 W/m ²
200	1992 W/m ²
300	500 W/m ²
400	611 W/m ²
500	127 W/m ²

Table 111: Worst hot case Conditions

With both worst case defined, we can run simulation to choose the correct materials, coatings, insulation, and radiators to build a reliable Passive Thermal Control System. This first step will reduce the temperature ranges but we will need to add active thermal control to have a well regulated system.

10.5.2 System analysis results

Following the table 107, we start with a first simulation without any additional coating in order to have an initial reference. The picture below represent the material repartition as a function of the emissivity of the applied material.

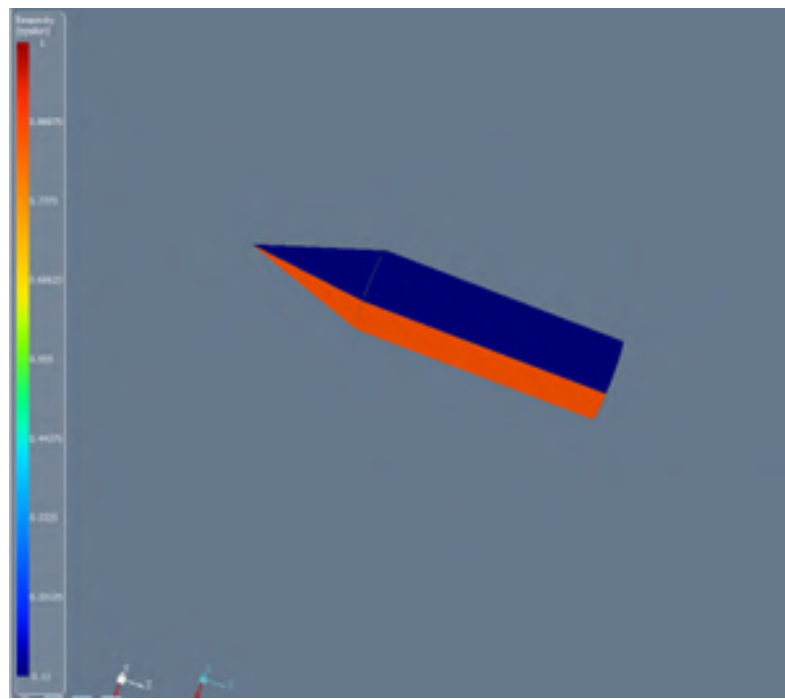


Figure 114: Emissivity representation of StarCheap without any coatings

Using this configuration, we computed the receive temperatures by each node of the shuttle. We obtained the graph below and clearly see that we have huge surface's temperature differences during each eclipse and sunlight exposure. We have a mean temperature range of **168,4°C** for the hot case and **172,8°C** for the cold case

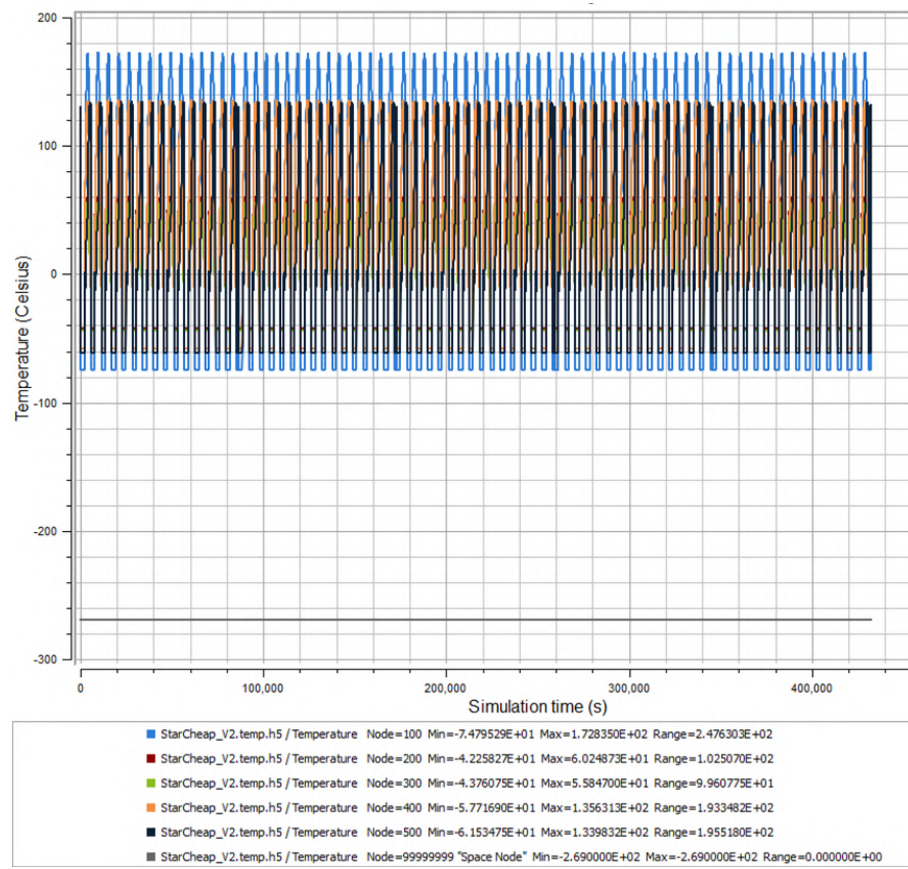


Figure 115: StarCheap's surface temperature with initial material - Hot case

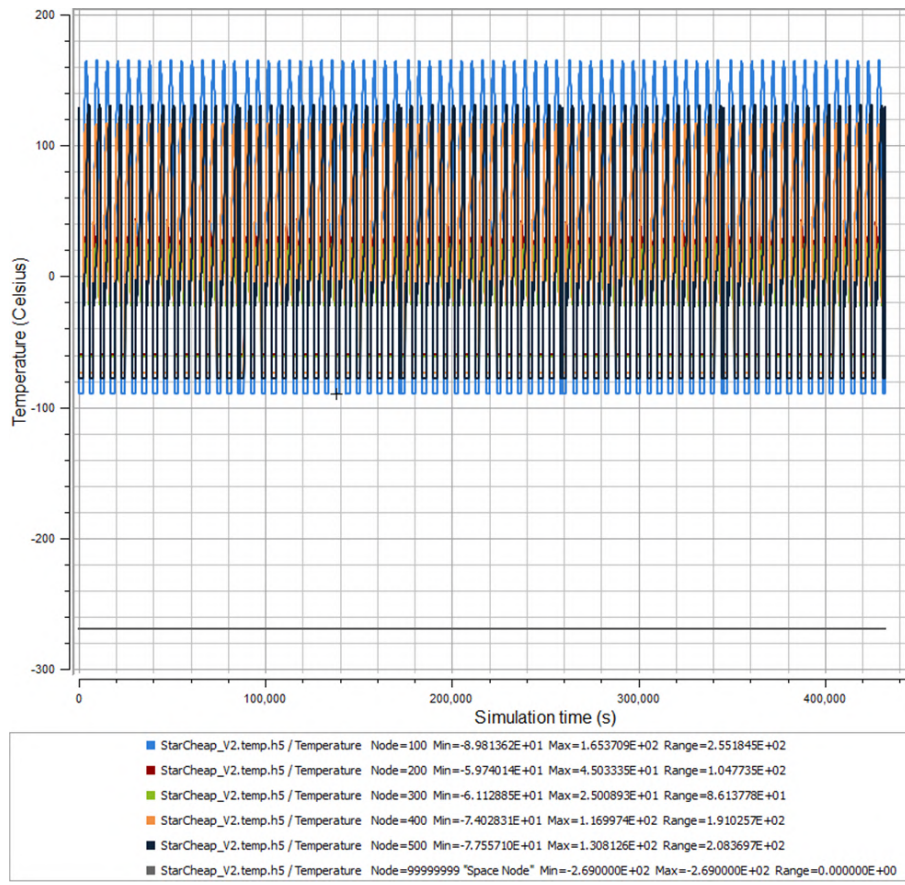


Figure 116: StarCheap's surface temperature with initial material - Cold case

We resume the inputs and results of our simulation in the following table.

Area	Node	Material	ϵ	α	Hot Case (°C)	Cold Case (°C)
Top Cylinder	100	Inox 310S	0.11	0.42	-74 to 173	-90 to 165
Bottom Cylinder	200	TUFI	0.873	NA	-42 to 60	-80 to 45
Bottom Cylinder	300	TUFI	0.873	NA	-44 to 59	-61 to 25
Top Nose	400	Inox 310S	0.11	0.42	-58 to 136	-74 to 116
Bottom	500	Alu-Li	0.10	0.20	-62 to 134	-77 to 131

Table 112: Temperature Ranges for Worst Hot and Cold Cases

These huge temperature ranges demonstrate the importance of implementing thermal control to avoid too many temperature gaps between successive thermal cycles along the orbit. Thus, thermal control is necessary for maintaining our shuttle and its components during its mission. In order to mitigate these differences, we apply several coatings on each node and evaluate the efficiency regarding the mission.

10.5.3 Final coatings choices

We based our coating choices on :

- The need to get colder. We are at 168.4°C in hot case and 172.8°C in cold case while we have a mean temperature operating range of 31.6°C (see thermal budget 108).

- The need to protect the heat shield tiles (TUF) against thermal cycling during the docked phase. Also from an environment point of view, we must protect the tiles from the UV and radiations (see 3.3).
- The need to protect the bottom part as it is close to the propulsion system.
- The need to reduce the temperature gaps in hot and cold cases. A temperature gap of $\pm 100^{\circ}\text{C}$ would be acceptable. If we want an efficient thermal conception, a temperature gap of $\pm 80^{\circ}\text{C}$ would be much better.

Top parts coating

For the top-facing surfaces, we choose the GSFC White Paint NS-74. This coating offers a high emissivity ($\epsilon = 0.92$) and a very low absorptivity ($\alpha = 0.17$), making it ideal for rejecting heat while minimizing solar gain. It was chosen specifically to help lower the overall temperature of these areas. Its reflective properties contribute to reducing the average and peak surface temperatures (up to 165°C , see table 112).

TUF coatings

We chose to use a silicate-based ceramic glaze similar to those used in NASA's Space Shuttle . These coatings:

- Increase the emissivity of the tiles and thus the heat rejection capacity
- Reduce fatigue from thermal cycling
- Protect against UV radiation and charged particles in orbit.

They are typically made of SiO (60–70%), AlO (15%), and LiO or MgO/ZnO/TiO for crystallization control. (see AZoM [2014])

Bottom part coating

For the bottom part of our shuttle, we choose to use the Thermal Barrier Coating (TBC). It is composed of multilayers with a metallic bond coat and a ceramic top coat (typically Yttria-Stabilized Zirconia - YSZ) (Nicholls and Duffy [2003]). This coating structure offer intersting properties (see Padture et al. [2002]) :

- can resist high thermal fluxes from propulsion systems
- Reduce temperature gradients and protect structural components
- Remain stable under prolonged high-temperature exposure

After implementing the defined coatings, we obtained the result below:

Area	Node	Material	ϵ	α	Hot case(°C)	Cold case(°C)
Top Cylinder	100	GSFC White P. NS-74	0.92	0.17	-93 to -13	-106 to -29
Bot. Cylinder	200	Silicate Coating	0.85	0.85	-55 to 26	-71 to 20
Bottom Nose	300	Silicate Coating	0.85	0.85	-53 to 11	-70 to -21
Top Nose	400	GSFC White P. NS-74	0.92	0.17	-70 to -17	-85 to -35
Bottom	500	TBC	0.75	0.80	-77 to 77	-92 to 74

Table 113: Temperature Ranges for Worst Hot and Cold Cases with coatings

For a better interpretation, we sum the temperatures gaps between the eclipse and the sunlight exposure for each case (see table below).

Area	Hot case(°C)	Without coating	Cold case(°C)	Without coating
Top Cylinder	± 80	± 247	± 77	± 255
Bot. Cylinder	± 81	± 102	± 91	± 125
Bottom Nose	± 42	± 103	± 49	± 86
Top Nose	± 53	± 194	± 50	± 190
Bottom	± 154	± 196	± 166	± 208

Table 114: Comparison of the temperatures ranges between the hot and cold cases with and without coatings

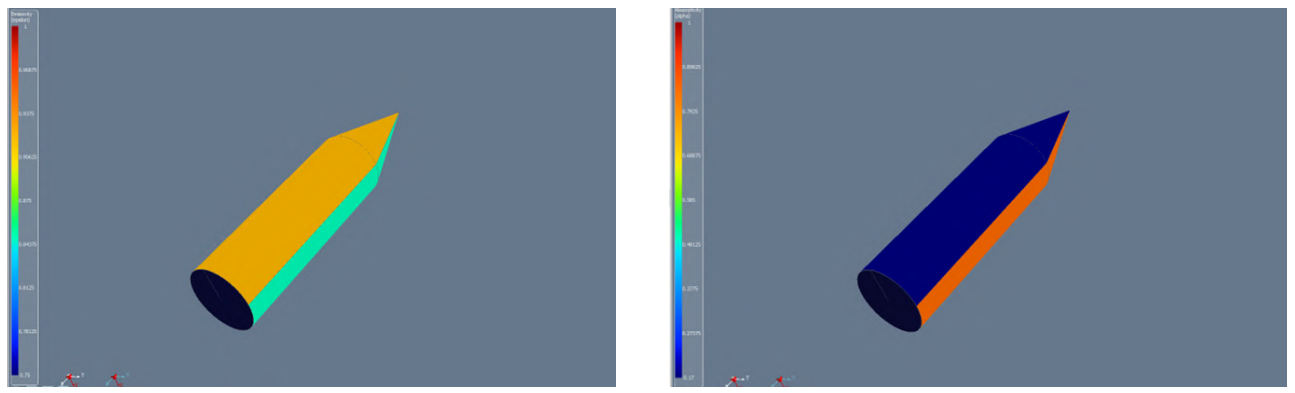
We note net improvement after applying the thermal coatings, when compared to the uncoated case. First, the top-facing surfaces (top cylinder and top nose) show a significant reduction in temperature range, thanks to the white paint (GSFC NS-74), which reflects most of the incoming solar radiation.

Secondly, the bottom cylinder and nose, facing toward Earth, display narrow temperature gaps across hot and cold cases. These materials help reduce thermal fatigue and maintain thermal stability throughout the docked phase where thermal cycling is critical.

Finally, The bottom area, which is the most exposed to propulsion heating, shows the largest temperature gap. However, even here, the TBC coating has reduced the temperatures ranges compared to the uncoated case : from 208°C to 166°C in hot case. However, it is not enough to meet the previous established requirement of $\pm 100^\circ\text{C}$. Futher studies need to be conducted to either find a better coating choice or implement a strong active thermal control.

The application of thermal coatings on the shuttle has effectively reduced the thermal amplitudes in both worst-case scenarios. For almost each areas, we ended up to meet and exceed the $\pm 100^\circ\text{C}$ requirement as it is the case for the nose, with only a 49°C range while we started at a 208°C range. This confirms the importance of tailoring the coatings to each zone based on exposure and functional needs.

The picture below present the final coating repartition on our shuttle as a function of the emissivity and the absorption.



(a) As a function of the emissivity

(b) As a function of the absorbtion

Figure 117: Final coating repartition

10.6 Active Thermal Control System (ATCS)

10.6.1 Active Thermal Control requierments

While the implemented passive thermal control reduces temperature fluctuations and limits excessive heat absorption, it is often not sufficient to ensure proper operating ranges for the component listed in the thermal budget (see 108). For this reason, we design an Active Thermal Control System (ATCS) to dynamically complete the passive control.

To maximize the effiency and mass of the thermal active control, we must gatter the equipement with a similar operating range together. The picture below describe the different temperature areas based on the thermal budget (108. We must note that this is a non scale schematic. However, having the dimensions of equipement, we ensured that they all fit in the same area. Proper design and placement need to be conduct in order to propose an efficient design while taking in account the thermal requirements.

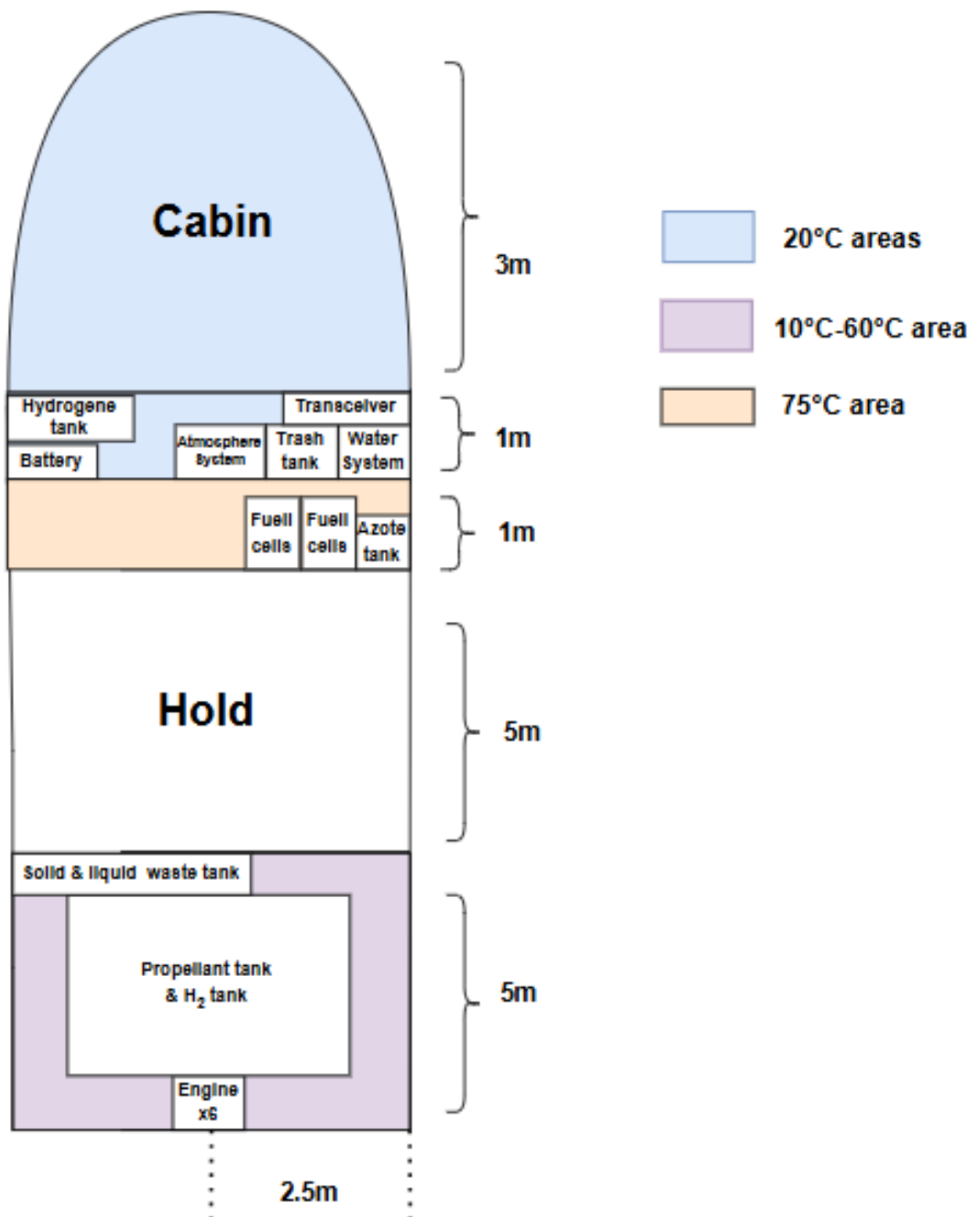


Figure 118: Schematic of the different temperature areas and the associated equipment

Crossing the data with the passive thermal control, we obtained the table below, which sum up the required temperature versus the surface temperatures.

Temperature required (°C)	Hot case (°C)	Cold case (°C)
Blue area		
20	-70 to -17	-85 to -35
20	-53 to 11	-70 to -21
Violet area		
10-60	-55 to 26	-71 to 20
10-60	-93 to -13	-106 to -29
Orange area		
75	-55 to 26	-71 to 20
75	-77 to 77	-92 to 74
75	-93 to -13	-106 to -29

Table 115: Comparison of the inside and the surface temperatures

Blue Area

Components in this area, such as the cabin or atmospheric control tanks, must be maintained at around 20°C. However, the observed surface temperatures are between -70°C and -17°C in the hot case and drop further in the cold case. These values show that passive control is insufficient, and active heating is mandatory. The issue becomes even more critical during eclipses, when sunlight is blocked for long durations, leading to deeper cooling.

Violet Area

These systems must operate between 10°C and 60°C. The surface temperatures fall far below these limits in both thermal cases, especially in the cold case (down to -106°C). Without active heating, the propellant could freeze, leading to mission failure. Therefore, thermal regulation is essential, including heaters and thermal sensors.

Orange Area

Subsystems like pressurized nitrogen tanks require 75°C to maintain proper pressure. However, even in the hot case, external surfaces are well below that target. In this situation, both active heating and insulation are needed to reach the required internal temperature.

10.6.2 Active Thermal Control equipments

Based on the temperature gaps observed in both hot and cold cases, different active thermal control strategies must be implemented for each zone. These strategies aim to maintain the equipment within their operating temperature ranges.

Blue Area : 20°C

- Electrical heaters must be placed inside the cabin walls and gas tanks to maintain a stable internal temperature.

- To ensure even distribution of heat from local sources (e.g., electronics), heat pipes are recommended. Their passive operation makes them reliable and energy efficient Agency [2019].
- To have a dynamic heating system, we must add temperature sensors to activate heaters if needed.

Violet Area : 10°C to 60°C

- Mechanical Pumped Fluid Loops can be implemented, they can transfer heat from warmer zones (e.g., fuel cells or batteries) to the tanks, using ammonia or Freon-based coolants Center [2017].
- Add Multilayer Insulation (MLI) to reduces heat loss and prevents rapid cooling during eclipses.

Orange Area : 75°C

- Again, heaters must be used to actively raise and maintain internal temperatures. We could also MLI for insulation purpose and avoiding using too much the heating system.
- Also, we must add thermal sensors to constantly monitor tank temperature and trigger heating only when needed, improving energy efficiency.

Each area presents different thermal challenges. The blue area requires moderate heating and efficient distribution, the violet area needs strong and reliable thermal protection to prevent freezing, and the orange area demands constant high temperatures. The combination of heaters, heat pipes, fluid loops, and smart control systems can ensures that all subsystems remain operational within their thermal constraints.

10.6.3 Feasibility and Limitations of the ATCS

Managing the thermal environment of the shuttle is a challenging task, especially in low Earth orbit (LEO) conditions. In our case, the spacecraft undergoes up to 16 eclipse periods per day, each lasting approximately 34 minutes. These regular transitions between sunlight and shadow create strong thermal cycling and require an efficient thermal control strategy. The combination of passive thermal coatings and active thermal control (ATCS) solutions such as fluid loops, radiators, and heat pipes can mitigate these effects and help maintain components within acceptable temperature ranges.

Our simulations with applied coatings already show a significant reduction in temperature fluctuations across key structural nodes. With additional ATCS components, the temperature can be more tightly regulated, especially for sensitive areas like tanks and electronics.

However, several limitations reduce the precision and reliability of our thermal pre-design. One of the major limitations is the absence of a complete Systema analysis. Without it, we cannot fully evaluate the capacity of the thermal system to handle all heat loads under varying orbital conditions.

Additionally, we do not have reliable data regarding the amount of heat dissipated by the various onboard components (fuel cells, electronics, tanks, etc.) and not the exact locations where these dissipations occur. This missing information prevents us from properly sizing the active thermal control system and estimating the real heat rejection capabilities of the shuttle.

Moreover, although we have divided the thermal control system into three main area, this approach remains a high-level simplification. It was guided by the current limited number of components and known constraints. In a reality, the thermal system would need to handle a much more complex distribution of hardware, varying heat loads, and structural interfaces. Each subsystem may impose its own requirements, including strict temperature tolerances, redundancy needs, and specific time responses to orbital transitions.

Therefore, our proposed solutions are technically viable, their implementation requires further detailed analysis to ensure proper sizing, redundancy, and integration of thermal hardware.

11 Docking

11.1 Introduction

The docking system [Aeronautics and Administration [2010]] relies on a process involving two essential stages: soft capture and hard capture. During the rendezvous phase, the active vehicle, StarCheap, uses targets provided by the passive vehicle, the station, to align precisely. Soft capture, performed by the Soft Capture System (SCS), is the first stage of docking. It stabilizes the vehicles and corrects initial misalignments using guide petals and mechanical latches.

Once the vehicles are aligned and stabilized, the Hard Capture System (HCS) takes over to ensure structural connection and interface sealing. The HCS uses active and passive hooks to provide a secure link, enabling the transfer of crew and cargo. The docking interface is designed to be androgynous, meaning it can mate with an identical interface, offering great operational flexibility.

11.2 Requirement

In the development of our StarCheap space shuttle, the design of the docking system relies on three essential categories of requirements: the functional requirements defined by the system analysis of our shuttle, the interface requirements necessary for interactions within the System of Systems (SoS) with the second space shuttle and the Space Station, as well as the requirements imposed by the International Docking System Standard (IDSS) Interface Definition Document.

11.2.1 System of systems Docking Requirements

The specific requirements for the Docking subsystem in context of SoS are resumed in the table below:

Requirement ID	Description
FUN-DOC-001	Shall be compatible with standards: IDSS Revision F 2022
FUN-DOC-002	Shall be able to comply with approach sequences.
FUN-DOC-003	The docking system shall operate autonomously with astronauts monitoring operations.
FUN-DOC-004	Shall communicate for status of approach.
FUN-DOC-005	Shall communicate for state on approach.
FUN-DOC-006	Shall comply with hatch opening requirements.
FUN-DOC-007	Shall comply with pressurization norms.
FUN-DOC-008	Shall comply with atmosphere leakage norms.
FUN-DOC-009	The station shall supply power to the shuttle while it is docked.
FUN-DOC-010	Shall have similar voltage.
FUN-DOC-011	Shall be electromagnetically compatible.
FUN-DOC-012	Shall function within standardized temperature range.
FUN-DOC-013	Shall process propellant refuelling.
FUN-DOC-014	Shall process O2 refuelling.
FUN-DOC-015	Shall process pressurant refuelling.
FUN-DOC-016	Shall process water refuelling.
FUN-DOC-017	Shall be able to communicate while docked.
FUN-DOC-018	Shall be compatible with linked communication protocols.

Table 116: List of Intergroup Requirements

11.2.2 Functional requirements

The specific functional requirements for the Docking subsystem are resumed in the table below:

Requirement ID	Description
Doc-REQ-001	The docking system shall include a secure locking mechanism to ensure firm attachment after docking.
Doc-REQ-002	The docking system shall operate autonomously with astronauts monitoring operations.
Doc-REQ-003	The docking system shall ensure a sealed environment to maintain atmospheric pressure.
Doc-REQ-004	The docking system shall include an airlock or hatch system for safe passage.
Doc-REQ-005	The docking system shall incorporate mechanisms to absorb minor impacts or vibrations.
Doc-REQ-006	The docking system shall be designed for reusability. [10 reuse cycles, lifetime 5 years]
Doc-REQ-007	The docking system shall include a reliable mechanism for quick undocking in emergencies.
Doc-REQ-008	The docking system shall be protected from specified environmental conditions.
Doc-REQ-009	The docking system shall incorporate fault tolerance and apply redundancy as needed.
Doc-REQ-010	The docking system shall include precise alignment systems for accurate approach.
Doc-REQ-011	The docking system shall not exceed a specified percentage of the total mass.

Table 117: List of Docking System Requirements

11.2.3 IDSS Requirements

Seals

The HCS (Show in Program [2013]) shall implement two concentric pressure seals that accommodate seal on seal mating, within (figure 126) dimensional constraints. The seal parameters are defined as below :

- DOCK-TEC-REQ-001 : Seal adhesion force $\leq 900N$ – defined as the required force to pull seals apart after being sealed together.
- DOCK-TEC-REQ-002 : Seal protrusion height in a free state above the HCS Mating Plane $\leq 2.1mm$.

Mechanisms Loads

The mechanisms shall have a given mechanical response:

- Preload of the hook system after locking, i.e., tightening load to exert a pressure on the HCS:
 - **DOCK-TEC-REQ-003:** Minimum Preload: 31,300N
 - **DOCK-TEC-REQ-004:** Maximum Preload: 44,340N
- **DOCK-TEC-REQ-005:** Design limit capability of the active and passive hook elements shall be $\leq 50,000\text{N}$.
- **DOCK-TEC-REQ-006:** The load response (stiffness) of the Active Hard Capture Hook Mechanism shall be between the following curves, (figure 119).
- **DOCK-TEC-REQ-007:** The load response of the Passive Hard Capture Mechanism shall be between the following curves, Figure (figure 120).

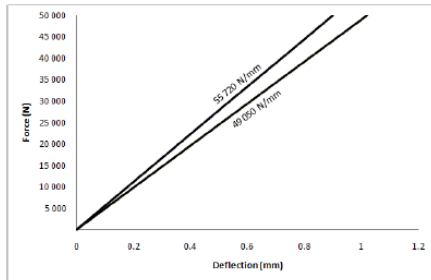


Figure 119: Load response of active hook mechanism

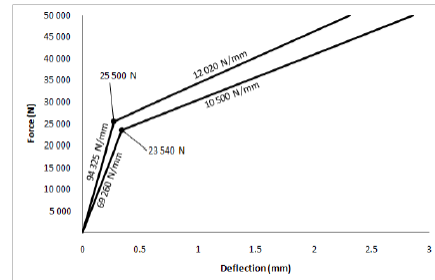


Figure 120: Load response of passive hook mechanism

Separation System

The separation system shall implement a retractable separation system that can be remotely commanded to fully retract below the interface plane without application of external forces, while providing symmetric separation force:

- **DOCK-TEC-REQ-008:** Total separation force shall be $< 2670\text{N}$ when HCS mated.
- **DOCK-TEC-REQ-009:** Total separation force shall be $\geq 1778\text{N}$ at 4.2mm above HCS Mating Plane.

Sensors Load

- **DOCK-TEC-REQ-010:** During docking or undocking phases, the resistance force that the sensors on the passive HCS system could provide shall be $\leq 85\text{N}$ for a separation $\geq 4.2\text{mm}$ between the HCS matching plates.

Electrical Bonding : SCS

- **DOCK-BOND-REQ-001:** IDSS compliant systems shall establish bond paths to mitigate electrical hazards on the integrated subsystem interfaces.

- **DOCK-BOND-REQ-002:** IDSS compliant mechanisms protect against electrostatic discharge through the soft capture system. The bond path may be through any metal-to-metal contact provisions for this purpose. The requirement is from initial contact to hard capture during the docking operation.
- **DOCK-TEC-REQ-011:** Bonding resistance for the SCS after soft capture shall be 1Ω or less.

Electrical Bonding : HCS

IDSS compliant mechanisms are to be protected against RF emissions. The bond path is through metal-to-metal contact on the seal interface between two IDSS compliant HCS mechanisms.

- **DOCK-TEC-REQ-012:** Bonding resistance for the HCS after latching shall be 2.5 milliohms or less.

Mechanical Bonding

Materials used in the construction of the docking interface shall allow proper mating while experiencing the following conditions:

- **DOCK-BOND-REQ-003:** Temperature difference between the two mating interfaces of up to 55°C .

Environment

Materials used in the construction of the docking interface shall allow proper mating while experiencing the following conditions:

- **DOCK-BOND-REQ-004:** External pressure environment $< 1.0 \times 10^{-4} \text{ Pa}$.

Contact Conditions

- **DOCK-AOCS-REQ-001:** The closing axial rate shall be limited to $0.1 \text{ m} \cdot \text{s}^{-1}$.
- **DOCK-AOCS-REQ-002:** The lateral radial rate shall be limited to $0.04 \text{ m} \cdot \text{s}^{-1}$.
- **DOCK-AOCS-REQ-003:** The pitch/yaw rate shall be limited to $0.2^\circ \cdot \text{s}^{-1}$ (vectorial sum of pitch/yaw rates).
- **DOCK-AOCS-REQ-004:** The roll rate shall be limited to $0.2^\circ \cdot \text{s}^{-1}$.
- **DOCK-AOCS-REQ-005:** The lateral radial misalignment shall be limited to 0.1 m.
- **DOCK-AOCS-REQ-006:** The pitch/yaw misalignment shall be limited to 4° (vectorial sum of pitch/yaw rates).
- **DOCK-AOCS-REQ-007:** The roll misalignment shall be limited to 4° .

11.3 Docking phases

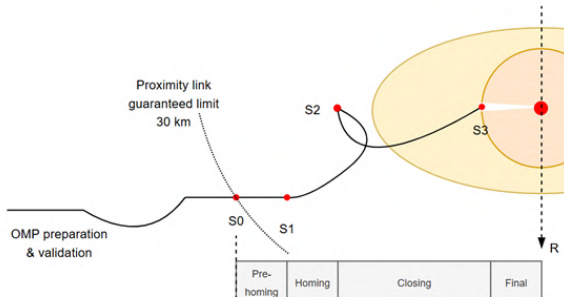


Figure 121: The series of orbital manoeuvres (OMP : On board Mission Plan)

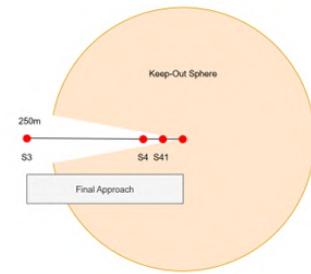


Figure 122: The final approach from point S3

11.3.1 Description :

This procedure offers a comprehensive description of the docking and undocking processes between the station and our shuttle StarCheap. It highlights the approach phases and specifies the requirements for the final rendezvous and undocking stages. The docking port facilitates electrical and data connections, fluidic interfaces for refueling, and mechanical docking of the interfaces. The procedure begins when the interface signals its intention to dock, just before the start of their phasing. It concludes when the interface initiates its departure burn.

The approach ellipsoid (AE) is a 4km by 2km ellipsoid centered at the station's center of mass. The Keep-out Sphere is a safety sphere with a 300m radius, also centered around the station's center of mass. The white corridor consists of two cones: 8° for distances between 200m and 20m, and 4° for distances less than 20m.

11.3.2 Phasing and pre-homing :

During this sequence, the interface must execute multiple phasing manoeuvres and orbit adjustments to increase its altitude and align with the station for rendezvous. The phasing should be completed within one orbit, culminating at point S0, which is 30 km from the station. The transition from S0 to S1 marks the pre-homing phase, lasting approximately 360 minutes. S1 is positioned 20 km behind the Station. At this stage, the interface must perform proximity link acquisition and homing manoeuvre calculations. Ground control must verify the GNC parameters, and both the interface and the Ground Station must approve the homing procedure.

11.3.3 Homing :

The homing phase initiates the rendezvous, transitioning from S1 to S2, which is located 3.5 km behind the station at the same altitude. This phase should take 90 minutes. During this period, the interface must complete half a revolution at point S2 to orient its thrusters correctly. Station-keeping must account for contingencies, requiring the interface to remain at the S2 position for one full orbit.

11.3.4 Closing :

The closing phase goes from S2 to S3 and should last around 120 minutes . S3 is located 250 meters behind the station. Another station-keeping orbit must be done.

11.3.5 Final Approach :

The final approach happens between the S3 and docking points and takes around 20 minutes. At 200 meters behind the station, the interface must be in the corridor. During the docking sequence from S3 to S4, the space shuttle maintains its position on the V-bar (velocity vector), using range and line-of-sight data from its navigation sensors to control its motion relative to the station. As it progresses from S4 to S4.1, the shuttle's sensor mode shifts to relative attitude measurement, ensuring that its docking port remains aligned with the station's port, thereby tracking any movements of the station. Upon reaching S4.1, approximately 12 meters from the docking port, the shuttle performs a final hold to allow both the crew and ground control to verify that all systems are ready for docking. The approach resumes on command from the mission control center, with no further changes to mode or configuration. Throughout this final phase, the crew closely monitors the shuttle's approach using independent data sources, such as visual images from the station's cameras and range data from the station's rendezvous system, ensuring a safe and precise docking procedure.

11.3.6 Docking Phase – Procedure with Station ASTROIKOS

As part of the System of System project, the station has sent us its list of procedures for checking and validating docking. The list of procedures is detailed in the following information :

Passive dock**Checklist for Station Docking and De-docking:**

1. Activate docking mode.
2. Test sealing integrity.
3. Isolate from the rest of ASTROIKOS.
4. Check connection integrity.
5. Check orbital parameters and position.
6. Prepare process for sensor contamination mitigation.
7. Potentially use multipath so that all the antenna is fixed.

Checklist for Exchange of Resources on the Docking:

8. Activate exchange mode.
9. Test sealing integrity.
10. Verify the position of the Astronauts.
11. Stop all the activities on the station.
12. Isolate from the rest of ASTROIKOS.
13. Check connection integrity.
14. Check the sensor for good transfer.
15. Prepare process for transfer of resource.
16. Transfer the resource.

Active dock

Checklist for the Shuttle:

- 17. Test sealing integrity.
- 18. Test docking system actuators integrity.
- 19. Test docking system sensors integrity.
- 20. Check atmosphere information.
- 21. Check orbital parameters and position.
- 22. Enter docking manoeuvre mode.
- 23. Check space station connection.

11.4 Architecture

The NDS users guide is making a perfect introduction to the Docking system interface, with various interfaces we will have to deal with in the design of the docking system.

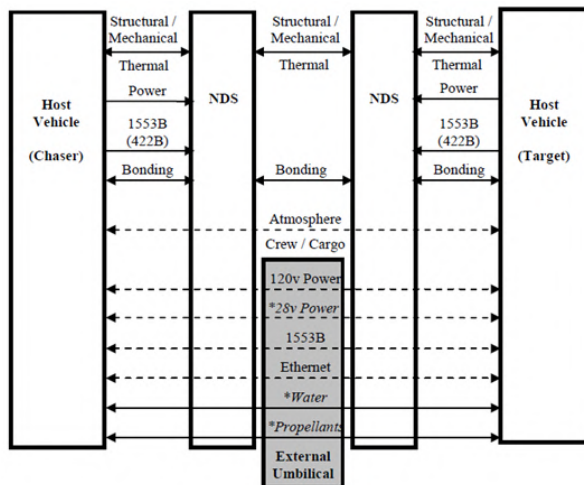


Figure 123: Mated NDS end-to-end Functional Interfaces

It is representing : the mechanical interface, the thermal interface, the power supply interface, the communication interface, the atmosphere exchange, the refuelling exchange, Additional interfaces. It is lacking the sensors and sensors strikers' interface between the chaser and the target. The NASA Docking System (NDS) [Program [2022]] was developed in compliance with the IDSS standard . The purpose of this document is to provide a fundamental understanding of the NDS technical and operations information. It must not be used as a design document.

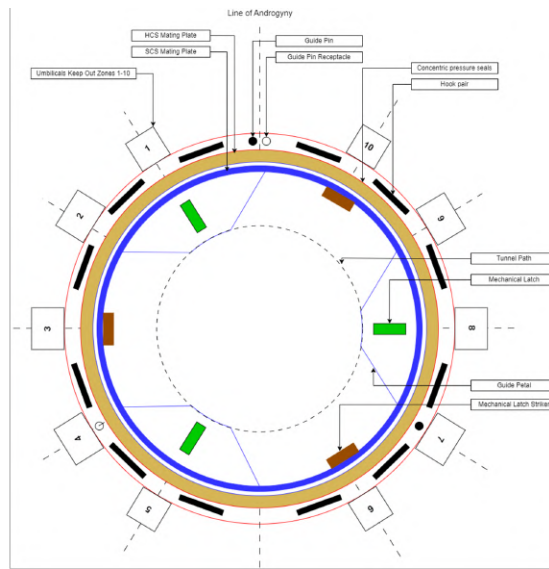


Figure 124: Docking Port IDSS Standard Design - Conceptual View

The Figure 124 is representing a conceptual view of the docking system according to IDSS standard. With various sizes of interfaces:

- Interfaces [1, 5, 6, 10]: $100 \times 136 \text{ mm}^2$
- Interfaces [2, 3, 4, 7, 8, 9]: $177.8 \times 136 \text{ mm}^2$

According to the NDS, as a reference base, we can make the hypothesis that our docking port will be similar to the ones depicted as NDS-301 and NDS-302, weighing respectively 340 kg and 320 kg. The principal differences between NDS-301 and NDS-302 [Program [2022]] are in the use:

- NDS-301 is designed to be both a passive and active system.
- NDS-302 is primarily designed to be passive, thus lacking certain components and capabilities.

A fundamental design choice on the 301 architecture is the use of pyrotechnic bolts that are by definition not designed for reusability and shall be changed between every mission.

11.4.1 SCS

The SCS is responsible for the initial alignment and capture of the two spacecraft. It uses guiding petals and mechanical locks to ensure smooth capture.

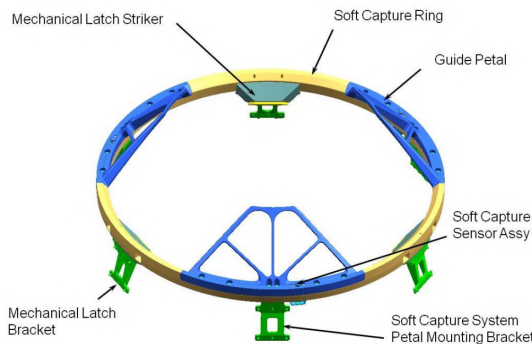


Figure 125: SCS

11.4.2 HCS

The HCS uses active hooks to engage opposing passive hooks to provide the structural connection and pressure seal compression. The HCS interface consists of a tunnel, 12 active/passive hook pairs on each side, dual concentric pressure seals, fine alignment guide pins and guide pin receptacles, sensors, sensor strikers, separation system, and resource umbilical.

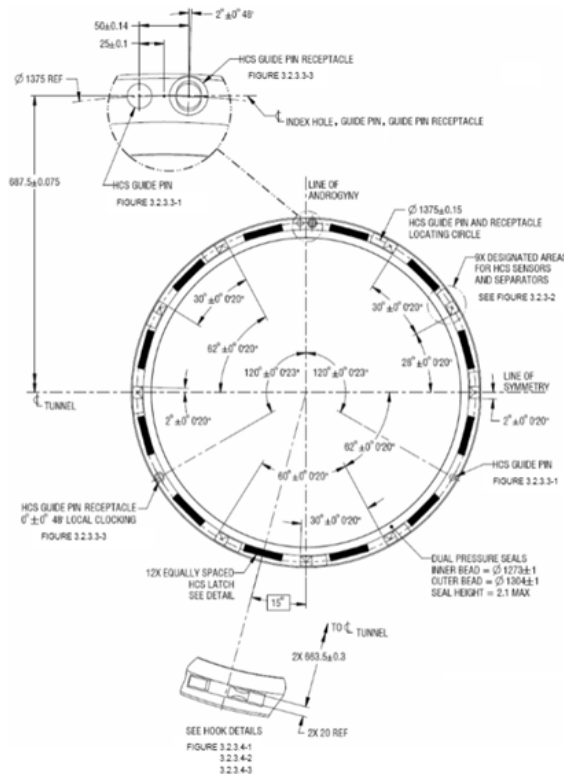


Figure 126: HCS

The hard capture hook system is defined as a combination of :

- Active Hook Mechanism
- Passive Hook Mechanism
- Structural elements in compression

The location of umbilical links is normalised and standardised to specific values, as well as the allowable area. There are 10 umbilical locations from 1 to 10.

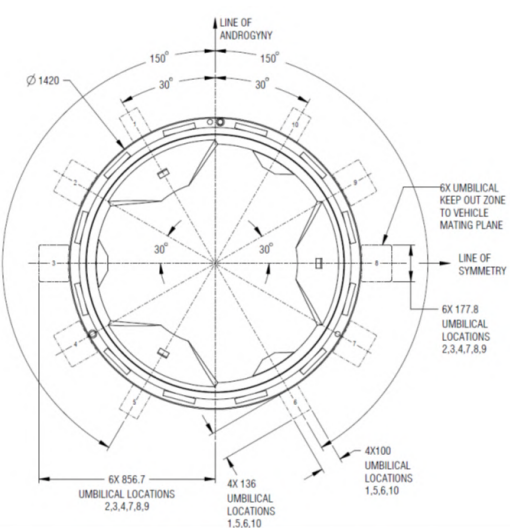


Figure 127: Umbilicals keep out zone

11.5 Interfaces

In addition to the main interface that represents the Docking port, more interfaces can be added between StarCheap S/C and space stations.

11.5.1 Additional Interfaces

The additional interfaces are being dealt with in the standard IDSS with chosen areas around the main docking interface, i.e., SCS and HCS. This allows the users and designers to add and use a variety of additional interfaces as needed. In our case design, the following additional umbilical interfaces have been selected:

Power Bus :

One or several Power Supply Bus will be added to the docking port. This interface will be used to supply power while StarCheap is docked to the space station.

Water Line :

One or several Water lines will be added to the docking port. This interface will be used to transfer water between StarCheap and the targeted spacecraft. It could be used either to resupply a space station or to resupply the StarCheap spacecraft.

Fuel Line :

The choice of in-orbit refuelling is necessary to carry out the mission of fetching debris. However, we're keeping open the option for the future of also refuelling the station with ergol, so the exchange must be bi-directional. Port number 4 of the HCS active docking interface is selected as the shuttle refuelling port.

Communication Bus :

This communication bus's purpose is to give redundancy to the spaceship's communication while being docked to a space station. In case of external communication system failure, it can still communicate with Ground Control using the space station's external communication system, and vice versa.

11.5.2 Interfaces Location :

In order to properly define the docking port, if new interfaces need to be added, their location need to be considered and defined.

Matching Plate :

The interfaces could be placed on the matching plate if the designed size is sufficient.

External Arm :

If the matching plate size is sizing, an external arm can be added. But it will increase the complexity and the weight of the system.

The choice has been made to integrate the interfaces in the interface area of the IDSS standard Figure 2 as following in the figure 128:

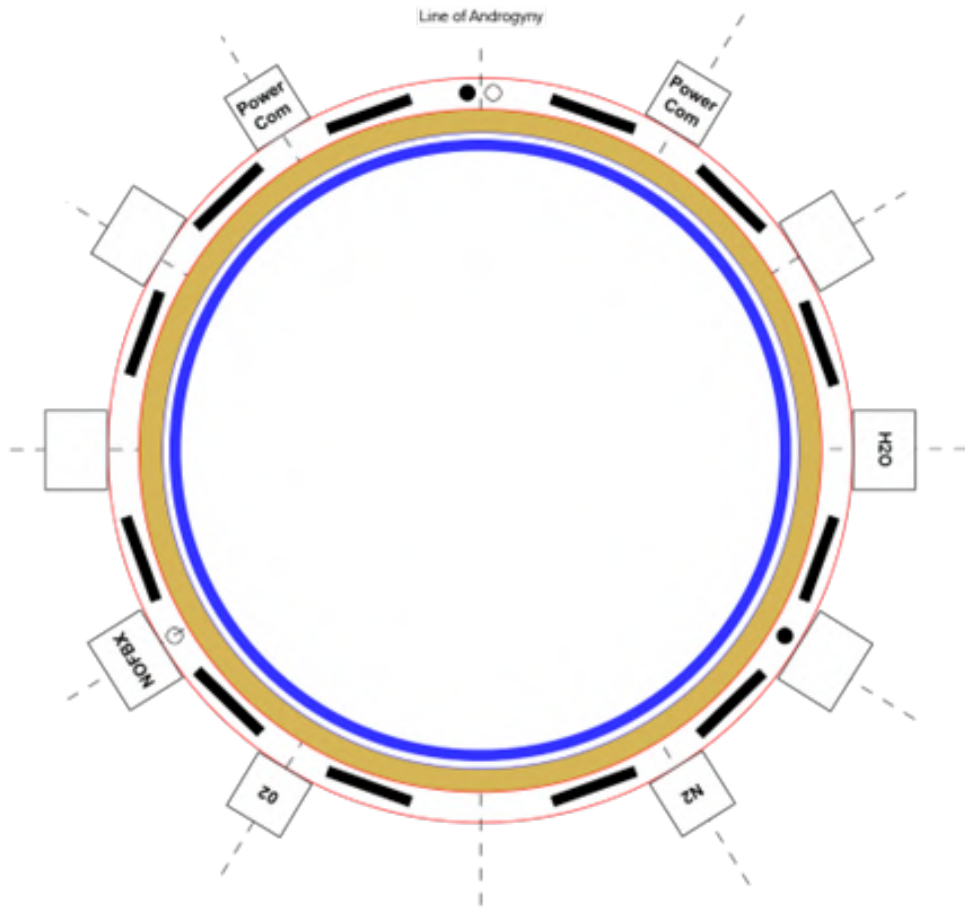


Figure 128: Docking port interfaces location choice.

- **Location 1:** Main Power Supply and Main Communication link
- **Location 4:** NOFBS Propellant for SpaceCheap Shuttle
- **Location 10:** Redundant Power Supply and Redundant Communication link
- **Location 5:** O₂ umbilical link
- **Location 6:** N₂ umbilical link
- **Location 8:** H₂O umbilical link

11.5.3 Interfaces Specifications

The interfaces will be designed using an automated retractable “arm”, that will be powered and actuated from the space station.

Water Line :

The water umbilical link needs to be designed according to the needs. It is necessary to define the required volume flow rate between the spacecrafts in order to design the umbilical diameter. As water freezes, it should be necessary to integrate heaters to prevent icing or to enable de-icing.

Power Transfer Interfaces :

Component	Specifications
Electrical Connectors	28V DC or 120V DC/AC depending on the system, EMI protection
Current	5-50 A
Power Capacity	3–5 kW per docking port
Protection	Circuit breakers, fuses, current overload detection
Usage	Charging visiting spacecraft, transferring power to subsystems or payloads
Cable Type	Shielded spiral cable (copper/silver)

Communication and Data Transfer :

Component	Specifications
Interfaces	Ethernet
Redundancy	Dual-redundant channels for safety
Data Rate	From kbps (command & telemetry) to Mbps (video, real-time systems) Up to 1 Gbps, Micro-D, CAN, SpaceWire connectors
Functions	GN&C synchronization, telemetry, remote control, payload uplink/downlink

Fluid Transfer Capabilities - Water :

Component	Specifications
Connectors	Self-sealing, auto-locking or semi-automatic hydraulic fittings Have heaters
Pressure Range	2–4 bar typical
Flow rate	1–5 L/min (depending on system configuration)
Cable type	Tygon / Teflon-type hose

O2 and N2 :

Component	Specifications
Regulation	High-precision pressure/temperature control valves
Safety	Non-return valves, leak sensors, purge capability
Pressure range	100 – 300 bars
Temperature	20-30 degrees
Flow rate	2-8 L/min
Valves / Regulation	High-pressure reducer + check valves
Needs	Have a pressure regulator
Purpose	Cabin pressurization, atmosphere regeneration, emergency reserve systems

Fuel Transfer :

Component	Specifications
Fluid type	NOFBX
Interfaces	Hermetically sealed Quick Disconnects (QDs), remotely actuated
Transfer Control	Fully automated sequence (software-controlled)
Safety systems	Double seals, pressure sensors, emergency cutoff valves Chemical compatibility, check valves
Cable type	Teflon-coated composite hoses

All cables have a thermal sheath and micrometeorite shielding.

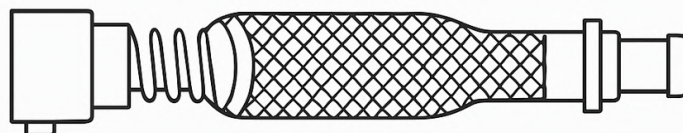
11.5.4 Interface Design

Design of the Cable Docking :

Component	Specifications
Name	Flexible multifunction umbilical (docking cable)
Function	Transfer of water, fuel, O ₂ /N ₂ gases, thermal fluid, power, and data
Integrated channels	6 (Water, Fuel, Communication, Power, O ₂ /N ₂ , Thermal Loop)
Length (contracted)	0.5 – 1.0 m
Length (extended)	up to 2.5 m
Minimum bend radius	15 cm
Mechanical life cycle	> 200 mating/un-mating cycles
Outer material	Nomex braided sleeve + micrometeorite shielding + UV coating
Sealing level	IP69 / vacuum compatible
Operating temperature	-40 °C to +100 °C
Gas pressure resistance	up to 250 bar (O ₂ /N ₂ line with steel mesh)
Dielectric resistance	1000 V with EMI/EMC shielding
Connector type	Self-aligning blind-mate, NASA/ESA standard compatible
Integrated regulation	2-stage pressure regulator for O ₂ /N ₂ included
Compliance	NASA-STD-5017, ECSS-Q-ST-70, ISO 14644
Estimated weight	3.5 – 6 kg depending on length and configuration
Volume (stowed)	< 0.015 m ³
Compatible connectors	QD hydraulic, Micro-D, D-Sub, power blind-mate, dual fluid QD
Integration method	Flexible routing within telescopic or coiled guide

Design of the Cable

This cable will permit the connection to the shuttle for the transfer of resource.



Extensible cable for transfer of resources

Figure 129: Cable design

11.6 Actuators Definition of the Docking System

In accordance with the IDSS standard, and the analysis of current solutions for IDSS compliant docking systems, Figure 130 shows the Docking Port IDSS Standard Design Conceptual View with actuators location. In red are shown the HCS actuators for the hook pairs, and in grey are shown the SCS actuators for the active system. A list of actuators is made available by Maxon group

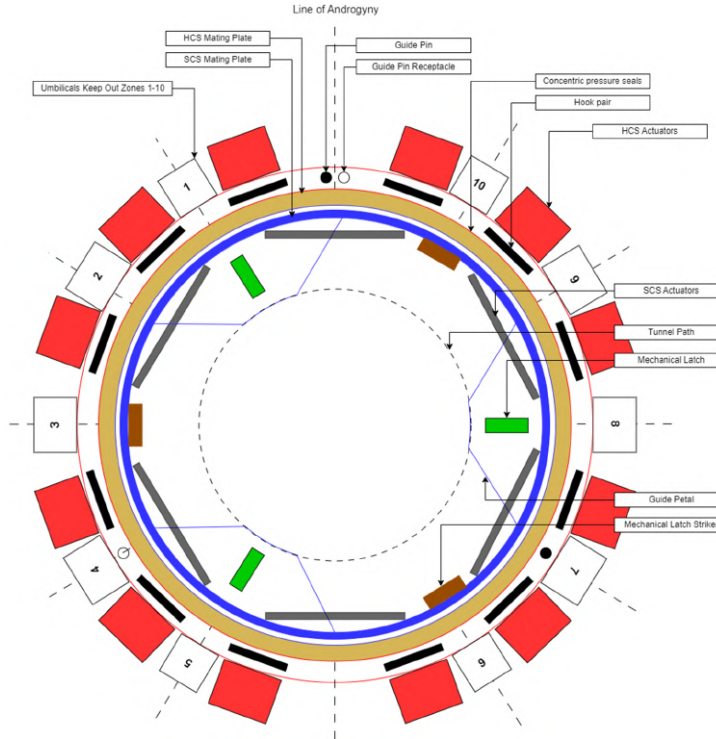


Figure 130: Docking Port IDSS Standard Design - Conceptual View with actuators

11.6.1 HCS Actuators

In accordance with the IDSS standard, the actuators used to power the hook pairs are electric motors. There are twelve drive systems that are used to power the locking hoods, each composed of two brushless motors - EC-4pole 30 motors, to enhance reliability, and one gearhead.

Value	Specification
V_{nom} [V]	24-32
P_{nom} [W]	150
N_{nom} [rpm]	17,100
η_{max} [%]	88
Mass [kg]	0.3

Table 118: EC-4pole 30 motors characteristics.

11.6.2 SCS Actuators

In accordance with the IDSS standard, the actuators that are used to power the system are not clearly described by Maxon group.

11.6.3 Other Actuators

There are 11 other actuators in the IBDM IDSS compliant design, that are composed of one dual-winding electrical motor - EC 32 flat motor, and a planetary gearbox.

Value	Specification
V_{nom} [V]	9-12-24-48
P_{nom} [W]	15
N_{nom} [rpm]	3,720 ... 4,780
η_{max} [%]	73
Mass [kg]	0.057

Table 119: EC 32 flat motor characteristics.

11.7 Sensors Definition

11.7.1 Proximity Sensors

The purpose of proximity sensors is to assess the relative distance between the chaser and the target and therefore positioning of the docking interfaces. This function can be realized using LIDAR. With one on the active system and 1 on the passive system provides a good balance between precision and efficiency as a first guess.

The proximity sensor will need to provide the system between the S/C and the space station from the S3 point. Therefore, it will need to have a range of 250m, and the according power.

The ATV and various systems are using the RVS-3000 product, presented in Figure 131 and Table 120, to monitor and measure the range between two cooperative spacecrafts.



Figure 131: RVS-3000. Jenaoptronik

Value	Specification
Field of View [°]	40x40 ... 1x1
Line of Sight 3σ noise [°]	≤ 0.05
Range min. [m]	<1
Range max. [km]	>2
$P_{\text{nom}}, P_{\text{max}}$ [W]	63, 85
Mass [kg]	12.4
Dimensions [mm]	342 x 267 x 215
Nominal Voltage [V]	28
Data Interface	MIL-1553

Table 120: RVS-3000 characteristics

11.7.2 Force Sensors

The purpose of force sensors is to assess the distribution of forces around the docking interfaces, ensuring a controlled engagement and identifying misalignment or excessive applied forces in the docking system that could damage it. These sensors are in the SCS' deployment axis. Their position is chosen to monitor the force on each axis.



Figure 132: Miniature in-line load cell.

Position Sensors

The purpose of position sensors is to assess the displacement and alignment of the docking mechanisms. These sensors would be used to measure the displacement of the SCS, and the angular positioning of the HCS hooks.

For angular positioning of the HCS hooks (12 of them) it will be measured with stock hall sensors.

Hall Sensor	Value
Output DC Voltage [V]	3 ... 24

Table 121: Hall sensor characteristics

For displacement of the SCS it could be measured by Linear Variable Differential Transformer (LVDT), which is measuring the linear displacement of a central core inside the coil assembly (Figure 133), whose will induce a magnetic field change, which can be measured. There will be one inside each SCS deployment “arm”, 6 of them.

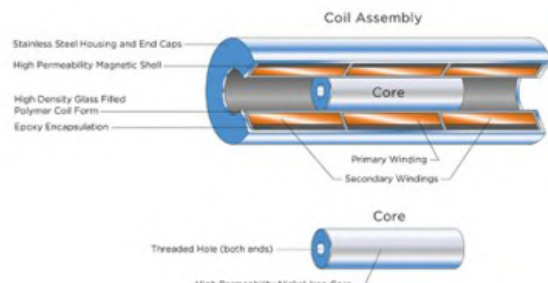


Figure 133: LVDT concept

Value	Specification
Linearity [%]	<0.2
Range [mm]	5 to 300
Operating T° [°C]	0 to 65
P _{max} [W]	0.75
Input DC Voltage [V]	10 to 30
Output	LD620, LD620

Table 122: LVDT sensor example

Optical Sensors

The purpose of optical sensors is to assess the attitude of the spacecraft with regard to the target. It provides a visual guide for the docking phase. This is usually done using cameras. Having 2 of them would provide a backup and enhance capabilities by providing depth measurement capabilities. With an additional for the docking itself.

The optical sensors will be empowered by VBN (Visual Based Navigation). The idea is to develop the functioning of the VBN w.r.t. the targeting and recognizing methodology from the chaser toward the target. The Auricam D80 (Figure 134) was used on the ATV and is going to be used on the Dream Chaser, the characteristics of this camera are presented in Table 123.



Figure 134: Auricam D80.

Strain Sensors

The purpose of these sensors is to assess the structural load in critical areas of the docking system. It helps monitor deformation of the docking interface, that is why 3, placed at opposite locations, for triangulation would be necessary to better monitor the structural health. The strain sensors are usually strain gauges (Figure 135), and possess the following characteristics:

AURICAM D80	Value
Resolution [pixel]	2048x2048
Frame rate [fps]	Up to 10
FoV [°]	80
Resolution [cm]	5 @ 100m
Mass [kg]	<0.42
Dimensions [mm]	140x71x65
Operating T° [°C]	-35 to +55
Input Voltage [V]	4.75 to 6
P_{nom} [W]	<2

Table 123: Auricam D80 characteristics

A camera will be placed to be able to see the docking port, in order to provide other sensing information.

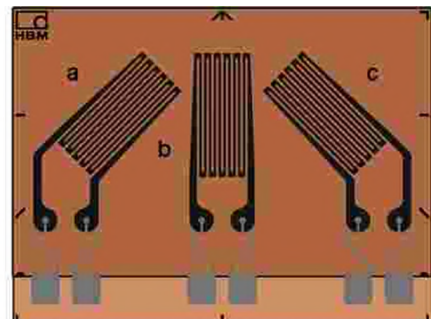


Figure 135: Strain gauges

Value	Specification
Maximum elongation [$\mu\text{m}/\text{m}$]	+10,000 / – 15,000
Temp range [°C]	–200 … + 250
P_{\max} [W]	0.3

Table 124: Strain gauge characteristics

Pressure Sensors

The purpose of these sensors is to assess the state of the docking seals and to ensure that the seals are intact – that there is no atmosphere leakage, and that there is no unexpected pressure differential. 3 sensors could be used to ensure reliability of the system, and to be FO/FS. A pressure sensor is shown in Figure 136, with the following characteristics :

Value	Specification
Mass [kg]	0.227
Dimensions [mm]	ø30, L79.5
Operating Temp [°C]	-25 … 85
Range [bar]	0 … 2.5
Resolution [bar]	0.01
Accuracy [%]	±0.5
Input DC Voltage [V]	9.6 … 36
P_{nom} [W]	<0.5

Table 125: Pressure sensor characteristics

One can also use space hardened technology.

Temperature Sensors

The purpose of these sensors is to assess the thermal conditions of the docking system. This monitors the thermal conditions to assess the possible impact on the docking performance as well as assessing the feasibility of crew/cargo transfer without injuries. We could place 3 sensors on the inside of the docking ring at opposite sides to ensure re-



Figure 136: Pressure sensor

dundancy in case of icing or other problems. The Figure 137 is showing a humidity and temperature sensor with the following characteristics Table 126 :

Value	Specification
Accuracy [%]	1.5
Input Voltage [V]	2.15 to 5.5
Dimensions [mm]	2.5 x 2.5 x 0.9
Accuracy [°C]	±0.2
Range [°C]	-40 to +125
P_{nom} [mW]	10

Table 126: Micro Humidity and Temperature sensor - SHT3x-DIS characteristics



Figure 137: Humidity and Temperature Sensor. SHT3x-DIS

One could use a more classical sensor such as a PT-100 temperature sensor

11.8 Docking System Power Supply

The docking sequence implies that the electrical motors are working by pairs and not all at once, this is an active strategy in current strategies to decrease power load and increase safety of the system.

Component	Number	Max Unit Power [W]	Total Power during docking [W]
EC-4pole 30 motor	24	150	300
EC 32 flat motor	11	15	165
Proximity Sensor	1	85	85
Force Sensor	6	<1	~2
Position Sensor	14	~0	~0
LVDT	6	0.75	4.5
Optical Sensor	2	2	4
Strain Sensor	3	0.3	0.9
Pressure Sensor	3	0.5	1.5
Temperature Sensor	3	0.01	0.03

Table 127: Power supply for docking components.

According to Table 127, the power budget for sensors is 98W. According to Table 127, the total required power budget for actuators is about 465W. The maximum power budget is when the EC-4pole 30 motor are used with the sensors, therefore using ~398W.

11.9 Conclusion

The StarCheap docking system is meticulously engineered to ensure safe and reliable spacecraft connections, adhering to rigorous standards and operational requirements. It features a two-stage process—soft capture for initial stabilization and hard capture for secure structural connection—both designed to be androgynous for operational flexibility. The system meets comprehensive functional, System of Systems (SoS), and IDSS requirements, ensuring compatibility, autonomous operation, and environmental resilience. The docking procedure involves precise orbital maneuvers and thorough checklists for both the station and shuttle, highlighting the system's robustness and reliability in facilitating crew and cargo transfers, as well as resource exchanges.

12 Command Data Handling

The function of an On-board Data Handling (OBDH) Subsystem, often referred to as the brain of the space shuttle, is to perform onboard operations and internal communication autonomously. This system manages the various phases of the mission, which can be activated by astronauts or the ground segment command. The OBDH is responsible for receiving, error-correcting, and decoding telecommands from the Telemetry, Tracking, and Command (TT&C) system, as well as forwarding them for execution by the target avionics. It stores telecommands until a specified time or position, measures discrete values such as voltages and temperatures, and collects data from other units via data buses like SpaceWire. Measurements are buffered in real-time and processed to achieve mission objectives. The OBDH compiles, encodes, and stores telemetry frames, transmitting them to the ground via TT&C, while managing and distributing time signals. Additionally, the OBDH handles all onboard data sent to actuators and sensors, ensuring the safety and reliability of the mission through redundant components.

12.1 CDH requirements

Requirement ID	Description
OBDH-REQ-001	The system must ensure continuous and reliable data management under mission conditions
OBDH-REQ-002	The system must process incoming and outgoing data efficiently to meet real-time mission needs
OBDH-REQ-003	System must include hot redundancy to ensure fault tolerance and high availability
OBDH-REQ-004	System must provide sufficient onboard storage for mission data
OBDH-REQ-005	System must be autonomous during the entire mission
OBDH-REQ-006	The system must ensure the integrity and security of onboard data
OBDH-REQ-007	The OBDH must support multiple communication interfaces with subsystems and payloads
OBDH-REQ-008	The OBDH system must be designed according to the SpaceWire standard
OBDH-REQ-009	OBDH should be responsible for going on safe mode at the shuttle level. (MSU chain)
OBDH-REQ-010	Astronauts shall be able to trigger the shuttle safe mode at any time
OBDH-REQ-011	The system shall receive telecommands from the TT&C subsystem
OBDH-REQ-012	The system shall perform error correction on received telecommands
OBDH-REQ-013	The system shall decode telecommands accurately for further processing
OBDH-REQ-014	The system shall ensure the integrity of telecommands during forwarding
OBDH-REQ-015	The system shall store time-tagged telecommands until their specified execution time
OBDH-REQ-016	The system shall measure discrete values such as voltages, temperatures, and binary statuses
OBDH-REQ-017	The system shall collect measurements from other units and subsystems SpaceWire
OBDH-REQ-018	The system shall encode telemetry frames for transmission
OBDH-REQ-019	The system shall ensure the integrity of stored telemetry frames
OBDH-REQ-020	The system shall ensure the reliability of telemetry downlink
OBDH-REQ-021	The system shall manage time signals accurately
OBDH-REQ-022	The system shall distribute time signals to relevant subsystems and components

Table 128: List of OBDH Requirements

12.2 Critical analysis

In the realm of space systems design and analysis, we define the criticality levels of functions and mission phases to ensure the reliability and safety of operations. The following tables present a classification of function criticality levels, along with various mission phases and their associated functions, thereby facilitating optimal risk management and performance throughout the project lifecycle.

Criticality level	Description	Tolerable failure
1	Function is not used	Any failure
2	Functions is used but not prevalent in the normal behaviour	Degraded state
3	Functions is used and important, but there is close to no time constraint	Outage of 1 minute
4	Functions availability is important	Outage of 1 second
5	Function availability	Outage of several milliseconds

Number Mission Phase	Description
P1	Launch
P2	Separation
P3	Orbital Insertion
P4	Docking phases
P5	Docked
P6	Undocking phases
P7	Debris orbit insertion
P8	Debris Capture
P9	Debris Storage/Removal
P10	Orbital correction
P11	Re-entry
P12	Landing

Function	Description
F1	Thermal Control
F2	Power Supply
F3	Power Distribution
F4	Comms with Ground
F5	Comms with station
F6	ECLS
F7	Propulsion
F8	Mission and Vehicle Management
F9	AOCS

Table 130: Functions

Table 129: Mission Phases

Criticality levels 4 and 5 impose stringent requirements for availability and fault tolerance, necessitating specific redundancy mechanisms to ensure the reliability and safety of operations. For criticality level 4, a maximum outage duration of 1 second is tolerated, which is typically met by warm redundancy. In this setup, redundant equipment is kept on standby, ready to be quickly activated in case of failure, allowing reconfiguration within less than a second to minimize disruptions. In contrast, criticality level 5, which tolerates only a 100-millisecond outage, requires hot redundancy. Here, redundant

equipment operates in parallel with the primary system, ensuring an almost instantaneous switchover and uninterrupted service continuity. These mechanisms are crucial for ensuring that space systems remain operational even in the event of failures, thereby safeguarding mission integrity and crew safety.

Function/Phase	Thermal Control	Power Supply	Power Distribution	Comms with Ground	Comms with station	ECLS	Propulsion	OBC	AOCS
Launch	3	3	3	2	1	4	1	5	1
Separation	3	3	3	3	1	4	2	5	4
Orbital insertion	3	4	4	3	1	4	5	5	4
Docking phases	3	5	5	3	4	4	4	5	5
Docked	3	1	3	1	1	1	1	3	1
Undocking phases	3	5	5	3	4	4	4	5	5
Debris orbit insertion	3	4	4	3	1	4	5	5	4
Debris Capture	3	4	4	3	1	4	3	5	5
Orbital correction	3	4	4	3	1	4	5	5	4
Re-entry	4	5	5	4	1	4	4	5	5
Landing	4	5	5	4	1	4	5	5	5
Max level	4	5	5	4	4	4	5	5	5

Table 131: Function/Phase Critical level

12.3 Management Mode analysis

Mode management is part of our shuttle's resilience process: the plurality of modes enables us to perform all the tasks of our multi-mission shuttle. These modes give us the ability to cope with the adversity and complexity of the environment in which our shuttle operates. These modes are separated into groups called: Principal Management Mode, Docked management mode ,Capture Management Mode, Landing Management Mode.

12.3.1 Principal Management Mode

- **LAM (Launch Mode):** The shuttle is in Launch Mode from the moment of transfer of power provision from ground to the on-board batteries, until the shuttle separation from the launcher. During LAM, the shuttle the receivers are on, the transmitter is on, and the shuttle communication buses are initialized. After having enabled all the analog and digital acquisition/commanding lines, the On-board Computer (OBC) waits for the separation signal to start the separation sequence.
- **INM (Initialization Mode):** Automatically activated after separation from the launcher. During this mode, the shuttle initializes all critical systems, checks for any post-launch anomalies, and prepares for transitioning into the next operational phase.
- **SBM (Stand-by Mode):** In Stand-by Mode, the shuttle acts as an inorbit spare not used for any operational service but able to become operational within a short time frame. Full health and safety activities are maintained, including continuous real time monitoring. Thrusters are disabled.
- **NOM (Nominal Mode):** In Nominal Mode, the shuttle along its payload and platform is fully operational. The shuttle is three axes stabilized ensuring the required trajectory and life support for astronauts.

- **OTM (Orbit Transfer Mode):** gives the capability of performing the transfer using the propellant, while maintaining the attitude compatible with this orbit correction. The mode is provided with a guidance profile uploaded from ground or from astronauts.
- **FSM (Fail Safe Mode):** The shuttle enters the Safe Mode under critical on-board anomaly detection, which cannot be autonomously recovered

or which, though recovered, could present a risk later on if normal operations are continued. Return to normal operations is completely carried out under ground control or pilot actions.

- **FOM (Fail Operational Mode):** The shuttle enters the Safe Mode under critical on-board anomaly detection, which cannot be autonomously recovered.

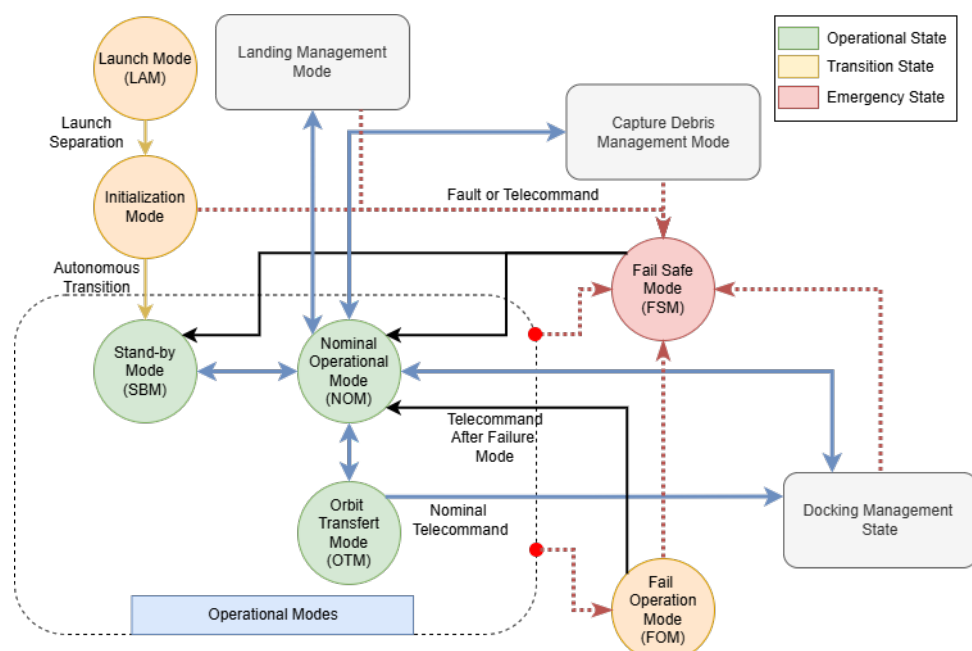


Figure 138: Principal Management Mode

12.3.2 Docking Management Mode

The docking management mode starts as soon as the shuttle enters the docking phase (S0 point), as explained in detail in the docking section. The docking management mode ends when the undocking phase is finished.

- **HDM (Hard-Dock Mode):** Once soft contact is confirmed, a more stable connection is established. All service connections (mechanical, electrical) must be engaged before refueling or maintenance operations begin.
- **SDM (Safe Docking Mode):** In the event of major problems during

the coupled phase, this mode puts the shuttle in a safe configuration. If possible, a controlled disconnection of the space structures is preferred. Otherwise, the system must avoid overloading the docking system while adjusting the attitude of the attached system.

- **RDM (Refueling Docked Mode):** Service operations such as fuel/gas changeover or maintenance are carried out. Attitude and orbital dynamics operations are controlled by the station. In the event of a problem, rapid separation or transfer to SDM is planned.
- **EDM (Escape Docking Mode):** Perform CAM maneuver Collision avoidance maneuver.
- **SFDM (Soft Docked Mode):** Transition mode between the phases when shuttle and station are still detached and the moment of first contact. The soft connection mechanism is activated to prevent the two from drifting apart.
- **RVDM (Rendezvous Docking Mode):** The shuttle approaches the target structure, using its sensors and actuators to perform the rendezvous. Once the distance and relative position are stable, the mode switches to BDM. In the event of ground segment failure or command, control switches to EDM.
- **BDM (Berthing Docking Mode):** From the end of RVDM until contact between shuttle and target structure, this mode brings the shuttle closer to the docking fixture on the target structure, maintaining relative position/velocity/attitude within defined limits. Can switch to EDM in the event of an unexpected event or ground segment command.

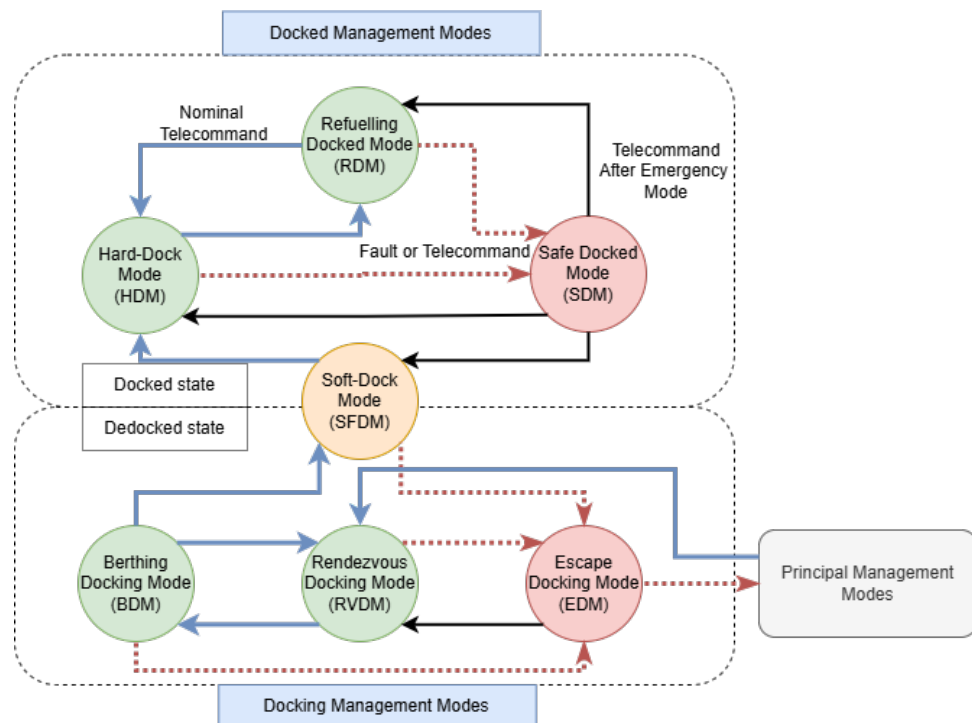


Figure 139: Docking Management Mode

12.3.3 Capture Management Mode

The capture management mode refers to the shuttle's modes during the debris capture phase. This phase involves a large number of mechanisms, which creates a risk of failure. In this study, we don't go into the details of countermeasures in the event of mechanical failure during debris capture and displacement in the cargo bay.

- **ICM (Inspection Capture Mode):** This mode enables our shuttle to make efficient use of its sensors and actuators to identify the debris, check its dynamics, and adapt our attitude to that of the debris.
- **RCM (Rendezvous Capture Mode):** The shuttle approaches the target debris, using its sensors and actuators to perform the rendezvous. Once the distance and relative position are stable, the mode switches to ICM. In the event of ground segment failure or command, control switches to ECM.
- **ECM (Escape Capture Mode):** Perform Collision Avoidance Manoeuvre
- **DCM (Deployment Capture Mode):** This mode allows the cargo bay to be opened, the grabb system to be deployed and the debris to be stored. When this mode is selected, shuttle functions must have a high level of criticality.
- **SCM (Safe Capture Mode):** In the event of major problems during the capture phase, this mode puts the shuttle in a safe configuration. If possible, the grapple is severed with the debris and the shuttle performs an anti-collision manoeuvre. If not, we force the debris into the cargo hold
- **HCM (Hard Capture Mode):** The shuttle is in contact with the debris and performs a debris storage maneuver in the cargo hold. This mode closes the hold. Without failure, once the debris has been correctly stored, the shuttle automatically transitions to nominal mode (NOM).

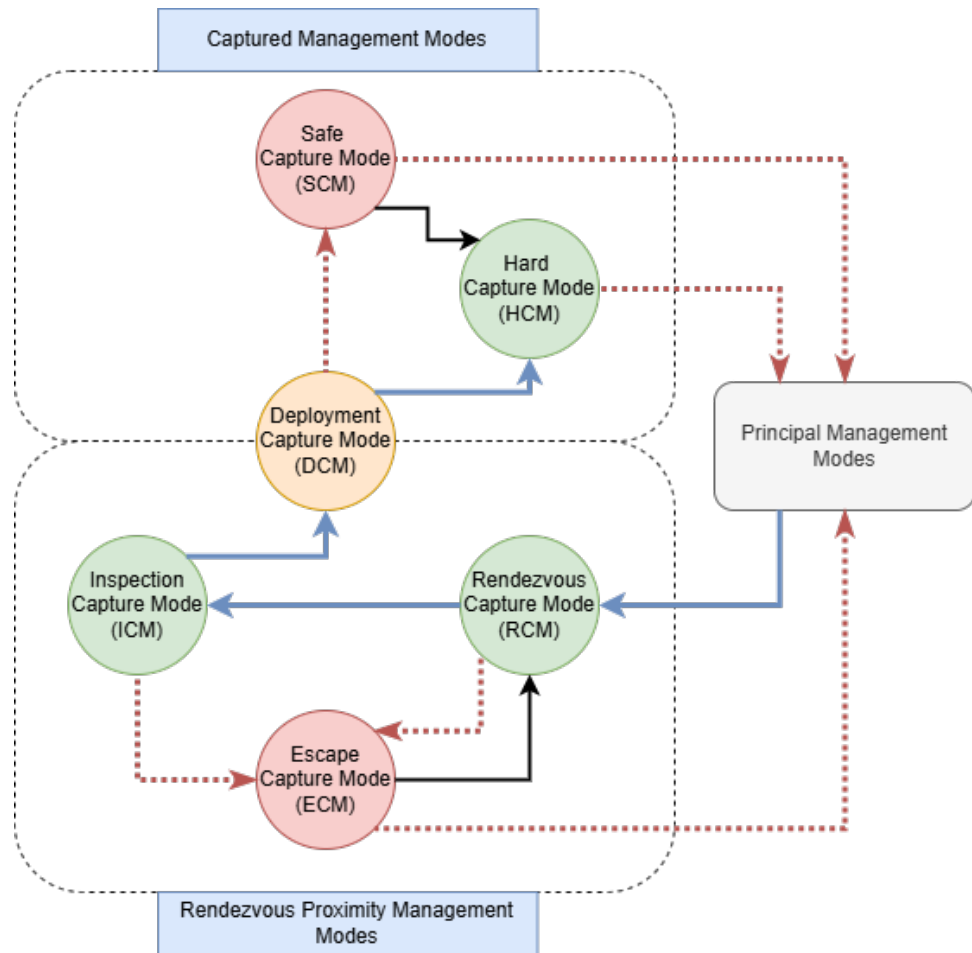


Figure 140: Capture Management Mode

12.3.4 Landing Management Mode

The landing management mode starts at an altitude of 200km, where we separate from the debris before re-entry. The re-entry phase is critical, as even a small deviation can cause the landing to fail. The safe mode of the landing management mode remains to be defined from the point of view of astronaut safety.

- **ECM (Ejection Bay Mode):** The shuttle approaches the target structure, using its sensors and actuators to perform the rendezvous. Once the distance and relative position are stable, the mode switches to BDM. In the event of ground segment failure or command, control switches to EDM.
- **RM (Re-entry Mode):** Gives the capability of performing the re-entry using propellant, while maintaining the attitude compatible with the re-entry trajectory. This mode allows astronauts to control the system more easily than the ground segment.
- **LM (Landing Mode):** Gives the capability of performing the belly flop et hover manoeuvres
- **SBLM (Stand-by Landing Mode):** In Stand-by Landing Mode, the shuttle checks the astronauts' living conditions and transmits vital information to the ground segment.
- **SLM (Safe Landing Mode):** TBD

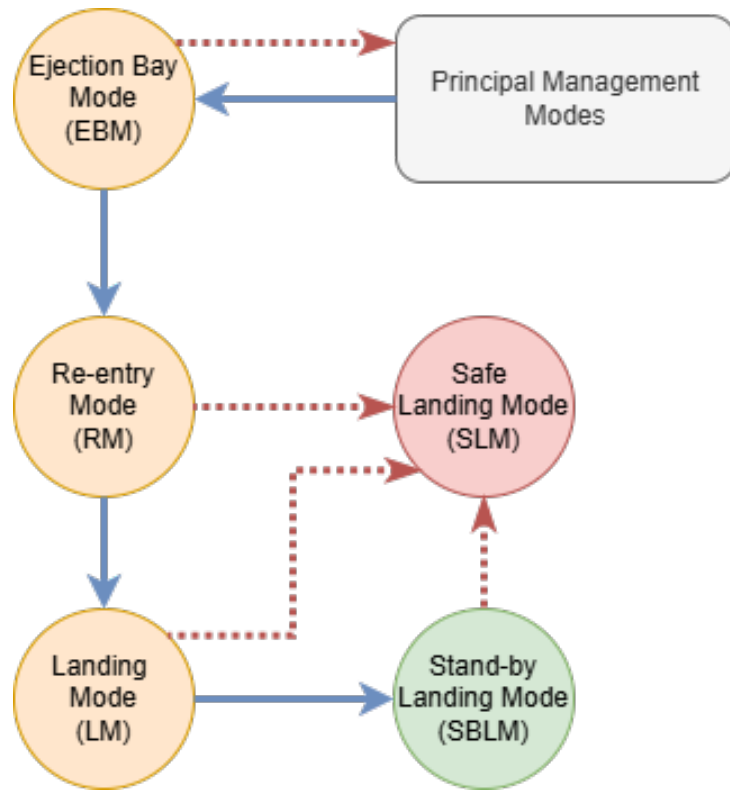


Figure 141: Landing Management Mode

The following table presents the different activity modes according to the phases of the mission as well as the sub-systems that it mainly requires

Phase/Mode	LAM	OTM	SBM	FSM	FOM	NIM	NOM	HDM	SDM	RDM	EDM	SFDM	RVDM	BDM	ICM	RCM	ECM	DCM	SCM	HCM	EBC	RM	LM	SBLM	SLM
Launch	X																								
Separation		X	X		X	X		X																	
Orbital insertion	X	X	X	X																					
Docking phases		X	X					X	X		X	X													
Docked			X					X	X	X	X														
Undocking phases				X	X				X	X		X	X												
Debris orbit insertion	X			X	X																				
Debris Capture				X	X			X	X																
Orbital correction	X	X	X	X																					
Re-entry			X					X																	
Landing				X				X																	
Subsystem																									
Thermal Control	ON	ON	ON	ON	ON	ON	ON	ON	ON	ON	ON	ON	ON	ON	ON	ON	ON	ON	ON	ON	ON	ON	ON	ON	ON
Power Supply	ON	ON	ON	ON	ON	ON	ON	OFF	ON	ON	ON	ON	ON	ON	ON	ON	ON	ON	ON	ON	ON	ON	ON	ON	ON
Power distribute	ON	ON	ON	ON	ON	ON	ON	ON	OFF	ON	ON	ON	ON	ON	ON	ON	ON	ON	ON	ON	ON	ON	ON	ON	ON
Comms with Ground	ON	ON	ON	ON	ON	ON	ON	ON	ON	ON	ON	ON	ON	ON	ON	ON	ON	ON	ON	ON	ON	ON	ON	ON	ON
Comms with station	OFF	OFF	OFF	OFF	OFF	OFF	ON	ON	ON	ON	ON	ON	ON	ON	ON	OFF	OFF								
ECLS	ON	ON	ON	ON	ON	ON	ON	OFF	ON	ON	ON	ON	ON	ON	ON	ON	ON	ON	ON	ON	ON	ON	ON	ON	ON
Propulsion	OFF	ON	OFF	OFF	OFF	OFF	OFF	IDLE	OFF	OFF	OFF	ON	IDLE	ON	ON	OFF	OFF	OFF	OFF	OFF	ON	ON	OFF	ON	ON
OBC	ON	ON	ON	ON	ON	ON	ON	ON	ON	ON	ON	ON	ON	ON	ON	ON	ON	ON	ON	ON	ON	ON	ON	ON	ON
AOCS	IDLE	ON	ON	ON	ON	ON	ON	OFF	ON	ON	ON	ON	ON	ON	ON	ON	ON	ON	ON	ON	ON	ON	ON	ON	ON

Figure 142: Subsystem and Phase by Mode

12.4 CDH Architecture

12.4.1 Global Architecture

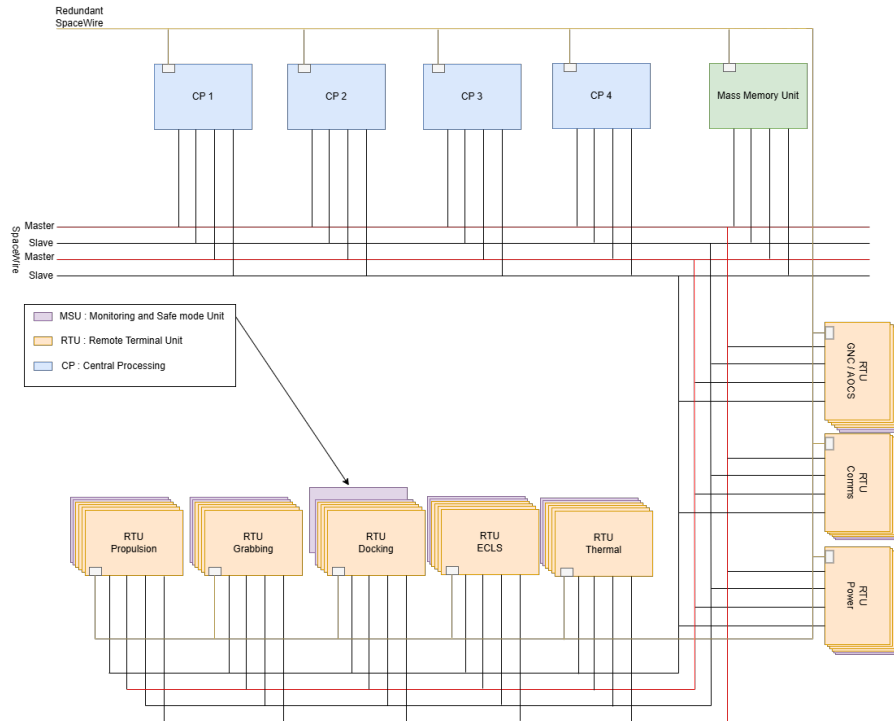


Figure 143: Global Architecture

The Remote Terminal Computer (RTC) [Terma [2023]] serves as a bridge between the SpaceWire network and low data rate sensor buses, collecting data from sensors, packaging it into SpaceWire packets, and sending it to the data handling system. It also distributes commands from the data-handling processor to the sensors or actuators. This setup allows multiple low data rate sensors to be integrated into the SpaceWire network and supports legacy devices like Mil-Std 1553 [Klar et al. [2023]]. However, it requires managing two types of bus/network. This Spacewire based architecture is ideal for our systems which has numerous low data rate sensors or legacy devices and can easily incorporate units like downlink telemetry and uplink telecommand systems into the SpaceWire network.

12.4.2 SpaceWire links

For our mission, the shuttle must exchange large amounts of information quickly and execute calculations to perform astronaut-ordered telecommands. The SpaceWire standard, ESA ECSS-E-50-12A [ecs [2010]], is based on two commercial standards: IEEE-1355 and LVDS (Low Voltage Differential Signaling). SpaceWire is a high-speed, low-power communications technology designed for easy implementation in digital logic [Parkes [2012]]. It supports rapid data transfer with link speeds over 200 Mbps and uses point-to-point connections, offering flexibility for integrating redundancy into spacecraft systems. This protocol also allows for the incorporation of future equipment using newer technologies not supported by older protocols.

SpaceWire's low power consumption is achieved through the LVDS protocol, which specifies a current value of ± 3.5 mA and a receiver terminal resistance of 100 ohms, resulting in a 350 mV potential difference. Additionally, SpaceWire is compatible with the CCSDS communication protocol, utilizing the CCSDS Packet Transfer Protocol [Habinc and Isomäki [2023]].

Physical Level

The SpaceWire cable comprises four twisted pair wires with a separate shield around each twisted pair and an overall shield. To achieve a high data signalling rate with SpaceWire over distances up to 10 m a cable. One of the drawbacks of SpaceWire is the mass of the cable which is around 87 g/m.

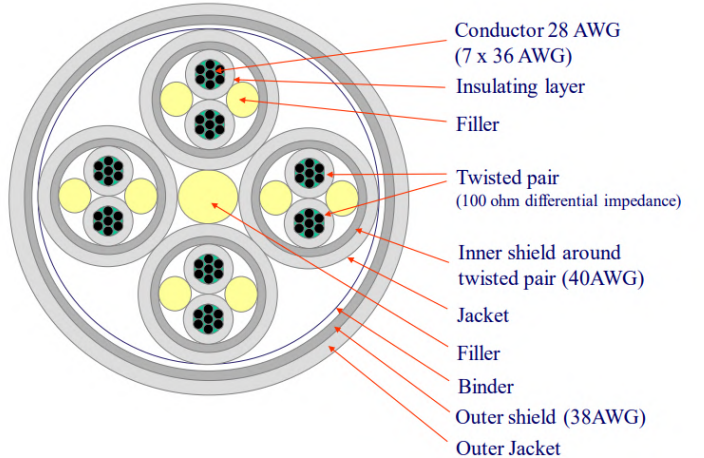


Figure 144: SpaceWire Cable Structure

Packet Level

SpaceWire transmits data in packets, each starting with a destination address followed by the data payload and ending with an End of Packet (EOP) marker. Transmission is managed through a credit-based flow control system, ensuring data is only sent when the receiver is ready, and operates over full-duplex links for simultaneous bidirectional communication. Routing in SpaceWire can be achieved through path addressing, where packets contain a list of directions for traversing the network, or logical addressing, where each node has a unique identifier, and routers use routing tables to forward packets. Fault recovery in SpaceWire, utilizing parity checking to detect errors and automatically reinitializing links upon fault detection. The system sends an Error End of Packet (EEP) to signal transmission errors, and higher-level protocols manage retransmission. Redundancy and error containment within the link layer further enhance reliability, making SpaceWire suitable for the demanding and critical conditions of space missions.



Figure 145

Address Range	Function
0	Internal Configuration Port
1-31 (01-1F hex)	Physical Output Ports
32-254 (20-FE hex)	Logical Addresses, which are mapped on to the physical output ports
255 (FF hex)	Reserved

Table 132: Router Addresses

12.4.3 Subsystems network

The command data handling architecture for a space shuttle, as illustrated in Figure 146, is based on a modular and redundant approach aimed at ensuring high availability and enhanced reliability of critical systems. Each subsystem is equipped with four Remote Terminal Units (RTUs) to provide high redundancy, thereby allowing operations to continue even in the event of a unit failure. Sensors are connected to all four RTUs, requiring a check of port availability and the potential addition of switches to manage the number of connections. Some sensors require analog-to-digital converters to adapt signals, while those requiring high data rates can be directly connected to the SpaceWire. The two MSUs (Monitoring and Safe mode Unit) must ensure safe mode in the event of a critical failure. These units are designed as independent units of the CDH team.

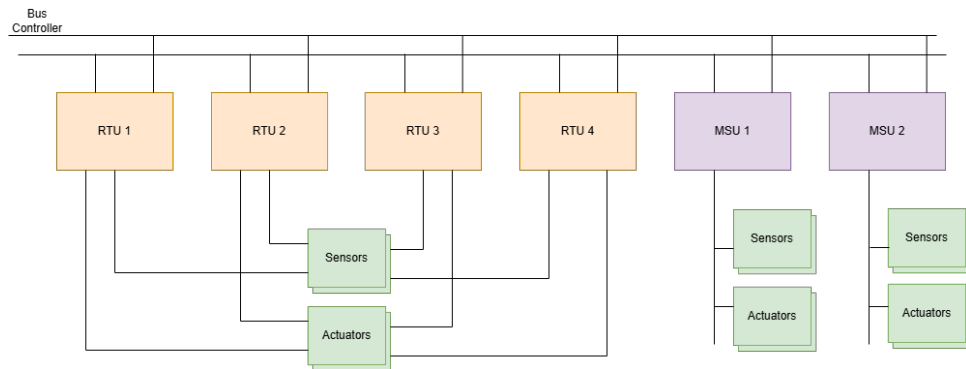


Figure 146: Subsystem Architecture

12.5 Component definition

As defined in the sub-system architecture presented earlier. We choose 3 components presented below : the OBC, the TMC and the RTU.

12.5.1 OBC : On-Board Computer

The Sirius OBC LEON3FT [AAC Clyde Space [2020a]] is an on-board computer designed for advanced space missions, providing fast and reliable operations with its fault-tolerant LEON3FT processor and RTEMS real-time operating system. It features two SpaceWire interfaces for high-speed communication while maintaining low power consumption and a compact design, ideal for space environments.

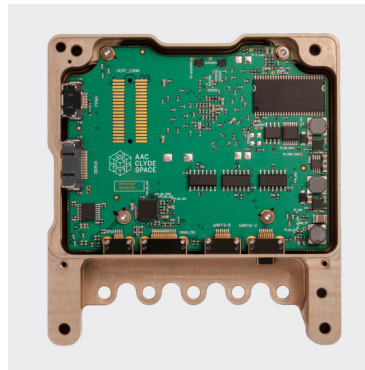


Figure 147: SIRIUS OBC LEON3FT

Feature	Value
SpaceWire	2 interfaces at 50 Mbps
Power Consumption	1.3 W
Dimensions	95.89 mm x 90.17 mm x 17.20 mm
Weight	130 g

Table 133: OBC specifications

12.5.2 TCM : Telemetry, Command, and Mass Memory

The Sirius Command and Data Handling system has a standard single string system that consists of an on-board computer (Sirius OBC[AAC Clyde Space [2020b]]) and a combined mass memory with CCSDS stack (Sirius TCM). The OBC runs mission specific software and manage the spacecraft system. The TCM receives and stores payload data and platform housekeeping data while at the same time distributing telecommands and serving mass memory data to the transceiver.

The Sirius TCM LEON3FT is a specialized Telemetry, Command, and Mass Memory system designed for advanced satellite missions. Equipped with a 50 MHz LEON3FT fault-tolerant processor and a real-time operating system, it ensures efficient mission management and data processing. The system features 32 GB of mass

storage, supports SpaceWire for high-speed data transfer, and utilizes CCSDS encoding for seamless satellite communication. Its design incorporates triple-modular redundancy and memory scrubbing to protect against radiation-induced errors, ensuring continuous operation in the harsh conditions of space

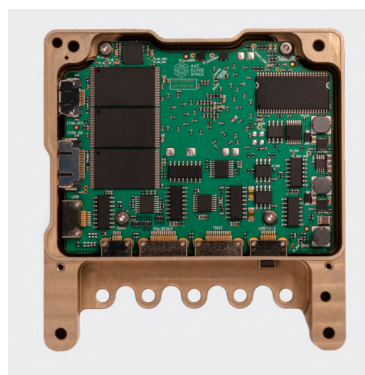


Figure 148: SIRIUS TCM LEON3FT

Feature	Value
Power Consumption	1.3 W
SpaceWire Interfaces	2 at 50 Mbps
Dimensions	95.89 mm x 90.17 mm x 17.20 mm
Weight	130 g

Table 134: TCM specifications

12.5.3 RTU : Remote Terminal Unit

To determine the number and types of RTUs needed for your satellite architecture, we can map each subsystem to the appropriate RTU modules based on their functions. In this preliminary design we are considering a redundancy of 4 RTUs per sub-system.



Figure 149: Terma - Remote Terminal Unit

Subsys.	Wt.(Kg)	Dim. (mm)	Pwr. (W)
Power	1.5	200 x 200 x 100	5
ECLS	1.2	180 x 180 x 80	4
Thermal	1.5	200 x 200 x 100	5
AOCS	1.8	220 x 220 x 120	6
Comm.	1.6	210 x 210 x 110	5.5
Prop.	1.7	215 x 215 x 115	5.5
Dock.	1.5	200 x 200 x 100	5
Grab.	1.5	200 x 200 x 100	5
Total	43.2	0.12 m ²	144 W

Table 135: RTU specifications

12.5.4 Sensors

Our OBDH subsystem must ensure the measurement of vital parameters for the space-craft, necessitating the integration of various sensors. To begin with, temperature sensors monitor the thermal conditions of critical components such as processors and memory units, allowing for the detection and mitigation of potential overheating issues to guarantee optimal performance and extended lifespan of electronic components. Voltage and current sensors provide real-time data on the power supply to the OBDH subsystem, essential for maintaining stable operation and preventing power-related failures. Error detection is integrated into the OBC, TCM, and RTU components, continuously monitoring data integrity and correcting errors in data storage and transmission, ensuring the reliability of data handling processes. Together, these sensors provide comprehensive insights into the OBDH subsystem's operational status, enabling proactive maintenance and enhanced mission reliability.

12.6 Conclusion

The Command and Data Handling (CDH) subsystem perform reliable and autonomous operation of our space shuttle. It efficiently manages onboard operations and internal communication by processing telecommands, collecting mission data, and ensuring real-time data handling. The system's design emphasizes continuous data management, real-

time processing, fault tolerance through hot redundancy, and robust data integrity and security.

Criticality analysis underscores the need for warm and hot redundancy to handle outages, ensuring mission integrity and crew safety. The CDH architecture, utilizing SpaceWire for high-speed communication, integrates redundancy for enhanced reliability. Key components, including the On-Board Computer (OBC), Telemetry, Command, and Mass Memory (TCM) system, and Remote Terminal Units (RTUs), ensure efficient data processing and communication. Sensors monitor vital parameters, providing a robust framework for the CDH subsystem.

Overall, the CDH subsystem's design balances performance, reliability, and safety, enabling effective mission execution and adaptation to operational challenges.

13 Debris Capture

13.1 Requirements

Table 136: StarCheap Grabbing Mechanism Requirements

Requirement ID	Description
Gra-REQ-004	The system is capable of safely capturing debris without damaging it or other spacecraft.
Gra-REQ-005	Captured debris shall be secured in the storage module.
Gra-REQ-006	The system should be fully autonomous, the astronauts' role will only be to monitor operations and be ready to abort if need be.
Gra-REQ-007	Grabbing shall be performed without EVA.
Gra-REQ-008	The system should be 90% reusable.
Gra-REQ-009	The mass of the system must represent 4% of the total mass of the shuttle.
Gra-REQ-010	Must take into account the fault tolerance and apply redundancy if needed.
Gra-REQ-011	Once debris is captured, the system must be able to stabilize it.
Gra-REQ-012	Once debris is captured, the system must be able to securely grip the object to prevent it from escaping.
Gra-REQ-014	The capture system should feature modular or adjustable tools to accommodate various types of debris and adapt to unexpected challenges in debris size, shape, material, and mission variety.
Gra-REQ-015	The mechanism must be capable of safely interacting with debris with different surface types and geometries (e.g., smooth, rough, sharp, or irregular surfaces).
Gra-REQ-016	The mechanism must be able to reach debris within reasonable distance of the shuttle.
Gra-REQ-017	The capture system should use an active, flexible method.

13.2 System Analysis

Capture of an orbital debris is an operation of very high risk for any ordinary space vehicle, and even more so for a vehicle with crew onboard.

Capturing space debris involves significant technical challenges primarily due to the high relative velocities (up to $\tilde{7.8}$ km/s in low Earth orbit) and the often uncontrolled, tumbling motion of debris objects. The spacecraft must execute highly precise approach maneuvers using advanced guidance, navigation, and control (GNC) systems to match the debris' orbit and attitude without inducing additional momentum. Any miscalculation can result in a high-energy collision, potentially fragmenting the debris and exacerbating the space debris problem.

The capture mechanism—whether robotic arms, nets, harpoons, or adhesives—must be designed to tolerate dynamic loads and unpredictable contact forces while ensuring secure attachment to often irregular, non-cooperative targets.

Debris retrieval operations must consider delta-v limitations, thermal and structural stress on the capturing spacecraft, and potential shifts in the system's center of mass that can impact post-capture stability and maneuverability.

The debris capture mechanism must be comprised of:

- **A deployment mechanism** responsible for extending and positioning the debris capture system from the spacecraft to the target debris
- **A tether** to secure the debris once captured and to allow for retraction back to the spacecraft. The tether needs to be designed to withstand the high tensile forces of pulling debris, potentially moving at high speeds, while being lightweight to avoid additional strain on the spacecraft
- **The capture mean** responsible for physically capturing the debris and securing it for the subsequent retrieval phase
- **A retrieval mechanism** that pulls the tether and debris back into the spacecraft's hold or storage area once it has been captured

The design strategy for this subsystem was to first and foremost assess the mechanism used for the capture of the debris most adapted to the most stringent class of debris considered in the case of the mission, and subsequently assess the specific needs for each component and their specifications.

13.3 Debris use case characteristics

The considered debris for the dimensioned mission in this report is a space debris in LEO originally from a launch on Wed, 13 Nov 2019 UTC launched from the Taiyuan Space Center, China (TSC). Its orbital parameters and physical characteristics are resumed below.

Parameter	Value
Altitude	896
Orbit Type	Circular
Inclination	45.01°
Mass	1000 kg
Shape	Cylindrical
Length	4 m
Radius	0.68 m
Surface	9.057 m ²

Table 137: Debris characteristics and orbital parameters

13.4 Choice of Mechanism

There are two ways of approaching space debris removal :

Active debris removal (ADR), which refers to using spacecraft or robotic systems to intentionally seek out and remove space debris from orbit.

Passive debris removal involves designing satellites and rockets to reduce debris creation over time. This includes features like deorbit sails, tethers, or making sure spacecraft naturally re-enter the atmosphere at the end of their mission without external intervention.

In the context of StarCheap’s mission, the goal is for the shuttle to remove the debris from the orbit into its hold and then deorbit it upon reentry. As such, passive debris removal is of no interest in this study.

A survey is made of existing and potential active debris capture technologies, based on the studies by Svitina and Cherkasova [2023] et Arshad et al. [2025]; their candidacy is subsequently assessed in the context of StarCheap’s mission.

Active debris removal methods can be with contact or contactless:

Contact methods	Contactless methods
Rigid methods	Ion beam shepherds
Tentacles	Laser-based approaches
Robotic arms	Electrostatic tractors
Deorbiter satellites	Gravity tractors
Sling-Sat	Foam-based methods
Flexible methods (tethers)	Solar concentrators
Nets	
Gripper	
Harpoons	

Table 138: Survey of contact and contactless debris removal methods

13.4.1 Tentacle-Based Clasping Mechanisms

The tentacle-based clasping mechanism is a novel approach developed for active debris removal missions. The system comprises multiple extendable booms—termed “tentacles”—which utilize a combination of rotary actuators, spring-loaded hinges, dampers, latches, and linear actuators to enclose and secure orbital debris. All components are flight-proven, with established heritage in previous missions, contributing significantly to the system’s overall reliability.

Several configurations have been investigated, ranging from two-tentacle to four-tentacle systems. In the two-tentacle design, each tentacle comprises two booms with two rotational degrees of freedom and extends to approximately twice the length of the chaser satellite. Capture is achieved using a combination of rotary and linear actuators, supported by a leaf spring mechanism that facilitates secure latching. In contrast, four-

tentacle systems, although mechanically more complex, typically omit linear deployment and rely solely on rotary actuation. These tentacles are stowed via hold-down and release mechanisms and deployed through rotational movement.

Despite their advantages in reliability and cost-efficiency, primarily due to the use of simple mechanical systems, tentacle-based designs exhibit limitations in reach and adaptability. Their effectiveness is reduced when targeting fast-tumbling or irregularly shaped debris, and coordinating multiple tentacles introduces additional mechanical and control complexity. Consequently, the concept has seen limited further development, with research shifting toward robotic manipulators offering enhanced precision and flexibility.

13.4.2 Robotic Manipulators

Space manipulators offer a more controlled solution for debris mitigation and consist of a spacecraft equipped with at least one robotic arm. These systems are categorized into free-floating and free-flying manipulators. Free-flying manipulators actively control both position and attitude of the base, whereas free-floating systems passively conserve fuel by allowing the base to drift during operations.

While robotic arms have been extensively studied and show promise for precise capture, their rigid structures risk fragmenting debris during contact, particularly when dealing with fragile or deteriorating targets.

13.4.3 Mothership-CubeSat (Deorbiter Satellite) Approach

In this concept, a larger mothership performs the initial rendezvous with the target orbit, after which it deploys CubeSats for individual debris capture. This two-stage process allows potential removal of multiple debris objects but introduces complexity. Fast-tumbling targets may evade capture during the rendezvous phase, and the CubeSat itself may suffer damage during collision or docking. Nonetheless, this method remains a scalable strategy for large-scale debris remediation.

13.4.4 Sling-Sat Method

The Sling-Sat concept, also referred to as the Space Sweeper with Sling-Sat (4S), uses a spinning spacecraft to capture debris and subsequently sling it into a decaying orbit. The spacecraft exploits the momentum from the debris for propulsion, thereby reducing onboard fuel consumption for subsequent maneuvers. Although fuel-efficient and capable of removing multiple objects in a single mission, the technique introduces complexity in dynamic control, especially during debris interactions, and remains a theoretical construct requiring further validation.

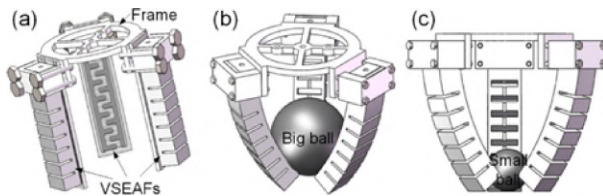


Figure 150: Soft gripper method for removing space debris Svtotina and Cherkasova [2023]

13.4.5 Tether-Based Systems

Tether systems—whether electrodynamic or momentum exchange-based—leverage long cables to facilitate propulsion or momentum transfer. Electrodynamic tethers interact with Earth’s magnetic field to produce thrust, enabling orbital adjustments or deorbiting without traditional propellants. Momentum exchange tethers, often rotating, transfer kinetic energy to debris to alter their trajectories.

Controlled deployment of tethers can be achieved via several methods, including impulse-based passive systems or thruster-assisted active deployment. Proper terminal conditions are ensured by adjusting initial deployment conditions, tension control, or thruster support. These systems offer significant propellant savings, particularly when the service spacecraft is substantially more massive than the debris.

The integration of robotic arms with tether systems enables combined detumbling and towing capabilities. However, tether dynamics introduce control challenges, particularly in microgravity, and exposure to environmental factors such as atomic oxygen, radiation, and micrometeoroids reduces long-term reliability.

13.4.6 Soft Gripper Technologies

Soft grippers are made from highly deformable elastomers and conform to the surface topology of the target, offering a low-damage alternative for delicate or irregular debris. Often integrated with electrostatic or gecko-inspired adhesives, these systems ensure reliable attachment in microgravity. Their compliance allows them to withstand partial failures and maintain function.

Nevertheless, they are susceptible to environmental degradation due to vacuum-induced outgassing, radiation exposure, atomic oxygen erosion, and thermal cycling. Electrorheological and magnetorheological actuators also face challenges related to arcing in plasma environments. These issues, along with vulnerability to puncture and material fatigue, necessitate careful material selection and robust protective coatings.

13.4.7 Net-Based Capture

Net-based systems are highly adaptable and capable of enclosing debris of various shapes and spin states without requiring direct contact. The net configuration—defined by geometry, size, and mass distribution—is tailored to the specific mission. Successful demonstrations, such as the one targeting the Envisat spacecraft, utilized nets with weighted

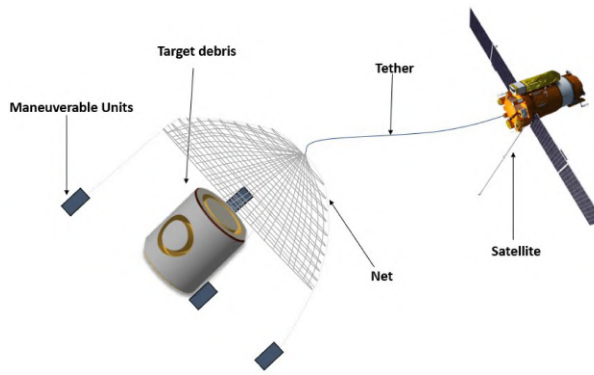


Figure 151: Net-based method for removing space debris Svtotina and Cherkasova [2023]

corners to ensure reliable entrapment.

The key advantages of this method include reduced reliance on specific contact points, lowered risk of fragmentation, and tolerance to debris inertia. However, the capture of fast-spinning or asymmetrically tumbling targets presents challenges, particularly regarding net stability and control during deployment.

13.4.8 ElectrodynamiC Tether Capture (EDDE)

The ElectroDynamic Debris Eliminator (EDDE) is a solar-powered spacecraft equipped with a conductive tether and a capture net. Operating without fuel, EDDE navigates via electrodynamiC forces generated through interaction with Earth's magnetic field. The system rotates to enhance control authority and can capture objects up to 8 tonnes depending on spin rate.

This method is ideal for removing large, slow-rotating debris (>100 kg), which constitute the majority of high-risk objects. However, reduced plasma density at higher altitudes limits efficiency, and aerodynamic drag in low Earth orbit may counteract generated thrust.

13.4.9 Tethered Gripper Systems

This concept employs a three-finger gripper attached via tether to a satellite. The gripper is launched toward the target and, upon successful capture, the tether facilitates detumbling or deorbiting. Advanced guidance and control algorithms govern rendezvous, capture, and stabilization.

While the approach is advantageous for its flexibility and reduced collision risk, it introduces complex dynamics due to tether behavior. Entanglement risks, stability loss upon impact, and high fuel demands for active stabilization are key limitations. Additionally, the method lacks generalizability, as the gripper must be tailored to each debris object.

13.4.10 Harpoon-Based Tether Systems

Harpoon-based capture employs a projectile equipped with barbs and a crushable tip, fired at the debris and tethered to the capturing spacecraft. Upon impact, energy is absorbed, and the barbs secure the harpoon in place, allowing detumbling or towing via the tether.

Although capable of capturing irregular debris, this method is prone to fragment generation due to the physical penetration of the target. It also suffers from potential targeting inaccuracies and remains under experimental evaluation regarding practical implementation and reliability.

13.4.11 Solar Concentrator Methods

Initially developed for asteroid deflection, solar concentrators have been adapted for orbital debris mitigation. The system focuses high-intensity light onto debris, inducing surface sublimation and generating thrust for orbit modification. Applicable to objects with specific area-to-mass ratios, this method operates over extended durations (hundreds of days), making it unsuitable for time-critical deorbiting missions.

13.4.12 Laser-Based Removal

Laser systems for debris removal operate in two primary modes: direct ablation, where surface material is vaporized, and ablation back-jet, where the reaction force from vaporized material modifies the object's trajectory. These contactless methods allow standoff operation but face limitations in debris breakup risk, reentry times, and reduced efficacy against rapidly tumbling targets.

13.4.13 Ion Beam Shepherding

The ion beam shepherd concept uses a spacecraft equipped with a low-divergence ion thruster to exert force on a debris target without physical contact. The spacecraft “parks” in front of the debris and directs ions at its surface, transferring momentum to alter its orbit.

While this approach eliminates the need for capture mechanisms, it requires substantial propellant to counteract its own thrust during operation, effectively halving usable fuel. This limits the number of objects that can be processed and reduces mission efficiency.

13.4.14 Origami-Inspired Capture Mechanism

Inspired by origami folding principles, this system proposes a multimodal, deployable structure capable of transforming into various capture geometries. For small debris (1–10 cm), a spherical caging configuration with a geodesic design is used, whereas larger debris is captured with a three-finger layout.

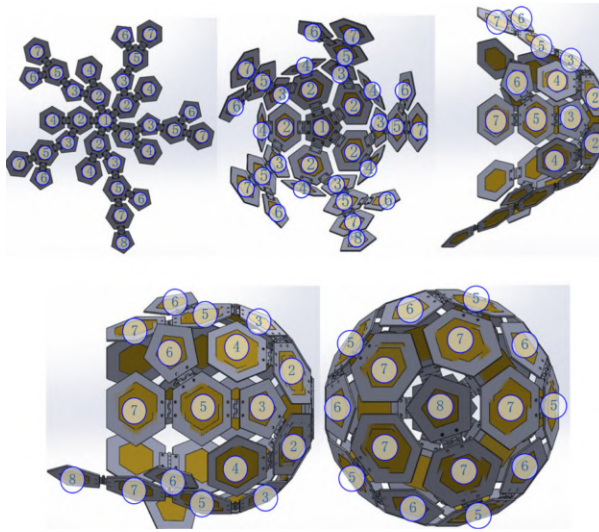


Figure 152: Novel origami Capture concept Svtotina and Cherkasova [2023]

Advantages include adaptability to debris geometry, compact storage volume pre-launch, and the ability to restrict target motion during capture. However, the mechanism is unproven, complex to control, and not currently scalable to larger debris objects.

13.5 Results and Choice

Choosing a candidate for a shuttle-based capture method demands 3 aspects, based on the requirement of capturing a debris and storing it within the storage module on-board in an efficient and safe manner:

- active capture contact-based system
- autonomy
- flexibility
- safety
- feasibility
- durability
- reusability

As such we can disregard the contactless active removal methods as they are not feasible for large debris.

From the survey, we evaluate 5 candidates based on the aforementioned criteria :

Solution	Advantages	Disadvantages
Nets	<ul style="list-style-type: none"> • no need for grasping point • wide variety of debris • less risk of fragmentation • no reliance on target inertia • reach possibility • flexibility • proven 	<ul style="list-style-type: none"> • control of target dynamics • asymmetric deployment • oscillations • tearing, twisting
Hard Gripper	<ul style="list-style-type: none"> • flexibility • proven 	<ul style="list-style-type: none"> • need for grasping interface • limited debris application • fragmentation • mechanical reliance • limited range
Harpoon	<ul style="list-style-type: none"> • no need for grasping point • proven • wide variety of debris 	<ul style="list-style-type: none"> • high probability of failure • debris degradation • system damage • limited range
Soft Grip	<ul style="list-style-type: none"> • no need for grasping point • lightweight, cost effective • wide variety of debris 	<ul style="list-style-type: none"> • novel • sensitivity to space env. • control of target dynamics
Origami	<ul style="list-style-type: none"> • no need for grasping point • wide variety of debris 	<ul style="list-style-type: none"> • novel • complex

Table 139: Assessment of candidate Active Debris Removal Methods

Due to the overwhelming advantages of the net-based solution, it is the chosen candidate for the debris capture method of the StarCheap shuttle.

13.6 System Specifications

The following preliminary specifications are established for the complete system, based on preliminary geometric analysis and loads assessments. Assumptions are made for required control authority and safety measures.

13.6.1 Deployment Mechanism

The deployment mechanism is responsible for extending the net structure from the spacecraft to a position suitable for capture, while maintaining appropriate spatial alignment with the debris. The deployment must be reliable, controlled, and minimize disturbances to the spacecraft.

A solution of an inflatable ring structure and a compressed gas launcher has been selected. The inflatable ring unfolds the net into a wide conical shape in zero gravity, maintaining uniform tension along the rim. This ensures full net opening without mechanical complexity.

The compressed gas-based deployment offers a clean, low-shock method of launching the net and corner weights away from the spacecraft. This avoids high mechanical forces and reduces risk to onboard systems.

We wish the system to extend up to 10–15 meters from the spacecraft, providing an adequate buffer zone for safe deployment away from sensitive instruments. We set a target 1–3 m/s to match debris velocity and close the distance without aggressive momentum exchange.

13.6.2 Tether

The tether connects the capture net to the spacecraft and transmits the forces required to secure and eventually retrieve the debris. It must withstand high tensile loads while remaining lightweight to avoid increasing spacecraft mass and inertia.

A high-strength, space-rated synthetic fiber such as Kevlar, Technora, or Dyneema should be selected for the tether due to their tensile strength-to-weight ratio and resistance to radiation and micrometeoroids.

We set a tether length of 30 meters to allow for flexible net deployment and maneuverability. This distance ensures the net can be projected at a safe distance without entangling the spacecraft and still provides enough room for maneuvering and damping retrieval motion.

The debris, with a mass of 1000 kg, could impart significant dynamic loads during capture and retrieval. Assuming a relative closing velocity of 0.5 m/s and a deceleration time of 0.5 seconds:

$$F = \frac{mv}{t} = 1000N \quad (158)$$

Applying a safety factor 3–5, we require a tether capable of withstanding 3000–5000 N. Using material strength of 3000 MPa, we assess that a 4–5 mm diameter rope provides sufficient tensile area while keeping system mass low (0.1–0.2 kg for 30 m length).

We note that considerations should be made for protection against UV exposure, atomic oxygen, and minor debris impacts, such as coating or an outer sheath.

13.6.3 Capture Mechanism - Net

The capture net serves as the primary physical interface between the spacecraft and the target debris object. Its function is to enclose the debris, conform around its geometry, and retain it securely throughout subsequent maneuvers. The net must be capable of capturing the object regardless of its orientation, provide reliable containment under dynamic conditions, and remain lightweight to minimize impact on spacecraft mass and inertia budgets.

13.6.3.1 Geometric Design and Sizing

A conical net geometry has been selected for its simplicity, scalability, and effective enveloping capability. The net is deployed in a cone shape with the wide opening facing

outward from the spacecraft, allowing for rapid expansion and maximum surface area during capture. A key driver in the sizing of the net is the requirement to accommodate the debris object in all possible approach orientations.

The target debris is a cylindrical object with a length of 4.0 meters and a radius of 0.68 meters, corresponding to a diameter of 1.36 meters. While a net sized to match this diameter would be sufficient for a frontal or axial approach (i.e., with the debris axis aligned with the net axis), this approach cannot be assumed in an uncontrolled environment. In the worst-case scenario, where the debris presents its long axis perpendicular to the net opening (i.e., side-on), the effective frontal projection of the debris equals its full length of 4.0 meters. To ensure successful capture in this configuration, the net must have a mouth diameter exceeding this maximum dimension

Taking into account this worst-case orientation, a net mouth diameter of 6.0 meters has been selected. This dimension provides a 2.0-meter margin over the projected length of the debris, allowing for positional inaccuracies and lateral drift during deployment. To fully envelop the debris, the net must also be sufficiently deep. A net depth of 6.5 to 7.0 meters is chosen to ensure that, even after accounting for folding and partial wrapping, the debris remains securely enclosed within the net volume.

The net is designed with a mesh size of 0.3 meters, which represents a compromise between mass efficiency and containment effectiveness. This spacing ensures that large features of the debris cannot pass through the mesh, while reducing the total material volume required. The mesh is composed of radial and circumferential threads, forming a flexible yet durable lattice that can deform under load and conform around the debris body.

In a similar fashion to the tether, the net should be fabricated using space-rated high-strength synthetic fibers such as Kevlar, Technora, or Dyneema. These materials are chosen for their excellent tensile strength-to-weight ratios (typically 2–3 GPa), resistance to UV radiation and atomic oxygen, and proven flight heritage in space tether and restraint applications. Individual thread diameters are selected in the range of 4 to 5 millimeters, ensuring sufficient tensile load capacity while maintaining flexibility.

Based on the projected deployment volume and material density, the total net mass is estimated at 5 to 10 kilograms, depending on mesh density and reinforcement details. In its stowed configuration, the net folds compactly to occupy a volume of approximately 0.015 to 0.03 cubic meters.

13.6.3.2 Closure Mechanism

In addition to the primary drawstring mechanism, a magnet-based closure system is proposed to secure the mouth of the capture net following engagement with the target debris. This method provides a passive, self-aligning means of closure that functions without the need for complex actuators or continuous power. The use of magnetic latches in space applications is advantageous due to their low mass, minimal mechanical complexity, and the ability to operate reliably in vacuum conditions.

The closure system consists of high-strength neodymium magnets (NdFeB, grade N52) embedded at discrete intervals along the net's outer rim. When the net wraps around

the debris object, these magnets are brought into contact across opposing edges of the net mouth, creating a set of magnetic latch points that hold the structure closed. The number, strength, and distribution of these magnetic pairs are sized to withstand the tensile loads generated during and after the capture event.

The design must account for the maximum radial force that may act to reopen the net during dynamic capture events. Based on the expected mass of the target debris (1,000 kilograms) and a conservative estimate of post-capture motion ($v=0.5 \text{ m/s}$, $t=0.5\text{s}$) the force acting on the closure due to the debris momentum is:

$$F = \frac{mv}{t} = 1000N \quad (159)$$

To ensure robustness under off-nominal conditions and include a safety margin, we apply a safety factor of 2.5 and account for radial tension due to net contraction and uneven load distribution with a factor of 1.5, bringing the total closure load requirement to approximately 3750 N.

To resist this load, twelve magnetic latch points are distributed evenly around the rim of the net's 6-meter diameter opening, resulting in one latch every 30 degrees.

The holding force required at each magnet pair is thus:

$$F_{\text{latch}} = \frac{F}{12} = 313N \quad (160)$$

Assuming available N52-grade neodymium magnets provide high attractive forces in compact forms, we size a single $50 \times 25 \times 10$ mm rectangular magnet which can produce approximately 250–300 N of holding force when paired face-to-face with an identical unit. To meet the required force per latch, two such magnets per side can be used, providing:

$$F_{\text{mag/pair}} = 2 \times 250 = 500N \quad (161)$$

which exceeds the required 313 N per latch with margin. This theoretically ensures that each latch point can tolerate localized spikes in load without detachment.

Considerations should be made so that the magnets are encapsulated in reinforced textile pouches or molded polymer housings sewn directly into the net's perimeter. Alignment tabs or tapered magnet edges could ensure reliable engagement upon contact. Nickel-coating could provide resistance to atomic oxygen and prevent degradation from thermal cycling.

13.6.3.3 Summary of Net Specifications

13.6.4 Retrieval Mechanism

The retrieval system gradually pulls the captured debris back toward the spacecraft while absorbing impact energy and controlling tether tension to avoid sudden impulses.

We consider a motorized winch system is used to reel in the tether. The winch includes a torque-limited spool, braking capability, and closed-loop tension control to manage load

Parameter	Value
Net Shape	Conical
Mouth Diameter	6.0 meters
Net Depth	6.5–7.0 meters
Mesh Size	0.3 meters
Material	Kevlar, Dyneema, or Technora
Thread Diameter	4–5 mm
Closure System	Magnetic Latching
Load Capacity	$\geq 5000 \text{ N}$ (with safety factor)
Net Mass (est.)	5–10 kg
Stowed Net Volume (est.)	0.015–0.03 m ³

Table 140: Summary of Net and Closure Mechanism Specifications

changes during retraction.

With a 1000 kg debris load and a winch drum radius of 0.05 meters, the winch must apply sufficient torque:

$$T^{\circ} \text{winch} = F_{\text{tether}} \cdot r = 50 \text{ Nm} \quad (162)$$

If the torque required by the winch to retrieve the captured debris is directly linked to the tension in the tether and the radius of the winch drum, then the torque at the winch must be sufficient to overcome the forces acting on the debris during retraction.

The retrieval speed determines how quickly the captured debris is reeled back into the spacecraft. For this system, the linear retrieval speed is arbitrarily designed to range from 0.1 m/s to 0.3 m/s.

The linear retrieval speed v is related to the angular velocity ω of the winch drum by the following equation:

$$v = \omega \cdot r,$$

where r is the radius of the winch drum. Assuming a winch drum radius of $r = 0.05 \text{ m}$ (5 cm), we can calculate the angular velocity required to achieve a retrieval speed of 0.1 m/s. Substituting into the equation:

$$\omega = \frac{v}{r} = \frac{0.1}{0.05} = 2 \text{ rad/s.}$$

Thus, to achieve a linear retrieval speed of 0.1 m/s, the winch drum must rotate at an angular velocity of 2 rad/s.

The power required by the winch to achieve this higher speed is:

$$P_{\text{winch}} = T_{\text{winch}} \cdot \omega = 50 \text{ Nm} \cdot 6 \text{ rad/s} = 300 \text{ W.}$$

Thus, the winch requires 300 W of power to achieve a retrieval speed of 0.3 m/s.

13.6.5 Specification Synthesis

Component	Specification
Net	Cone, 6.0 m diameter, 6.5–7.0 m depth, 0.3 m mesh
Tether	20–30 m, 4–5 mm diameter, 3000–5000 N capacity
Deployment	Inflatable ring + compressed gas launch
Retrieval	Motorized winch, 500 Nm torque, 0.1–0.3 m/s speed

Table 141: Summary of System Specifications

13.7 System Limitations

The previous section outlined a preliminary concept and design for StarCheap’s debris capture mechanism. While the proposed solution appears promising, several aspects of the system could present challenges during deployment or operation.

Specifically, the initial positioning of the magnets on the shuttle may impede the deployment of the net if not carefully planned, particularly when accounting for potential movements of the system during operations before deployment.

Additionally, considerations must be made for scenarios involving tumbling or unstable debris, which could exceed the handling capabilities of the winch or tether. In a worst-case scenario, there is also the risk of debris colliding with the shuttle or becoming lodged in the cargo bay doors.

To ensure the system’s viability, a detailed study is recommended, where the dynamics of net unfolding are simulated under various debris conditions. Software such as Matlab/Simulink could be used for such simulations, with the system’s specifications adjusted based on the results obtained. A node-based model of the net dynamics would provide valuable insight into the feasibility of the system.

13.8 Operational Assessment

A high-level operational flowchart for the process of capturing the debris and later disposing of it before reentry is made. It outlines not only the operational processes necessary for capture, but also the escape routes in case of anomaly or critical issues.

We note that the previsional operational scenario accounts for multiple checks (Go/No Go) before initiating the capture operation.

Within the operation, multiple failure scenarios are considered, from deploying the net and having to abort to an issue during the retrieval of the debris to the shuttle.

The operational flowchart has highlighted the necessity to include a mechanism that will full cut the tether between the shuttle and the debris should the need arise.

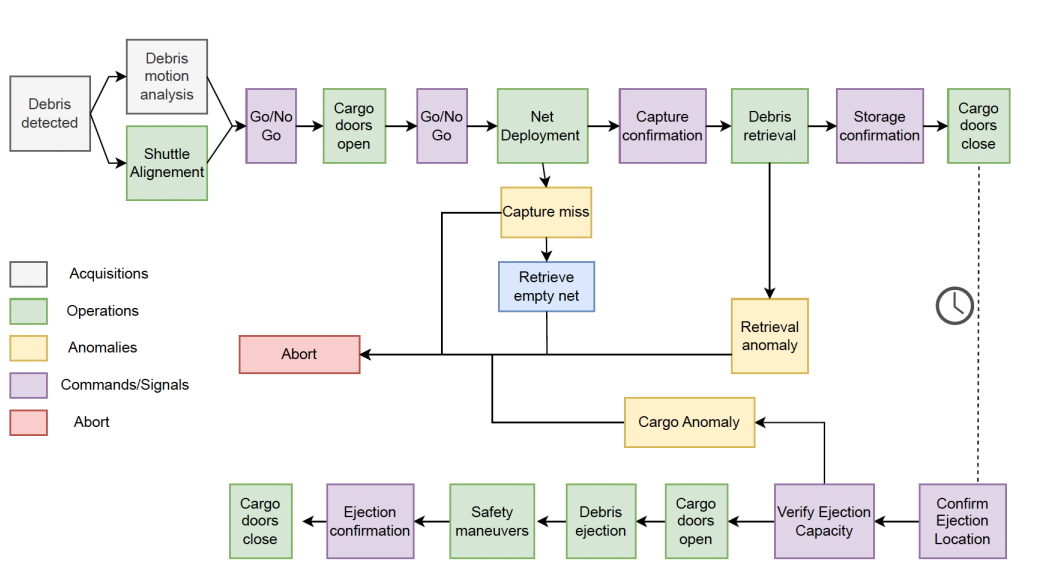


Figure 153: Capture Operational Flowchart

14 System Lifecycle Implementation

14.1 Manufacturing

The manufacturing of the StarCheap is a key phase in the transition from design to hardware. It involves the production of flight-representative components and is structured in a modular and phased approach. Subsystems are manufactured in parallel—such as the propulsion module, crew capsule, and cargo bay with independent quality loops to allow faster iteration and validation. All modules then converge toward a single final assembly line, located in a cleanroom facility compliant with *ISO-8* standards. Long lead-time items, including tanks, engine nozzles, and composite skins, are identified early in the project and prioritized to ensure integration flow.

14.1.1 Supplier Strategy and Make-or-Buy Logic

A hybrid production strategy is applied, combining different sourcing approaches based on component sensitivity and complexity. In-house production is reserved for sensitive or IP-critical items, such as CDH boards, ignitors, and fuel cells. Components requiring high-complexity manufacturing or those that are space-qualified are procured from external suppliers. For propulsion and structural assemblies, long-term strategic industrial partners are selected to reduce development risk. Each supplier is qualified through a standard process involving audits, capability matrices, and Production Part Approval Process (PPAP), and must comply with ECSS or NASA quality standards.

14.1.2 Quality Control and Inspections

Quality assurance (QA) follows a dual approach to ensure manufacturing reliability and compliance. Inline quality is maintained through visual and dimensional inspections conducted after each manufacturing step, using predefined go/no-go criteria. At the end of the process, final verifications are carried out using Non-Destructive Testing (NDT) methods. These include ultrasonic testing for composite bonding, X-ray imaging for welded joints, CT scans for 3D-printed parts, and pressure as well as leak tests for tanks.

14.2 Assembly, Integration and Testing

The AIT phase is a critical part of the development of the StarCheap. It ensures that all hardware and software subsystems are physically assembled, functionally integrated, and verified under mission-representative conditions. This process includes three main stages: assembly, integration, and testing.

14.2.1 Assembly

Assembly refers to the mechanical and electrical construction of each subsystem prior to full vehicle integration. Each functional module—such as the propulsion module, cargo bay, or pressurized crew capsule—is assembled individually in an *ISO-8* cleanroom using dedicated tooling (jigs, alignment frames, ESD-safe platforms).

Mechanical, thermal, and electrical interface compatibility is verified at this stage using Interface Control Documents.

14.2.2 Integration

Integration refers to the physical and logical connection of all subsystems into the final spacecraft configuration. This includes:

- Routing of fluid lines (NOFBX, helium, cooling),
- Connection of data buses (SpaceWire, MIL-STD-1553) and power lines,
- Installation of thermal protection systems and micrometeoroid shielding,
- Mounting of the spacecraft on its ground support equipment (MGSE),
- Use of mass or payload simulators if necessary.

The goal is to obtain a flight-representative configuration suitable for testing. Integration follows detailed AIT procedures defined in the AIT Plan (AITP) and is aligned with the program's industrial and verification schedule.

Particular attention is given to several key aspects during manufacturing and integration. Harnesses are routed in a clean and secured manner to minimize the risk of electromagnetic interference. All critical components and connectors are positioned to ensure easy accessibility for testing and maintenance. Furthermore, every operation is fully documented through detailed work orders, checklists, and activity logs, ensuring traceability and compliance throughout the process.

14.2.3 Testing Campaign

After assembly and integration, a comprehensive series of functional, performance, environmental, and safety tests are performed. The table below summarizes the key tests identified for the StarCheap.

Table 142: AIT – Assembly, Integration and Testing Test Matrix

Test Type	Name	Objective	Description
Functional Test	CDH Safe Mode Test	Validate MSU triggering on anomalies	Simulate subsystem failure and verify CDH switches to safe mode via Monitoring and Safe mode Unit (MSU).
Performance Test	Docking Sensors Calibration	Validate sensor accuracy for docking maneuvers	Verify LIDAR, force, position, and strain sensors during approach phase (S3 to S4.1), including relative pose measurement.
Integration Test	Docking System Interface Test	Ensure mechanical and communication interface compatibility	Test passive and active docking ports, SCS/HCS alignment, and sealing integrity procedures as per IDSS standard.

Test Type	Name	Objective	Description
Functional Test	Power Distribution Validation	Check EPS distributes power within specs	Inject load profiles and verify PCDU switches, current sensors and regulators within tolerance across operation modes.
Environmental Test	Thermal Cycling	Validate thermal resilience	Perform thermal vacuum testing for critical components (e.g. CDH, sensors) across -65°C to $+125^{\circ}\text{C}$ ranges.
Functional Test	Gimbal and TVC Actuation Test	Validate thrust vectoring system	Run actuation cycles on spherical gimbal to assess movement range and bearing friction limits during hover/reentry.
Performance Test	Autonomous Rendezvous Sequence	Evaluate VBN and GN&C system integration	Simulate full autonomous rendezvous using visual-based navigation (Auricam D80) and Kalman-filter-based sensor fusion.
Safety Test	Abort System Activation Test	Ensure emergency sequence is reliable	Trigger manual and automatic aborts from critical phases (reentry, docking) and assess ejection, system reset, and alerting.
Functional Test	SpaceWire Network Routing Test	Verify internal communication and error handling	Inject packet errors, monitor MSU detection, test routing through logical and physical SpaceWire addresses.
Integration Test	Payload Grabbing and Securing Test	Assess capture system reliability	Test CPTR mechanism on simulated debris in motion and confirm gripping, stabilization, and locking sequence.
Functional Test	GNSS + IMU Fusion Test	Validate position and velocity estimation accuracy	Assess GNSS signal handling and drift correction via Kalman filter over time and maneuvers.

14.3 Maintenance and Refurbishment

To ensure safe, efficient, and repeatable missions, the StarCheap system incorporates a robust maintenance and refurbishment plan. This plan is informed by the system's design, its operational constraints, reliability targets (RAMS), and risk mitigation strategies. Maintenance is triggered at the end of each mission cycle—specifically after return to Earth—and aims to guarantee airworthiness and flight-readiness for the next launch.

The current scope covers servicing operations following standard round-trip missions be-

tween Earth and an orbital station. Maintenance activities begin upon vehicle recovery and continue until preparations are complete for the next rollout. The servicing strategy combines cycle-based maintenance—performed after each use or after a specified number of cycles—with condition-based maintenance, which is driven by telemetry analysis, diagnostics, or the detection of anomalies during or after flight operations. This dual approach ensures both reliability and efficiency in vehicle turnaround.

14.3.1 Post-Mission Preliminary Inspection

After every mission, a preliminary inspection is conducted to detect any signs of damage or degradation that could impact future operations. This process includes a visual inspection of external components such as the structure, thermal insulation, and docking ports. In parallel, post-flight telemetry logs are analyzed to identify performance anomalies, parameter drifts, or any limit violations. Special attention is given to critical safety checks, particularly for crew-rated systems, propulsion safety loops, and life support equipment, to ensure continued compliance with safety and mission-readiness standards.

14.3.2 Diagnostic Testing

Functional testing is carried out on all major systems to assess wear and verify operability:

- **Electronics:** test of OBC, CDH, attitude and orbit control systems (AOCS), and avionics buses.
- **Propulsion:** leak and performance tests on tanks, thrusters, valves, and gimbals.
- **Communications:** RF link tests, antenna alignment, and transceiver health checks.

14.3.3 Corrective Maintenance After Anomalies

When anomalies are observed during flight or test, targeted investigations are launched:

- **Root cause analysis:** supported by test logs, telemetry, and component history.
- **Failure resolution:** redesign, shielding, or operational constraint added if needed.
- **Component reinforcement:** if needed to avoid recurring failure in future missions.

14.3.4 Maintenance Scheduling and Cycles

Three levels of intervention are defined:

- **Immediate post-mission maintenance:** performed after every mission, includes visual inspection and diagnostics.
- **Intermediate servicing:** after a defined number of cycles or upon early degradation signs; includes partial disassembly.
- **Overhaul:** after a major cycle count; includes deep disassembly, replacement of life-limited parts, and full recertification.

The frequency and nature of intervention are determined by the component specifications, RAMS targets, and accumulated flight data.

14.4 End-of-Life and Sustainability

The StarCheap system is designed with sustainability as a core principle, both in terms of its impact on the space environment and its lifecycle footprint on Earth. The end-of-life (EOL) phase is carefully planned to ensure full compliance with international debris mitigation guidelines and to support environmentally responsible operations.

14.4.1 End-of-Life Strategy

The default EOL strategy for StarCheap depends on its mission role:

- **Nominal case:** the shuttle returns to Earth for refurbishment and reuse after completing its orbital mission. This reusable approach significantly reduces waste and long-term orbital congestion.
- **Contingency case:** if safe return is not possible (e.g., propulsion failure, irreversible anomaly), a controlled deorbit maneuver is executed to ensure atmospheric burn-up or disposal to a graveyard orbit (depending on altitude and orbit class).

The CDH subsystem includes autonomous EOL logic with fail-safes to trigger passivation or disposal if required.

14.4.2 Environmental Impact

A preliminary lifecycle assessment (LCA) has been carried out to evaluate the environmental performance of the StarCheap system across its manufacturing, operational, refurbishment, and end-of-life phases. One of the key findings is a significant reduction in the CO₂ footprint, with hardware reuse expected to lower emissions per mission by over 60% compared to traditional single-use launchers. The adoption of a modular servicing strategy also contributes to waste minimization by avoiding full system disposal and reducing production scrap. Additionally, the handling of hazardous materials is carefully managed, ensuring that all fluids or components classified as hazardous are either fully recoverable or effectively neutralized following mission completion.

15 Conclusion

The OrbitXplorer project in designing the StarCheap space shuttle is challenging.

Developing a system capable of operating in LEO while interacting with various space assets required a comprehensive approach. More than just a standalone spacecraft, the StarCheap is part of a system of systems, interacting with other vehicles. In a context where the number of objects in orbit continues to increase, addressing the issue of space debris has become essential. Our shuttle contributes to this effort by offering a modular platform capable of capturing, transporting, and safely deorbiting objects.

From a technical perspective, we made several key design choices to meet the mission objectives. The structure is based on a carbon shell and aluminium reinforcements, offering a compromise between mechanical strength and low mass. For propulsion, we selected a green propellant that combines efficiency with reduced toxicity. The vehicle is wingless and relies on retropropulsion for controlled re-entry. Electrical power is provided by a fuel cell, enabling high energy density and continuous power delivery during capture operations. To ensure autonomous and safe debris removal, we integrated a net-based capture system. Communication with mission control is maintained through relay satellites. Finally, the system is designed for in-orbit refueling via docking.

Beyond the technical outcome, this project helped us apply our knowledge to a complex space engineering problem. We gained experience in design trade-offs, teamwork, and systems integration. We also improved our ability to manage constraints related to mass, power, volume, and reliability.

References

- Spacewire - ccstds packet transfer protocol. Standard ECSS-E-ST-50-53C, European Space Agency, ESTEC, Noordwijk, The Netherlands, February 2010.
- Aerospace structural design – course notes. Lecture notes, 2023. Politecnico di Milano, MSc Aerospace Engineering.
- AAC Clyde Space. Sirius obc leon3ft. AAC Clyde Space Datasheet, 2020a. Accessed on 2023-10-01.
- AAC Clyde Space. Sirius tcm leon3ft. AAC Clyde Space Datasheet, 2020b. Accessed on 2023-10-01.
- National Aeronautics and Space Administration. Nasa docking system (nds) users guide. Technical Report NAS15-10000, Johnson Space Center, Houston, Texas, Nov 2010.
- European Space Agency. Esa - heat pipes in space applications, 2019. URL https://www.esa.int/Enabling_Support/Space_Engineering_Technology/Heat_Pipes_in_Space. Accessed 2025-04-10.
- H. Julian Allen and A. J. Jr. Eggers. A study of the motion and aerodynamic heating of ballistic missiles entering the earth's atmosphere at high supersonic speeds, 1958.
- Muneeb Arshad, Michael C.F. Bazzocchi, and Faraz Hussain. Emerging strategies in close proximity operations for space debris removal: A review. *Acta Astronautica*, 228: 996–1022, March 2025. doi: 10.1016/j.actaastro.2024.12.017.
- AZoM. Materials used in space shuttle thermal protection systems. <https://www.azom.com/article.aspx?ArticleID=11443>, 2014. Accessed April 2025.
- D. R. Bartz. A simple equation for rapid estimation of rocket nozzle convective heat transfer coefficients. *Jet Propulsion*, 27(1):49–51, 1957.
- BASF. Sorbead® co2 dehydration. <https://chemical-catalysts-and-adsorbents.basf.com/global/en/adsorbents/sorbead-for-ccs>, 2023.
- Michael Belair, Marcus Hennekens, Stephen Barsi, Pedro Herraiz Alijas, Tobias Langner, and Jan-Hendrik Meiss. Artemis i orion-esm propulsion system engine performance. In *Proceedings of the Conference*, Glasgow, Scotland, May 2024. Conference Paper.
- John J. Bertin. *Hypersonic Aerothermodynamics*. American Institute of Aeronautics and Astronautics, 1994. ISBN 9781563470367.
- D. BLEVINS and C. HOHMANN. Description of the space shuttle reaction control system. *11th Propulsion Conference*, 1975.
- NASA Johnson Space Center. Nasa thermal control handbook: Satellite thermal control, 2017. URL https://www.nasa.gov/sites/default/files/atoms/files/nasa_thermal_control_handbook.pdf. Accessed 2025-04-10.
- Dean R. Chapman. *An Approximate Analytical Method for Studying Entry into Planetary Atmospheres*. NACA TN 4276. NACA, Washington, D.C., 1958.

Scott Dickerson Stephen Didziulis Peter Frantz Charles Gurrisi, Raymond Seidel and Kevin Ferguson. Space station control moment gyroscope lessons learned. January 2009.

Thomas T. Chen, Camilah D. Powell, and Michael K. Ewert. Life support baseline values and assumptions document. Technical Report NASA/TP-2015-218570, Rev2, NASA Johnson Space Center, 2022. URL https://ntrs.nasa.gov/api/citations/20210024855/downloads/BVAD_2.15.22-final.pdf. Accessed: 2025-04-18.

John D. Star ship aerodynamics estimate. <https://forum.nasaspacesflight.com/index.php?action=dlattach;topic=56619.0;attach=2109604;image>, 2022.

et al. Davidson. Nofbx monopropellant for space propulsion applications. Technical Report NASA/TM-2012-217569, NASA, 2012.

European Cooperation for Space Standardization. Ecss-e-hb-32-26a: Mechanical shock design and verification handbook. <https://ecss.nl/standard/ecss-e-hb-32-26a-mechanical-shock-design-and-verification-handbook/>, 2010. Accessed: 2025-04-15.

C. Gibson and C. Humphries. Orbital maneuvering system design evolution. Technical report, NASA Lyndon B. Johnson Space Center, Houston, Texas 77058, 1988. Technical Report.

John L. Goodman. Rendezvous and proximity operations of the space shuttle. Technical report, United Space Alliance, LLC, NASA Johnson Space Center, Houston, Texas 77058, 1988. Source of Acquisition: NASA Johnson Space Center.

Sandi Habinc and Marko Isomäki. Implementing the ccsds packet transfer protocol for ecss spacewire links. *SpaceWire Standardisation (Poster)*, 2023. Aeroflex Gaisler, Kungsgatan 12, SE-411 19 Göteborg, Sweden.

Robert A. Hall, Steven Hough, Carolina Orphee, and Keith Clements. Design and stability of an on-orbit attitude control system using reaction control thrusters. Technical report, Jacobs ESSSA Group, Huntsville, AL, 35812, 2023.

Dieter K. Huzel and David H. Huang. *Modern Engineering for Design of Liquid-Propellant Rocket Engines*, volume 147 of *Progress in Astronautics and Aeronautics*. American Institute of Aeronautics and Astronautics, 1992. ISBN 978-1563470134. URL https://books.google.com/books/about/Modern_Engineering_for_Design_of_Liquid.html?id=TKdIbLX51NQC.

James F. Marchman III. *Aerodynamics and Aircraft Performance*. James F. Marchman III in association with the University Libraries at Virginia Tech, 3rd edition, 2021.

ECAPS / IspKart. Lmp-103s and nofbx performance datasheet. Technical datasheet, 2019. Green monopropellant engine specifications.

M. Kaushik. Hypersonic flows. In *Theoretical and Experimental Aerodynamics*. Springer, Singapore, 2019. ISBN 978-981-13-1677-7. doi: 10.1007/978-981-13-1678-4_10. URL https://doi.org/10.1007/978-981-13-1678-4_10. Chapter 10.

Robert Klar, Christopher Mangels, Sandra Dykes, and Michael Brysch. Design considerations for adapting legacy system architectures to spacewire. *SpaceWire Networks and Protocols*, 2023. Short Paper, Southwest Research Institute, San Antonio, TX.

Anett Krammer, Luc Blecha, and Marc Lichtenberger. Fin actuation, thrust vector control and landing leg mechanisms design for the retalt vtv launcher. *CEAS Space Journal*, 14:577–591, 2022. doi: 10.1007/s12567-021-00421-0. URL <https://doi.org/10.1007/s12567-021-00421-0>. Received: 15 July 2021 / Revised: 15 November 2021 / Accepted: 31 December 2021 / Published online: 13 January 2022.

Koushal Kumar, Manish Kumar, and Arun Kumar. Design and analysis of composite overwrapped pressure vessel with analysis of various overwrapping pattern. *International Journal for Modern Trends in Science and Technology*, 8(6):33–46, 2022. doi: 10.46501/IJMTST0806005. URL <https://www.researchgate.net/publication/361465349>. ISSN: 2455-3778.

Hailian Li, Mohamed Eddaoudi, Thomas L. Gro, and O. M. Yaghi. Establishing micro-porosity in open metal-organic frameworks: Gas sorption isotherms for zn(bdc) (bdc = 1,4-benzenedicarboxylate). *Communication*, August 1998. Accessed through your institution.

Martin-Baker Aircraft Company Limited. US18E Ejection Seat for F-16 Block 70/72. <https://www.martin-baker.com/>, 2025. Data Sheet.

Pat B. McLaughlan, Scott C. Forth, and Lorie R. Grimes-Ledesma. Composite overwrapped pressure vessels, a primer. Technical Report NASA/SP-2011-573, NASA Johnson Space Center, 2011. Available at <https://ntrs.nasa.gov/citations/20110008406>.

Heather Mera, Joel A. Kirkland, Ryan E. Wall, and Timothy Cichan. Integrating orion and initial lunar gateway environmental control and life support systems. Technical report, Lockheed Martin Space, 12257 S. Wadsworth Blvd, Littleton, CO 80127, 2023. Technical Report.

Jacques MOULIN. System aspects of the atmospheric re-entry.

G. S. Mungas, D. J. Fisher, C. D. Mungas, and B. Carryer. Nofb monopropellants – background, characterization, and testing. nofbxTM: A new non-toxic, "green" propulsion technology with high performance and low cost. nofbxTM single stage to orbit mars ascent vehicle. In *Joint Army, Navy, NASA, Air Force (JANNAF) Interagency Propulsion Conference*, number SPS-I-11, Colombia, MD, December 2008. CPIA/JHU.

Greg S. Mungas, David Fisher, Joanne Vozoff, and Marco Villa. NofbxTM single stage to orbit mars ascent vehicle. In *IEEE Aerospace Conference Proceedings*. Firestar Technologies, mv2space, IEEE, 2012. doi: 10.1109/AERO.2012.6187299. URL https://www.researchgate.net/publication/261075483_NOFBX_single_stage_to_Orbit_Mars_Ascent_Vehicle. Conference held in March 2012.

Richard NAKKA. Introduction to rocketry: Fins. https://www.nakka-rocketry.net/RD_fin.htm, 2024.

- NASA. Nasa spaceflight human-system standard volume 2: Human factors, habitability, and environmental health. Technical Report NASA-STD-3001, Volume 2, Revision D, NASA, 2023. URL <https://www.nasa.gov/wp-content/uploads/2023/11/nasa-std-3001-vol-2-rev-d-with-signature.pdf>. Accessed: 2025-04-18.
- NASA. Environmental control and life support system (eclss). https://www.nasa.gov/wp-content/uploads/2020/10/g-281237_eclss_0.pdf?emrc=67ffdc, 2024.
- Axel Neumann and Martin Sippel. Critical analysis of spacex's next generation space transportation system: Starship and super heavy. In *HiSST: 2nd International Conference on High-Speed Vehicle Science Technology*. DLR – German Aerospace Center, 2022.
- J.A. Nicholls and T.E. Duffy. Thermal barrier coatings for gas turbine engines. Technical Report NASA/TM-2003-212310, NASA Glenn Research Center, 2003. URL <https://ntrs.nasa.gov/citations/20030093404>.
- NASA NOAA and U.S. Air Force. U.s. standard atmosphere, 1976. Technical report, U.S. Government Printing Office, Washington, D.C., 1976. NOAA, NASA, and USAF collaboration.
- N.P. Padture, M. Gell, and E.H. Jordan. Thermal barrier coatings for advanced gas-turbine engines. In *Science*, volume 296, pages 280–284, 2002. doi: 10.1126/science.1068609.
- Steve Parkes. *SpaceWire User's Guide*. STAR-Dundee Limited, Dundee, 2012. ISBN 978-0-9573408-0-0. Copyright © 2012 STAR-Dundee Limited. All rights reserved.
- Development Projects Office International Space Station Program. Nasa docking system (nds) interface definitions document (idd). Technical Report JSC 65795, National Aeronautics and Space Administration, Houston, Texas, Nov 2013. Revision H.
- International Space Station Program. International docking system standard (idss) interface definition document (idd). Technical Report Revision F, National Aeronautics and Space Administration, Houston, Texas, Jul 2022.
- North American Rockwell Rocketdyne Engineering Division. Advanced ignition systems: Final report. Technical Report NAS8-25126, NASA, Canoga Park, California, 1971. URL <https://ntrs.nasa.gov/api/citations/19710025676/downloads/19710025676.pdf>. Prepared under Contract NAS8-25126.
- Martinez Santiago, Catherine Hourtolle, Pierre Labourdette, Jean-François Goester, Sylvain Delattre, Véronique Tyrou, and Emilio De Pasquale. High reactivity maneuver design in atv missions. Technical report, CNES, 18 av. E. Belin 31401 Toulouse Cedex 9, FRANCE, 2009. Technical Report.
- Richard L. Sauer and David J. Calley. Apollo experience report: Potable water system. Technical Report NASA TN D-7291, NASA Manned Spacecraft Center, Houston, TX, 1973. URL <https://ntrs.nasa.gov/citations/19730016147>. Accessed: 2025-04-18.
- John H. Scott. Fuel cell development for nasa's human exploration program. Technical report, NASA Johnson Space Center, 2007. URL <https://ntrs.nasa.gov/api/citations/20070023719/downloads/20070023719.pdf>.

- Jason Silverman, Andrew Irby, and Theodore Agerton. Development of the crew dragon ecls. Technical report, Space Exploration Technologies, Hawthorne, California, 90250, 2023. Technical Report.
- George P Sutton and Oscar Biblarz. *Rocket propulsion elements*. John Wiley & Sons, 2017.
- V.V. Svitina and M.V. Cherkasova. Space debris removal – review of technologies and techniques. flexible or virtual connection between space debris and service spacecraft. *Acta Astronautica*, 204:840–853, March 2023. doi: 10.1016/j.actaastro.2022.09.027. URL <https://doi.org/10.1016/j.actaastro.2022.09.027>.
- Terma. Remote terminal units for all types of satellites. Terma Datasheet, 2023. Accessed on 2023-10-01.
- the Space Techie. How rockets navigate? <https://www.thespacetechie.com/how-rockets-navigate-gimballed-engines/>, 2020.
- Juan E. Tibaquirá, Kiril D. Hristovski, Paul Westerhoff, and Jonathan D. Posner. Recovery and quality of water produced by commercial fuel cells.
- Martin J. L. Turner. Rocket and spacecraft propulsion. January 2009.
- Kishor kumar Ukirde, Swaraj Pawar, Darshan Rahane, Bhushan Sagar, and Tushar Shinde. Aerodynamic study of various fins for missile body. *International Journal for Research in Applied Science & Engineering Technology*, 11(2), February 2023. ISSN 2321-9653. doi: 10.22214/ijraset.2023.49235. URL <https://doi.org/10.22214/ijraset.2023.49235>. Available at: www.ijraset.com.
- Unknown. Space shuttle guide. <https://spaceshuttleguide.com/>, 2025. Accessed: 2025-04-18.
- Antonio Viviani and Giuseppe Pezzella. Heat transfer analysis for a winged reentry flight test bed. In *Proceedings of the International Astronautical Congress*, Napoli, Italy, year unknown. URL <https://your-link-if-available>. Accessed April 2025. Affiliation: DIAM (SUN), CIRA.
- James R. Wertz and Wiley J. Larson. *Space Mission Analysis and Design*. Microcosm Press and Springer, Hawthorne, CA, 3rd edition, 2011.
- Wikipedia contributors. Apollo command and service module. https://en.wikipedia.org/wiki/Apollo_command_and_service_module, 2025. Accessed: 2025-04-18.
- . Etude des phénomènes thermiques dans un tube de hartmann-sprenger. *International Journal of Heat and Mass Transfer*, 16(3):529–538, 1973. doi: 10.1016/0017-9310(73)90221-4. URL <https://www.sciencedirect.com/science/article/pii/0017931073902214>.

List of Figures

1	System of System interfaces	10
2	ConOps phase 1	13
3	ConOps phase 2	13
4	ConOps phase 3	14
5	ConOps phases/modes	14
6	Debris Inclinaison vs. altitude	16
7	Propellant characteristics	18
8	Propellant mass for insertion depending on propellant choice	18
9	Trajectory representation	19
10	Remaining fuel mass	20
11	Inclination (tilt) evolution	20
12	Altitude evolution	21
13	Psimu Reentry Ground track	22
14	Psimu Reentry Used DeltaV Plot	23
15	Psimu Reentry Mach vs Time Plot	23
16	Psimu Reentry Mach vs Altitude Plot	23
17	Psimu Reentry Acceleration vs Altitude Plot	24
18	Psimu Reentry Acceleration vs Time Plot	24
19	Psimu Reentry Altitude vs Time Plot	24
20	Psimu Reentry Velocity vs Altitude Plot	25
21	Psimu Reentry Velocity vs Time Plot	25
22	Psimu Atmospheric Density Model US76	25
23	Atmospheric Re-entry	28
24	Anomalies environment causes	29
25	Orbit Average Flux	29
26	Solar Particle Fluences	30
27	Heavy Ions Fluxes	30
28	Meteoroids impacts in LEO over 5,7 years (LDEF mission)	31
29	O ⁺ density on Station & Debris orbits	31
30	Dose in function of the thickness on Station & Debris orbits	32
31	TNID Equivalent Fluences	33
32	Grun Meteroid Flux on Station Orbit	34
33	Comparison of different marterials exposed to a LEO orbit over 5.7 years (LDEF mission)	35
34	Wipple Shield used on NASA's stardust probe	36
35	Architecture diagram of the propulsion system	39
36	Engine geometry	43
37	Engine 3D view	44
38	RCS Engine 3D view	45
39	Top-view schematic of the injector plate	47
40	Acoustic ignitor geometry	49
41	Cooling system with 1 channel	52
42	Cooling system with 50 channels	52
43	Ariane 5 TVC geometry Turner [2009]	53
44	Gimballed engine assembly architecture Huzel and Huang [1992]	53
45	Ring-type Gimbal Mount Huzel and Huang [1992]	55

46	Spherical Gimbal Mount Huzel and Huang [1992]	56
47	Merlin Engine Gimbal Frame the Space Techie [2020]	58
48	Gimbal frame 2D schematic	58
49	Gimbal frame 3D schematic	59
50	He Tanks	62
51	NOFBX tank	62
52	NOFBX + He tanks architecture	63
53	ISS Control Moment Gyroscopes Charles Gurrisi and Ferguson [2009] . .	69
54	Shuttle Axis Denotation	71
55	Schematics of RCS placements	89
56	Starship Aerodynamics Estimates	91
57	Estimated drag force upon ballistic reentry	92
58	Estimated drag acceleration with increased profiles	93
59	Resulting accelerations for reentry with and without flaps	94
60	Hypersonic flow representation Kaushik [2019]	96
61	Existing flap geometries NAKKA [2024]	97
62	General Flap geometry denomination III [2021]	97
63	Impact of nose shape on the hypersonic shock wave Allen and Eggers [1958]	99
64	Flaps geometry and implantation schematic	101
65	Propulsive module	110
66	Structure idealization of the Cargo Module	112
67	Hoop stress on the Cargo Module	113
68	Coefficients of Axial Compressive Buckling for Long Curved Plates . . .	114
69	Stringer and Ring Arrangement for the Cargo Module	115
70	Life module	120
71	Structural frame	121
72	Propulsion layout	122
73	Propulsion section	122
74	Detail of the docking interface	123
75	Cargo hatch in open and closed positions	123
76	Engine injector and ignitor	124
77	Capsule layout	124
78	Martin Becker seat	125
79	Access Windows between StarCheap and Ground Stations (Satorb Analysis)	130
80	Communication Architecture	131
81	Ka-Band Antenna - BAE Systems	134
82	SWIFT-X KTRX Transceiver	134
83	Communication Hardware Architecture of StarCheap	139
84	CCSDS Space Packet	140
85	CCSDS Packet Transfer Protocol packet	141
86	Initial Estimation of the Power Budget	143
87	Schematic Diagram of PEMFC	145
88	Gravimetric and volumetric energy densities of various fuels	146
89	Schematic architecture of the primary energy source	147
90	SAFT VES100 Battery	149
91	Final architecture of the Electrical Power System (EPS)	151
92	ECLSS Architecture	157
93	CO ₂ and Humidity Removal System Architecture	162

94	Air Filtration Architecture	164
95	Example of water dispenser to rehydrated the meals	168
96	Illness Classification from NASA/TP-2015-218570	172
97	Examples of hygiene means in the ISS	175
98	Chris Hadfield brushing his teeth in the ISS	176
99	Potable water microbiological limits from NASA-STD-3001	177
100	Diagram representing the drinkable water production chain	179
101	Water consumption and production during the day	182
102	NASA's Space Shuttle water tank Unknown [2025]	186
103	Schematic of the CSM management system in Apollo Sauer and Calley [1973] Wikipedia contributors [2025]	188
104	Water system architecture	190
105	Picture of the urine funnel in the ISS	195
106	Representation of the different fluxes on a capsule during the re-entry, extract from MOULIN	198
107	Graphics from the study of Antonio Viviani and Giuseppe Pezzella	201
108	Material repartition on the Nasa's space shuttle	203
109	Heat shield structure of the Starship	204
110	Thermal map of the StarCheap during its re-entry	208
111	Picture of the TUF material	209
112	Systema modelisation of StarCheap	213
113	Trajectory definition on Systema	213
114	Emissivity representation of StarCheap without any coatings	216
115	StarCheap's surface temperature with initial material - Hot case	217
116	StarCheap's surface temperature with initial material - Cold case	218
117	Final coating repartition	221
118	Schematic of the different temperature areas and the associated equipment	222
119	Load response of active hook mechanism	229
120	Load response of passive hook mechanism	229
121	The series of orbital manoeuvres (OMP : On board Mission Plan)	231
122	The final approach from point S3	231
123	Mated NDS end-to-end Functional Interfaces	233
124	Docking Port IDSS Standard Design - Conceptual View	234
125	SCS	235
126	HCS	235
127	Umbilicals keep out zone	235
128	Docking port interfaces location choice.	237
129	Cable design	239
130	Docking Port IDSS Standard Design - Conceptual View with actuators	240
131	RVS-3000. Jenaoptronik	241
132	Miniature in-line load cell.	242
133	LVDT concept	242
134	Auricam D80.	243
135	Strain gauges	243
136	Pressure sensor	244
137	Humidity and Temperature Sensor. SHT3x-DIS	245
138	Principal Management Mode	250
139	Docking Management Mode	251

140	Capture Management Mode	253
141	Landing Management Mode	254
142	Subsystem and Phase by Mode	255
143	Global Architecture	256
144	SpaceWire Cable Structure	257
145	257
146	Subsystem Architecture	258
147	SIRIUS OBC LEON3FT	259
148	SIRIUS TCM LEON3FT	259
149	Terma - Remote Terminal Unit	260
150	Soft gripper method for removing space debris Svitina and Cherkasova [2023]	266
151	Net-based method for removing space debris Svitina and Cherkasova [2023]	267
152	Novel origami Capture concept Svitina and Cherkasova [2023]	269
153	Capture Operational Flowchart	276